THE UNIVERSITY *of* EDINBURGH

PROTEOMIC INVESTIGATION OF THE MDM2 INTERACTOME AND LINEAR MOTIF INTERACTIONS

Judith Nicholson BSc(Hons)

Thesis submitted for the degree of Doctor of Philosophy

University of Edinburgh

2011

In the beginning the Universe was created. This has made a lot of people very angry and was widely regarded as a bad move.

- *Douglas Adams*

The Universe has as many different centres as there are living beings in it

- *Aleksandr Solzhenitsyn*

Declaration

I declare that this thesis has been composed by myself, Judith Nicholson

and that this work is entirely my own unless otherwise clearly acknowledged.

This work has been submitted for the degree of Doctor of philosophy and has not been submitted for any other qualification, professional or otherwise.

Signature:

Table of Contents

Acknowledgments

Firstly my amazing supervisors Ted Hupp and Perdita Barran, who have been supportive and encouraging all the way through my PhD. Euan Murray, for his help with my lab work, for hundreds of interesting conversations about very important things and for bringing me a sombrero from Mexico. Alex Scherl, for his collaboration and immense proteomics expertise, even though it meant Team AGR2 was a bit annoyed at me for deserting them for Team Nutlin. On that note, Team AGR2 (Magda, Euan, Mel, Hannah, Terry) – this year must finally be the year of AGR2… A big thank you to Mark Molloy, Thiri Zaw and everyone I worked with at Sydney for welcoming me at sunny APAF. Erin, Susy, Bart and Jenny for MDM2 related help and advice. Everyone at the CTCB, particularly Janice Bramham, Liz Blackburn and Malcolm Walkinshaw, as well as Martin Wear and Hugh Morgan for CypB and PK. Chandra, for inviting me to Singapore and finding great food for me there. Everyone who organized and attended the Brno conferences, particularly Borek for inviting us all because the wine cellar visits were MINT. All of the support staff at ECRC, particularly Andrea, Jim, Jed and Shirley.

My friends and colleagues at the Hupp and Ball labs while I've been working there, too many to list by name but everyone was brilliant, thanks for making my PhD so much fun.

AND the Barran group – Martin, Peter, Jason, Stefan, Yana, Roland, Hattie, Ewa, Kamila, Sophie and the project students, making Friday afternoons even better than they intrinsically are.

For stopping me from being mental while I was writing this, Glenogle Swim Centre, Leith FM, tweeters and anyone who asked me if I fancy a pint at the exact moment I fancied a pint.

Finally, Mam, Dad and Sarah for encouraging me while I decided to stay in full-time education for as long as possible, it worked!

Abstract

The oncoprotein MDM2 has an integral role in cancer development via multiple signalling pathways. Two proteomic mass spectrometry screens, label-free with spectral counting quantitation and 8-plex iTRAQ were used to identify proteins up or downregulated over time by the MDM2 targeting drug Nutlin. A subset of previously identified MDM2 binding partners were identified as altered after Nutlin treatment, along with proteins which have not as yet been linked to MDM2 or p53. Proteins altered two hours after Nutlin treatment were screened for sequence similarity to an MDM2 binding consensus motif based on the BOX-I region of p53. Peptides corresponding to this motif were validated for MDM2 binding, and the mode of binding investigated using competition ELISA and thermal denaturation assays. Known MDM2 ligands such as Nutlin were shown to have a range of effects on the binding of these newly identified MDM2 peptides, which may be attributed to allosteric regulation of MDM2. The effects of Nutlin on two full length proteins identified by the MS screens, CypB and NPM, were confirmed *in vivo*. *In vitro* binding of MDM2 to CypB and PK, which contain BOX-I like motifs, was also demonstrated validating proteomic mass spectrometry screens as a method to identify new protein-protein interactions. To further investigate the potential of linear motifs to modulate protein-protein interactions, a peptide aptamer targeting the protein AGR2 was tested for effect on AGR2 and p53 in a cancer cell line.

Abbreviations

17-AAG – 17-N-Allylamino-17-demethoxygeldanamycin

Abl – Abelson murine leukaemia viral oncogene homolog 1

Acc. – Accession number

AD – Acidic domain

ADP – Adenosine diphosphate

AGR2 – Anterior gradient 2

Akt – RAC-alpha serine/threonine-protein kinase

ALK – Anaplastic lymphoma kinase

APE1 – DNA-(apurinic or apyrimidinic) lyase

APS – Ammonium persulphate

AQUA – Absolute quantification

ARF – ADP ribosylation factor

ATM – Ataxia telangiectasia mutated

ATP – Adenosine triphosphate

BAX – Apoptosis regulator BAX

Bcr – Breakpoint cluster region protein

BRAF – Serine/threonine-protein kinase B-raf

BRET – Bioluminescence resonance energy transfer

BSA – Bovine serum albumin

CHIP – Carboxy terminus of Hsp70-interacting protein

CID – Collision induced dissociation

CK1 – Casein kinase 1

CML – Chronic myeloid leukaemia

CMV – Cytomegalovirus

COP1 – Constitutive photomorphogenesis protein 1

CypB – Cyclophilin B

DD – Data dependent

ddH_20 – Double distilled H_2O

DI – Data independent

DIGE – Difference gel electrophoresis

DMEM – Dulbecco's modified eagle medium

DMSO – Dimethylsulfoxide

DNA – Deoxyribonucleic acid

DNA-PK – DNA-dependent protein kinase

DTT – Dithiothreitol

E2F1 – Transcription factor E2F-1

ECL – Enhanced chemiluminescence reagent

EDTA – Ethylene diamine tetraacetic acid

EGTA – Ethylene glycol tetraacetic acid

ELISA – Enzyme linked immunosorbent assay

ER – Endoplasmic reticulum

ESI – Electrospray ionization

FCS – Foetal calf serum

FRET – Fluorescence resonance energy transfer

GPP – Gas phase fractionation

GST – Glutathione s-transferace

HECT – Homologous to the E6-AP carboxyl terminus

HEPES – 4-(2-hydroxyethyl)-1-piperazineethanesulfonic acid

Her2/Neu – Receptor tyrosine-protein kinase erbB-2

HPLC – High performance liquid chromatography

HRP – Horseradish peroxidase

HSP90 – Heat shock protein 90

IPTG – isopropyl β-D-1-thiogalactopyranoside

IRES – Internal ribosomal entry site

IRF2 – Interferon regulatory factor 2

iTRAQ – isobaric tags for relative and absolute quantitation

LB – Luria-bertani (or lysogeny broth) mediuam

LC – Liquid chromatography

LC-MS – Liquid chromatography-mass spectrometry

MALDI – Matrix assisted laser desorption ionization

MDM2 – Mouse double minute 2

MDM4/MDMX – Mouse double minute 4/mouse double minute X

MOPS - 3-(N-morpholino)propanesulfonic acid

MRM – multiple reaction monitoring

mRNA – Messenger ribonucleic acid

MS – Mass spectrometry

MS/MS – Tandem mass spectrometry

m/z – mass/charge

NEDD8 - Neural precursor cell expressed developmentally down-regulated protein 8

Ni-NTA – Nickel nitrilotriacetic acid

NMR – Nuclear magnetic resonance

NP40 - Nonyl phenoxypolyethoxylethanol 40

NPM - Nucleophosmin

NT – N-terminal

PAcIFIC – Precursor acquisition independent from ion count

PCR – Polymerase chain reaction

PBS – Phosphate buffered saline

PBS-T – Phosphate buffered saline with 0.05% Tween

PDB – Protein data bank

PenStrep – Penicillin and streptomycin

Pirh – p53-induced RING-H2 protein

PK – Pyruvate kinase

PPI – Protein-protein interaction

PRIMA - 2,2-bis(hydroxymethyl)-3-quinuclidinone

RB1 – Retinoblastoma 1

RFU – Relative fluorescence units

RING – Really interesting new gene

RLU – Relative luminescence units

RNA – Ribonucleic acid

RPL – Ribosomal protein large subunit

RPMI – Roswell park memorial institute

RPS – Ribosomal protein small subunit

rRNA – Ribosomal RNA

SAFA – Scaffold attachment factor A

SAXS – Small angle X-ray scattering

SDS – Sodium dodecyl sulphate

SDS-PAGE – Sodium dodecyl sulphate polyacrylamide gel electrophoresis

SCX – Strong cation exchange

SDS – sodium dodecyl sulphate

SFM – Serum free medium

SILAC – Stable isotope labeling of cells in culture

siRNA – Small interfering ribonucleic acid

SUMO – Small ubiquitin like modifier

TAD – Transactivation domain

TBS – Tris buffered saline

TBS-T – Tris buffered saline with 0.05% Tween

TEAB – triethylammonium bicarbonate

TEMED – Tetramethylethylenediamine

TET – Tetramerisation domain

TFA – Trifluoroacetic acid

TGF – Transforming growth factor

TOF – Time of flight

Tris – Tris(hydroxymethyl)aminomethane

Triton X-100 - Polyethylene glycol p-(1,1,3,3-tetramethylbutyl)-phenyl ether

Tween - Polyoxyethylene (20) sorbitan monolaurate

Ub - Ubiquitin

UBE1 – ubiquitin-like modifier-activating enzyme 1

UbcH5 – Ubiquitin conjugating enzyme E2 D1

UV – Ultraviolet

UV/Vis – Ultraviolet/visible light

ZF – Zinc finger

1 Introduction

1.1 Overview of the molecular basis of cancer

1.1.1 Carcinogenesis and the cancer phenotype

Cancer is a disease arising from a combination of factors which have their basis in genetic mutations, and around 13% of worldwide deaths are attributable to cancer[1]. Cancer cells are unable to arrest or die, which leads to uncontrollable cell proliferation eventually resulting in a tumour. There is huge diversity between different types of cancer, and each tumour has a unique molecular signature. The mechanisms by which a healthy cell transforms into a cancer cell, carcinogenesis, include a range of pathways and events which accumulate to finally result in a malignant tumour. A combination of immunity to growth signals, cell immortality, increased proliferation, ability to invade surrounding tissues, resistance to the immune system and altered metabolism may contribute to carcinogenesis[2]. The micro-environment of a tumour can include non-cancerous cells, altered extracellular matrix and cancer stem cells which cooperate with the cancer cells, further complicating the phenotype of a tumour[3]. Genetic mutations giving rise to altered expression of proteins, expression of mutant proteins and deletion of regulatory proteins are factors which can give rise to a cancerous phenotype[4]. Constitutively active or inactive fusion proteins also contribute to carcinogenesis through the activation of cancer promoting pathways[5]. Some of these cancer promoting mutations are in the genes controlling cell cycle progression, and pathways which control checkpoints to prevent cells with DNA damage from dividing and proliferating, the deregulation of which can immortalize cells[2]. Mutations causing loss or gain of

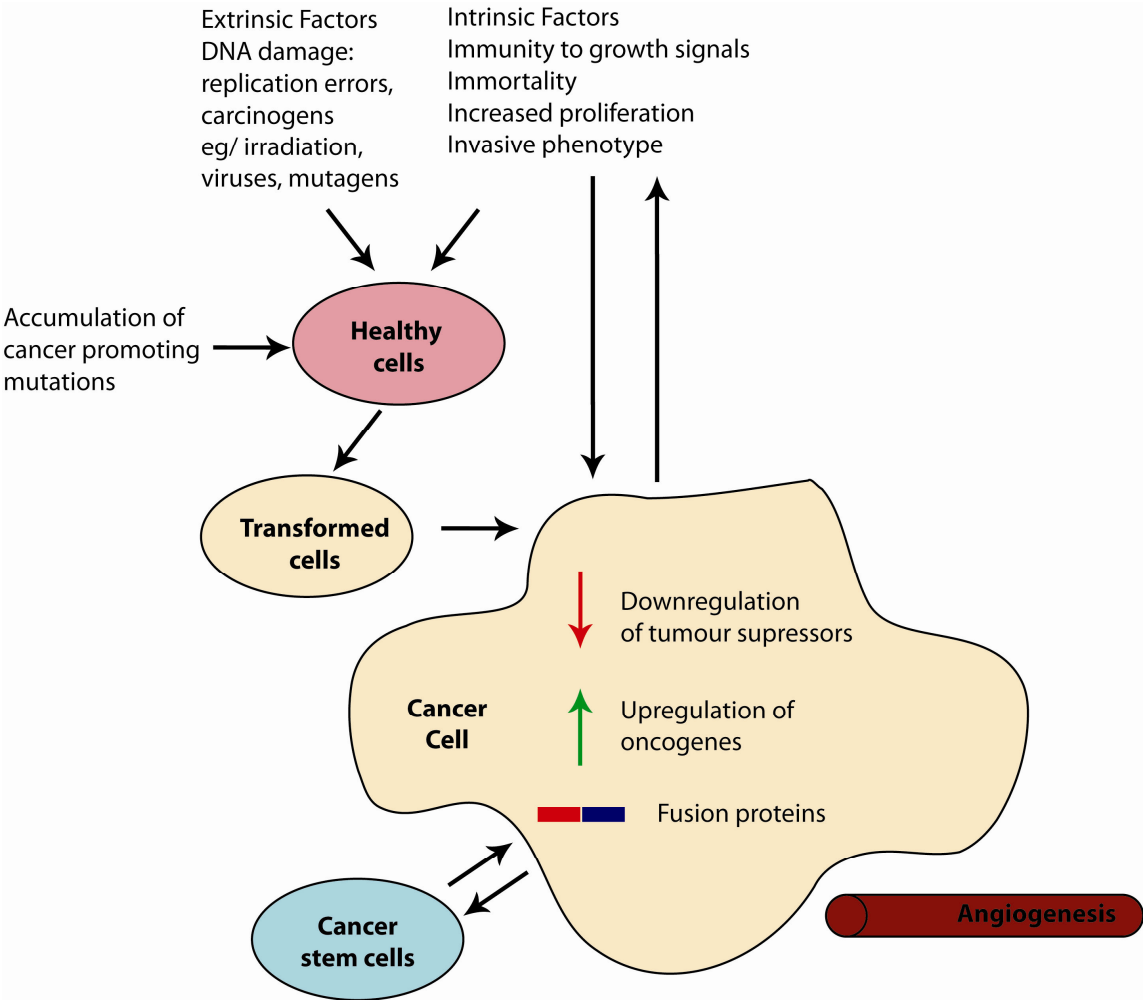

Figure 1.1- Summary of factors contributing to carcinogenesis, tumour microenvironment and tumour progression

function in proteins can also disrupt other intracellular signalling pathways, and deregulation of a combination of pathways regulating the other processes described above can contribute to the transformation of a cell into a cancerous cell (Fig. 1.1).

Genetic instability therefore leads to misregulation at the protein level, which is where the changes which cause a cell to become cancerous are effected. Pathways misregulated in cancer also include growth factor response, metabolic pathways, transcription and translation machinery, protein degradation and apoptosis[2, 6]. In summary, many normal cellular processes are misregulated and aberrant in cancer cells, and the genetic instability of cancer cells translates to proteome level alterations which manifest as the altered behaviour observed in cancer.

1.1.2 Current cancer therapeutic strategies

There is diversity in mutations causing misregulation of cancer pathways and cancer survival mechanisms which raises a problem for designing new cancer therapeutics. Cancer treatments can include surgery and radiotherapy, however these methods of treatment may leave cancer cells behind which can continue proliferating. Cancer drugs targeting the proteins which cause transformation and cell survival are a more directed type of therapy[7]. With a wide range of proteins and pathways involved in the survival of a cancer cell, there can be difficulty in choosing targets for drug development. The drug must preferably target only cancer cells, and cause the arrest or death of cancer cells to such an extent that no cancerous cells remain to continue proliferating. Pathways and proteins which are central to carcinogenesis can provide rich sources of targets for cancer therapeutics due to their vital role in the continued survival of a cancer cell. Cell signaling pathways regulating proliferation, cell cycle checkpoints and apoptosis are obvious targets for cancer therapeutics. Additionally, the environment of a cancer cell may have unnatural metabolic conditions due to increased hypoxia, reliance on

glycolysis rather than oxidative phosphorylation[8] and over or underexpression of proteins required to maintain the correct balance of protein synthesis and degradation, also known as proteostasis[9].

Cell surface receptors and kinases which regulate cell signaling pathways are attractive targets, due to the availability of a substrate binding interface or pocket which allows rational design of drugs to fit the binding site[10]. Targeting receptors and kinases has the potential to knock-out or activate a whole pathway by targeting a single protein. Successes in cancer therapy have included drugs which target general features of cancerous cells which are also required for the survival of healthy cells. Examples are paclitaxel, or taxol which targets microtubule dissassembly[11] and cisplatin which targets DNA transcription[12], both of these therapeutics are based on the principle that cancer cells are more rapidly dividing and therefore will be more negatively affected by these drugs than slower dividing healthy cells. A recently developed drug which fits this profile is bortezomib also known as Velcade™, which targets the proteasome, the theory behind this being that cancer cells produce more misfolded proteins than healthy cells which places a higher burden on the proteasome[13]. Drawbacks with these drugs which broadly affect cellular processes are that they can also affect healthy cells, and are not targeted directly to cancerous cells, which results in the side effects of these treatments. More specific drugs have been developed which are targeted to particular proteins, such as kinases, ATP binding proteins or cell surface receptors. Successes in this area include the bcr-abl tyrosine kinase inhibitor, Gleevec™, which targets the oncoprotein fusion of Bcr and abl often found in chronic myeloid leukaemia (CML) and is constitutively

activated[14]. Antibody therapeutics such as anti-Her2/neu, known as Herceptin™, which specifically binds the Her2 receptor are another example of precisely targeted therapeutics[15]. These drugs are effective for specific types of cancer, however they will only work for cancer cells with a specific mutation or characteristic and therefore are limited to the treatment of particular types of cancer. Discovery of new targets alongside tried and tested treatments is required to broaden our arsenal of available cancer treatments and find drugs to treat cancers which do not respond to the current repertoire of anti-cancer therapeutics.

1.1.3 Hub proteins and interactomes as drug targets

Proteins which are at the junction of multiple pathways can promote cancer cell survival and transformation. These proteins are attractive targets for therapeutics, because targeting them could have effects against a wide range of cancer cells without a negative effect on healthy cells. They also have potential as targets for combination therapies to enhance the effect of precisely targeted drugs. The chaperone HSP90 is an example of a hub protein, it is widely involved in cancer related protein folding pathways for example p53 pathways, BRAF and Akt pathways[16]. Targeting HSP90, for example with the inhibitor geldanamycin and the geldanamycin derivative 17-AAG[17], has been shown to be very effective as a potential anti-tumour therapeutic. Another advantage of targeting heat shock proteins is that cancer cells exhibit altered proteostasis, due to the requirement of a higher rate of production of proteins to support the accelerated proliferation and division of cells[18]. Proteostatic pathways encompass translation and

degradation machinery, and finding out the molecular details of these pathways will be useful for cancer research. The p53 tumour suppressor is another important example of a hub protein, mediating transcription and regulating cell cycle checkpoints and apoptosis, and participating in multiple pathways including TGF-beta, ubiquitin proteasome pathway and cell cycle regulation[19] (Fig. 1.2). It is often quoted that p53 is mutated or deactivated in 50% of tumour cells, and it is the case that many tumours can be classed

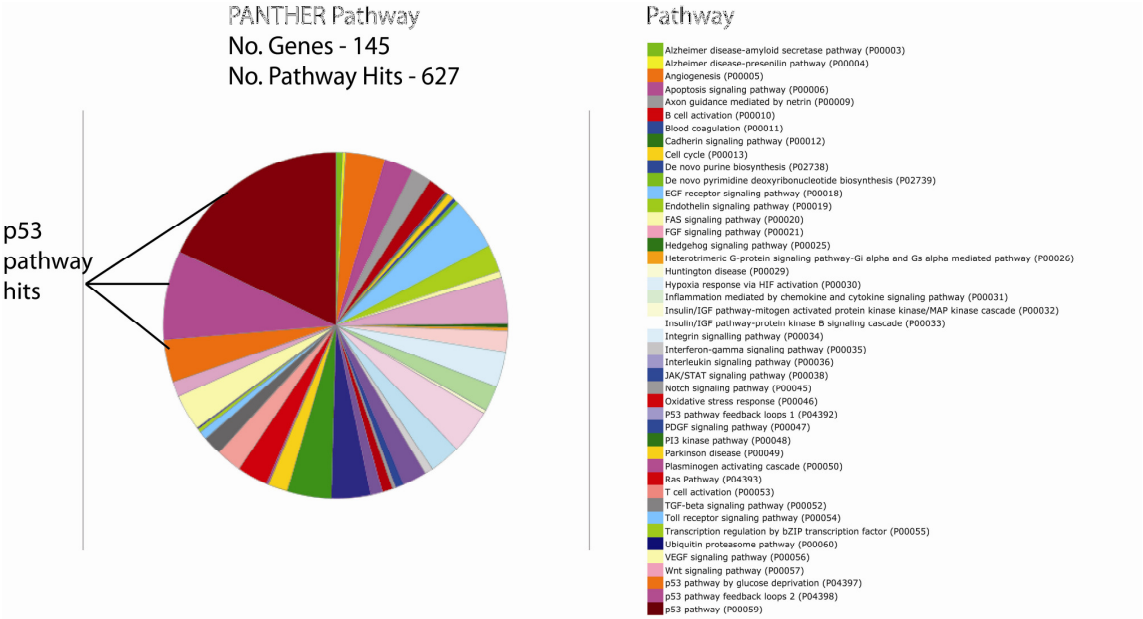

Figure 1.2 – Summary of pathways which contain proteins in the p53 regulatory network generated using PANTHER database, segments represent the number of proteins in each pathway and some proteins are represented in more than one pathway, 16th May 2011[20, 21].

based on their p53 status which may eventually be regularly tested for as an indicator as to which drugs will be effective[22]. To verify this statistic, it would be necessary to carry out widespread proteomic studies on tumours as well as genetic studies, due to regulation on the protein level often being a cause of p53 misregulation. Targeting p53 for reactivation is an extremely attractive cancer target, as this can result in the

activation of cell cycle arrest and apoptosis pathways, and many cancer research efforts have focused on this.

It is becoming widely acknowledged that cellular proteins are regulated by an 'interactome' rather than by individual binary protein-protein interactions. A protein interactome can be defined as all of the proteins which bind to or are regulated by the protein of interest[23]. Proteins are part of complexes, which are dynamic and regulated by multiple factors, and their interactome is variable and responsive to the cellular environment. It is possible to investigate the interactome of a protein by using protein-protein interaction identification techniques such as yeast two-hybrid, phage peptide display and affinity purification as well as mass spectrometry[24]. The proteome could be described as a collection of overlapping interactomes, since proteins share common transcription, translation and degradation machinery all cellular proteins will be linked *via* their interactomes in a vast cellular network. The environment inside cells means that most proteins are tightly packed with other proteins, and are surrounded from translation to degradation, thus the linkages between proteins in pathways or cellular functions are highly regulated and highly complex[25].

1.2 p53 structure and functions in cancer

1.2.1 p53 role in cancer

The tumour suppressor p53 has been the subject of a vast amount of cancer research since being discovered in 1982 by Levine *et al*[26]. Activation of p53 can cause cell cycle

arrest or apoptosis in cancer cells as part of the DNA damage response pathway, and is central to the cells defense against cancer. p53 is therefore an important target for cancer therapeutics, and a critial protein to study to enhance our understanding of the mechanisms involved in carcinogenesis and cancer cell survival.

1.2.2 The structure of p53

p53 was named after it was discovered to migrate at 53 kDa on an SDS-PAGE gel[26],

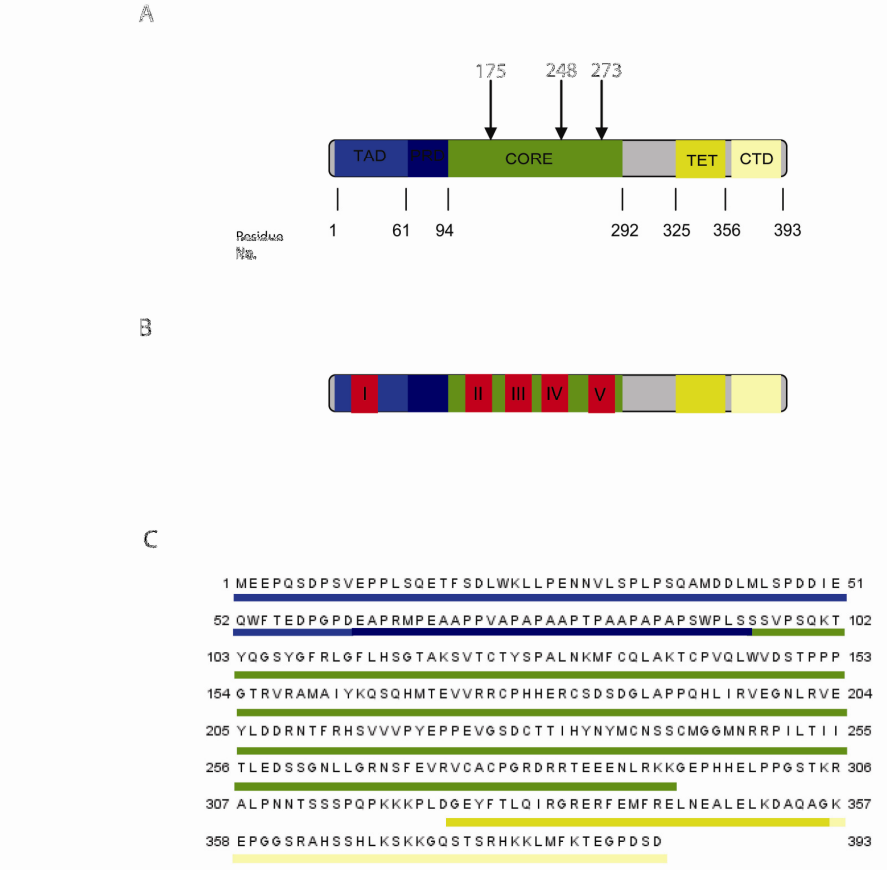

Figure 1.3 – A) Domain structure of p53 with domains highlighted and location of three most common p53 mutations in cancer TAD – transactivation domain (contains two TAD motifs[27]), PRD – proline rich domain, CORE – Core domain, TET – tetramerisation domain, CTD – C-Terminal domain B) Location of conserved BOX regions of p53. C) Amino acid sequence of human p53 with domains highlighted

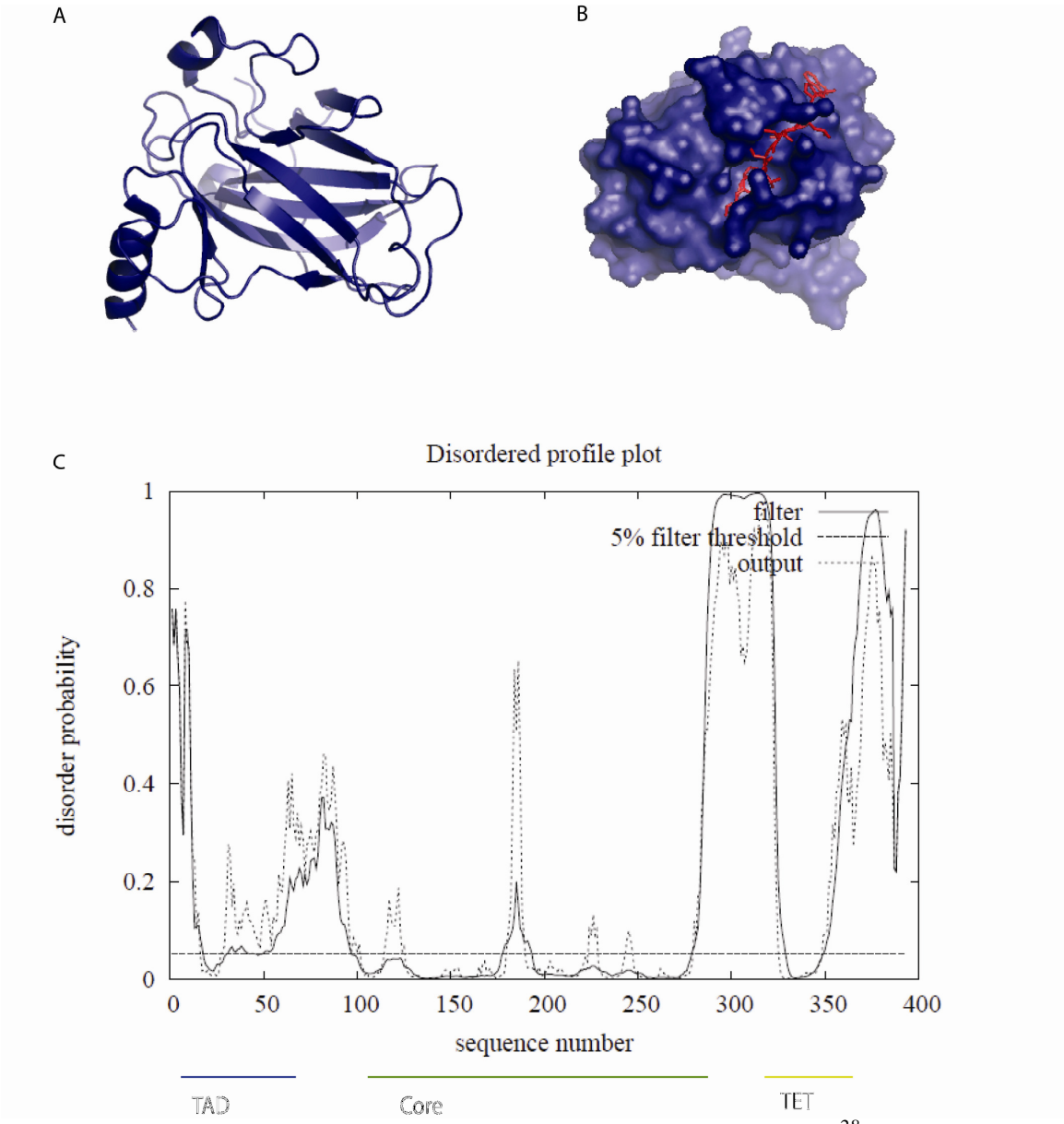

Figure 1.4 – A) Representation of p53 core domain structure residues.[28] B) p53 core domain with disordered N-terminal region of core highlighted in red. PDB: 2WXR C) Disopred[29] prediction of stuctural disorder in full length p53, TAD – transactivation domain, Core – core domain, TET – tetramerisation domain

however the molecular weight of p53 is actually 43.7 kDa. p53 has a high degree of disorder and has been shown to form both dimers and tetramers[30, 31]. The protein is 393

amino acids long, and contains several distinct domains, and conserved regions of p53 have also been designated BOX-I, II, III, IV and V (Fig. 1.3)[19]. The domains of p53 are the N-terminal transactivation domain, a proline rich domain, the core DNA binding domain, the tetramerisation domain and the C-terminal regulatory domain. The core domain (Fig. 1.4a,b) and the tetramerisation domain structures of p53 have been solved by X-ray crystallography and small angle X-ray scattering (SAXS), both for wild type p53 and several p53 core domain mutants[28, 32-34]. Although the core DNA binding domain is an ordered region of p53 there are still many disordered loops in the core structure, and SAXS has revealed the high degree of disorder in the p53 structure[32]. The tetramerisation domain is an alpha helical domain which forms a helix-helix interface with other p53 monomers[35]. Overall p53 is a highly unstructured protein, with large predicted regions of disorder[29] (Fig. 1.4c). Full-length p53 readily unfolds at elevated temperatures, this inherent flexibility may facilitate degradation, and be linked to the necessity to quickly degrade p53 in order to allow cell cycle progression[36]. Some p53 mutants are associated with lower thermostability, which could contribute to p53

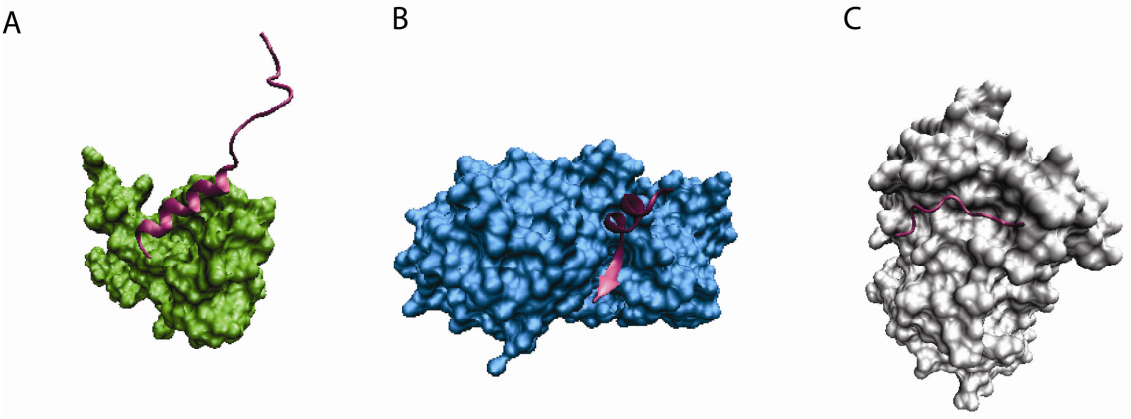

Figure 1.5 – Disordered C-terminal domain of p53 bound to A) S100b as an alpha helix B) sirtuin as a beta strand C) cyclin A2 in an extended conformation PDB: 1DT7, 2H2D and 1H26 respectively[37]

degradation and deactivation of the p53 response in cancer cells[34]. The core domain in isolation has a higher degree of stability than the full-length protein, this may be due to this domain mediating DNA binding and requiring a more ordered structure. However many of the p53 protein interaction interfaces are located in other domains. In particular the N-terminal and C-terminal domains of p53 are highly disordered, and both of these regions have been proposed to have a role in binding the negative regulator of p53, MDM2[38, 39]. Interestingly, it has recently been shown that the disordered region of p53 between the proline rich domain and the core domain confers stability to the core through binding to it as a linear motif[28] (Fig. 1.4b), highlighting the important functional role of disordered regions of p53. The C-terminal domain of p53 has also been shown to adopt multiple conformations in the presence of different protein ligands, an example of binding induced folding and a mechanism by which p53 can bind multiple proteins (Fig. 1.5)[40]. The high degree of disorder in p53 structure, and observed changes in p53 structural rearrangement on binding in crystal structures, suggests p53 interactions may be extensively regulated by mechanisms involving 'folding on binding' which is a concept central to disordered protein binding mechanisms[41].

1.2.3 Functions of p53 in tumour suppression

p53 is a transcription factor which promotes cell cycle arrest proteins such as p21, and apoptotic effectors such as BAX. Increased levels of p53 therefore correlate with a higher incidence of apoptosis and cell cycle arrest[42]. p53 is central to the DNA repair pathway, stimulus such as UV and X-ray which cause DNA damage activate p53 as a

transcription factor and stabilise cellular levels of p53. It is interesting to note that p53 has been reported to have greater than 300 interactions[43] (Fig. 1.2), and participates in many multi-protein complexes. Roles for p53 have been proposed in aging[44], metabolism[45] and development[46] as well as functioning as a tumour suppressor. This is an intriguing example of one cancer related protein participating in a diverse interactome, and mediating the cross-talk between multiple cellular pathways. A large amount of research has been focused on p53, and it is a possibility that other less well known proteins may have equally large interactomes.

1.2.4 Misregulation of p53 in cancer and therapeutic targeting

The inactivation of p53 can occur by deletion or downregulation, as well as through the production of mutant p53 with aberrant functions. p53 mutants are common in cancer, and there are mutation hotspots in the p53 sequence, particularly focused in the core DNA binding domain[19]. It is often the case that p53 mutant proteins are dominant over the wild type form of the protein where both are expressed, and in these cases mutant p53 acts as an oncoprotein[43]. Therefore there are two ways to target the p53 pathway in cancer: reactivation of wild type p53 or inhibition of mutant p53. Other mechanisms by which p53 can be misregulated in cancer include an increase in negative regulators of p53 such as MDM2 and other E3 ubiquitin ligases[47, 48], the cytoplasmic relocalisation of p53 which downregulates p53 functions and misregulation of downstream targets of p53[49]. Drugs which have been developed with the aim of reactivation of p53 related processes include molecules which bind and inactivate or rescue mutant p53. The drug

CP-31398 for example binds to mutant p53 and abrogates the oncogenic effects of this protein by stabilizing the protein[50]. Mutant p53, such as Y220C, has a binding pocket which can be targeted by rational drug design, and studies have shown that this may be a viable route for reactivating p53[51]. The anti-cancer compound PRIMA covalently modifies reactive cysteines, which affects p53 due to the dependence of p53 on reactive cysteines for function[52]. However it is possible that the anti-cancer activity of this drug

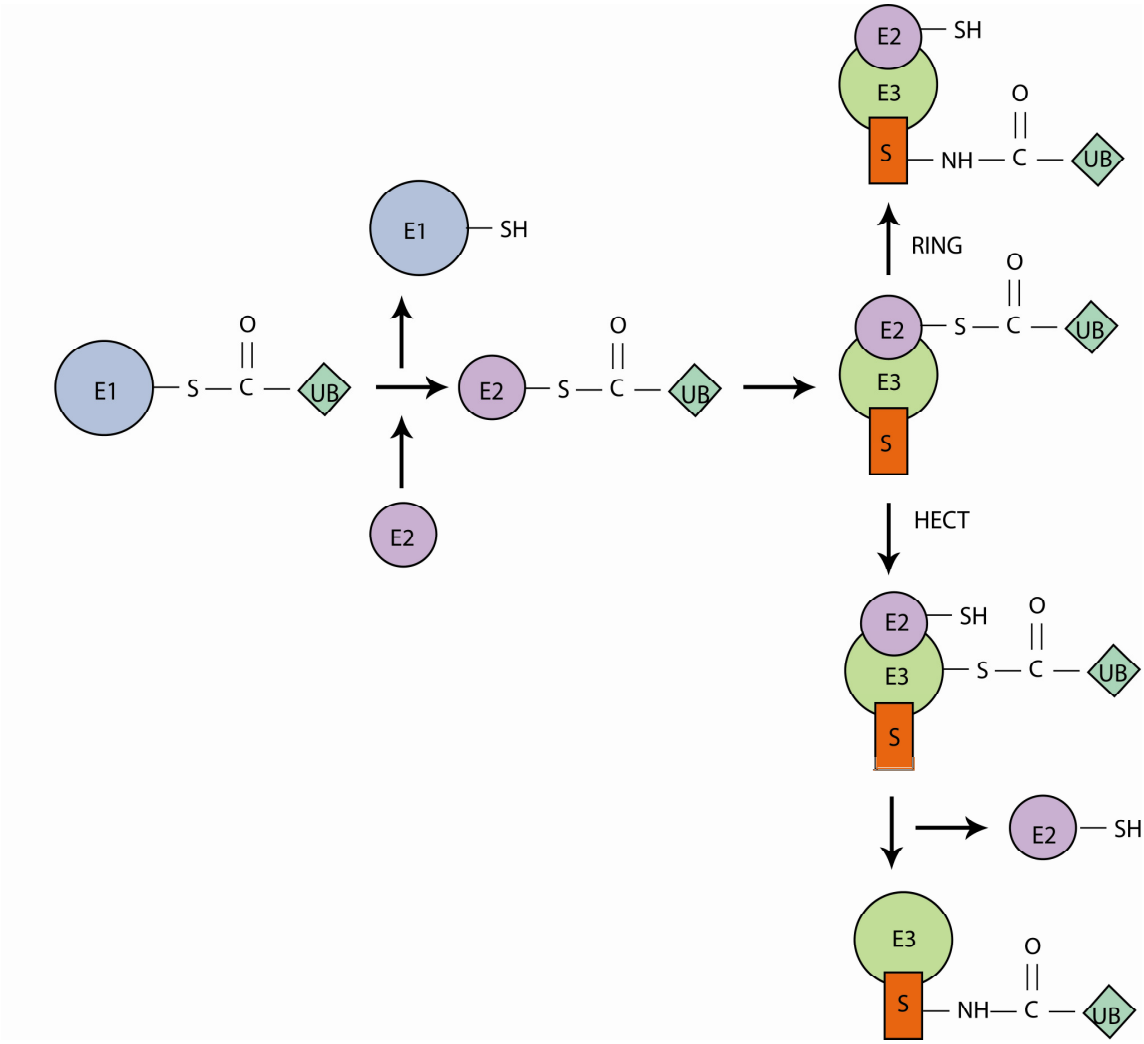

Figure 1.6 – Mechanism of ubiquitination mediated by E1, E2 and E3 ligases. RING E3 ligases conjugate ubiquitin directly to substrate lysine residues, HECT E3 ligases transfer ubiquitin to substrate via an intermediate step where ubiquitin is conjugated to the E3 via a thiol linkage. S – substrate, Ub – ubiquitin.

is due to it attacking a broad range of reactive cysteines and is not necessarily p53 specific. Many p53 targeting strategies focus on MDM2 which is an E3 ligase for p53[47]. E3 ligases function as enzymes which catalyse the ubiquitination of a substrate which targets the substrate for proteasomal degradation. E3 ligases work as part of an ubiquitination pathway, which includes the transfer of ubiquitin from an E1 and E2 enzyme. The E3 which makes contact with the substrates, can ubiquitinate proteins *via* two known mechanisms, RING E3 ligases directly transfer ubiquitin from the E2 to the substrate and HECT E3 ligases form a thiol bond with the ubiquitin prior to transfer to the substrate[53] (Fig. 1.6). NEDD8 and SUMO are ubiquitin-like proteins, and can be conjugated to substrates, including p53 and MDM2, although this is not linked to proteasomal degradation in the same way as ubiquitination[54]. MDM2 is not the only p53 E3 ligase, others include Pirh[55], CHIP[56] and COP1[57], as such these proteins may also represent targets for reactivation of p53. The MDM2 p53 binding interfaces are well-characterised and it has also been shown in many studies that MDM2 regulates p53 transactivation, cellular localization and mRNA translation[58, 59]. Although targeting MDM2 has primarily been investigated as a means of reactivating p53, MDM2 also has a complex interactome and participates in many cellular pathways which are not necessarily p53 dependent. These pathways are not yet characterized to the extent of p53 pathways. Discovering more about MDM2 related pathways would be instructive, as these two proteins are major 'hubs' in cancer.

1.3 The role of MDM2 in cancer

1.3.1 Functional roles of MDM2

MDM2 is a multi-functional, multi-domain protein primarily characterized as an E3 ubiquitin ligase targeting the tumour suppressor p53[47, 60]. As well as an E3 ligase targeting p53, MDM2 has been shown to be involved in ribosomal pathways, translation[59], nuclear localisation and chaperone functions[61]. Over 150 proteins have been reported as MDM2 interacting proteins[43], and although there is an

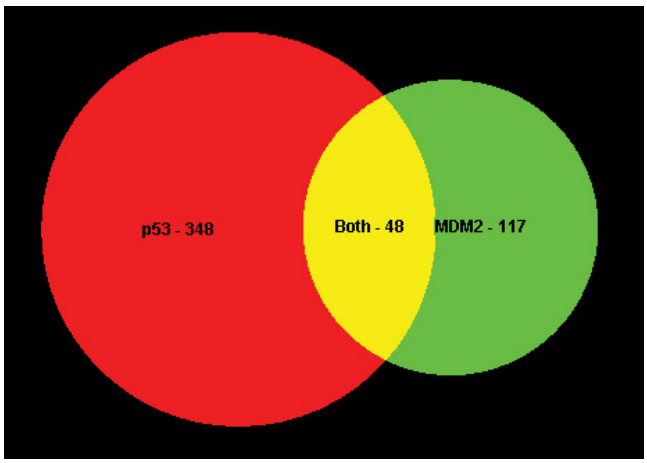

Figure 1.7 – Overlapping p53 and MDM2 interactomes

overlap with the p53 interactome (Fig. 1.7) MDM2 also has many binding proteins not known to be associated with p53 and therefore the inhibition of MDM2 in cancer could have wider ranging effects than an increase in p53 levels. Similarly p53 has many non-MDM2 related binding partners, suggesting that targeting MDM2 may not re-activate all of the functions associated with p53.

1.3.2 Structure of MDM2

MDM2 is a 55 kDa protein of 491 amino acids, expressed as a range of splice variants

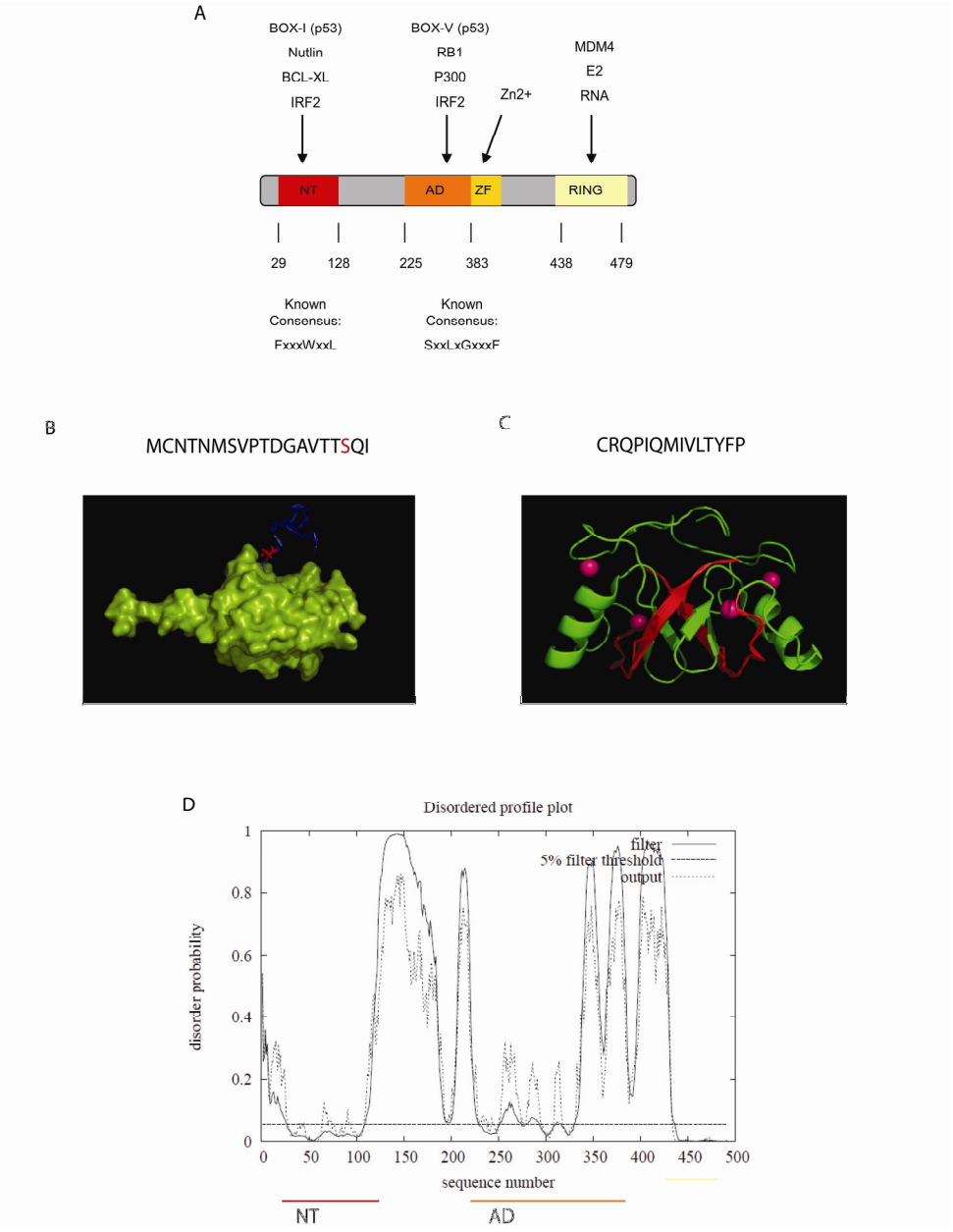

Figure 1.8 – A) Domain structure of MDM2 and binding site of a selection of known ligands NT – N-terminal domain, AD – Acidic domain, ZF – zinc finger, RING – RING domain B) Sequence of lid domain and position in NMR structure, lid highlighted in blue, Ser17 highlighted in red PDB: 1Z1M C) Sequence of tail domain and position in RING dimer structure, tail highlighted in red, zinc highlighted in pink PDB: 2HDP D) Disopred[29] disorder prediction of MDM2 structure and position of major domains

which can also promote carcinogenesis[62]. The overall domain structure of MDM2 is illustrated in Figure 1.8a, MDM2 has a structured N-terminal domain with a hydrophobic pocket, a disordered central acidic domain containing a nuclear localization signal, a zinc finger, and a C-terminal really interesting new gene (RING) domain which has similarity to other members of the RING E3 ligase family[63]. The RING domain contains an ATP binding site with sequence similarity to the P-walker ATP binding loop and a zinc coordination site[64]. There are also two mini-domains at the N and C-terminus of MDM2, the disordered N-terminal lid and the C-terminal tail which mediate MDM2 ligand binding and possibly RING oligomerisation respectively (Fig 1.8b, c)[65, 66]. Overall the full-length MDM2 protein is predicted to have a high level of disorder, particularly in the acidic domain (Fig. 1.8d), which may contribute to the difficulties encountered in determining the structure of full-length MDM2.

1.3.3 MDM2 N-terminal structure

The structure of the N-terminal domain of MDM2 has been solved by x-ray crystallography and NMR, in an apo form and in complex with drugs and peptide ligands derived from p53[67, 68]. There are interesting differences between the X-ray structure and the NMR structure which hint at a degree of flexibility in this domain (Fig. 1.9a,b). The N-terminal domain contains a hydrophobic pocket, and there is an electrostatic patch around the ligand binding pocket, with a region of negative charge including the residue glutamate 25 (1.9a,b,c). Although the N-terminal domain overall is relatively structured, the N-terminal lid is flexible and unstructured and can act as a pseudosubstrate to bind into the hydrophobic pocket[65]. The N-terminal domain,

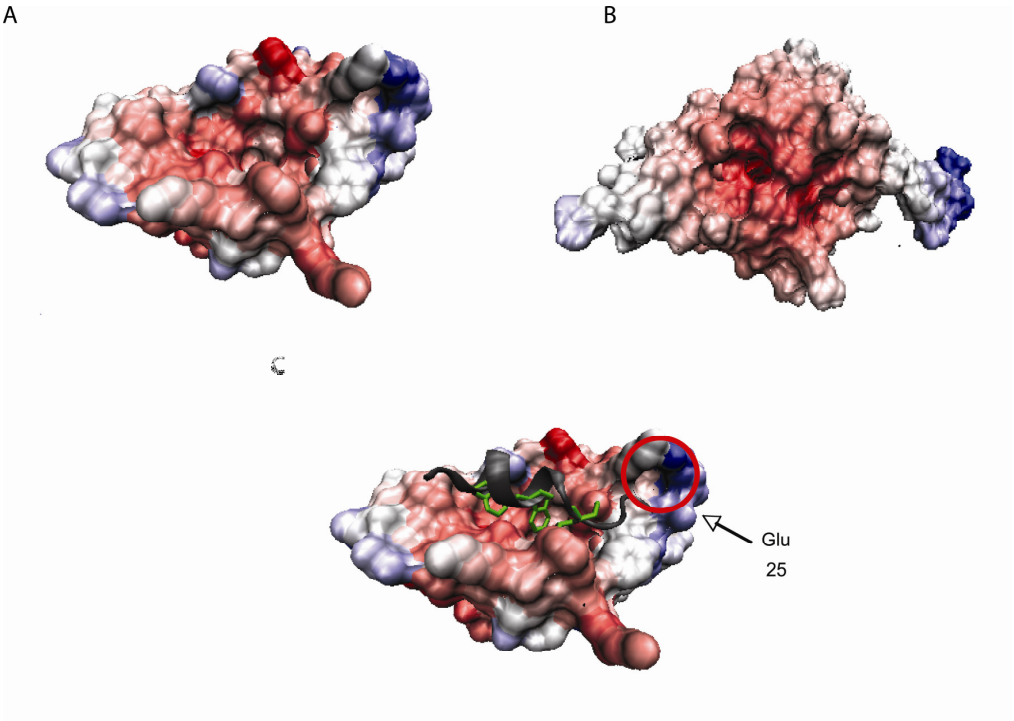

Figure 1.9 – N-terminal structures of MDM2. A) X-ray structure of N-terminal domain showing hydrophobic pocket, PDB: 1YCR B) NMR structure of N-terminal domain PDB: 1Z1M C) p53 N-terminal BOX-I sequence binding MDM2 with Glu25 highlighted

particularly the hydrophobic pocket and the RING domain, of MDM2 is partially conserved in organisms as diverse as *Trichoplax adhaerens, Danio rerio* and *Mytilus trossulus*.(Fig. 1.10)[69, 70] which supports the idea that there is a vital role of the p53-MDM2 axes in non-cancerous pathways. The lid and tail regions are also well conserved, indicating a functional role for these disordered regions.

1.3.4 RING domain structure

RING E3 ubiquitin ligases, which contain a zinc finger motif, interact with an E2 conjugating enzyme to transfer ubiquitin to the substrate. This is in contrast to HECT ligases which are covalently modified with ubiquitin by a thiol linkage before transferring ubiquitin to the substrate[71]. The MDM2 RING domain structure has also

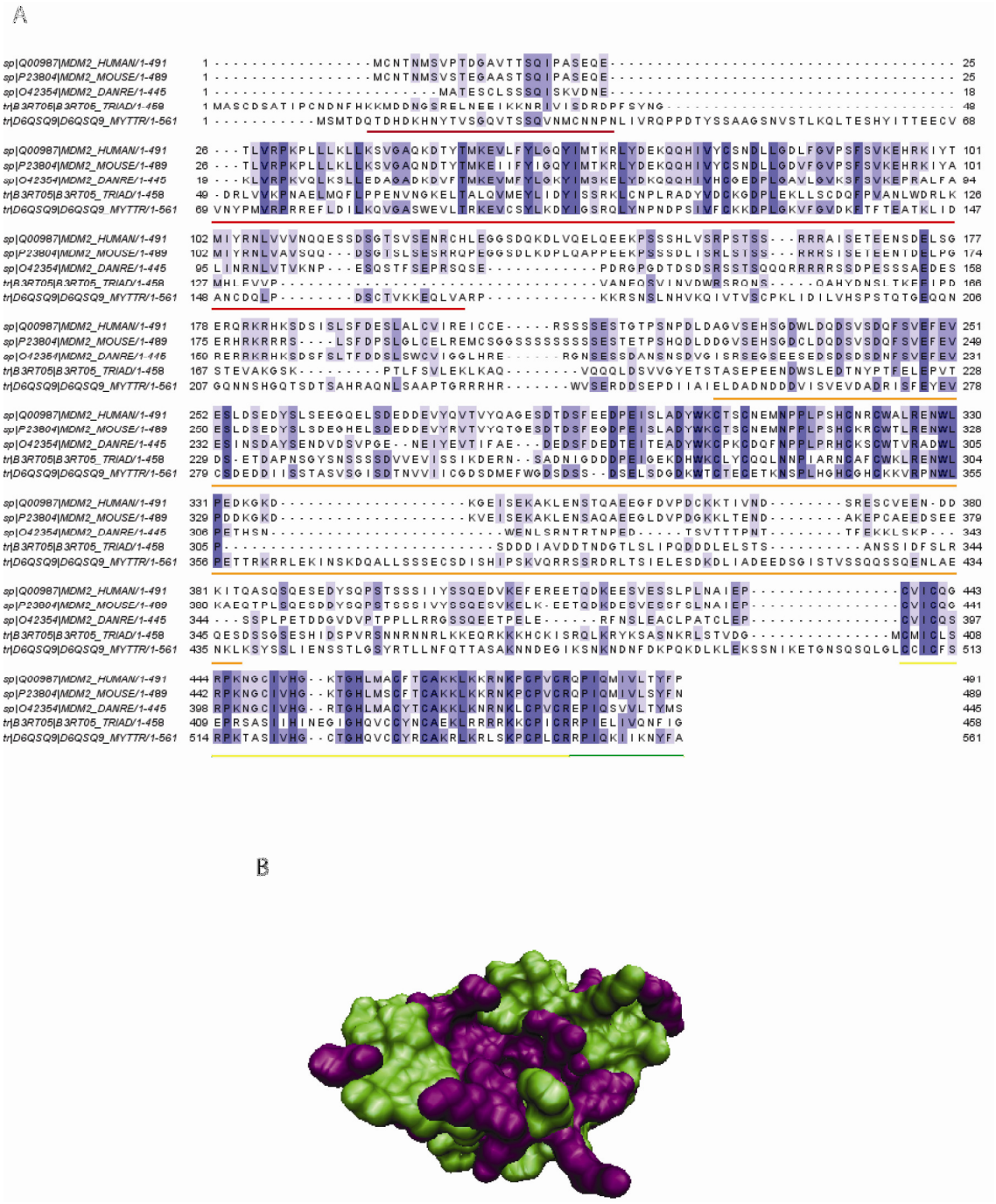

Figure 1.10 – A) Alignment of human, mouse, zebrafish, Trichoplax and Mytilus MDM2 homologs with main domains highlighted maroon – lid, red – N-terminal domain, orange – acidic domain, yellow – RING domain, green - tail[72] B) Structure of human MDM2 with conserved residues in Trichoplax highlighted in purple

been obtained, both as a homodimer by NMR and as a dimer with the MDM4 RING domain by x-ray crystallography[73] (Fig. 1.11), and has similarity to other members of the RING E3 ligase family[63]. Mutation of residues in the RING domain which coordinate the zinc results in loss of ubiquitin ligase activity of MDM2, and ability to ubiquitinate p53[60]. The RING domain in isolation has been shown to function as an E3 ligase[74], with no requirement for the other MDM2 domains which may therefore confer specificity to MDM2.

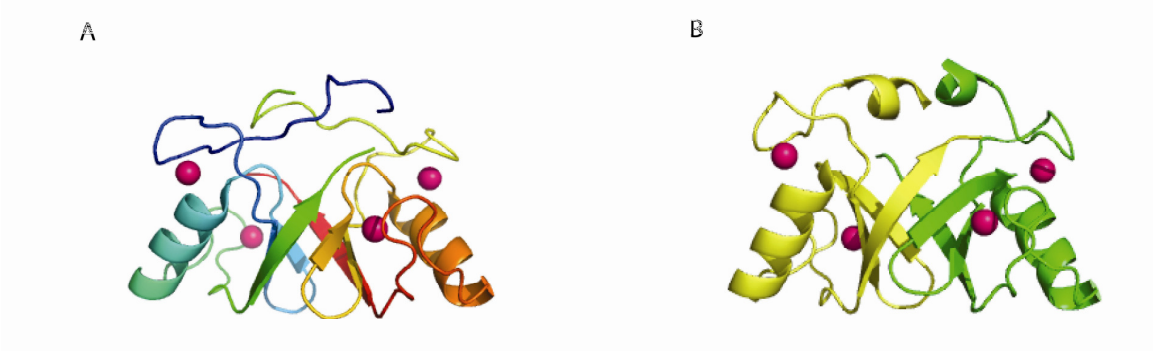

Figure 1.11 – A) RING domain dimer of MDM2 PDB: 2HDP, zinc atoms highlighted in pink B) RING dimer of MDM2 and MDMX RING domains, zinc atoms highlighted in pink PDB: 2VJE

1.3.5 The MDM2 acidic domain

The central domain of MDM2, known as the acidic domain is highly unstructured. However it has been shown to form higher order structures with the unstructured domain of ARF which may be an indication of a folding on binding mechanism, as ARF is a known MDM2 ligand[75]. The structure of full-length MDM2 has not been obtained, and is unlikely to be viable for crystalisation due to the disorder and flexibility of the acidic domain and other regions of the full-length protein. There are two putative beta sheets

located in the acidic domain, however overall this region appears to be highly plastic[76, 77].

1.3.6 Known MDM2 ligands and cofactors

As the structure of MDM2 suggests, it is a complex protein with the capacity to bind multiple ligands which facilitate cross-talk between MDM2 domains. MDM2 binds zinc, both at the zinc finger in the acidic domain and in the RING domain and it has been demonstrated that zinc may enhance some anti-MDM2 therapeutics[78]. RNA is bound by the RING domain[79], and there is also an ATP binding site in the RING domain. These co-factors can mediate the function of MDM2, for example zinc and RNA inhibit the MDM2 interaction with a p53 derived peptide known as BOX-I, and also with the chaperone HSP90[80]. RNA may stimulate ubiqutination by MDM2, and has been shown to potentiate the interaction between MDM2 and the interferon regulatory protein IRF2[81]. MDM2 has been shown to bind p53 mRNA in particular, and mediate the translation of p53 which is another interesting aspect of MDM2 functional regulation of p53[59]. This may link to the MDM2 role in binding ribosomal proteins, and it is interesting to speculate whether MDM2 can bind multiple mRNAs, possibly *via* a consensus sequence, and thus act as both a mediator of translation and protein degradation.

1.3.7 Post-translational modification of MDM2

MDM2 has multiple phosphorylation sites, and is phosphorylated in response to DNA damage, growth factor mediated signaling and also dephosphorylated in some sites after

DNA damage. Serine 17 has been shown to be particularly important in regulation of the N-terminal lid which can regulate availability of the N-terminal domain of MDM2 to ligand binding and is phosphorylated by DNA-PK[82]. Other phosphoylation sites in MDM2 include multiple ATM sites near the RING domain, which when phosphorylated prevents p53 from exporting p53 to the cytoplasm[83]. The degradation of MDM2 has been demonstrated to be controlled by the phosphorylation of sites in the acidic domain by CK1 which mediates SCF βTRCP degradation pathways[84]. As an E3 ligase, MDM2 is also ubiquitinated, and can auto-ubiquitinate as well as neddylating substrates such as p53[85] and the ribosomal protein L11 with the ubiquitin like modifier NEDD8[86]. Sumo specific protease can modulate MDM2 regulation of p53, indicating MDM2 may be sumoylated and this regulates MDM2 function[87].

1.4 MDM2 regulation of p53

1.4.1 p53 and MDM2 feedback loop

p53 and MDM2 are in a feedback loop, which regulates the level of p53 and therefore downstream functions of p53 activity, and *vice versa*. As well as MDM2 catalysing the ubiquitination of p53 which targets it for proteasomal degradation MDM2 also prevents the p53 transactivation domain binding to transcriptional coactivator proteins, halting the transcription of genes which effect the activation of p53 regulated pathways. p53 promotes the transcription of MDM2 as a downstream target, and this linked with the MDM2 mediated degradation of p53 forms a negative feedback loop (Fig. 1.12a)[19]. It is emerging that MDM2-p53

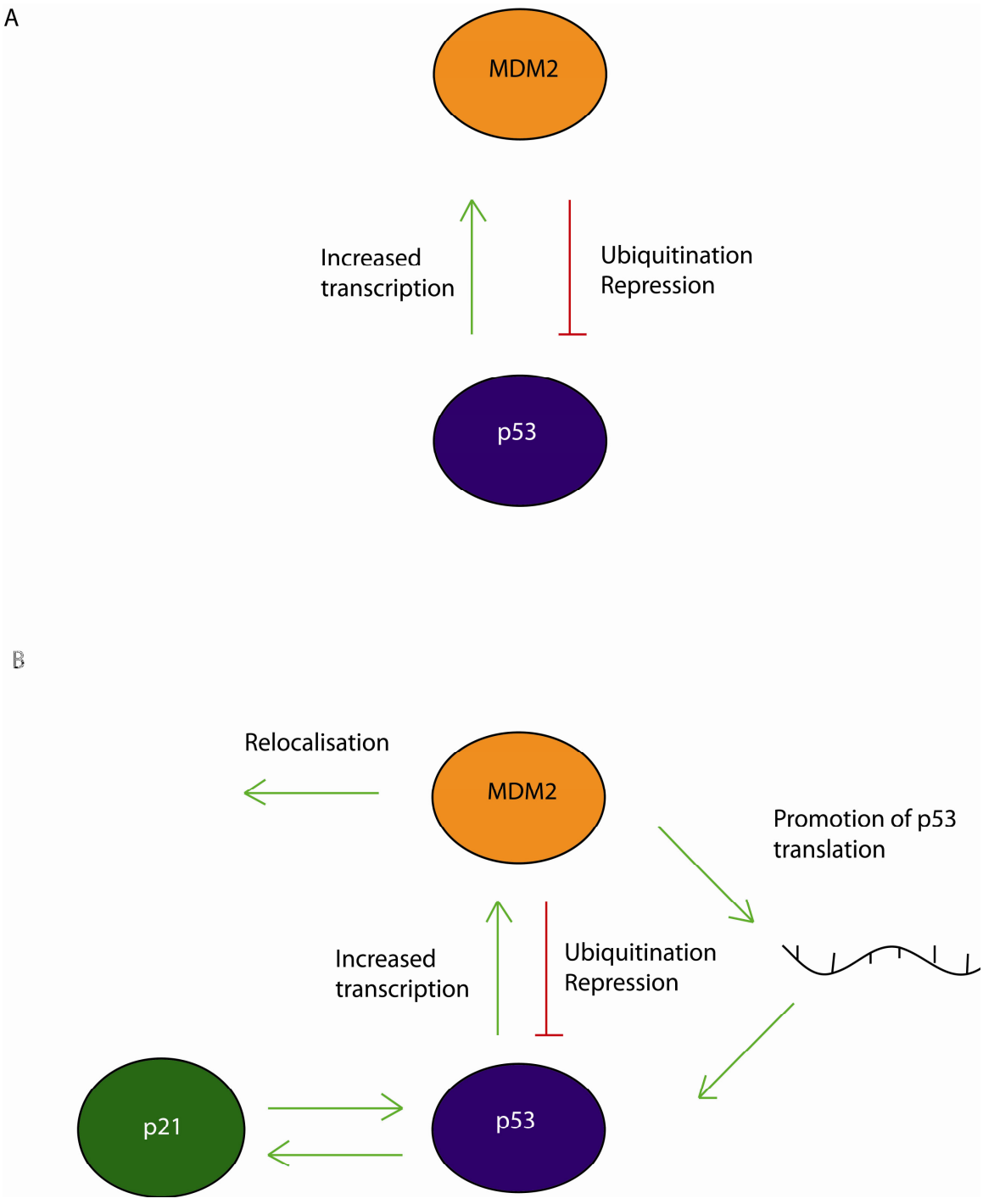

Figure 1.12 – A) Basic MDM2-p53 feedback loop B) Other factors in MDM2-p53 regulation

regulation mechanisms may be more complex than this simple feedback loop (Fig. 1.12b). ARF and ribosomal proteins can cause relocalisation of MDM2 which prevents ubiquitination of p53[79, 88]. It has also been proposed that p21 acts as a positive regulator of p53, due to the cyclical behaviour observed for both p53 and p21 levels in cells which are not stimulated by DNA damage to activate p53[89]. As previously mentioned, MDM2 also regulates the translation of p53 mRNA, linked to MDM2 regulation by ribosomal proteins. MDM2 can stimulate internal ribosomal entry site (IRES) translation of p53 mRNA, which is an alternative method of translation initiation. MDM2 is therefore also a positive regulator of p53 levels, particularly when ER stress mechanisms are activated[90]. There are doubtless many other factors influencing these feedback mechanisms, and the balance between these opposing functions of MDM2 determines the level of p53 in the cell.

1.4.2 Dual site MDM2 ubiqutination mechanism

The mechanism by which MDM2 ubiquitinates p53 has been extensively studied, and has been shown to be mediated by multiple binding interfaces between p53 and MDM2, particularly the conserved BOX-I and BOX-V regions. The current model proposes that the BOX-I region of p53 binds the N-terminal domain of MDM2 with high affinity which allosterically activates the acid domain and stimulates the p53 BOX-V domain to bind MDM2[91] (Fig. 1.13). This BOX-V binding site is sometimes referred to as the 'ubiquitination signal' and subsequent to p53 binding this domain the RING domain

catalyses mono and poly ubiquitination of p53. The allostery between these two domains is highly complex; N-terminal ligands such as p53 can activate binding at the acidic

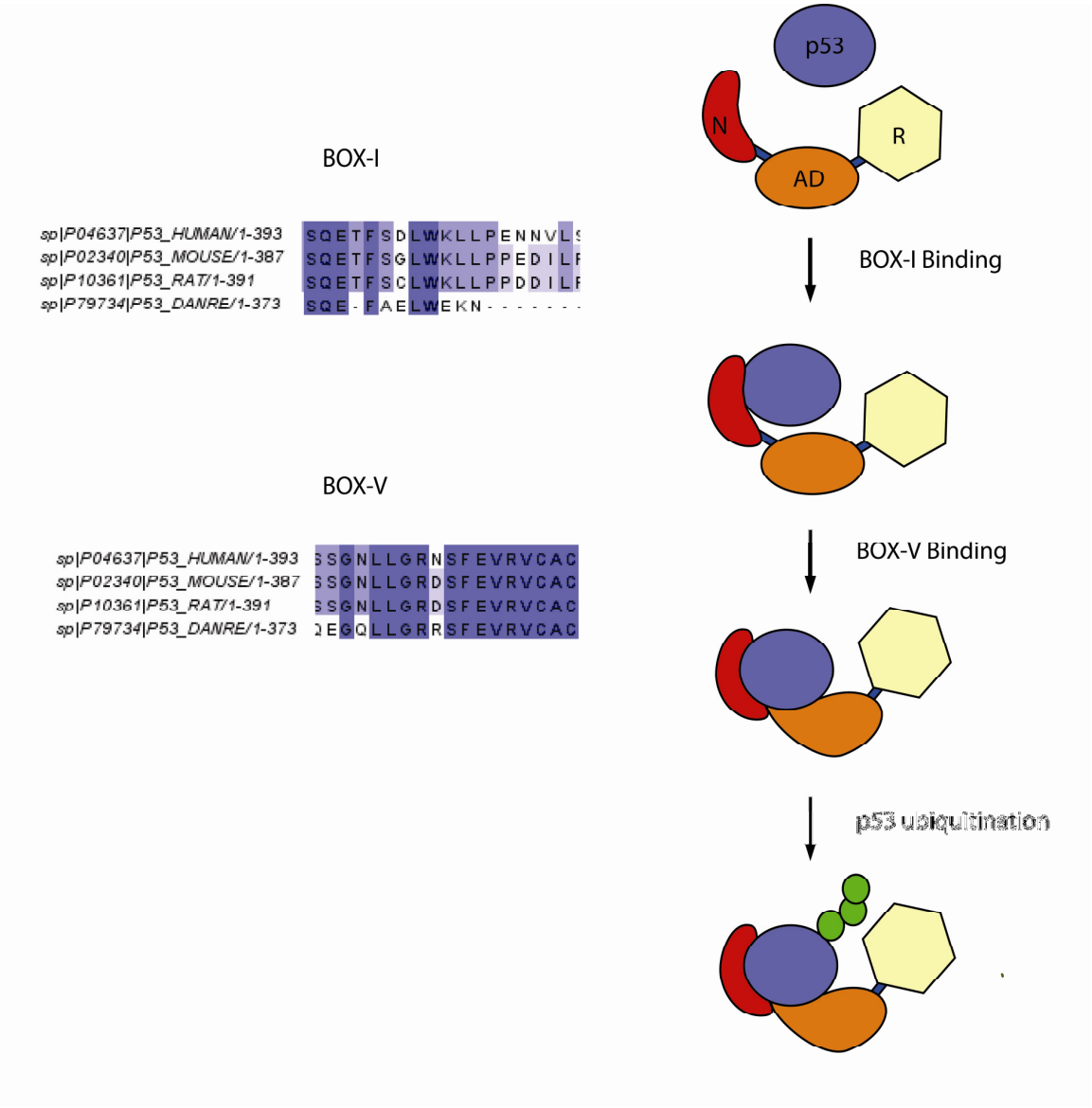

Figure 1.13 – Dual site mechanism of MDM2 ubiquitination of p53[91] *and conserved MDM2 binding motifs BOX-I and BOX-V. N – N-terminal domain, AD – Acidic domain, R – RING domain.*

domain, however inhibitors of binding at the N-terminus such as the drug Nutlin can actually enhance p53 ubiquitination although overall the protein is stabilized[91]. It has also been shown that acid domain ligands strongly inhibit ubiquitination and also weakly inhibit binding at the N-terminus of MDM2, which suggests this allostery can function in both directions[81, 91]. The dual site mechanism is further complicated by the role of the tail for MDM2 dimerisation[66], and the lid domain regulation of the hydrophobic pocket[65]. It is unclear what effect dimerisation or indeed the formation of higher order oligomers would have on MDM2 function. MDM2 runs at a range of molecular weights on an SDS-PAGE gel, which can be a characteristic of disordered proteins, and elutes at multiple peaks by size exclusion chromatography[92]. These data suggest that there are a range of conformations or oligomers possible for full length MDM2, and MDM2 allostery may depend on conversion between these conformers. The RING domain has also been shown to exert an allosteric effect on MDM2 binding p53, with RING mutants affecting the zinc coordination site or exhibiting different binding and ubiquitination of p53 compared to the wild type protein[60, 64]. Cofactors also play a role in the allosteric regulation of MDM2, as described previously, the presence or absence of zinc and RNA regulates the binding of MDM2 to BOX-I peptide and also HSP90 derived peptides[80, 92]. Phage peptide display results show that different consensus sequences are obtained when MDM2 is pre-incubated with different cofactors, highlighting the importance of structural rearrangements of MDM2 in response to binding ligands[80]. It has been demonstrated that both the N-terminal domain of MDM2 and the RING domain are involved in ubiquitinating p53. Perhaps it is the combination of these domains in one allosteric protein which facilitates the multiple mechanisms of p53 regulation by

MDM2, with the acidic domain functioning as a regulatory module and a signal transducer between the various domains.

1.4.3 Proteins regulating the MDM2-p53 feedback loop

Other MDM2 binding proteins can regulate the p53-MDM2 feedback loop. The tumour suppressor RB1 has a binding site in the acidic domain of MDM2, and can prevent p53 binding at this site[91]. ARF also interacts with MDM2 in this domain, and regulates MDM2 activity. Various kinases, such as DNA-PK, interact with MDM2 to post-translationally modify the protein which has also been shown to affect p53 binding[82, 93], and MDM4 has widely been suggested to participate in a regulatory network with MDM2 and p53, although the exact details of this mode of regulation are not yet fully understood. There is a recently discovered phosphorylation site in the BOX-V region of p53, with an unknown kinase which may regulate MDM2 binding and p53 ubiquitination[94]. Ribosomal proteins which bind MDM2 have been shown to have an effect on the regulation of p53 as they occupy the p53 binding sites of the acidic domain of MDM2 and move it into a different subcellular localization and pathway[88].

1.5 The MDM2 interactome

1.5.1 Non-p53 related MDM2 mechanisms

Amongst the functions for MDM2 that have been characterized are as an E3 ligase, a ribosomal regulator, a chaperone and a signaling molecule. MDM2 has been described as a 'partially disordered hub protein' and as it is situated at the intersection of multiple signaling pathways it is an attractive target for anti-cancer therapeutics[95]. Although

MDM2 is important for regulation of p53, it is becoming clear that the non-E3 ligase functions of MDM2 are also important in cancer cells.

1.5.2 MDM2 as an E3 ligase

As well as ubiqutinating p53, MDM2 has been shown to ubiquitinate the ribosomal protein S7[96], IRF2[81] and the endonuclease APE1[97] amongst other targets. It is not known whether the MDM2 ubiquitination mechanism is identical for each of these proteins, the S7 binding site has been mapped to the acidic domain[96], whereas IRF2 appears to have MDM2 binding sites in both the N-terminus and acidic domain[81]. Further research is required to determine whether or not the MDM2 ubiquitination mechanism must always have multiple domain contacts, as is the case with p53. Proteomics methods have previously been used to attempt to determine the substrates of E3 ligases[98], however in practice this is a difficult problem due to the abundance of ubiquitinated proteins in a cell and the potential for substrates to be ubiquitinated by multiple E3 ligases. In the case of MDM2, many binding proteins have been shown to be ubiquitinated, however as the RING ubiquitinates in the absence of the other regulatory domains of MDM2 these results should be treated with caution.

1.5.3 MDM2 and ribosomal proteins

MDM2 has been extensively shown to interact with multiple ribosomal proteins, including RPL11, RPS7, RPL5, RPL26, RPL5 and RPL23[88]. These ribosomal proteins are part of the regulatory pathway of MDM2, and can mediate MDM2 localisation and function with regards to p53 regulation. The regulation of MDM2 by RPL11 is mediated

by MDM2 neddylation of RPL11 which results in it localizing to the nucleolus. In nucleolar stress situations RPL11 is relocated to the nucleoplasm and it is proposed that binding of MDM2 by RPL11 here overrides MDM2 binding to p53 and this inhibits the downregulation of p53 by MDM2[86, 99]. S7 is another interesting ribosomal MDM2 ligand, it has also been proposed to prevent MDM2 binding to p53[100] and has been mapped to a binding interface in the MDM2 acid domain. S7 has also been shown to be ubiquitinated by MDM2 and this is linked to increased degradation of ribosomal protein S7[96]. The ribosomal mediation of MDM2 activity may be ARF independent, although ARF relocalises MDM2 to the nucleolus[101]. RPL26 has been shown to be polyubquitinated by MDM2 and RPL26 may promote the translation of p53, which is negatively regulated by MDM2[102]. MDM2 also binds nucleophosmin, which can shuttle it to and from the nucleolus, indicating the nucleolar localization of MDM2 is an important factor in the regulation of p53 and other MDM2 functions[103]. Overall, misregulation of the level of ribosomal proteins or rRNA synthesis can activate p53 *via* an MDM2 dependent pathway[104]. The balance of proteins present in the ribosome is an important mechanism for maintaining proteostasis, and further understanding of the role of in the regulation of these proteins will clarify what role this has in cancer cells and healthy cells.

1.5.4 MDM2 stabilisation of E2F1

In contrast to the regulation of p53 by MDM2, the transcription factor E2F1 is stabilized by MDM2 and inhibition of MDM2 binding to E2F1 with the drug Nutlin results in the

degradation of E2F1[105]. This protection of E2F1 from degradation by MDM2 is due to the fact that MDM2 sequesters E2F1 to protect it from other ubiquitin ligases. As E2F1 binds the N-terminus of MDM2, disrupting this domain with Nutlin results in the release and subsequent degradation of E2F1[105, 106]. The kinase CK1α, which increases in response to cellular stresses linked with cancer such as X-ray irradiation and virus infection also participates in stabilization of E2F1 in a complex with MDM2[107]. MDM2 mediated regulation of the stabilization of E2F1 illustrates the ability of MDM2 to function as a stabilizing binding partner, unlike as destabilizing binder mediating p53 ubiquitination.

1.5.5 MDM4 influence on MDM2

MDM4, also known as MDMX, has a high degree of homology to MDM2 and has been shown to form a RING domain dimer with MDM2 (Fig. 1.11b)[73]. MDM4 can bind p53, although it has not been shown to have E3 ligase activity. MDM4 has an overall similarity to the domain structure of MDM2, although structural studies have shown extensive differences in the p53 N-terminal binding domain[108]. Studies show that MDM4 can inhibit the transactivation of p53, facilitate the MDM2 ubiquitination of p53, and affect the localization of the p53-MDM2 complex. Although links have been found between MDM4 and MDM2 with regards to p53 regulation, there are also instances where these proteins are independently amplified in cancer, indicating they have independent roles[109]. MDM4 is undoubtedly part of the MDM2 interactome, however it is unclear how many of MDM2 functions are dependent upon MDM4 activity.

1.6 Linear motifs, disorder and the MDM2 interactome

1.6.1 Linear motifs as mediators of protein-protein interactions

Linear motifs are sequence features which mediate protein-protein interactions, usually located in disordered regions of proteins[110, 111]. It has been thought of as particularly difficult to target protein-protein interactions due to larger surface areas involved in the interaction compared with a substrate binding pocket. In fact, many protein interactions are mediated by these short peptide motifs and have critical residues which make contact with a binding partner which can be represented as a consensus motif. As it is widely

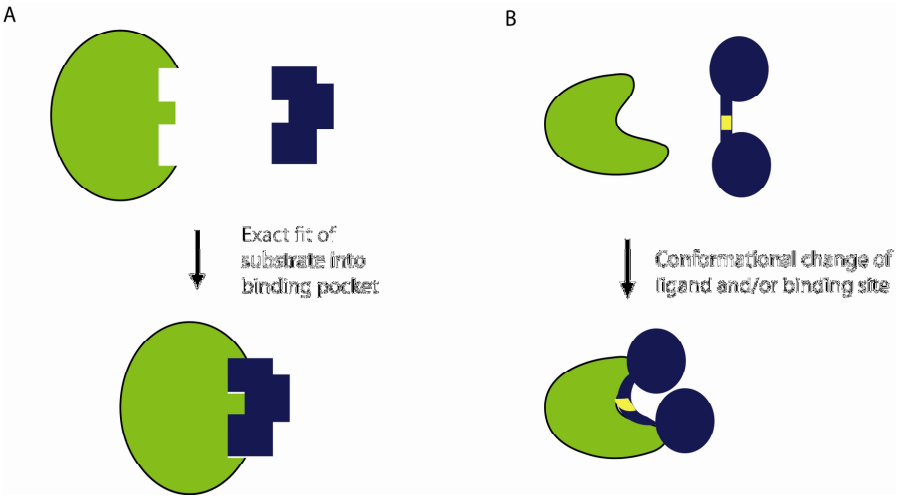

Figure 1.14 – A) Lock and key mechanism of enzyme substrate interaction. B) Schematic of linear motif interaction, yellow - motif

thought for many enzyme substrate reactions, this is not based on the classic 'lock and key' mechanism proposed by Emil Fischer[112, 113], but an induced fit or 'folding on binding' mechanism (Fig. 1.14)[114]. Examples of these peptide motifs can occur in loops between structural features like alpha helices and beta strands, which are hotspots for

protein-protein interactions. The word 'linear' is slightly misleading, as these motifs are flexible and adopt structure on binding[115]. A linear motif may correspond to a consensus sequence based on residues which are necessary for binding to a target protein, examples of this are: the HSP90 binding motif, 14-3-3 protein binding motif, kinase binding motifs which can be as simple as two amino acids, and numerous targeting or signal sequences such as KDEL in endoplasmic reticulum targeting[110]. A linear motif is a short amino acid sequence, which can act as the binding site for another protein similarly to a ligand. Linear motifs can also adapt to bind different target proteins, their plasticity means they can adapt to fit a given target. The C-terminal region of p53 is a good example of this kind of plasticity (Fig. 1.5). Linear motifs are frequently associated with disordered regions of proteins, and programs for locating linear motifs such as DILIMOT[110] and SLiMFinder[116] incorporate this into the criteria for identifying a linear motif. An interesting example of protein-protein interaction mediation by linear motifs and how they can mediate to the mechanism of disordered proteins is the highly disordered yeast E3 ligase San1. San1 binds disordered substrates in a 'quality control' mechanism, to degrade misfolded proteins which are also chaperoned by San1. This involves the recognition of linear motifs by the disordered region of San1 coming into contact with these motifs which induces folding on binding[117]. Linear motifs are also interesting for the paradigm of allosteric proteins, due to a concept known as 'fuzziness', which describes the phenomenon where a bound ligand can continue to move or alter the conformation of a binding partner[118]. A known linear motif is attractive as a starting point to develop protein-protein interaction inhibitors which mimic these motifs, peptidomimetics and drugs which match the pharmacophore of interaction peptides can

be developed based on a known peptide. The drug Nutlin, discussed in section 1.6.6 is an example of how this can be put into practice.

1.6.2 Discovery of linear motifs and protein-protein interaction inhibitors

It is possible to target protein-protein interactions (PPI), although this is not yet as amenable to chemical and computation screening as substrate binding pockets. Phage peptide display is a developing method by which is it possible to find high affinity peptide ligands. Proteins, and peptides obtained by phage display can both be used to search databases for proteins which contain similar sequences, and as the starting point for developing peptidomimetic drugs[119, 120]. Other methods of finding protein-protein interaction motifs are to search for similarity in known binding partners of a protein, or search yeast two hybrid assay results. If there is a known peptide binder of the protein of interest, it is also possible to map the residues required for a binding interface using peptide arrays. Miniaturised SPOT based arrays can be employed to substitute every residue to every other residue and find optimized and high affinity binding peptides for purified proteins[121]. Protein-protein interactions are a relatively new target for drug development, peptides themselves are not yet considered optimal for use as drugs due to poor cell permeability and may be quickly degraded in the cell. This can be improved by adding cell penetrating sequences, such as penetratin, or creating versions of the peptide with peptoids, hydrocarbon stapling of the peptide backbone or retro-inverso peptides with D-amino acids in reverse sequence which are not targeted for proteolysis. Chemical optimization can improve upon the basis of a known structure to create peptidomimetics

which are drug-like and inhibit protein-protein interactions[122]. Although this is a difficult route for drug discovery the number of proteins targeted for drug development has leveled off in recent years, and the number of proteins which are extensively studied only includes a small percentage of the proteome. Disordered proteins, which have a propensity to interact *via* linear peptide motifs could be targeted by protein-protein interaction inhibitors. They make up approximately 50% of the proteome[95], and represent a neglected category of proteins for research into drug discovery. This is perhaps due to the reliance of current methods on crystal and NMR structures, and the success of drug design using these methods.

1.6.3 Discovery of a potential linear motif representing peptide by phage display

Phage peptide display is a method of acquiring high affinity peptide ligands to a protein target, these peptides can then be used as tools or to investigate consensus binding sequences for a protein. Antibody epitope mapping is one example of how phage display can find consensus sequences, and this was carried out previously for p53[123]. A study to expand the interactome of a protein and develop peptide ligands for a protein using phage display was carried out on the protein AGR2[124].

The protein AGR2 was discovered as an overexpressed protein in Barrett's oesophagus, which is a metaplastic tissue associated with progression to oesophageal cancer. AGR2 has been implicated in the negative regulation of p53, and as a biomarker for various types of cancer[125-127]. Peptide phage display and sequence optimization revealed the

AGR2 binding peptide PTTIYY, which was subsequently shown to bind AGR2 and affect the subcellular localization of both AGR2 and p53, and possibly re-activate the p53 pathway[124, 128]. Although AGR2 has few known binding partners, this peptide represents a potential AGR2 binding motif and is a starting point to search for proteins containing this sequence which may then be validated as AGR2 binding partners. This illustrates the potential of linear motifs as a starting point to find new protein-protein interactions, which is the reverse of using protein-protein interaction interfaces to design drugs based on linear motifs. Phage peptides may also represent a starting point for the design of drugs, so it is possible to find new therapeutic leads both from optimized peptide ligands, and from mimickry of naturally occurring linear motif interfaces.

1.6.4 Representative MDM2 binding motifs in p53, BOX-I and BOX-V

The dual site mechanism of MDM2 binding to p53 is mediated by BOX-I and BOX-V regions of p53, in particular two linear motifs which are bound by the N-terminal domain and acidic domain respectively[91]. The BOX-I motif binds the MDM2 N-terminus at the hydrophobic pocket region (Fig 1.15a). It has been shown that mutation of the BOX-I motif at three critical residues (Fig. 1.15a, b) abrogates MDM2 binding to p53. These residues intercalate into the MDM2 hydrophobic pocket creating a strong binding interface, electrostatic attraction of the residues surrounding this hydrophobic core also contribute to the BOX-I-MDM2 interaction[39, 129]. Other residues such as the positively charged glutamine residues to the C-terminus of the core of this sequence also

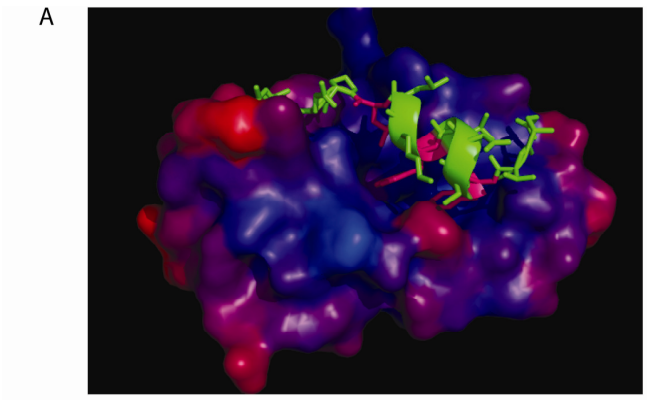

Figure 1.15 A) N-terminal domain of MDM2 in complex (coloured according to b-factor) with BOX-I peptide (green), key binding residues highlighted in pink PDB:1YCR B) BOX-I sequence, MDM2 binding residues highlighted in red C) Full p53 sequence with BOX-I highlighted in orange and BOX-V highlighted in green D) BOX-V (yellow) position in core domain of p53 PDB: 1UOL

contribute positively to the BOX-I-MDM2 interaction. The BOX-V motif, located in the DNA binding domain of p53 (Fig. 1.15c) in a region known to contain a mutation hotspot, binds the acidic domain with a lower affinity than the N-terminal interface, and this region of MDM2 also binds peptide motifs derived from the RB1 tumour suppressor and is a docking site for multiple ribosomal proteins and the ARF tumour suppressor[77, 88, 91]. It is interesting to note that the BOX-V domain is slightly buried on the p53 structure, which may account for the lower affinity of this motif for MDM2 and require structural rearrangement to bind MDM2 (Fig. 1.15d). Phage display against MDM2 yielded consensus binding peptide sequences corresponding to these p53 motifs[80, 92]. This suggests that these motifs are dominant MDM2 binding sequences. Other motifs were also discovered which do not correspond to sequences in p53 but do have similarity to the protein SAFA, subsequently shown to bind MDM2. The chaperone HSP90 also contains sequence similarity to peptides which bind MDM2 obtained by phage display[80], and has also similarly been validated as an MDM2 binding protein. The motifs discovered by phage display were varied based on the presence of different MDM2 cofactors, indicating structural changes in MDM2 mediate which motifs the protein can bind to.

1.6.5 Peptide ligands of MDM2 obtained by p53 optimisation

The BOX-I motif was optimised to develop high affinity ligands for MDM2, some of which have the ability to also bind the less well defined hydrophobic pocket of MDM4[130]. This is interesting because it has been suggested that the dual inhibition of

MDM2 and MDM4 would result in a greater effect than inhibiting MDM2 alone. The PMI peptide was the result of optimization of the BOX-I motif, and differs in sequence to BOX-I (Fig. 1.16a), although the residues necessary to contact the hydrophobic pocket are conserved[130]. The K_d for PMI binding to the N-terminus of MDM2 is 3.2 nM compared with the BOX-I peptide (440 nM). Systematic mutation of the BOX-I and

A

	1	2	3	4	5	6	7	8	9	10	11	12
BOX-I	E	T	F	S	D	L	W	K	L	L	P	E
PMI	T	S	F	A	E	Y	W	N	L	L	S	P

B

BOX-I	E	T	F	S	D	L	W	K	L	L	P	E
		+	+++			+	+++			++	-	
PMI	**T**	**S**	**F**	**A**	**E**	**Y**	**W**	**N**	**L**	**L**	**S**	**P**
	+	++	+++		+	+	+++	-		+		

Figure 1.16 A) BOX-I and PMI peptides, important binding residues highlighted in red B) Residues in each peptide and contribution to MDM2 interaction (positive: +, neutral or deleterious: -)

PMI peptides reveals which residues are neutral, contribute to binding or are deleterious in each peptide (Fig. 1.16b)[131]. This study is instructive for understanding linear motifs, because it reveals that the consensus sequence found in a linear motif which gives rise to high affinity interactions is important, but there is also considerable room for non-essential residues to vary without affecting binding activity. It is interesting to note that the proline residue in BOX-I and the glutamine residue in PMI contribute negatively to BOX-I affinity, these residues might be important for docking, resulting in a higher

dissociation constant. The concept that variable sequences are tolerated in linear motifs is illustrated by numerous 'non-canonical' motifs found in proteins which are still bound by a protein which recognizes a consensus. The peptides investigated in these studies have high affinity for MDM2, however lower affinity binding peptides may also be biologically relevant as transient interactions in the cellular environment can be significant. The BOX-V and RB1 interactions with MDM2 for example are weak compared to BOX-I, however this interface actually forms the ubiquitination signal for p53 and both of these peptides can affect, albeit mildly, binding at the N-terminal domain of MDM2[91]. Transient motif binding is likely to be highly dependent on other proteins participating in a complex and the environment of the protein interaction, which are predicted to increase by orders of magnitude the affinities and activities observed *in vitro* due to proximity of ligand and binding partner. It has been shown by ion mobility mass spectrometry that small heat shock protein has up to 300 oligomerisation states and conformers[132]. Due to the observed allostery of MDM2 and internal disorder it is possible that it is also converting between conformers in order to bind different peptide ligands.

1.6.6 Nutlin as an MDM2-p53 protein-protein interaction inhibitor

MDM2 has many of the characteristics of a promising target for cancer therapeutics. It is at the hub of multiple signaling pathways, is the binding partner of the important tumour suppressor p53, is aberrantly regulated in many cancers and has a drug binding pocket in the form of the hydrophobic cleft. A small molecule screen for MDM2 inhibitors

identified cis-imidazolines know as ‘Nutlins’ named for ‘Nutley inhibitor’ as a high affinity MDM2 binding molecule[133]. The Nutlins are cis-imidazolines which are synthesized as two enantiomers, one of which is 150 times more effective than the other. Nutlin-1, 2 and 3 (Fig. 1.17a) are all effective MDM2 binders, with Nutlin-3 having the highest affinity for MDM2 at 90 nM. The mode of action of Nutlin is that

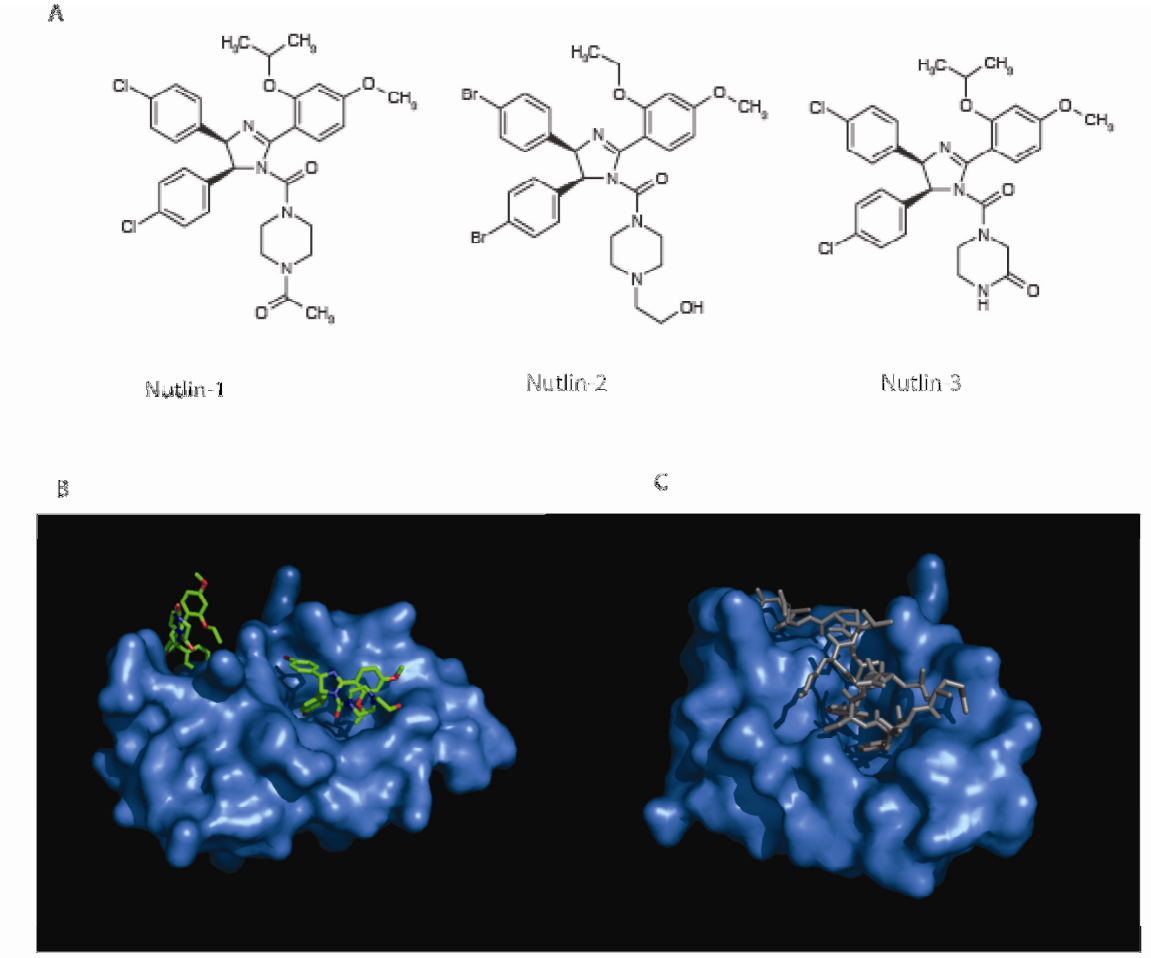

Figure 1.17 A) Chemical structure of Nutlin-1, 2 and 3 B) Structure of Nutlin-2 bound to MDM2 N-terminus PDB: 1RV1 C) Structure of BOX-I (grey) bound to MDM2 PDB: 1YCR

it binds the MDM2 hydrophobic pocket in the same region as the BOX-I peptide from p53, mimicking the residues which intercalate into the hydrophobic pocket (Fig. 1.17b,c). The p53 residues which are mimicked are F19, W23 and L26 which have been shown to contribute to the high affinity of BOX-I for MDM2. Interestingly, the original x-ray structure of MDM2 with Nutlin shows more than one molecule of Nutlin bound to the N-terminus, although it is clear that the Nutlin in the hydrophobic pocket is a molecular mimic of the corresponding BOX-I residues which have previously been shown to be vital for BOX-I MDM2 binding. The affinity of Nutlin-3, is 90 nM compared to the BOX-I Kd of 440 nM and it effectively competes both BOX-I and full-length p53 tetramer from the N-terminal domain of MDM2[65, 91]. It has also been shown that Nutlin can bind the hydrophobic pocket of Bcl-xl, which has some similarity to the MDM2 pocket, and is a protein involved in apoptosis[134]. Nutlin does not have a high affinity for MDM4, which is appealing as a specific inhibitor of MDM2, although some studies suggest dual inhibition of MDM2 and MDM4 is desirable[108, 135].

1.6.7 Computational studies of MDM2 N-terminal binding

There are different components to the MDM2-BOX-I interaction, the core hydrophobic packing contributes to a decrease in the entropy of the BOX-I peptide, and around the hydrophobic pocket electrostatic interactions with residues around the hydrophobic core also stabilise the peptide binding to MDM2[108]. Nutlin takes advantage of disrupting the entropic component of this interaction, which for the BOX-I peptide is the dominant force maintaining contact between the linear motif and MDM2. Each residue in the BOX-I motif contributes to the interaction to a slightly different extent, shown by

molecular dynamics modeling of the residues involved[108] as well as substitution analysis *in vitro* which optimized the BOX-I peptide to the PMI inhibitor[131]. These computational studies reveal that other residues than those which intercalate BOX-I or Nutlin also mediate peptide binding by forming interactions around the hydrophobic cleft. The Tyr100 residue has been referred to as a 'gatekeeper' of the pocket, and can flip between 'open' and 'closed' positions to ostensibly block the hydrophobic pocket[136]. Charged residues, particularly glutamate 25 also potentiate BOX-I binding by attracting the positively charged C-terminus of the peptide before it packs into the hydrophobic pocket[108]. It is not inconceivable that these electrostatic interactions are required to dock this peptide before it 'snugly' binds into the hydrophobic pocket. Given that at this position in MDM4 this residue is represented by a glutamine, this would result in the loss of the electrostatic effect and would account partially for the lower affinity of MDM4 for BOX-I. As previously described, p53 regulation by MDM2 depends on an allosteric mechanism in MDM2[91]. This allostery is regulated by the transduction of signals binding at the N-terminal domain to the disordered acidic domain. N-terminal MDM2 regulation is actually even more complicated, with recent studies showing that phosphorylation of the lid domain at serine 17 in the lid of the N-terminus of the protein can mediate 'opening' and 'closing' of the hydrophobic pocket[65, 137]. This has been shown by Worrall *et al*. although NMR studies suggested the lid did not bind at the N-terminus[137, 138]. Molecular dynamics based computational studies have indicated that there are minor differences in the structure of the phosphorylated residue and the phospho-mimic, which lead to slightly different conformations of the lid over the hydrophobic pocket, and it is possible for the lid to occlude peptide but allow the

binding of Nutlin into the pocket[139]. This indicates that although Nutlin is an effective inhibitor of the BOX-I MDM2 interaction, it may be possible for other MDM2 N-terminal interactions to be affected differently by Nutlin due to slight differences in the binding site.

1.6.8 Therapeutic significance of Nutlin

As a potent inhibitor of the interaction between the N-terminal interface of p53 and MDM2, Nutlin has been investigated as a drug with therapeutic potential. There have been studies showing nutlin may be effective in retinoblastoma[140] and melanoma in cells with wild type p53. However there are some drawbacks to using Nutlin as a drug. Some studies show Nutlin has a wide range of affects in non-cancerous cells, and the MDM2-p53 axis although aberrant in cancer cells cannot be totally abolished as this would cause widespread cell death. Nutlin has been shown to be effective in combination with the proteasome inhibitor bortemozib[141] which is promising for the use of nutlin as part of combination treatments which target multiple aspects of cancer cells in one course of treatment. Although there are conflicting results about how effective Nutlin would be in the clinic, it remains a useful tool for investigating MDM2 and p53 pathways. It is also the case that Nutlin may be a scaffold for the development of more advanced therapeutics targeting MDM2.

1.7 Proteomics methods

1.7.1 Overview of proteomics methods

Although the human genome project catalogued the complement of genes present in the human genome, this base of knowledge is perhaps immeasurably complicated when translated to the protein level. The term proteomics was coined by Marc Wilkins at Macquarie University in 1994, to mean the protein complement of the genome[142]. Although many proteomics efforts are in progress, it is not yet possible to identify every protein in the human proteome. This is partly because of the increased complexity of the proteome compared to the genome, and partly because there is no one technology which can 'read' the proteome of a cell, such as DNA sequencing can 'read' the genome. The major differences between the proteome and genome are that the former is dynamic and constantly changing and adapting to stimulus over short timescales whereas the genetic code is stable to preserve information between generations and stable mutations arise over a longer period of time. When the proteome of a cell is discussed, this is different for every cell type, organism and environment of the cell, as it is primarily on the protein level that cells respond to stresses[143]. Post-translational modifications such as glycosylation, phosphorylation and proteolytic cleavage alter proteins on a proteomic level. Although these modifications are not directly coded for in the genome sequence they could be regulated epigenetically, by the silencing and activation of different genes or miRNAs due to DNA and histone modifications[144, 145]. Splicing events can alter mRNA prior to translation, sometimes resulting in multiple protein products from the same gene which further increases the complexity of the proteome[146]. Efforts to improve

knowledge of the proteome have focused on improving proteomic methods to absolutely validate the amount of protein in a cell, or relatively quantify protein levels in different states of the same cell type. This involves both improving technology used to measure the level of multiple proteins in a cell, and also optimizing the way proteomic data is analysed and validated. The aims of proteomic experiments can include finding out more about the interactome of a known protein, detection of new biomarkers for cancer and other diseases and to compare to microarray data for investigating whether genes are regulated on the transcriptional or translational level. Mass spectrometry (MS) is undoubtedly the key method which makes it possible to carry out large scale proteomics, due to the capability to sequence peptides without using chemical methods[147].

1.7.2 Quantitative proteomic methods – gel based

Some of the earliest methods used for quantitative proteomics were based on 2D gel electrophoresis, and detection of differences between the intensity of spots representing proteins on a 2D gel. This was developed further into difference gel electrophoresis (DIGE) which runs two samples on the same gel labeled with two different fluorescent dyes to simultaneously compare the expression of two proteins and eliminate errors introduced due to reproducibility of electrophoresis[148]. Gel based methods can suffer from inadequate separation, as many proteins cluster at similar isoelectric points or molecular weights and a single spot can represent multiple proteins. The benefit of this method however, is that it is quick and simple to carry out without the need for specialist equipment.

1.7.3 Shotgun proteomics

A commonly used non-gel based method for proteomic analysis of many proteins from a cell lysate is shotgun proteomics[149]. This technique involves the enzymatic digestion of a cell lysate proteolytically to yield peptide fragments from the cellular proteins, typically by trypsin. This is followed by sequencing detectable peptides by tandem mass spectrometry, also referred to as MS/MS, to identify which proteins are present in a mixture based on the presence of unique peptides (Fig. 1.18a,b)[150]. Tryptic peptides are detected in a primary MS scan, and selected peptides are subsequently sequenced by MS/MS[147, 151]. The primary peptide is referred to as the precursor or parent ion and the fragmented peptide known as product or daughter ions. The precursor ions are usually fragmented by collision induced dissociation (CID), and product ions are detected after separation by a second MS scan[147]. The difference in mass/charge (m/z) of the product ions can be used to determine the sequence of the peptide. If sufficient fragments are generated and detected in the MS/MS scan it is possible to calculate the mass of each individual amino acid present in the peptide from the difference in m/z between peaks, i.e. a loss representing 75.07 Da would represent loss of a glycine residue. There are different species of fragmented peptide ions which can be formed, which can depend on the fragmentation method and mass spectrometer. The reliability of the sequenced peptide is increased if there is good coverage over an ion series, for example the b and y series (Fig 1.18c). The sequences of the fragment ions can be used to determine the peptide sequence if enough fragment ions are obtained to calculate the loss of single amino acids. Files containing MS data which lists all of the peptides detected and sequenced in the sample can then be used as search queries for theoretical digest

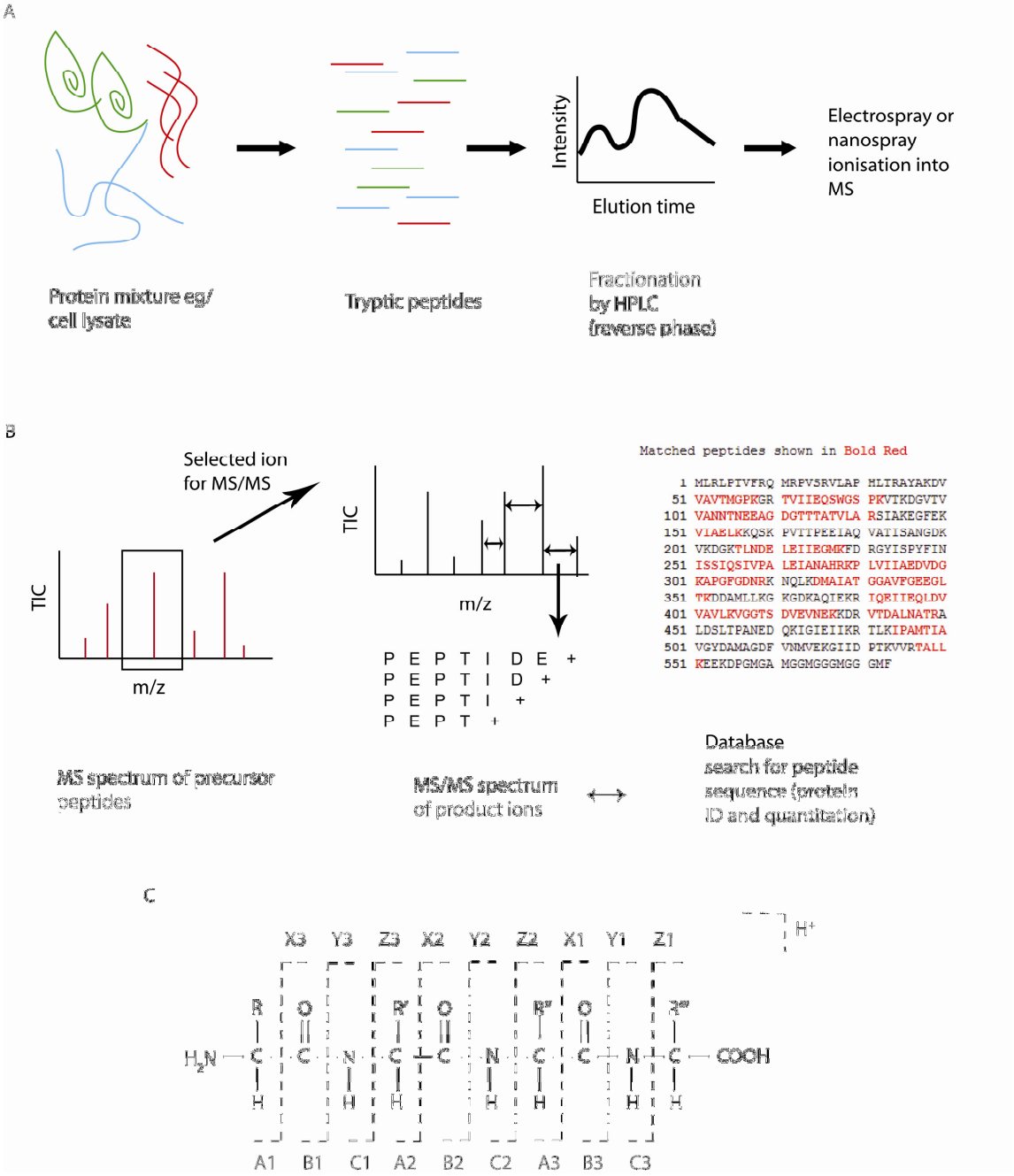

Figure 1.18 Overview of MS based shotgun proteomics A) Sample digestion and pre-fractionation B) MS based stages in protein identification C) Fragmentation at the peptide bond yielding different ion series[147]

databases such as MASCOT (Matrix Science), which return a list of the proteins present in a sample[151, 152]. This method is fairly straightforward for identification of single proteins, or relatively abundant proteins which have been pre-separated for example by electrophoresis, however for complex samples such as whole cell lysates there are several obstacles. Some drawbacks with this method are that it relies on a wide dynamic range of the mass spectrometer to detect low abundance as well as high abundance peptides, and because the tryptic digests are complex also requires high resolution[153]. Shotgun MS is closely related to the power of liquid chromatography methods to initially separate peptide mixtures, and reproducibility in LC increases the confidence in proteomics results due to the ability to obtain reliable replicates. It is also possible to use other fractionation methods prior to shotgun MS to obtain a number of fractions with reduced complexity to aid detection of lower abundance peptides. These fractionation methods include subcellular fractionation, strong cation exchange or other chromatography methods and gas phase fractionation[154]. UltraHPLC and nanospray can also increase the power of shotgun MS due to the constant flow rate they create into the mass spectrometer[155]. Using high resolution mass spectrometers, such as those which contain Orbitraps (Thermo) and linear ion traps allows the complexity of a high number of precursor peptides to be resolved and this increases the number of proteins detectable in one mass spectrometry experiment. New methods have been developed to avoid some of the data analysis problems associated with shotgun proteomics. One of these methods is data-independent acquisition, such as the precursor acquisition independent from ion count (PAcIFIC) method[156]. Typically the ions selected for fragmentation are chosen because they are more intense than the other ions in a data-dependent method of mass

spectrometry, and product ions are assigned to mass of the precursor ion to determine the peptide sequence. Alternatively, data-independent acquisition fragments every peptide in a small mass/charge window, and assigns them to a m/z in the centre of the window (Fig. 1.19). The m/z window is small so the difference in the precursor peptide

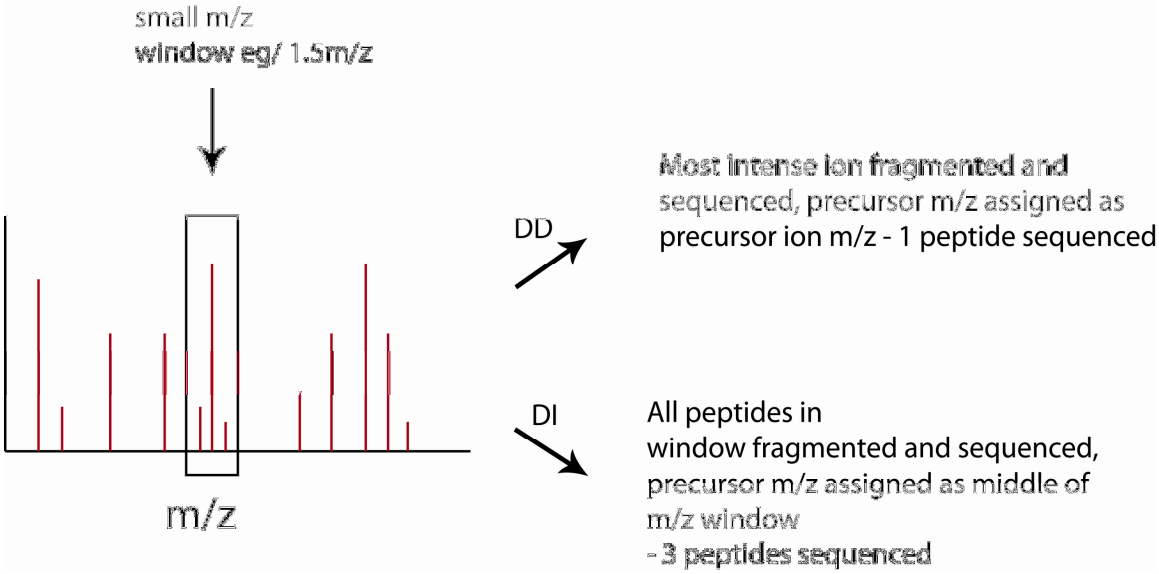

Figure 1.19 A) Data-dependent selection of ions for sequencing vs. PAcIFIC data-independent acquisition. DD – data dependent, DI – data independent

mass of peptides within the window is not significant. This results in a larger number of peptides being sequenced and a larger coverage of the proteome. Data-dependent acquisition can miss detection of lower abundance peptides which may nonetheless represent interesting proteins, p53 for example is an low abundance protein.

1.7.4 Proteomic quantitation methods

Many of the problems in proteomic experiments arise from quantitation of the detected proteins. For proteomics experiments to be reliable they should ideally be carried out

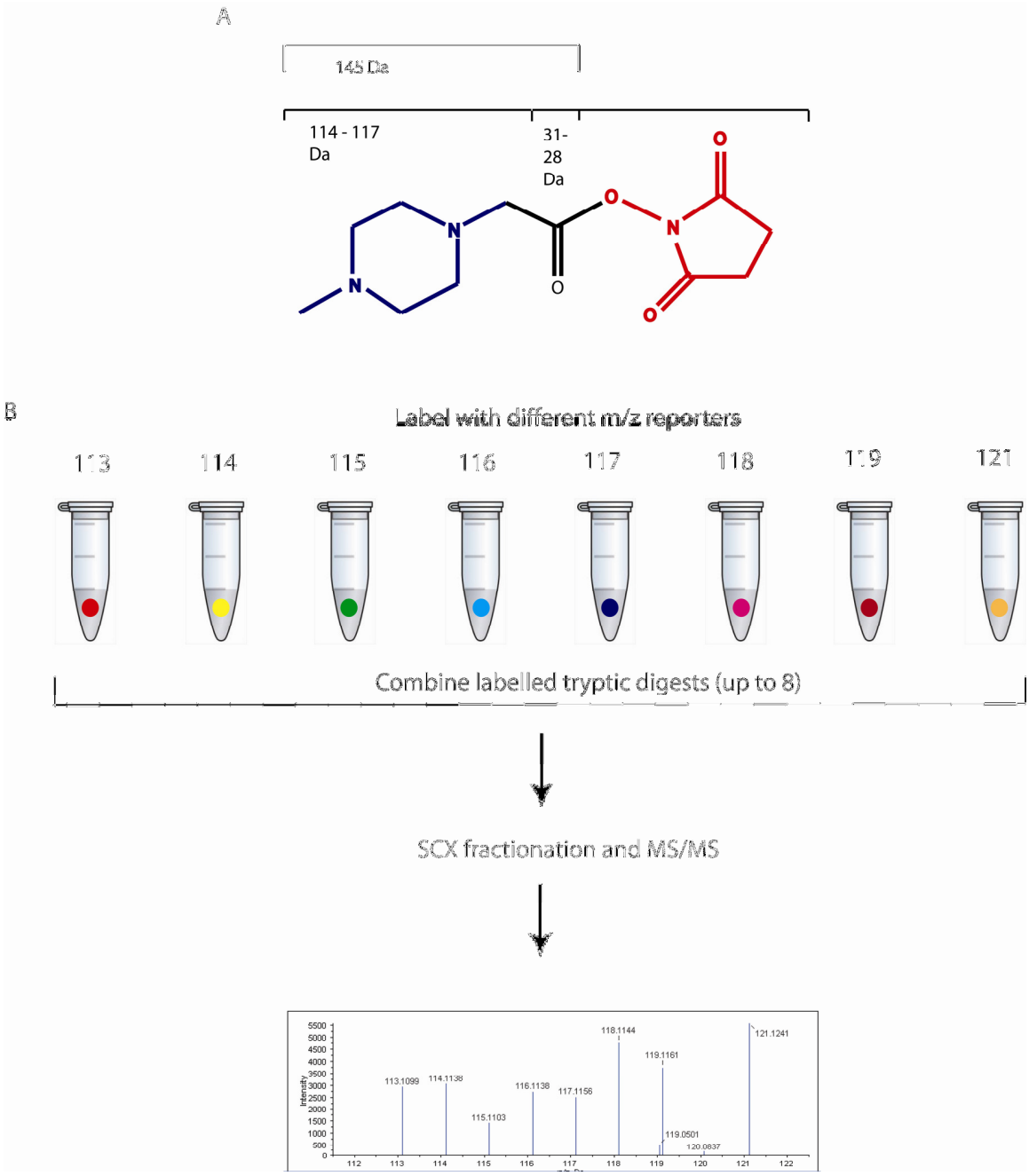

Figure 1.20 A) iTRAQ labels (Applied Bioscience) Reporter ion – blue, balance group – black, peptide reactive group - red B) iTRAQ workflow

with at least three biological and technical replicates. The aim of this is to minimize the impact of sample variation, LC conditions and variation in detection of peptides between

LC runs, as a single run may contain false negatives or positives. There are several well investigated methods of proteomic quantitation. As mentioned in the previous section, in 2D electrophoresis and DIGE quantify protein levels by measuring the intensity of a spot in a gel or a fluorescently labeled protein can be compared using specialized software, such as Progenesis (Nonlinear Dynamics).

In LC based shotgun proteomics, there are a wider variety of quantitation methods available. Techniques which chemically label the tryptic peptides have been shown to be effective, particularly isobaric tags for relative and absolute quantification (iTRAQ) which labels up to 8 samples with isobaric tags which are released when a peptide is fragmented in the MS, the piperazine region of the tags have different combinations of heavy and light carbon isotopes resulting in a range of masses[157] (Fig. 1.20a). The tags are initially isobaric to avoid any differences in peptide ionization or retention time for different iTRAQ labels. The ratio between these tags can then be used as a quantitation measure to detect the difference between the levels of proteins in different samples (Fig. 1.20b). Care has to be taken however to use several unique peptides for iTRAQ quantitation, as variation between the ionization efficiencies of peptides can result in anomalous results, as can difference between the labeling reaction in two samples which may not have occurred to an identical extent in all samples[158]. iTRAQ can also suffer from the 'compression effect', which is the quenching of iTRAQ ratios in complex samples due to detection of a less intense change in ratio between protein levels than is detected by other methods[159]. Another labeling method is stable isotope labeling of cells in culture (SILAC)[160], which involves cells in culture being grown in a heavy medium to

incorporate amino acids containing isoforms of amino acids with heavy elements into one sample to compare to a sample which has not been grown in heavy media[160] (Fig. 1.21). This method results in mass differences between otherwise identical precursor peptides which can be detected and used as a measure of

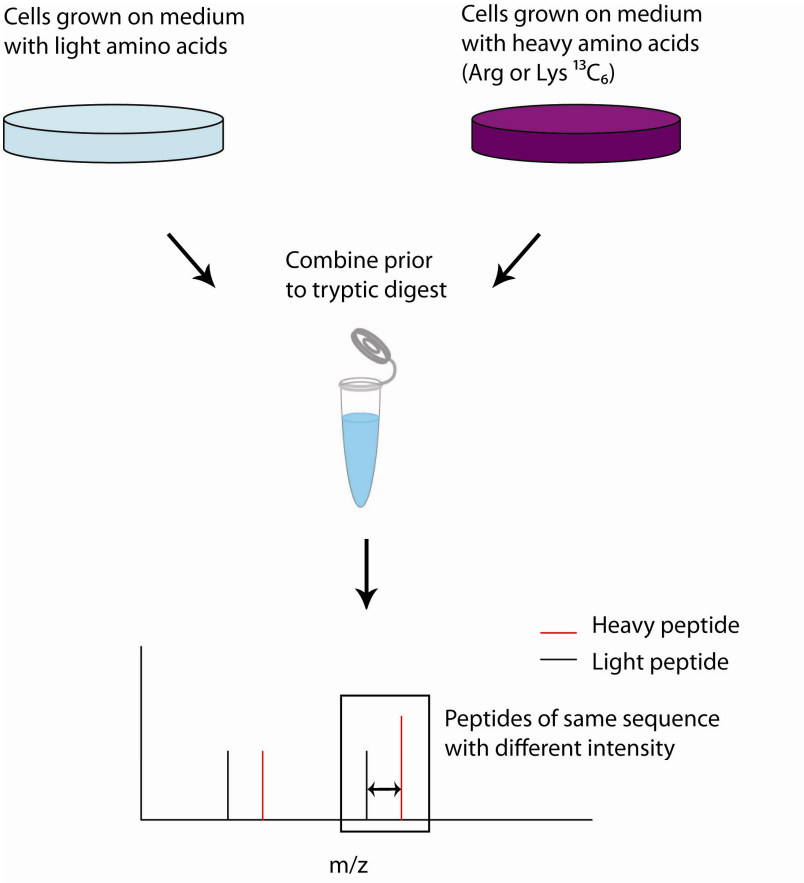

Figure 1.21 SILAC workflow – various combinations of ^{13}C and ^{15}N labeled arginine and lysine can be combined for multiplex quantitation

quantitation, and this method can be multiplexed by using different heavy amino acid combinations for different samples. This route has proven effective, however cells have to be propagated in heavy medium for several passages before they can be used for SILAC, which can result in difficulties if a phenomenon is dependent on passage

number. This is also an approach which is not suitable, for example, to analyse biomarkers in clinical samples, due to the impossibility of heavy labeling a patient; although SILAC has been demonstrated on *Drosophila*[161], mice[162] and *C. elegans*[163].

^{18}O labeling is a method which takes advantage of the trypsin digestion step, by using heavy water in the trypsin digest step which results in the incorporation of one or two heavy oxygen atoms into the tryptic peptide[164]. Where one sample is digested in heavy water, and a second sample digested in light water the peptides obtained by digestion will have a mass difference, and this allows relative quantitation of the peptide by comparing intensities[164]. Although SILAC and ^{18}O labeling do create peptides which have a different m/z, they do not contain a chemical labeling reaction step which is an advantage over methods like iTRAQ. Label free methods can avoid the problems in labeling peptides which can occur because of chemical reaction differences[165]. Label free quantitation methods include spectral counting, which simply counts the number of times a peptide appears in the initial MS spectrum and this can be compared to other samples[166]. This method requires algorithms which normalize the quantitation results based on the length of the protein a peptide is derived from, because longer proteins have more chance of the detection of multiple peptides[167]. This method also requires very reproducible LC conditions, as this can affect the number of times a peptide is detected. An alternative to spectral counting is to quantify peptides by measuring the area under the peak, which is the method usually used for multiple reaction monitoring (MRM) quantitation[165].

All of the methods above are relative methods of quantification, i.e. they compare two or more samples to each other. Absolute quantification is also possible with mass spectrometry based proteomics. Absolute quantification (AQUA) is a method which has been used to quantitate particular proteins by spiking lysates with a heavy peptide of a known protein, and using the known concentration of the spiked peptide to determine how much protein is present in a sample[168]. Variations on this technique include transfection of proteins which are concatomers of AQUA peptides which can be freed by tryptic digestion to quantify multiple proteins at once using this absolute quantitation method[169]. Drawbacks with these methods are that you have to know which proteins you want to quantify initially, which makes this a useful technique

Quantitation Method	Label	Relative or Absolute	Advantages	Disadvantages
DIGE	Fluorescently labelled proteins	Relative	Measures full length protein	Dynamic range issues
iTRAQ	Cleavable isobaric tag	Either	Opportunity for multiplexing	Extra labelling step
SILAC	Heavy amino acids	Relative	No chemical labelling	Several generations of cell culture required, not for use *in vivo*
18O Labelling	Heavy oxygen	Relative	Labelling intrinsic to tryptic digest step	Relies on enzymatic reaction
Spectral counting	None	Relative	No labelling	Requires very reproducible LC conditions
AQUA	Spiked heavy peptide	Absolute	Absolute quantitation	For known targets only
				Requires synthetic peptide for each quantitation

Table 1.1 Summary of quantitation methods for proteomics

for measuring known biomarkers but not discovering new biomarkers. Shotgun proteomics experiments which rely on relative quantitation takes a snapshot of the whole proteome, and results may include new hits which have not been discovered by traditional cell biology and genetics methods. Proteomic MS quantitation methods are summarized in Table 1.1.

1.7.5 Validation of proteomic data

If an appropriate number of replicates have been carried out, proteomic data can be very reliable, and it is often possible to find internal validation in a proteomic dataset of known proteins linked to the phenomenon being studied. For reasons of large data volume, a proteomics dataset can be difficult to interpret. In a quantitative proteomics experiment it is necessary to choose cut offs to represent up or downregulation of a protein, and assign significance values to the quantitations obtained. In the absence of rigorous statistical validation of proteomic datasets, traditional biochemical and cell biology methods can be used to validate individual hits, however it is unlikely that it would be possible to do this for every interesting hit generated in a proteomic mass spectrometry experiment. Various bioinformatics efforts are aiming to deal with this problem, for example using meta-data associated with identified proteins such as subcellular localization and known functions to classify proteomics results[170]. Creation of machine learning models has also been used to carry out unbiased filtering of proteomic data[171], and other bioinformatics based methods are very promising for continuing to make sense of the proteome and the dynamic nature of interactomes.

1.8 The aim of this project

MDM2 has diverse functions, a complicated molecular mechanism and a large interactome. By finding out more about the wider MDM2 interactome, new cancer targets as well as means to re-activate cell arrest and apoptotic pathways may be found. This in turn will improve our understanding of the way proteins have multiple binding partners and regulate multiple pathways. It is becoming clear that the cellular environment is complex and dynamic, and one method of measuring this dynamic environment is by using quantitative proteomics. The aim of this work was to perturb the MDM2 interactome using the drug Nutlin, and to use quantitative proteomic screens to detect proteins which have altered levels after Nutlin treatment (Chapter Three). Results were filtered using a model based on linear motifs binding of MDM2, and MDM2 binding peptides derived from proteins affected by Nutlin validated using biochemical methods such as ELISA and biophysical assays, in particular thermal denaturation (Chapter Four). Full-length proteins were then validated for MDM2 interaction and Nutlin response (Chapter Five). By targeting our efforts on a protein that is already relatively well characterised, MDM2, it can be evaluated whether this is a valuable method for interactomics and how successful the strategy of filtering of proteomic results by linear motifs is. Additionally, the concept of linear motif mediated interactions was investigated using the BOX-I and BOX-V motifs (Chapter Four). An AGR2 binding peptide and the mode of action of Nutlin were also investigated (Chapter Six).

2 Experimental Methods

2.1 Cell culture

2.1.1 Mammalian Cell Culture

MCF7 human breast adenocarcinoma cells were seeded on 6-well, 10 cm or 20 cm plates with 2 ml, 10 ml or 20 ml respectively DMEM growth medium (Invitrogen) supplemented with 10% foetal calf serum (FCS, Biosera) and 1% penicillin and streptomycin (PenStrep) (Invitrogen). Cells were incubated at 37°C with humidity, with a CO_2 level of 5 or 10%. To maintain cultures, cells were grown until 90-100% confluent, washed twice with sterile phosphate buffered saline pH 7.4 (PBS) then incubated with 3 ml trypsin-ETDA (Invitrogen) at 37°C for 5-10 mins to detach from the plate. Trypsinised cells were then diluted 1:1 with fresh DMEM 10% FCS, 1% penicillin and streptomycin and seeded onto new plates at the desired density. A375 human melanoma cells were also cultured in the same way using DMEM, and H1299 human lung carcinoma cells were cultured in RPMI medium supplemented with 10% FCS and 1% PenStrep (Invitrogen) with all other methods the same as for MCF7 cells.

2.1.2 Freeze down of cell cultures

For long term storage cells were stored in liquid nitrogen. Confluent cells were trypsinised as before with 3 ml trypsin-EDTA then diluted to 10 ml with growth medium. Cells were centrifuged at 1000 rpm for 5 mins and supernatant discarded. Pellets were resuspended in 5 ml freezing medium (FCS with 10% DMSO), aliquoted into cryovials and incubated at -80°C in an isopropanol chamber overnight before

transferring to liquid nitrogen. Cells were thawed by bringing an aliquot to 37°C and added to 5 ml growth medium supplemented with FCS and PenStrep to a 6 cm plate. Cells were washed with sterile PBS and fresh medium added the following day.

2.1.3 Harvesting of cells

Cells were harvested by washing twice with ice cold PBS, then scraping cells away from the plate into a small volume of ice cold PBS and transferring to a microfuge tube. Cells were then centrifuged for 3 mins at 3000 rpm, and the supernatant removed by pipetting before either snap-freezing the cell pellet in liquid nitrogen or proceeding directly to lysis.

2.2 Plasmids and transfection

2.2.1 Plasmids

Plasmids for transfection were purified by mini or maxi-prep (Qiagen) and concentration determined by measuring A_{260} on a NanoDrop UV/Vis spectrometer (Thermo). Plasmids are detailed in Table 1.

Vector	Size (kb)	Antibiotic Resistance	Supplier	Insert	Sequencing Primer
pcDNA3	5.4	Ampicillin, Neomycin	Invitrogen	Empty p53 MDM2 His-tagged ubiquitin	5'-TAATACGACTCACTATAGGG-3'
pCMV-6-XL5	4.7	Ampicillin	Origene	RPS7 ERp60	5'-GGACTTTCCAAAATGTCG-3'

Table 2.1 – Plasmids for transfection

2.2.2 Transfection protocol

Transfection mixture (for a 10 cm plate):

0-10 µg plasmid DNA
15 µl Attractene (Qiagen)
Made up to a final volume of 300µl with serum free growth medium (SFM)

Cells were allowed to grow to 90-100% confluence, washed twice with sterile PBS, and 10 ml growth medium supplemented with FCS and PenStrep. Transfection mixture was added to cells dropwise and they were incubated overnight at 37°C and 5% CO_2. After incubation cells were harvested as described.

2.2.3 siRNA Treatment of Cells

siRNA Transfection Solution 1:
190 µl SFM
10 µl siRNA (final concentration 1 µM)

siRNA Transfection Solution 2:
196 µl SFM
4 µl Dharmafect (Dharmacon)

siRNA stocks were prepared in ddH_2O to 20 µM in 1x siRNA buffer (Dharmacon). Cells were grown on 6-well plates to approximately 60% confluence, washed twice with sterile PBS and 1.6 ml fresh medium containing FCS was added per well. The two transfection solutions were prepared and incubated for 5 mins before solutions 1 and 2 were combined and incubated at room temperature for 20 mins. 400 µl per well of this solution was added to each well dropwise. Cells were harvested after 24 or 48 hrs as previously described.

2.3 Drug treatment of cells

2.3.1 Nutlin treatment of cells

A stock solution of 43 mM Nutlin-3 (Alexa Biochemicals) was prepared in 100% DMSO. Nutlin was added to medium to a final concentration of 0-40 µM and then added to cells after washing them twice with sterile PBS. Cells were harvested at the desired time point (Between 0-48hrs). Control cells were treated with DMSO only.

2.3.2 MG-132 treatment of cells

A stock solution of 10 mM MG-132 (VWR) was prepared in 100% DMSO. MG-132 was added to medium at a final concentration of 10 µM and then added to cells after washing them twice with sterile PBS. Cells were harvested after 4-5 hrs. Control cells were treated with DMSO only.

2.3.3 Cycloheximide treatment of cells

A stock solution of 10 mg/ml cycloheximide was prepared in 100% ethanol. Cycloheximide was added to fresh medium to a final concentration of 10 µg/ml and added to cells after washing twice with sterile PBS. Cells were harvested at time points between 0 and 2 hrs. Control cells were treated with ethanol only.

2.3.4 Peptide aptamer treatment of cells

Penetratin (RRMKWKK) tagged peptide aptamers (Clonestar) were dissolved to a stock concentration of 2.5 mM in ddH2O and neutralized to pH 7.0 with 5 M NaOH. Peptide

aptamers were diluted in growth medium to the desired final concentration between 0 and 50 µM and cells were washed twice with sterile PBS before adding peptide containing medium to plates. Cells were harvested 6-72 hrs after aptamer treatment, lysed and analysed by SDS-PAGE.

2.4 Cell lysis and subcellular fractionations

NP40 Lysis Buffer:
150 mM NaCl
1% NP40
50 mM Tris.HCl pH 8.0
50 mM NaF
5 µM EDTA

SDS Lysis Buffer
0.15% SDS
20 mM HEPES pH 8.0
10 mM NaF
150 mM NaCl
1 mM EDTA
1 mM EGTA

Urea Lysis Buffer
50 mM Tris.HCl pH 8.0
150 mM NaCL
6 M Urea pH 8.0
50 mM NaF
5 µM EDTA

Cell pellets were lysed in NP40 lysis buffer, SDS lysis buffer or urea lysis buffer. Cell pellets were incubated with 100-400 µl lysis buffer for 30 mins on ice, then centrifuged for 30 mins at 13 000 rpm to obtain lysate and an insoluble pellet. The insoluble pellet was either discarded or lysed with urea lysis buffer. Concentrations of lysates were obtained by Bradford assay[172]. For subcellular fractionation, cell pellets were lysed as per manufacturers instructions with a subcellular proteome extraction kit (calbiochem) to obtain cytoplasmic, membrane, nuclear and cytoskeletal fractions for each cell pellet.

2.5 Assays

2.5.1 Bradford Assay[172]

200 µl aliquots of Bradford reagent were incubated for 5 minutes with 1-2 µl bovine serum albumin (BSA) standards between 0-2 mg/ml. The same volume of each sample of unknown concentration was also added to a 200 µl aliquot of Bradford reagent. 50 µl of each standard and unknown sample were pipetted into a clear 96-well plate in triplicate and absorbance at 595 nm read using a VICTOR^3 1420 multi-label plate reader (PerkinElmer). Standards graph was constructed using absorbances from the BSA samples, fit with a straight line equation and concentration of unknown samples calculated from standard fit.

2.5.2 Peptide enzyme-linked immunosorbent assay (ELISA)

ECL I:	ECL II:
2.5 mM luminol	0.02% v/v H_2O_2
100 mM Tris.HCl pH 8.5	100 mM Tris.HCl pH 8.5
0.4 mM p-coumaric acid	

White 96-well plates (Costar) were incubated with 50 µl per well 16 µg/µl streptavidin (AnaSpec) overnight at 37°C to coat plate with streptavidin. Plates were washed 6 times with 200 µl PBS 0.05% Tween-20 (PBS-T) and then incubated with 1-5 µg biotinylated peptide (Mimotopes) per well for 1 hr with shaking on a rotating table. Plates were washed as before, prior to blocking with 200 µl 3% bovine serum albumin (BSA) PBS-T per well for 1 hr at room temperature. Blocking solution was removed and peptide coated wells were then incubated with 50 µl protein diluted in 3% BSA PBS-T. To show

peptide-protein binding titrations of protein serial dilutions were prepared with a non-binding peptide or protein as a negative control. If the assay was to measure competition the protein was incubated with competitor for 30-60 mins prior to addition to plate. Wells were washed as before, then incubated for 1 hr at room temperature with 50 µl per well primary antibody diluted in 3% BSA PBS-T (Antibodies – 2.3.3) and gentle shaking. Wells were washed again as before and incubated for 1 hr at room temperature with 50 µl per well secondary antibody diluted in 3% BSA PBS-T. After washing as before, ECL1 and ECL2 were combined in equal volumes directly before adding 50 µl of ECL mixture to each well. Plates were exposed to X-ray film which was developed as described in immunohistochemistry section, and also luminometry measurements were taken using a Labsystems Fluoroskan Ascent FL plate reader and the Labsystems Picogreen program to interpret data.

2.5.3 Protein-protein ELISA

White 96-well plates were coated with 10-50 µg protein diluted in 50 µl 0.1 M $NaCHO_3$ pH 8.0 per well overnight at 4°C, then washed as in the peptide ELISA and blocked with 200 µl 3% BSA-PBST. Plates were then incubated with protein and antibodies and developed as described for the peptide ELISA.

2.5.4 In vivo His-Ubiquitin assay

H1299 cells were transfected with pcDNA His-Ubiquitin, candidate protein (p53, CypB, S7) with or without cotransfection of pcDNA-MDM2 (Table 1.1). After 24 hrs transfected cells were treated for 4-5 hrs with the proteasome inhibitor MG-132

(Calbiochem) at a concentration of 10 µM prior to harvesting and snap freezing in liquid nitrogen.

Buffer A (100 ml)
6 M Guanidinium
47.35 ml 0.2 M Na_2HPO_4
2.65 ml 0.2 M NaH_2PO_4
10 mM Tris.HCl pH 8.0
70 µl 14.3 M β –mercaptoethanol
Adjust to final pH of 8.0

Buffer B
(100 ml):
8 M Urea
23.7 ml 0.2 M Na_2HPO_4
1.33 ml 0.2 M NaH_2PO_4
10 mM Tris.HCl pH 8.0
35 µl 14.3 M β -mercaptoethanol
Adjust to final pH of 8.0

Buffer C (50 ml):
8 M Urea
11.25 ml 0.2 M Na_2HPO_4
38.75 ml 0.2 M NaH_2PO_4
10 mM Tris.HCl pH 8.0
70 µl 14.3 M β-mercaptoethanol

Buffer D
Buffer C + 0.2% Triton X-100

Buffer E
Buffer C + 0.2% Triton X-100

Ub Lysis Buffer:
100 ml Buffer A
5 mM imidazole

Elution Buffer (1 ml)
200 mM imidazole
5% SDS
150 mM Tris-HCl pH 6.7
10% Glycerol
50 µl 14.3 M β -mercaptoethanol

Cells were lysed in 1 ml lysis buffer, pipetting through an 8 µ syringe several times to enhance lysis. 800 µl of lysate was transferred to a 15 ml falcon tube containing 4 ml of lysis buffer. The remaining 200 µl of lysate was retained for loading controls. 75 µl of Ni-NTA agarose beads (Qiagen) were added to the falcon tube and samples were incubated on a rotary shaker at 4°C overnight. Beads were then collected by centrifuging at 2000 rpm for 3 mins and the supernatant discarded. Beads were resuspended in 750 µl Buffer A, transferred to a microfuge tube and incubated at room temperature with

rotation for 15 mins. Mixtures were then centrifuged as before, supernatant discarded and beads washed with buffers B, C, D and E by resuspending in 750 µl of buffer then centrifuging as before and discarding supernatant. To elute His-ubiquitin tagged proteins beads were incubated with 75 µl elution buffer for 30 mins at room temperature, then centrifuged at 14 000 rpm for 5 mins at 4°C. Supernatant was collected and analysed by SDS-PAGE using Novex 4-12% pre-cast gels (Invitrogen).

2.5.5 In vitro His-Ubiquitin assay

Reaction mix for 16 reactions:

25 mM HEPES pH 8 (4°C)
6 mM $MgCl_2$
0.05% v/v Triton X-100
0.5 mM DTT
1 mM Benzamidine
80 µg/ml ubiquitin
3 mM ATP
Make up to a final volume of 400 µl with ddH2O

Fresh in vitro ubiqutination mixture was prepared on ice and mixed gently by inversion. 4 µl 1 M creatine phosphate and 2 µl 10 mg/ml creatine kinase were added and again mixed gently by inversion. 0.78 µl E1 UBE1 and 0.48 µl E2 UbcH5 (Boston Biochemicals) were added to the mixture along with substrate (p53 or CypB) and a titration of MDM2. Tubes were incubated at 30°C for 15 mins, then transferred back to ice, mixed with sample loading buffer and incubated at 95°C for 2 mins before analysis by SDS-PAGE using Novex 4-12% pre-cast gels (Invitrogen).

2.5.6 CelluSpots[173] peptide arrays

Slides functionalized with candidate peptides (Intavis) were blocked for 4 hours at room temperature in Tris buffered saline (TBS), 0.05% Tween (TBST) containing 5% BSA. Slides were then rinsed in TBST and incubated with 10 µg MDM2 or N-terminal domain MDM2 diluted in TBST 0.5% BSA overnight at 4°C. 3 x 10 min washes with TBST were carried out on slides, before incubation with primary antibody diluted in TBST 1% BSA for 1 hr at room temperature. Slides were washed as before, and incubated with LiCor IRDye 800CW donkey anti-mouse secondary antibody for 1 hr at room temperature. Slides were read on a LiCor Odyssey plate reader, and analysed using the LiCor software.

2.5.7 Co-immunoprecipitations

Cells were lysed in NP40 lysis buffer. 100 ml protein G sepharose beads (Sigma Aldrich or Expedeon) were washed with 1 ml cold lysis buffer three times by resuspending and centrifuging at 5000 rpm for 1 min, discarding the supernatant. Lysates were then pre-cleared of proteins which bind to protein G or sepharose beads by incubating lysate with 100 µl protein G beads for 40 mins on a rotary shaker at 4°C. This mixture was centrifuged at 13 000 rpm for 2 mins and supernatant transferred to a fresh eppendorf. 2 µg of anti-MDM2 (2A10) was added to the lysate and incubated overnight at 4°C with rotation. 15 µl protein G beads which had been washed as before were added to the lysate-antibody mixture and incubated for 1 hr at 4°C with rotation. Beads were washed by centrifuging at 5000 rpm for 2 min at 4°C, discarding supernatant and resuspending

in fresh lysis buffer for each wash. Antibody-protein complexes were eluted by boiling for 3-5 min with SDS sample loading buffer, then centrifuging at 5000 rpm for 5 min to obtain supernatant. Supernatant, load and wash fractions were then analysed by SDS-PAGE and western blot.

2.6 SDS-PAGE and western blotting

2.6.1 SDS-PAGE

5x Sample Loading Buffer:
250 mM Tris.HCl pH 6.8
50% v/v glycerol
5% w/v SDS
0.5% w/v bromophenol blue
250 mM DTT

10x Running Buffer:
250 mM Tris.HCl
2 mM Glycine
1% w/v SDS

10x Transfer Buffer
250 mM Tris.HCl
2 mM Glycine

Running Gel:
30% acrylamide mix (diluted to required percentage)
375 mM Tris.HCl pH 8.8
0.1% w/v SDS
0.1% w/v APS
0.04% v/v TEMED

Stacking Gel:
5% v/v acrylamide mix (Protogel)
125 mM Tris.HCl pH 6.8
0.1% w/v SDS
0.1% w/v APS
0.04% v/v TEMED

Whole cell lysate concentration was measured by Bradford assay and then normalized using water or lysis buffer. Sample loading buffer was diluted 1 in 5 into samples and 5-10 µg of total protein was analysed in each gel lane. Gels were either Novex pre-cast with a 4-12% gradient (Invitrogen), or running buffer and stacking buffer were prepared

as above at the desired percentage of acrylamide (10, 12 or 15% v/v). Gels were run at 180-200 V with the appropriate running buffer (MOPS for pre-cast (Invitrogen) or SDS for freshly prepared gels), using Bio-Rad gel apparatus and power pack until markers and protein standards (Fermentas) reached the bottom of the gel. Gels were either stained with coomassie stain or RapidBlue (Expedeon) and destained in 10% methanol, 7% acetic acid, transferred to water or used for western blotting.

2.3.2 Western blots

Transfer buffer was diluted to 1x with a final concentration of 20% v/v methanol. After SDS-PAGE gels were transferred to western blotting cassettes as follows from negative to positive electrode - sponge, two sheets of blotting paper, gel, membrane (Hybond, GE), two sheets of blotting paper, sponge, with all components soaked in transfer buffer. Cassettes were transferred to an electrophoresis tank with an ice pack, and transfer buffer was added to tank covering gel and membrane completely. Transfers were run at 300 mA for 1 hr, and either rinsed in H_2O before Ponceau staining to visualize bands or immediately blocked. Nitrocellulose membranes were blocked with 3% milk powder (Marvel) PBS-T for 1 hr at room temperature with gentle shaking. Membranes were then incubated with primary antibody diluted in 3% milk PBS-T at 4°C overnight. After incubation with primary antibody membranes were washed three times for 10 mins in PBS-T and incubated with secondary antibody diluted in 3% milk PBS-T at room temperature for 1 hr. Membranes were washed as before, then blotted dry and incubated on a glass sheet with ECL for 1 min after combining ECL1 and ECL2 directly before use. ECL was completely blotted off membrane before exposing x-ray film to

membranes in a dark room for variable exposure times. Films were developed with an Xograph developing machine.

2.3.3 Antibodies

2.3.3.1 p53 and MDM2 antibodies

p53 and MDM2 antibodies were all obtained from Moravian Biotechnology

p53 antibodies – DO1 (mouse monoclonal), DO12 (mouse monoclonal), CM1 (rabbit monoclonal)

MDM2 antibodies – 2A10 (mouse monoclonal), 4B2 (mouse monoclonal), 3G5 (mouse monoclonal), polyclonal anti-MDM2 (rabbit polyclonal)

2.3.3.2 Other antibodies

p21 (mouse monoclonal, Calbiochem), E2F1 (mouse monoclonal, Santa Cruz), β-actin (mouse monoclonal, Sigma Aldrich), Anti-AGR2 K47 (rabbit monoclonal, Moravian Biotechnology), RPS7 (mouse monoclonal, Abnova), CypB Poly (rabbit polyclonal, Abcam), CypB Mono (mouse monoclonal, Abnova), DNA-PK (goat monoclonal, Santa Cruz), NME1 (rabbit monoclonal, Cell Signalling), APEX1 (mouse monoclonal, Abcam), ERp60 (rabbit polyclonal, Abcam), NPM (rabbit polyclonal, Cell Signalling Technology), HMGB1 (mouse monoclonal, Abnova), Anti-His-tag (mouse monoclonal, Sigma Aldrich).

2.3.3.3 Secondary antibodies

HRP conjugated rabbit anti-mouse (Dako), HRP conjugated swine anti-rabbit (Dako) and HRP conjugated donkey anti-goat (Santa Cruz).

2.4 Mass spectrometry

2.4.1 PAcIFIC sample preparation and mass spectrometry

MCF7 cells grown on 20 cm culture plates and treated with 40 µM Nutlin-3 were harvested at 0, 2, 4, 8 and 12 hrs and lysed in NP40 lysis buffer. Lysates were analysed at the Proteomics Core Facility in University of Geneva by Precursor Acquisition Independent from Ion Count (PAcIFIC) LC-MS/MS on a linear ion trap Orbitrap (ThermoFisher) as described in[156], (A. Scherl). Identifications were obtained using the Phenyx database (GeneBio, Switzerland), with a false positive identification rate of less than 5%. Peptides were quantified by spectral counting, discarding any quantitations which rely on less than three spectral counts, and normalized to the length of the identified protein.

2.4.2 iTRAQ cell lysis and trypsin digestion

MCF7 cells were grown to confluence on 20 cm plates and treated with 40 µM Nutlin-3 were harvested at 0, 1, 2, 4, 8, and 12 hrs after nutlin treatment, lysed in 1 ml SDS lysis buffer per sample and briefly sonicated to fragment genomic DNA. The soluble fraction was obtained by centrifuging at 10 000 rpm and removing supernatant by pipetting into a clean microfuge tube. Total protein content was determined by Bradford assay. 80 µg of each lysate was incubated with 2 µl reducing agent (Applied Biosystems) for 1 hr at 60°C, followed by incubation with 1 µl cysteine blocking reagent (Applied Biosystems)

for 10 mins at room temperature. After reduction and alkylation three volumes of 0.25 M triethylammonium bicarbonate (TEAB) pH 7-9 were added to each sample. Trypsin (Promega Gold) was resuspended to a final concentration of 1 µg/µl in MilliQ purified H_2O and added 1:20 protease:protein to samples which were then incubated overnight at 37°C.

2.4.3 iTRAQ labeling reactions

Trypsin digested samples were lyophilized using a vacuum centrifuge for 1-3 hrs and pellets resuspended in 30 µl 0.5 M TEAB pH 7-9. 8 separate iTRAQ labels, which yield reporter ions at 113, 114, 115, 116, 117, 118, 119 and 121 m/z units (Applied Biosystems) were resuspended in 70 µl isopropanol. Trypsin digests were then labeled with one iTRAQ reagent per sample by incubation of digest with iTRAQ reagent for 2 hr at room temperature. 2 µl of each labeled digest was mixed and desalted by zip-tipping (Millipore).

2.4.4 Desalting peptide mixtures and MALDI MS

C18 zip-tips (Millipore) were activated by washing five times with 10 µl 90% acetonitrile, 0.1% TFA, then washed five times with 10 µl 0.1% TFA. 10 µl of sample was pipetted into the zip-tip, and re-pipetted ten times. Zip-tips were then washed three times with 0.1 % TFA and desalted sample eluted with 2-3 µl 4 mg/ml MALDI matrix resuspended in 70% acetonitrile, 0.06% TFA and spotted onto a 384 Opti-TOF MALDI target plate adjacent to MALDI peptide standards. Samples were analysed with an AB

SCIEX 4800Plus Proteomics Analyser automated MALDI-TOF/TOF to check for the presence of iTRAQ labels.

2.4.5 iTRAQ analysis by LC-MS/MS

All 8 iTRAQ labeled tryptic digests were combined in a microfuge tube and lyophilized in a vacuum centrifuge for 1-3 hrs. Samples were separated by strong cation exchange (SCX) and fractions containing peptides were resuspended in 100 µl 0.1% TFA, 2% acetonitrile, with several fractions with lower peptide content pooled to create a total of 20 separate samples for MS analysis. Fractions were then analysed by nanoLC ESI MS/MS with a QStar XL mass spectrometer (Applied Biosystems, Australian Proteome Analysis Facility) using positive nanoflow electrospray analysis in a data dependent acquisition mode. Proteins were identified using ProteinPilot (Applied Biosystems, Version 2.01) to submit a query via the MASCOT (Matrix Science) search engine. Parameters for searching were: Database – SwissProt, Labelling - iTRAQ, Fixed modifications - cysteine alkylation, Variable modifications – methionine oxidation, Enzyme - trypsin, Instrument - Qstar, Species - *Homo sapiens*. Peptides were quantified through the Paragon algorithm in the ProteinPilot programme after background correction and bias correction by the software (Applied Biosciences).

2.5 Protein Purification

2.5.1 Plasmids and Constructs

Full length MDM2 (FL-MDM2) and N-terminal domain MDM2 (NT-MDM2) were both expressed from pGEX-6p vectors, with an N-terminal GST tag cleavable at the

Precission protease™ (GE Healthcare) target site, LEVLFQGPL, which has a cleavage site between the glutamine and glycine residues. CypB is in the pDEST14 vector with an N-terminal His-tag sequence. AGR2 is in the pDEST17 vector with an N-terminal his tag sequence.

2.5.2 Transformations

Competent BL21(DE3) *E.coli* were incubated with 1-2 µl plasmid DNA on ice for 1 hr then incubated at 42°C for 45 secs to heat shock. 1 ml LB medium was added to bacteria which were then incubated for 1 hr at 37°C with shaking. Cells were centrifuged at 6000 rpm for 2-5 mins and 800 µl of the supernatant discarded. Pellet was resuspended in the remaining 200 µl LB medium, spread onto pre-warmed LB agar plates ampicillin at 100 µg/ml and incubated overnight at 37°C. Plates were sealed with parafilm and stored at 4°C until required.

2.5.3 GST-MDM2 Purification

Lysis Buffer:
10% sucrose
50 mM Tris.HCl pH 8.0
150 mM NaCl
0.5% NP40
5 mM DTT
1 mM Benzamidine
1 protease inhibitor tablet (Roche Complete) per 10 ml of buffer
Lysozyme 150 µg/ml

Wash Buffer 1:
20 mM HEPES pH 7.5
150 mM NaCl
1 mM DTT
0.1% NP40

Wash Buffer 2:
20 mM HEPES pH 7.5
0.5 M NaCl
1 mM DTT
0.1% NP40

Glutathione Elution Buffer:
25 mM HEPES pH 7.5
1 mM DTT
1 mM Benzamidine
50 mM Glutathione
10% Glycerol
150 mM NaCl

Precission Elution Buffer:
25 mM HEPES pH 7.5
1 mM DTT
10% Glycerol
150 mM NaCl
Protease Inhibitor (Roche Complete)

Plasmids were transformed into *E. coli* BL21(DE3) and single colonies picked into 50 ml LB supplemented with 100 µg/µl ampicillin. This starter culture was incubated overnight at 37°C with shaking. The starter culture was then diluted 1:100 into 500 ml LB supplemented with 100 µg/µl ampicillin in 2 L conical flasks and incubated at 37°C with shaking until an OD_{600} of 0.6 was reached. Flasks were then transferred to a room temperature shaker and induced with 1 mM isopropyl β-D-1-thiogalactopyranoside (IPTG) for 4-5 hrs. Cells were then centrifuged at 6000 rpm for 10-15 mins and pellets snap frozen in liquid nitrogen. Pellets were defrosted at room temperature then lysed in 20 ml lysis buffer per 1 L of culture by resuspending the pellet in lysis buffer on ice and incubating for 30 mins. Lysates were sonicated for 10 secs three times (Soniprep 150 plus), with 10 secs rest on ice between sonications. Lysates was then split into microfuge tubes and centrifuged for 10 mins at 10 000 rpm, to separate cell free extract (supernatant) from the insoluble fraction (pellet). 500 µl of glutathione sepharose beads slurry per 1 L of culture (GE healthcare) were washed three times with lysis buffer, and

then incubated with lysate for 1-2 hrs with the supernatant from the centrifuged lysate. Beads and lysate were transferred to a column jacket with a filter (VWR) and washed three times with wash buffer 1, a further three times with wash buffer 2 and then 0.5-1 ml elution buffer was added to the beads and they were incubated for a further 1-4 hrs. Glutathione elution buffer was used to obtain GST tagged MDM2 and Precission buffer to obtain cleaved MDM2. After incubation with elution buffer, fractions of approximately 100 µl were collected in microfuge tubes and analysed by SDS-PAGE. Protein concentrations were determined by Nanodrop (ThermoFisher) Uv/Vis absorbance at 280 nM, Bradford assay or as compared to BSA standards on SDS-PAGE.

2.5.4 Purification of His-AGR2 and His-CypB

Lysis Buffer:
20 mM Tris.HCl pH 8.0
150 mM NaCl
10 mM MgCl2
0.1% NP40
10% Glycerol
20 mM imidazole

Wash Buffer 1:
As lysis buffer with 40 mM imidazole

Elution Buffer:
As lysis buffer with 150 mM imidazole

E. coli BL21 (DE3) transformed with his-tagged protein vectors were picked from previously transformed plates and grown in 50ml LB medium containing 100µg/ml ampicillin overnight to make a starter culture. The starter culture was then diluted 1 in 10 into 500ml LB 100µg/ml ampicillin and cells grown with shaking at 37°C to an OD_{600} of 0.6. Cells were then induced with 0.5 mM IPTG and grown for 3-4 hours at room temperature. Cells were harvested by centrifuging at 6000 rpm for 20 mins at 4°C and pellet snap-frozen in liquid nitrogen. For lysis cells were incubated on ice for 30

mins after being resuspended in lysis buffer. Lysate was sonicated three times for 15 secs with a 15 secs break on ice between sonications, and centrifuged at 13 000 rpm for 10 mins in microfuge tubes to obtain soluble fraction. 1 ml Ni-NTA agarose (Qiagen) was washed three times with lysis buffer, then supernatant from lysed cells was added to beads and incubated on a rotary shaker for 1 hr at 4°C. Mixture was transferred to a 6 ml column jacket and flow-through collected to analyse by SDS-PAGE. Beads were washed 2 times with 5 ml lysis buffer, then a further three times with 5 ml wash buffer 1. Elution buffer was added to the column and 500 µl fractions collected and analysed by SDS-PAGE.

2.5.5 Buffer exchange

Zeba desalting columns (ThermoFisher) were washed 3-5 times with 300 µl desired buffer by adding to column and centrifuging for 1 min at 1 500g. 50-70 µl purified protein was then added to the column and eluted by centrifuging as before.

2.6 Site directed mutagenesis

2.6.1 Primers

CypB W47A primers (mutated bases highlighted in bold)

Forward – 5'-GAAAGTGACCGTGAAAGTG**GCG**TTTGATCTCGGATTGGTG-3'

Reverse – 5'-CACCAATGCGCAGATCAAA**CGC**CACTTTCACGGTCACTTTC-3'

2.6.2 Protocol

PCR reactions were carried out with template DNA (CypB pDEST 14) and appropriate primers.

PCR reactions for site directed mutagenesis were set up with:

12.5 µl 2X Pfu MasterMix (Stratagene)
2.5 µl Band Doctor (Stratagene)
50 ng plasmid template
0.13 µl forward primer (100µM stock)
0.13 µl reverse primer (100µM stock)
Nuclease free water to a final volume of 25 µl

Thermal cycling conditions:

95°C for 1 min
95°C for 50 sec
55°C for 1 min
68°C for 12 mins (adjust for larger plasmids)
repeat steps 2-4 for 15 cycles (or more)
68°C for 30 min
4°C forever.

PCR reaction products were digested using 5 U DpnI (Invitrogen) at 37°C for 90 mins and reaction stopped by incubating at 65°C for 90 mins. 5 µl of digested or undigested plasmid were transformed into *E. coli* DH5 alpha and streaked on LB-Agar plates containing the appropriate antibiotic. Colonies from bacteria transformed with digested plasmid were picked and grown in LB with appropriate antibiotic overnight, plasmids extracted by mini-prep (Qiagen) and sequenced.

2.6.3 DNA sequencing reactions

Sequencing primers

T7 (for pGEX and pDEST vectors) – 5'- 3'

Internal CypB sequencing primers

Forward - 5'-GGAAAGCACCAAAACCGATA-3'

Reverse – 5'-CTTTCGGGGCTTTGTTAGCAG-3'

Sequencing reactions were carried out with the following recipe:

1 µl Purified plasmid DNA (to be sequenced)
1 µl sequencing primer
1 µl BigDye (Applied Biosystems)
2 µl BigDye 5x buffer (Applied Biosystems)
5 µl nuclease free H2O

Thermal cycling protocol:

1. 96°C for 1 min
2. 96°C for 10 sec
3. 50°C for 5 sec
4. 60°C for 4 min
5. Go to step 2 for 24 cycles
6. 4°C forever

DNA was cleaned up by adding 2.5 µl 125 mM EDTA and transferring to a tube containing 30 µl ethanol, mixing and incubating for 15 min, then centrifuged at 13 000 rpm for 20 min. Supernatant was discarded, residual removed after centrifuging again. 30 µl 70% ethanol was added to the sample, then the sample was centrifuged as before for 5 mins. Supernatant was removed and discarded, then sample was re-centrifuged to remove residual. Pellet was air dried, then sent to Source Bioscience sequencing service. Results were analysed using Chromas and Expasy Translate.

2.7 Thermal Denaturation

Protein was prepared by diluting in appropriate buffer to a range of concentrations and incubated with ligands or DMSO control for 30 mins. Sypro orange (Invitrogen) was added to 200 µl of protein/ligand to be analysed at a final concentration of 5x (stock is 5000x). Protein-Sypro orange mixture was transferred to 96-well PCR plates (BioRad) in three identical replicates of 50 µl per well. PCR plates were sealed with film and centrifuged at 4000 rpm for 2 mins to ensure solution was at the bottom of the wells. Plates were analysed on a BioRad IQ5 ICycler using the BioRad ICycler software. Samples were heated in 1°C increments from 25°C to 95°C with a 30 second dwell time at each temperature and RFU of sypro orange measured at each degree. Melt-peaks were generated by plotting -dRFU/dt vs. temperature and determining the temperature at which the integrated peak minimum occured.

2.8 Super Arrays

cDNA was purified from cell lysates treated with aptamer as in section 2.3.4 and hybridized to arrays with genes representing p53 related pathways according to array manufacturers instructions (SABiosciences). Signal was detected using ECL and X-ray film and analysed using SABiosciences software, normalizing signal between arrays using the housekeeping genes GAPDH, Alpha-actin and CypB.

2.9 Reagents

All reagents were acquired from Sigma-Aldrich unless otherwise specified.

3 - Proteomic investigation of Nutlin effects on MCF7 cells

3.1 - Introduction

Proteomic mass spectrometry can simultaneously identify many proteins which respond to a drug or stimulus, and thus detect previously unidentified proteins which are up or downregulated. The p53-MDM2 interaction inhibitor Nutlin has principally been characterized with regards to the effect it has on the p53 response. However since MDM2 is highly allosteric[91], and off-target effects of Nutlin have not been widely characterized there are potentially also less well understood aspects to the Nutlin response. Two different MS based screens were carried out to investigate changes in global protein levels after Nutlin treatment. Results are considered in terms of whether any of these proteins are MDM2 or p53 binding or regulated proteins. Time points soon after Nutlin treatment were investigated with the aim of identifying proteins closely related to MDM2 before downstream responses to Nutlin treatment are activated. The two different MS methods chosen to analyse MCF7 cell lysates after a time course of Nutlin treatment, were 1) a label-free method, precursor acquisition independent from ion count MS/MS (PAcIFIC)[156], with quantitation by spectral counting to measure protein levels, and 2) a screen where the peptides from a tryptic digest are labeled for quantitation, using isobaric tag for relative and absolute quantitation (iTRAQ)[157] (Chapter 1).

3.2 Confirmation of early time point increase in level and activation of p53 by Nutlin treatment

The human breast cancer cell line MCF7 expresses wild type p53 and MDM2[48], and Nutlin treatment of these cells results in an increase in the level of p53 as early as 1 hour after treatment, which persists for up to 12 hours after treatment with a slight drop in the level 24 hours after treatment (Figure 3.1a, b). The p53 responsive protein p21 is observed to increase between 4 and 8 hours, following the increase in p53 which is an indication that the p53 which has increased in level is transcriptionally active[174], and that this is dominant over the degradation promoting effect MDM2 has been observed to have on p21[175]. The observed effect of Nutlin on E2F1 levels over this time course is to destabilise E2F1 more gradually than p53, the level can be observed to have decreased very slightly at 2 hours and continues to drop up to an 8 hour time point (Figure 3.1c). The interaction between MDM2 and E2F1 has previously been described[105, 107] and inhibition of the MDM2-E2F1 interaction destabilizes E2F1. Ubiquitination of p53 is also observed after Nutlin treatment when an SDS containing lysis buffer with reduced salt is used. This is likely due to increased levels of p53 and potentially the agonistic effect of Nutlin on p53 binding at the acidic domain[91]. MDM2 stabilisation is also observed after Nutlin treatment at 2 hours onwards (Figure 3.1c). This can be explained by a combination of p53 promoting MDM2 expression[174] and the stabilizing effect of Nutlin binding to MDM2. These results confirm that very early time-points are also significant in the MDM2-p53 axis and potentially in the wider MDM2 interactome.

3.3 Summary of label-free quantitative mass spectrometry screen results

Samples from 0, 2, 4, 8 and 12 hours after Nutlin treatment were analysed by PAcIFIC mass spectrometry coupled with gas phase fractionation (GPP) prior to LC-MS

(Described in Chapter 2). This pilot screen was carried out with two technical replicates on different LC runs. The PAcIFIC screen identified 321 proteins in one replicate and 362 in the second replicate distributed across all time points. Some proteins were detected at multiple time points, and some at a single time point. Identified proteins were categorized as being up or downregulated based on whether a two-fold change in the corresponding spectral count after Nutlin treatment relative to the spectral count in an untreated control sample was observed. The results are summarized in Figure 3.2 and fully listed in Appendix 1. Proteins which show a two-fold or greater change in both replicates are fully listed in Appendix 2. Detection in two replicates increases the likelihood that the changes observed are genuine, as detection of a two-fold change in only a single replicate may be due to poor or enhanced ionization of the peptides used for quantitation as well as other experimental errors. Overall, a greater amount of proteins were detected downregulated than upregulated (Figure 3.2b), and the number of proteins detected with altered levels at 4, 8 and 24 hours after treatment are slightly more than at the 2 hour time point. Of proteins identified as altered after Nutlin treatment many proteins were detected at two time points, whilst others were only detected at a single time point. For example the protein EIF4A1 is detected as upregulated two-fold or more in 2, 4 and 8 hour samples in replicate 2 relative to the level of detection in the 0 hour sample, but is undetected at 0 hours in replicate 1 and so exhibits an on/off style response at all other times for this replicate (Figure 3.3). It is possible to correct for this category of results by using a ratio based on log2 of each spectral count with 1 added to calculate fold change[176]. However as this screen did not include a robust number of replicates this kind of analysis may mask potential false

positives. Agreement between quantitations in both replicates increases the likelihood that the result is not simply due to missed detection of peptides from the protein of interest. A subset of proteins was detected as changed at multiple time points (Table 3.1, 3.2), with each time point representing a separate lysis, digest and LC-MS run. A number of proteins identified in a single replicate are observed at multiple time points. These results are less reliable than those from two replicates however proteins detected in a single replicate can be tentatively used as leads for further validation or to compare to future MS results, particularly if they are detected at multiple time points (Figure 3.4). There are also a large number of proteins detected in either replicate with an altered level, but unchanged in the other replicate. To verify if Nutlin treatment has a reproducible effect on these proteins, as well as those identified in only a single replicate further MS repeats or further validation by another method would be necessary. The final class of proteins identified in this pilot screen are those which have conflicting quantitation results (Table 3.5). Many of these quantitations have missed detections at either time point, such as splicing factor U2AF, and this illustrates why it is important to do multiple biological and technical replicates in a quantitative mass spectrometry experiment. If this project was to completely depend on the label-free proteomic mass spectrometry results more replicates and statistical analysis would be necessary.

3.4 Specific examples of protein level changes over time

Proteins which are detected with altered levels at several times represent pathways which are affected by Nutlin over the whole time course, and proteins which are only

altered at a single time point may be regulated by different mechanisms. The amount of the MDM2 binding protein HSP90[177] detected for example, increases at two hours and remains high over the whole time course which is a similar pattern as observed for p53 regulation by MDM2 (Figure 3.5a), whereas the amount detected of the previously identified MDM2 binding protein SAFA[92] is decreased over time (Figure 3.5b). Other proteins exhibit different patterns of regulation, such as the cancer cell proliferation marker prohibitin-2[178], which decreases at four hours then shows a recovery to near original levels (Figure 3.5c). Proteins which have not already been identified as part of the MDM2 interactome exhibiting similar patterns of regulation, for example CypB and stomatin like protein 2(Figure 3.5d, e) and are therefore potentially interesting leads for new MDM2 binding or regulated proteins.

3.5 Comparison of identified proteins to MDM2 and p53 known interactomes

Of hits which are up or downregulated in this screen, the presence of MDM2 or p53 related proteins serves as an internal validation of the dataset. MDM2 and p53 binding proteins which have been validated have been catalogued[43] and there are >150 and >300 known interactions for each protein respectively. These interactomes were compared to the proteins which are detected as upregulated or downregulated in the PAcIFIC MS experiment to evaluate whether this pilot screen yielded results which have previously been validated biologically, and to investigate if the less confident results from single replicates are linked to the known biological data. Four proteins from the known MDM2 interactome, HSP90[177], DNA-PK[82], PCNA[179] and PSME3[180] were modulated by Nutlin treatment in two replicates and eight proteins from the known p53 interactome were

detected, topoisomerase 1[181], S100-A11[182], TCP1 epsilon[183] and PARP-1[184], as well as DNA-PK, HSP90 PCNA and PSME3. Of the proteins detected only in a single replicate, no proteins were identified which are already known to participate in the known MDM2 interactome. One protein from each replicate, TFAM[185] and transcriptional activator BRG1[186], were identified which participate in the p53 interactome. Other proteins identified in both replicates include proteins with functions related to cancer, and although these proteins have not to date been identified as directly binding to p53 or MDM2 they are associated with processes which have been attributed to MDM2 and p53 related pathways. Examples include stomatin-like protein two which is associated with metastasis and tumour progression[187], eIF4G1 which binds mRNA in a pre-initation complex and is regulated by p53[188], CypB which is an immunophilin linked to cancer mechanisms[189] and XRCC5 (Ku) which plays a role in the DNA repair pathway along with DNA-PK[190]. A STRING database pathway map which links proteins based on known protein-protein interactions as well as well as predicted relationships[191] shows that many of the proteins identified by this screen are linked in a wider network. There are well-validated sub-complexes amongst these results, such as the T-complex proteins, calnexin and protein disulphide isomerase complexes[192], eIF proteins and ribosomal proteins[193] and heterogenous nuclear ribonucleoproteins[194] (Figure 3.6).

3.6 Overview of iTRAQ mass spectrometry screen

An 8-plex iTRAQ screen was carried out on the same MCF7 cell line treated with Nutlin and harvested at several time points. A one hour time point was included to investigate whether the response to Nutlin is more acute than shown by two hours in the PAcIFIC

screen and a 12 hour time point was also included. After this time cells can start to enter apoptosis or cell cycle arrest and widespread activation of downstream p53 related pathways[107] may obscure effects which are directly attributable to modulation of MDM2 interactions. As described in Chapter One, iTRAQ relies on a labeling step for quantitation, which adds an additional step in sample preparation before quantitation compared with PAcIFIC. Eight samples were combined and analysed simultaneously, and 1323 proteins detected in total (Table 3.5).

3.7 Quantitation of Nutlin regulated proteins by iTRAQ

Cut-off ratios of <0.77 or >1.33 were chosen to select proteins which are up or downregulated. For complex samples analysed by iTRAQ although the direction of the change in level, i.e. up or downregulated, is reliable, it has been reported that the numerical change may not be directly quantitative[159] (Chapter One). Therefore for cell lysates analysed by iTRAQ a large change in protein expression may be accompanied by a small change in iTRAQ ratio, compared to methods which measure fold change such as spectral counting. The total number of up and downregulated proteins identified in the iTRAQ screen are summarized in Figure 3.7 and all proteins identified across the time course are listed in Table 6. 10 of the detected proteins occur over multiple time points, including DNA-PK, NONO, and the APEX1 protein which is closely linked to regulation of p53 DNA repair[97]. Interestingly, many more proteins were identified in one of the replicates at 12 hours than at the earlier times, with less shared identifications with the earlier time points (Figure 3.7). The majority of the proteins identified at 12 hours were detected in a single replicate, this may be due to differences in the efficiency of the

lysis for the two replicates, or differences in the efficiency of one labeling reaction compared with the other samples. This further illustrates the importance of carrying out multiple replicates of the same sample. The overall trend is an increase after Nutlin treatment over time of the amount of proteins detected at each time point, with a the largest amount of detections at the 12 hour time point (Figure 3.7).

3.8 Comparision of iTRAQ hits with the known interactomes of MDM2 and p53

Many ribosomal proteins were identified in the second replicate of the 12 hour time point (Table 3.6), which is interesting since MDM2 has been shown to be extensively involved in ribosomal pathways[88]. DNA-PK and nucleophosmin (NPM) were identified at multiple time points in the iTRAQ results and are known to interact with MDM2 at the N-terminal domain, where the Nutlin binding site is located[82, 103]. p53 interacting proteins identified include APEX1[97], SUB1[195] and HMGB1[196] suggesting the possibility that these are part of larger complexes or networks which participate in a response to Nutlin treatment either through direct interaction with MDM2 or further downstream. Other than known MDM2 binding proteins other notable proteins identified in this screen include VDAC proteins VDAC1 and VDAC2, which have been implicated in apoptotic pathways[197] and these were detected here elevated at later time points. Another interesting identification is IQGAP1 which is regulated by S100 proteins and altered in hepatocellular cancer[198].

3.9 Comparison of label-free PAcIFIC and iTRAQ MS screens

There were fewer proteins with changes in detected levels after Nutlin treatment identified by iTRAQ than by the PAcIFIC screen, despite the higher number of identifications. This is likely due to the very high stringency conditions applied for iTRAQ quantitation. The iTRAQ MS screen identified 359 out of 417 unique proteins identified by PAcIFIC, and 1024 proteins which were not detected in either PAcIFIC replicate (Figure 3.8). Although the iTRAQ coverage is much greater there are still proteins which were only identified by PAcIFIC. This may be because PAcIFIC is optimized for detecting lower abundance proteins. The iTRAQ results however, contain all of the known p53 and MDM2 related proteins identified by the PAcIFIC screen. Four proteins were detected in the highest confidence set of results which were detected by both screens at any time point, NONO, ribosomal protein L6, DNA-PK and paraspeckle component 1. Of these proteins only DNA-PK has previously been characterized as important in the p53-MDM2 interactome[82], however the others are new interesting new leads which may warrant further investigation. There are major differences in the quantitation between the two mass spectrometry screens. DNA-PK is the protein which occurs most frequently in both datasets over all time points, and is detected upregulated in the iTRAQ screen whereas it is seen as downregulated in the PAcIFIC screen. Paraspeckle component 1 and NONO also exhibit this contradiction, whereas ribosomal protein L6 is detected upregulated in both screens.

3.10 Discussion

A principal aim of the proteomics experiments carried out here was to find protein-protein interaction leads from proteomics data. In turn these candidates validate further

and can be used to expand the MDM2 interactome, either with more comprehensive proteomics or coupled with biological validation (Chapter Four, Five). Label-free (PAcIFIC) proteomics revealed an extensive list of potential hits. However there were insufficient replicates in this experiment to rely on this as stand alone data. Comparison with the iTRAQ screen, which makes use of stricter quantitation and statistical analysis, revealed both features in agreement with the PAcIFIC screen and also some notable differences. Although some proteins were detected at multiple time points in both experiments, the two different MS methods resulted in different quantitation results. For example DNA-PK appears downregulated in the PAcIFIC screen but upregulated in the iTRAQ screen. A major factor in these discrepancies could be localization, as each method used a different lysis method. A relatively mild lysis buffer was used with the PAcIFIC samples and SDS containing lysis buffer and sonication was used to lyse the cells for iTRAQ. It is likely that this would result in the iTRAQ samples containing more nuclear and membrane proteins than the samples analysed by PAcIFIC. Although the quantitation results for some proteins obtained are contradictory between the two methods, these results are still informative because they indicate changes occur in the MDM2 interactome either by change in protein levels or localization. MDM2 subcellular localization changes cell in response to different stimuli[199] and a change in localization can result in significant alterations in the interactome of a protein. Indeed the protein nucleophosmin, frequently detected in the iTRAQ screen has previously been shown to regulate MDM2 localisation[103]. Other quantitation issues include the fact that the methods in these screens do not actually measure the level of intact protein, but peptides from tryptic digests. This is why it is important in the case of iTRAQ to use

more than one unique peptide for quantitation. The quantitations obtained here are also relative rather than absolute, with each time point being compared to a control sample which has not been treated with Nutlin. This means that any errors in the control sample due to detection issues or sample preparation are propagated in the values calculated at the other time points. Spectral counting, although it has been shown to correlate well with protein abundance[176], requires normalization, very reproducible LC conditions and at least three replicates to be relied upon as a stand alone method. iTRAQ problems can include the compression effect[159], which results in a reduction the magnitude of change in iTRAQ ratio in complex samples, and requires correction for the relative intensities of labeling reactions. In particular the 113 m/z label is often more intense than the other labels, and it is therefore inappropriate to use this label as a control[159]. Despite these drawbacks the data acquired from these experiments provides a wealth of information, and although the approach was applied to the MDM2 interactome it could also be used to investigate the interactomes of other proteins.

Although only two technical replicates were examined for the PAcIFIC screen, and two biological replicates for the iTRAQ spectrometry screens, the time course format of this experiment allows greater confidence results which are detected at multiple time points. Each time point represents a separate lysis, digest and in the case of iTRAQ labeling step, and it is possible to observe trends over time. It is interesting that conflicting results were detected within the two replicates in the PAcIFIC screen, and some of these were observed over the whole time course in both replicates. One reason for this could be that if the protein is simply not detected in the control sample and it is detected at other time

points or vice versa it will appear to be up or downregulated. This problem may be solved by using more replicates for each individual time point.

Proteins identified by both screens can be classified based on whether they are up or downregulated, and many exhibit a continued trend over time. An example of this is HSP90, however some proteins appear to stabilise to their original level after an initial change for example Prohibitin-2. This may be similar to the oscillation of a feedback loop, such as that exhibited by p53[89], as observed by the slight decrease in level of p53 at 24 hours in Figure 3.1a, or indicate entry into another pathway quickly after modulation of MDM2 activity by Nutlin. It is also interesting to note the difference between the early 1-4 hours modulated proteins in the iTRAQ screen, including APE1, NDKA and nucleophosmin which are already known to be closely related to MDM2, and increasing numbers of as yet unrelated proteins identified as up or downregulated at later times. This may be due to the early effects of targeting MDM2 with Nutlin causing a cascade of downstream effects from proteins in complex or regulated directly by MDM2. This highlights the utility of analyzing proteomic data over time courses, rather than choosing a fixed window to look at the effects of a drug, which gives us an insight into the complexity of the interactome of a protein over time.

Although the label-free screen represents preliminary data, and more biological replicates are desirable for the iTRAQ screen, a number of interesting leads have been generated from these screens. Internal validation of the dataset is provided in both screens by the detected changes of known MDM2 binding and regulated proteins, such

as PCNA, DNA-PK, NPM and HSP90. In the PAcIFIC screen more of these proteins were identified in two replicates than a single replicate, illustrating the fact that identifications from multiple replicates are more reliable than those from single replicates. The presence of these known MDM2 and p53 interacting proteins increases our confidence that some of the other proteins identified may represent new participants in these pathways and interactomes, and as such may warrant futher validation. These proteins would require biological validation, further mass spectrometry replicates or a combination of both. For example the presence of the NDKA protein at all time points in the iTRAQ screen, and splicing factor U2AF from 2 hours onwards suggests that these are important components of the Nutlin response. The presence of a dense network of chaperone proteins (Figure 3.6, Table 3.1, Appendix 2) also links to an MDM2 role in proteostasis[9], which is recognised as a mechanism that cancer cells use to cope with the increased folding burden, and involves a balance between E3 ligases and degradation pathways with chaperones and ribosomal pathways. It has also recently been shown that the central proteome of a cell is centered around cell death, cell cycle, proteostasis and metabolism[200], which is significant for MDM2 because it has been implicated in a number of these functions. Metabolic enzymes identified in these screens such as DLDH and citrate synthase warrant further investigation of these pathways in relation to MDM2. It is interesting to speculate how much a small change in the interactome of a protein, as with using Nutlin to target MDM2, can potentially have massive effects on the cellular interactome. An alternative hypothesis would be that feedback loops and proteostasis mechanisms compensate for these changes, however in this case the

induction of cell cycle arrest or apoptosis by Nutlin treatment do suggest cellular changes after Nutlin treatment are substantial.

Absolute methods of quantitation such as those based on heavy peptide standards to obtain values corresponding to an absolute level of protein in the cell are being developed. One example of this quantifies ubiquitin bound proteins[201], and these methods mainly focus on sample preparation to get maximum reproducibility. If the strict requirements for a reliable proteomic experiment, such as number of replicates, are not followed precisely, it is essential to do further experiments to validate any pilot data obtained by quantitative proteomics experiment. Two different kinds of proteomic experiment were carried out here, label-free (PAcIFIC) and peptide labeling (iTRAQ), and we found agreement in identifications between the two methods, but with significant differences in the quantitation results we obtained. As lead generating experiments these screens have succeeded, and there are multiple interesting proteins which respond to Nutlin treatment. However there are many more questions raised regarding how the novel proteins found in these screens are regulated by MDM2, and what the actual effects of Nutlin are on these proteins. This validation can take the form of either further, more comprehensive proteomic mass spectrometry experiments, or biological validation of some of the leads obtained in these screens. Further work detailed in Chapter 4 and 5 describes biological validation methods used to further investigate the mass spectrometry results and their significance for the MDM2 interactome.

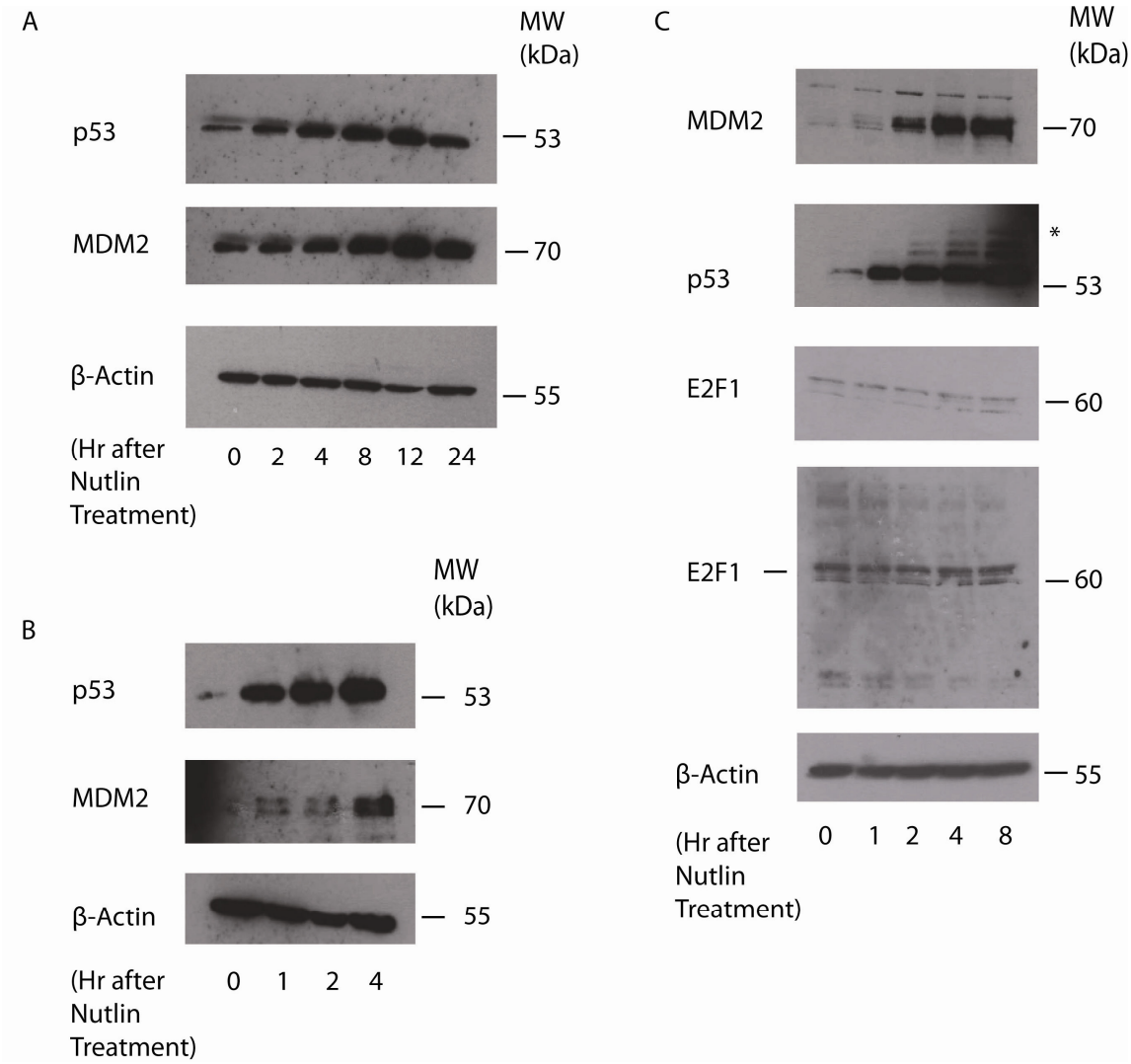

Figure 3.1 – MCF7 cells were treated with 40 uM Nutlin, lysed and proteins levels visualized by western blot (Antibodies described in section 2.3.3). β-actin levels were detected as a loading control. A) p53 and p21 increased protein levels after 40 μM Nutlin treatment at different time points for cells lysed with NP40 containing buffer. B) Early increase in p53 and late increase in MDM2 levels 1-4 hours after Nutlin treatment. C) p53, MDM2 and E2F1 levels in cells lysed in SDS containing buffer at various points after Nutlin treatment, ubiquitination bands indicated by asterisk. Apparent MW of principle band indicated on right of each blot.

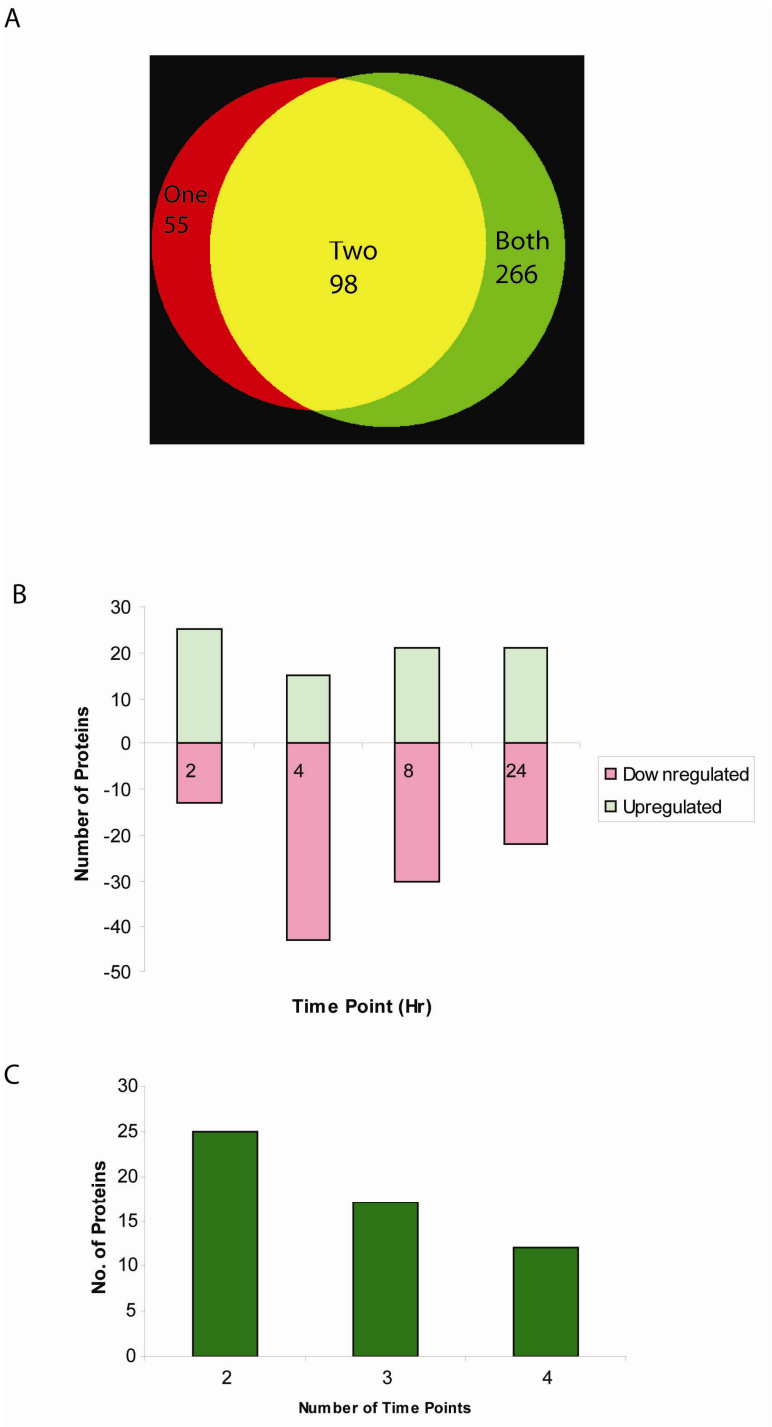

Figure 3.2 – A) Overall identifications between two replicates analysed by PAcIFIC MS/MS B) Number of proteins identified in two replicates at each time point quantified as up or downregulated two-fold by spectral counting C) Number of proteins identified at more than one time point

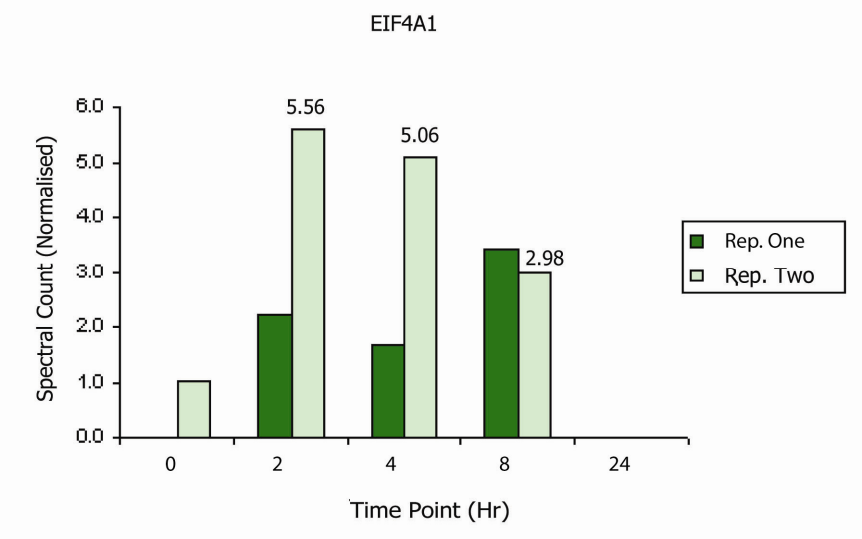

Figure 3.3 - Spectral counts at each time point after Nutlin treatment from PAcIFIC mass spectrometry screen for the protein EIF4A1. Counts are normalized based on the length of the protein sequence. Fold changes for replicate 2 are indicated by numbers on graph, for replicate 1 fold change was not calculated due to lack of detection in the 0 hour sample.

Acc.	Protein	Gene	FC 2Hr (1)	FC 2Hr (2)	FC 4Hr (1)	FC 4Hr (2)	FC 8Hr (1)	FC 8Hr (2)	FC 24Hr (1)	FC 24Hr (2)
Q13162	Peroxiredoxin-4	PRDX4	3.296	3.892	2.766	5.064	3.767	4.967	3.369	6.405
P14625	Endoplasmin (Heat shock protein 90 kDa beta member 1)	HSP90B1 GRP94 TRA1	3.570	5.931	4.150	2.813	4.521	6.292	6.002	6.405
Q14697	Neutral alpha-glucosidase AB	GANAB	4.760	3.707	4.426	3.939	4.521	3.312	4.633	5.338
P50454	Serpin H1 (47 kDa heat shock protein)	SERPINH1	4.760	2.780	4.426	3.376	4.144	3.726	5.896	4.003
P13667	Protein disulfide-isomerase A4	PDIA4	9.338	3.892	7.469	2.954	7.912	5.216	8.213	4.003
Q9Y5L4	Mitochondrial import inner membrane translocase subunit Tim13	TIMM13	Up	Up	Up	Up	Up	Up	Up	Up
P12004	Proliferating cell nuclear antigen (PCNA)	PCNA	2.197	2.224	2.213	3.376	2.637	2.980		
P60842	Eukaryotic initiation factor 4A-I (eIF-4A-I)	EIF4A1	Up	5.560	Up	5.064	Up	2.980		
P13010	X-ray repair cross-complementing protein 5	XRCC5	2.197	3.336			2.260	3.974	2.527	8.007
P12532	Creatine kinase U-type, mitochondrial	CKMT1A	9.887	2.780			5.651	3.477	6.317	3.203
P07237	Protein disulfide-isomerase (p55)	P4HB	3.042	3.830	3.320	4.689			3.888	3.737
Q15084	Protein disulfide-isomerase A6	PDIA6	3.515	3.336	4.648	3.135			3.790	2.974
Q9Y4L1	Hypoxia up-regulated protein 1	HYOU1	Up	Up			Up	Up		
Q9Y6X8	Zinc fingers and homeoboxes protein 2	ZHX2	Up	Up					Up	Up
Q969H8	UPF0556 protein C19orf10 (Interleukin-25) (IL-25)	IL25	Up	Up			Up	Up	Up	Up
Q8NBS9	Thioredoxin domain-containing protein 5	TXNDC5	Up	Up			Up	Up	Up	Up
P55145	Mesencephalic astrocyte-derived neurotrophic factor (Arginine-rich protein) (Protein ARMET)	MANF	Up	Up			Up	Up	Up	Up
Q9BSH4	Translational activator of cytochrome c oxidase 1 (Coiled-coil domain-containing protein 44)	TACO1	2.746	2.224					2.527	4.804
P23284	Peptidyl-prolyl cis-trans isomerase B (Cyclophilin B)	PPIB	2.197	Up	2.213	Up			3.369	Up
Q16740	Putative ATP-dependent Clp protease proteolytic subunit, mitochondrial	CLPP					3.391	Up	2.527	Up
P33991	DNA replication licensing factor MCM4 (CDC21 homolog)	MCM4			3.320	Up	3.391	Up		

Table 3.1 - Summary of upregulated proteins obtained at each time point after Nutlin treatment. Fold change (FC) of the spectral count of each protein for both replicates is shown, replicate indicated in brackets under time point. Where protein is not detected at either replicate at 0 Hr after Nutlin treatment proteins are categorised as 'up' for upregulated

Acc.	Protein	Gene	FC 2Hr (1)	FC 2Hr (2)	FC 4Hr (1)	FC 4Hr (2)	FC 8Hr (1)	FC 8Hr (2)	FC 24Hr (1)	FC 24Hr (2)
P53396	ATP-citrate synthase	ACLY	Down	Down	Down	0.563				
Q07065	Cytoskeleton-associated protein 4 (63 kDa membrane protein)	CKAP4			Down	Down	0.226	0.331	0.253	Down
P62834	Ras-related protein Rap-1A	RAP1A			Down	Down	Down	0.497	Down	Down
P42704	Leucine-rich PPR motif-containing protein, mitochondrial	LRPPRC			Down	Down	Down	0.248	Down	0.400
P58107	Epiplakin (450 kDa epidermal antigen)	EPPK1			0.383	0.169	0.087	0.199	Down	0.160
P50990	T-complex protein 1 subunit theta (TCP-1-theta)	CCT8	0.366	0.222			0.377	0.397	0.421	0.320
P28331	NADH-ubiquinone oxidoreductase 75 kDa subunit, mitochondrial	NDUFS1	Down	Down	Down	Down	Down	Down		
Q04637	Eukaryotic translation initiation factor 4 gamma 1	EIF4G1	0.366	Down	Down	Down				
P56385	ATP synthase subunit e, mitochondrial (ATPase subunit e)	ATP5I	0.471	Down	Down	0.422				
Q9Y383	Putative RNA-binding protein Luc7-like 2	LUC7L2	2.197	2.224	Down	Down				
Q9NX63	Coiled-coil-helix-coiled-coil-helix domain-containing protein 3, mitochondrial	CHCHD3			Down	0.281	0.161	0.331		
Q86U42	Polyadenylate-binding protein 2 (PABP-2)	PABPN1			Down	Down	0.283	0.497		
P54886	Delta-1-pyrroline-5-carboxylate synthase (P5CS)	ALDH18A1			Down	Down	0.161	N/A		
P30519	Heme oxygenase 2 (HO-2)	HMOX2			Down	Down	0.188	0.497		
P27824	Calnexin (IP90) (p90)	CANX			Down	0.375	0.323	0.221		
P11387	DNA topoisomerase 1	TOP1			Down	Down	0.452	0.331		
P62318	Small nuclear ribonucleoprotein Sm D3	SNRPD3			0.474	0.482	0.323	0.284		
P29401	Transketolase (TK)	TKT			2.490	5.064	3.391	3.974		
P60981	Destrin (Actin-depolymerizing factor) (ADF)	DSTN	0.275	0.477	0.415	0.482			0.316	0.229
P55011	Solute carrier family 12 member 2 (Basolateral Na-K-Cl symporter)	SLC12A2	0.366	Down	Down	Down			Down	Down
P78527	DNA-dependent protein kinase catalytic subunit (DNA-PK catalytic subunit)	PRKDC	0.471	0.318	0.474	0.241			0.361	Down
P43243	Matrin-3	MATR3					Down	0.397	0.421	Down
P30041	Peroxiredoxin-6	PRDX6					Down	0.331	Down	0.534
P20700	Lamin-B1	LMNB1					Down	Down	Down	Down
Q16891	Mitochondrial inner membrane protein (Mitofilin) (p87/89)	IMMT					0.141	0.284	0.316	0.458
O43290	U4/U6.U5 tri-snRNP-associated protein 1 (SNU66 homolog)	SART1	0.275	Down			Down	Down		
O95831	Apoptosis-inducing factor 1, mitochondrial	AIFM1	0.366	0.463			0.377	0.414		
P14314	Glucosidase 2 subunit beta (80K-H protein)	PRKCSH	2.563	2.224			2.826	2.129		
P51991	Heterogeneous nuclear ribonucleoprotein A3 (hnRNP A3)	HNRNPA3			Down	Down			Down	Down
P48643	T-complex protein 1 subunit epsilon	CCT5			Down	Down			Down	Down
Q92841	Probable ATP-dependent RNA helicase DDX17	DDX17			0.184	Down			0.281	Down
Q9UJZ1	Stomatin-like protein 2	STOML2	Down	0.477	Down	0.241	Down	0.426	Down	Down

Table 3.2 - Summary of downregulated proteins obtained at each time point after Nutlin treatment. Fold change (FC) of the spectral count of each protein for both replicates is shown, replicate indicated in brackets under time point. Where protein is not detected at either replicate at 0 Hr after Nutlin treatment proteins are categorised as 'down' for upregulated

A

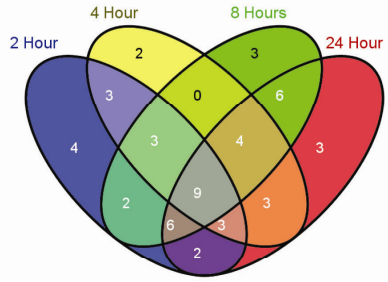

B

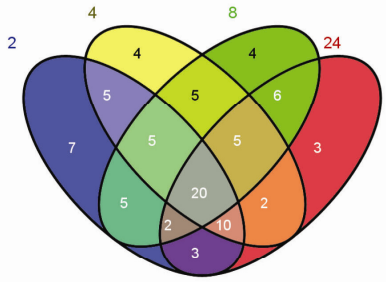

C

Acc.	Protein	Gene	0 Hr	2 Hrs	4 Hrs	8 Hrs	12 Hrs
O95292	Vesicle-associated membrane protein-associated protein B/C	VAPB	7.000	1.098	0	0	0
P40227	T-complex protein 1 subunit zeta (TCP-1-zeta)	CCT6A	5.000	2.197	0	2.260	1.263
O00148	ATP-dependent RNA helicase DDX39	DDX39	5.000	2.197	0	2.260	1.263
Q8NFV4	Abhydrolase domain-containing protein 11	ABHD11	0	1.098	3.319	3.390	2.526

D

Acc.	Protein	Gene	0 Hr	2 Hrs	4 Hrs	8 Hrs	12 Hrs
O75396	Vesicle-trafficking protein SEC22b	SEC22B	7.045	1.119	1.699	2.000	3.223
O75533	Splicing factor 3B subunit 1	SF3B1	5.032	1.119	0	1.000	0
P62753	40S ribosomal protein S6	RPS6	1.006	2.238	0	0	0
P27797	Calreticulin	CALR	1.006	7.835	5.097	7.000	6.447
Q9Y285	Phenylalanyl-tRNA synthetase alpha chain	FARSA	0	3.357	1.699	1.000	1.611
Q9NR28	Diablo homolog, mitochondrial (Smac)	DIABLO	0	1.119	1.699	4.000	3.223
Q96I99	Succinyl-CoA ligase [GDP-forming] subunit beta, mitochondrial	SUCLG2	0	3.357	1.699	3.000	1.611
P09493	Tropomyosin alpha-1 chain	TPM1	0	1.119	1.699	2.000	1.611
P07339	Cathepsin D	CTSD	0	10.073	1.699	7.000	4.835

Figure 3.4 – Overlapping identifications detected in single replicates at various time points. A) Replicate one; B) Replicate two. C) Spectral counts of proteins detected at multiple time points in replicate one excluding proteins which are only detected at one time point; D) proteins detected at multiple times in replicate two excluding proteins which are only detected at one time point.

Accession	Protein	Gene	Rep. 1 (Time after Nutlin Treatment (Hr))					Rep. 2 (Time after Nutlin Treament (Hr))				
			0	2	4	8	24	0	2	4	8	24
Q9BR76	Coronin-1B	CORO1B	1.000	0.000	0.000			1.007	2.239	1.699		
P11177	Pyruvate dehydrogenase E1 component subunit beta, mitochondrial	PDHB	4.000	1.099	0.000			1.007	2.239	3.398		
P45880	Voltage-dependent anion-selective channel protein 2 (VDAC-2)	VDAC2	2.000	5.493				8.052	2.239			
P06753	Tropomyosin alpha-3 chain (Gamma-tropomyosin)	TPM3	1.000	4.394				5.033	2.239			
Q8WU68	Splicing factor U2AF 26 kDa subunit	U2AF1L4	0.000	0.000	0.000	2.260	0.000	3.020	1.119	0.000	0.000	0.000
P62081	40S ribosomal protein S7	RPS7	0.000	1.099				1.007	0.000			
Q9UQ80	Proliferation-associated protein 2G4	PA2G4	1.000		0.000		0.000	0.000		0.000		1.612
Q9BQE3	Tubulin alpha-1C chain	TUBA1C	4.000		0.000			8.052		11.893		
Q00341	Vigilin	HDLBP	3.000		0.000	0.000	0.000	0.000		0.000	2.000	1.612
P62857	40S ribosomal protein S28	RPS28	1.000		0.000	0.000	0.000	0.000		1.699	1.000	1.612
O75607	Nucleoplasmin-3	NPM3	6.000		0.000			4.026		8.495		
O43175	D-3-phosphoglycerate dehydrogenase	PHGDH	5.000		1.660			1.007		3.398		
P62879	Guanine nucleotide-binding protein G(I)/G(S)/G(T) subunit beta-2 (G protein subunit beta-2)	GNB2	4.000		1.660			1.007		3.398		
P11142	Heat shock cognate 71 kDa protein	HSPA8	6.000		13.279			49.321		18.689		
O60506	Heterogeneous nuclear ribonucleoprotein Q (hnRNP Q)	SYNCRIP	2.000		4.979			9.059		3.398		
Q99798	Aconitate hydratase, mitochondrial	ACO2	1.000		3.320			5.033		1.699		
Q02878	60S ribosomal protein L6 (Neoplasm-related protein C140)	RPL6	1.000			0.000		0.000			1.000	
P18621	60S ribosomal protein L17	RPL17	3.000			0.000	0.000	0.000			1.000	3.224
B2RPK0	Putative high mobility group protein B1-like 1	HMGB1P1	6.000			0.000		4.026			9.000	
P11142	Heat shock cognate 71 kDa protein	HSPA8	6.000			14.693		49.321			21.000	
P08708	40S ribosomal protein S17	RPS17	9.000				2.527	3.020				6.447
Q99733	Nucleosome assembly protein 1-like 4	NAP1L4	3.000				1.263	1.007				3.224
P60660	Myosin light polypeptide 6	MYL6	2.000				6.317	7.046				3.224

Table 3.3 – Conflicting quantitation results over the 24 hour time course, spectral counts are shown for both technical replicates where the direction of regulation after Nutlin treatment (up or down) are contradictory between the two replicates.

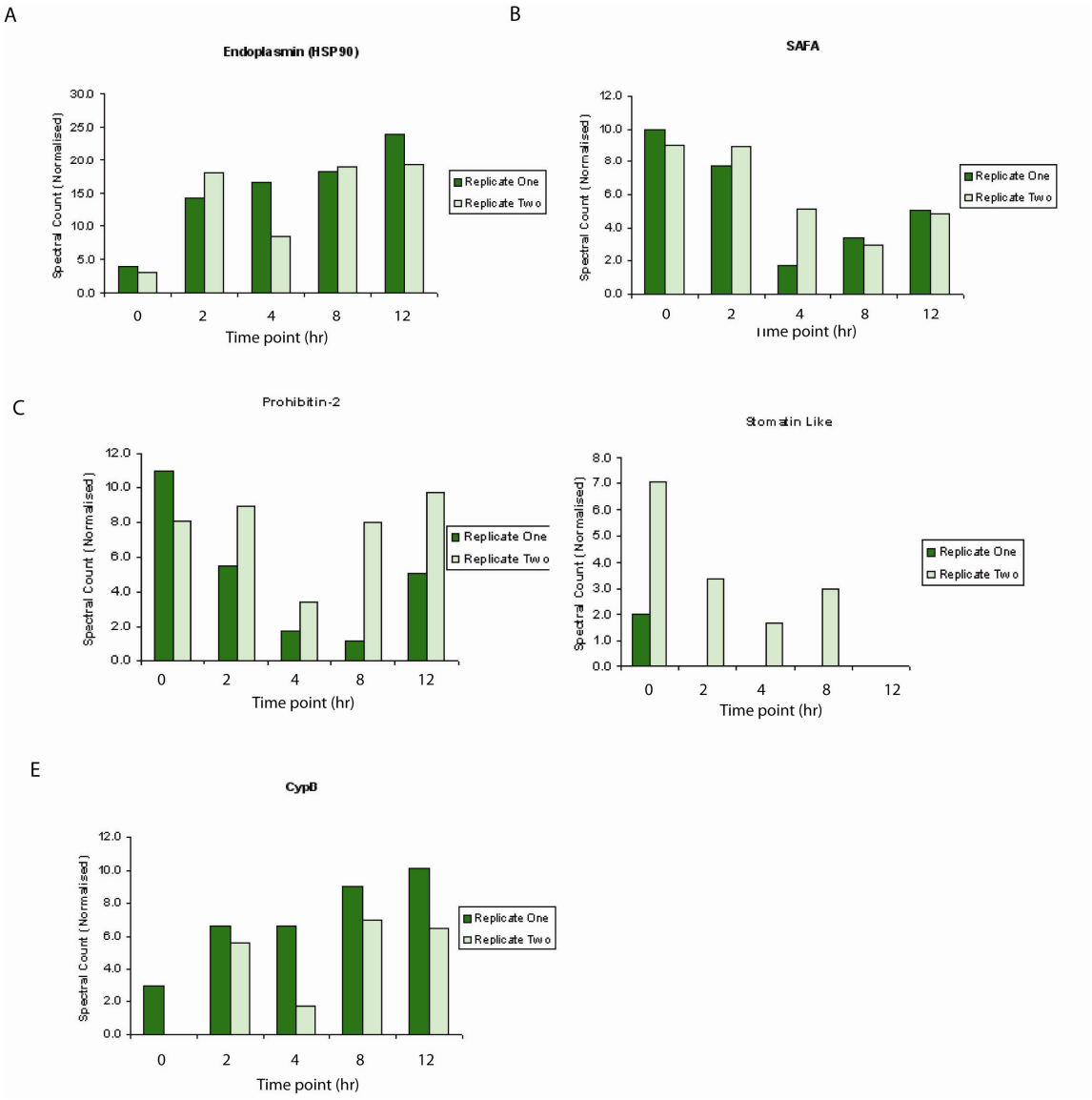

Figure 3.5 – Examples of protein regulation trends over the Nutlin time course, for a selection of known and unverified MDM2 interacting proteins. Spectral counts over time for known MDM2 binding proteins; A) HSP90 B) SAFA and unverified MDM2 binding proteins; C) Prohibitin-2 D) Stomatin-like protein 2 E) CypB.

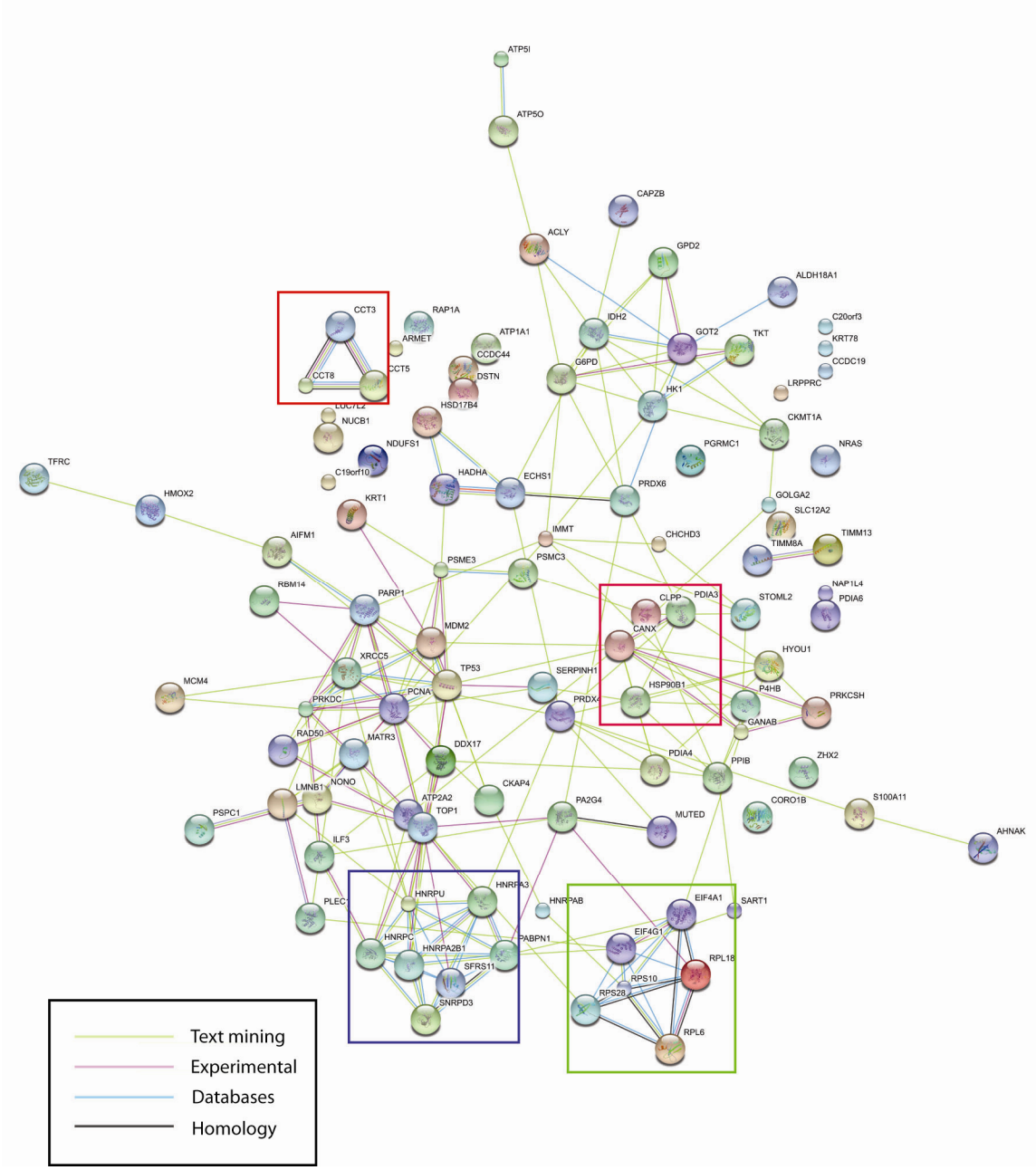

Figure 3.6 – Search tool for the retrieval of interacting genes/proteins (STRING) interaction network for proteins identified at each time point. Complexes are highlighted as follows, Pink – HSP90, Green – eIF and ribosomal proteins, Red – T complex proteins, Blue – hnRNPs. Colour of nodes does not represent function, larger nodes indicate that structural information is available for the protein represented.

iTRAQ Label	113	114	115	116	117	118	119	121
Sample (Hours post Nutlin)	1Hr	0Hr	2Hr	4Hr	8Hr	12Hr	2Hr (R)	12Hr (R)

Unused Cutoff	Proteins Detected	Proteins Before Grouping	Distinct Peptides	Spectra Identified	% Total Spectra
>2.0 (99)	1071	1341	13185	48921	84.2
>1.3 (95)	**1323**	**1579**	**13694**	**49980**	**86.0**
>0.47 (66)	1468	1770	14089	50595	87.1

Table 3.4 – Labelling scheme for 8-plex iTRAQ experiment and summary of results. Cut-off used highlighted in bold, >1.3 (95) represents the score assigned to each identification by protein pilot, 1.3 indicating 95% confidence in the identification.

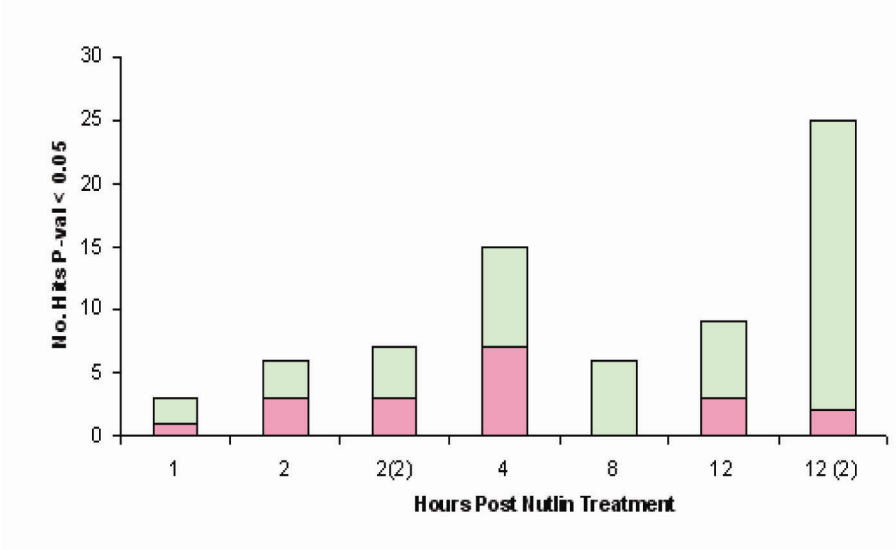

Figure 3.7 – Overview of number of proteins identified in iTRAQ results across the Nutlin time course which are up or downregulated and have a p-value <0.05 and a ratio of either >1.33 or < 0.77 relative to the control sample from cells which were not treated with Nutlin. Green – upregulated proteins, Red – downregulated proteins. (2) – Second biological replicate.

Protein	Gene	Peptide (95%)	1 Hr	P-Val	2 Hrs	P-val	4 Hrs	P-val	8 Hrs	P-Val	12 Hrs	P-val	% Cov.
Cleavage and polyadenylation specificity factor subunit 6	CPSF6	3	1.522	0.037			1.412	0.042					10.53
DNA - (apurinic or apyrimidinic site) lyase	APEX1	8	1.348	0.032	1.548	0.016							47.17
Nucleoside diphosphate kinase A	NDKA	13	0.757	0.001	0.656	0.017					0.685	0.040	73.68
Nucleophosmin	NPM	42					1.744	0.002	1.627	0.006			8.427
Splicing Factor U2AF 35kDa	U2AF1	9			1.347	0.008	1.429	0.002	1.378	0.030	1.572	0.004	55
Dihydrolipoyl dehydrogenase, mitochondrial precursor	DLDH	8					1.410	0.043	1.325	0.011			23.97
ATP Synthase D Chain, mitochondrial	ATP5H	6											49.07
4F2 cell-surface antigen heavy chain	4F2	9											41.59
Voltage-dependent anion-selective channel protein 1	VDAC1	16					1.428	0.002			1.392 (1.773)	0.000 (0.000)	59.72
Non-POU domain-containing octamer binding protein	NONO	12			1.478	0.009					1.386	0.003	41.61
DNA-dependent protein kinase catalytic subunit	PRKDC	23			1.415	0.000	1.652	0.000	1.377	0.001	1.497 (1.599)	0.000 (0.000)	18.31
Annexin A5	ANXA5	7			0.625	0.020							49.69
ADP/ATP translocase 2	ADT2	28					1.410	0.029	1.345	0.027			76.17
Cathepsin D precursor	CATD	9					1.410	0.043					34.71
Ras GTPase-activating-like protein IQGAP1	IQGA1	10					0.772	0.028					16.78
Phosphoglycerate kinase 1	PGK1	18					0.764	0.000					51.8
Ezrin-radixin-moesin-binding phosphoprotein 50	NHERF	12					0.748	0.004					34.36
High mobility group protein B1	HMGB1	14					0.747	0.001					55.81
Acidic leucine-rich nuclear phosphoprotein 32 family member E	AN32E	2					0.738	0.004					14.93
Peptidyl-prolyl cis-trans isomerase A	PPIA	21					0.737	0.006					90.91
Heterogenous nuclear ribonucleoprotein G	HNRPG	3									1.381	0.040	15.35
Voltage-dependent anion-selective channel protein 2	VDAC2	8									1.443 (1.734)	0.029 (0.021)	48.3
Heterogenous nuclear ribonucleoprotein D-like	HNRDL	4											28.81
Partitioning defective 6 homolog beta	PAR6B	3									0.714	0.000	25
Acidic leucine-rich nuclear phosphoprotein 32 family member B	AN32B	7									0.654	0.035	33.47
60S ribosomal protein L15	RL15	2									2.127	0.022	24.51
60S ribosomal protein L4	RL4	12									2.123	0.000	43.33
60S ribosomal protein L13	RL13	3									1.932	0.025	26.11
60S ribosomal protein L7a	RL7A	8									1.731	0.001	31.2
Acidic leucine-rich nuclear phosphoprotein 32 family member A	AN32A	9									1.630	0.039	35.34
60S ribosomal protein L28	RL28	3									1.596	0.029	43.8
Splicing factor, proline- and glutamine rich	SFPQ	12									1.561	0.002	31.54
60S ribosomal protein L6	RL6	7									1.551	0.000	50.35
Paraspeckle component 1	PSPC1	4									1.494	0.001	21.8
B-cell receptor-associate protein 31	BAP31	7									1.476	0.002	38.62
Cytochrome c oxidase subunit 5A, mitochondrial precursor	COX5A	7									1.463	0.016	62.67
60S ribsoxomal protein L8	RL8	5									1.435	0.007	29.96
Transmembrane protein 43	TMM43	3									1.429	0.013	20.75
60S ribosomal protein L21	RL21	5									1.418	0.032	36.25
40S ribosomal protein S9	RS9	5									1.400	0.003	54.64
Protein S100-A13	S10AD	3									1.351	0.035	59.18
Adenlylate kinase isoenzyme 2, mitochondrial	KAD2	7									0.682	0.010	48.12
Phosphate carrier protein, mitochondrial precursor	MPCP	4									1.346	0.022	41.99

Table 3.5 – All iTRAQ up and downregulated identifications with p-value < 0.05 represented as ratio to control (untreated) sample. Values in brackets represent identifications from the second biological replicate. % Cov. – percentage coverage of protein sequence detected.

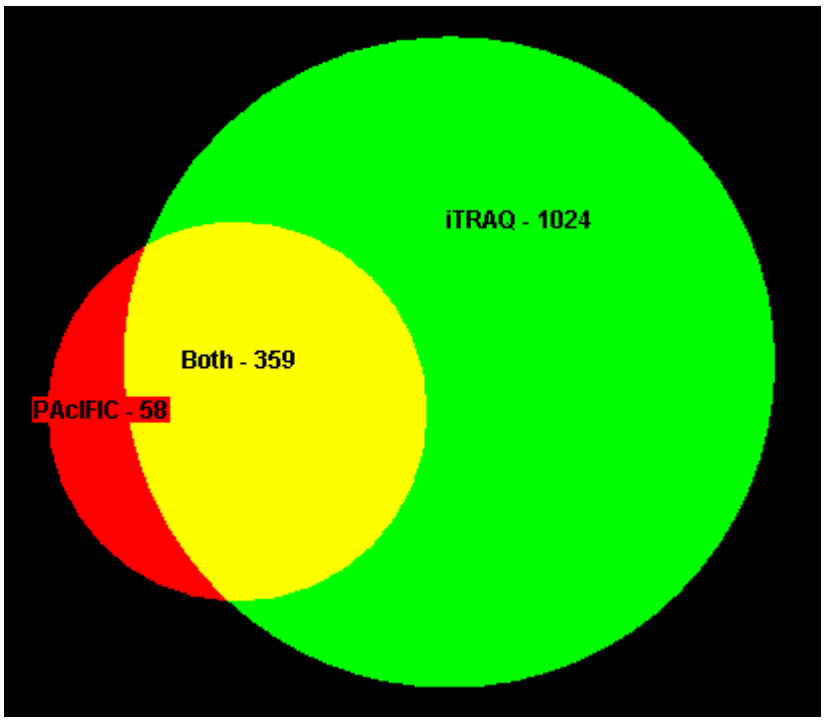

Figure 3.8 – Overlapping PAcIFIC and iTRAQ identifications

4 - Identification and validation of new MDM2 binding peptides derived from proteins affected by Nutlin treatment

4.1 Introduction

Quantitative shotgun proteomic mass spectrometry can yield a large amount of information, as shown in Chapter Two, which creates the problem of finding meaningful results in a substantial dataset. It could be argued that all proteins identified exhibiting an altered response to Nutlin in Chapter Two warrant further investigation. As this is not feasible here a subset of proteins were selected to be validated biologically. MDM2 has been shown to participate in networks extensively based on the ability to bind linear motifs[80], and the MDM2-p53 interaction is a model example of this[91]. The large disordered region in the acidic domain of MDM2 also makes it a likely candidate for interacting via linear motif mechanisms. A screen was carried out on the MS leads acquired in this experiment for the presence of motifs homologous to p53, and peptides corresponding to these motifs were investigated for MDM2 binding.

4.2 BOX-I like loose consensus motif

The BOX-I region of p53 includes F19, W23 and L26 (Chapter One). It has previously been shown that the MDM2 binding protein IRF2 has a BOX-I like sequence and a BOX-V like sequence[81], which is also found in the other IRF family member IRF1 (Figure 4.1a). The core tryptophan residue which is mimicked by Nutlin in the case of BOX-I[133] is replaced by a tyrosine in the IRF peptides and the leucine which is also mimicked by Nutlin is also present. The phenylalanine which is mimicked by Nutlin is

not found in either IRF1 or IRF2 sequence and is replaced by an alanine in these peptides. A hydrophobic residue to the N-terminus (Position 11) of the aromatic residue is found in all three peptides, as is a proline to the C-terminus of the core hydrophobic section. In the centre of the conserved hydrophobic residues in this motif is a positively charged residue; a lysine (BOX-I) or an arginine (IRF1, IRF2). The IRF1 and IRF2 peptides also contain a charged region at the C-terminus of the sequence which is not present in the BOX-I sequence. Two very loose consensus motifs were constructed based on these hydrophobic and aromatic core residues found in both BOX-I and IRF peptides (Figure 4.1b). These low complexity motifs were chosen to select peptides with variation around this hydrophobic core.

4.3 Comparison of BOX-I and IRF peptides binding to MDM2

Relative binding of BOX-I and IRF peptides shown in Figure 4.1 to full-length recombinant MDM2 was measured by ELISA (Figure 4.2a). The BOX-I peptide bound MDM2, purified by cleavage from a GST tag, to a greater extent than both IRF peptides. However although SP column purified MDM2 still bound all three peptides, BOX-I bound this MDM2 to a lesser extent than the IRF peptides (Figure 4.2b, c). This indicates that the purification method affects MDM2 peptide binding, possibly due to the retention of cofactors by one method and not the other. Zinc competes BOX-I well, however it only has an effect on IRF peptides binding at higher concentrations (Figure 4.2d) suggesting that zinc is a potential cofactor retained by SP column purification which affects BOX-I binding. These data taken together demonstrate that although the BOX-I and IRF peptides both bind MDM2 there are potentially differences in the

binding site or mechanism by which MDM2 binds these peptides. BOX-I has a Kd of 440 nM for MDM2 compared with 90 nM for Nutlin[131, 133], hence the efficacy of Nutlin as an MDM2-p53 protein-protein interaction inhibitor. Interestingly, the IRF1 and IRF2 peptides do not exhibit this response to Nutlin or BOX-I (Figure 4.3b) and are competed effectively by the RB1 or BOX-V peptides (Figure 4.3d, e) which bind the MDM2 acid domain and mildly compete with BOX-I. IRF1 and IRF2 peptides may bind a different region of MDM2 than BOX-I or bind the hydrophobic domain in a site it is not possible for Nutlin to compete for.

4.4 Screening of mass spectrometry hits using BOX-I like motif

Using the loose consensus motif which links IRF and BOX-I peptides, the mass spectrometry results from the 2 hour time point of the PAcIFIC mass spectrometry screen were searched using prosite[202] for the presence of BOX-I like motifs. Low confidence (ie/ single replicate) hits were also included. The stricter motif containing the charged residue in the centre of the motif was found in 38 proteins, and the looser motif was found in 145 proteins (Figure 4.4). A number of proteins contained multiple occurrences of this motif, notably DNA-PK which contains 28 instances of the motif.

4.5 Investigation of peptides corresponding to the motif by ELISA

Peptides corresponding to the core motif sequences found in these proteins, along with the 5 N-terminal and 10 C-terminal surrounding residues, were screened by ELISA for binding to full length MDM2. After removing peptides with very low complexity or located in the transmembrane region of membrane proteins, 94 peptides containing the

motif (Appendix 3) were tested by ELISA for binding to MDM2 and 20 peptides from the total tested showed some binding to MDM2. These binding peptides were categorized based on how stable the extent of this binding was relative to BOX-I (Figure 4.5). A subset of peptides actually exhibited a higher level of binding by ELISA than BOX-I, others exhibited an intermediate amount of binding (Figure 4.5a, b), whereas some were weak or very weak binders (Fig 4.5c, d). The affinity of BOX-I for MDM2 is approximately 400 nM[131], therefore it is important to note that those binders classed here as 'weak' exhibit in this assay around 10% of the BOX-I to MDM2 interaction intensity. These peptides are therefore weak in comparison to BOX-I, but still bind MDM2 higher than the background level. To further validate these motifs, peptides with the critical core aromatic residue mutated to an alanine were compared to the wild type peptides (Figure 4.6). In most cases the substitution of this residue resulted in a loss of binding to full length MDM2, highlighting the importance of this residue in the motif as previously reported[131]. Exceptions are the reptin peptide which is unaffected by the W to A mutation, and the UBF1, SERCA2 and IL25 peptides which show enhanced binding with the alanine mutation (Fig 4.6 a, b). This could be experimental error, or demonstrate that these peptides are non-specifically binding to MDM2. This confirms that the majority of the peptides selected depend on the core motif aromatic residue for binding to MDM2.

Alignment of the peptides which bind to MDM2 (Figure 4.7) reveals two of the stronger binding peptides RPS7 and APIF-1 have a proline to the C-terminus of the core motif, correlating with the BOX-I and IRF peptides. 11 out of 20 new MDM2 binding peptides

have a positively charged residue in the centre of the hydrophobic motif, and none of these peptides are categorized as weak binders. 8 out of the 20 new peptides identified have a charged region at the far C-terminus of the motif similar to the IRF peptides, and for the weaker binders this frequently includes negatively charged residues alongside the positively charged residues. RPS23, calreticulin and RAB8A peptides have tyrosine or phenylalanine in position 3 which has previously been shown to be important for BOX-I binding into the hydrophobic pocket[131]. The ERp60 peptide has very low complexity around the motif, which may contribute to nonspecific binding to hydrophobic regions of MDM2.

Overall the peptides which bind MDM2 compared to those which did not bind by ELISA have a higher representation of arginine residues in the core and N-terminal to the core motif, and are more likely to have a leucine/proline directly to the C-terminal of the core motif, and an aspartate at position 14. For an initial investigation this was calculated by noting the number of times a residue occurred in a peptide and counting it as 'over-represented' if it occurred in more than 20% of the peptides (Figure 4.8), a method which has previously been used to examine DAPK binding peptides[203]. Non-binding peptides did not have any over-represented residues other than the core residues which were set in the prosite search, in particular there were no over-represented positively charged amino acids in the core of the motif. Leucine, valine, tyrosine and phenylalanine were more likely to appear than tryptophan, isoleucine and methionine, which may be due to the lower occurrence in general of the latter amino acids.

4.6 Competition assays with known MDM2 ligands

Similarly to the IRF peptides, Nutlin does not compete with all of the newly identified MDM2 binding peptides (Figure 4.9b). The peptides from nTPR, SNF2L4, SERCA2, Mitofilin RAB8a, calreticulin and SFRS11 are competed by Nutlin. However the DBC1 peptide is enhanced by Nutlin, an effect which has previously been observed for acid domain ligands. BOX-I has a less pronounced effect than Nutlin as a competitor, with very few peptides competed by BOX-I (Figure 4.9c). The RAB8A peptide which is competed well by Nutlin is also competed by BOX-I. Some peptides are enhanced for MDM2 binding by the addition of BOX-I. For example the peptides from DBC1, SNF2L4, calnexin and ERp60 all show increased binding with a higher concentration of BOX-I peptide. RB1 competes many of the peptides to a greater extent than it does BOX-I; including the IRF peptides as previously seen (Figure 4.9d). Unexpectedly, enhancement of MDM2 binding to some peptides is caused by RB1, the peptides derived from RPS23, SFRS11 and calnexin for example. The enhancement of the RPS23 peptide is quite pronounced, as this is a very weak binder when no other ligand is present. We can therefore classify the newly identified MDM2 peptides based on which MDM2 ligands compete or enhance their binding (Fig 4.9e).

4.7 Peptide binding to the N-terminal domain of MDM2

BOX-I binds to the N-terminal domain, amino acids 1-126, of MDM2 with a higher intensity than any of the newly identified peptides (Figure 4.10). Many of the newly identified peptides do show some binding to this domain which is abrogated by the aromatic to alanine mutation in the core motif (Figure 4.10a). RPS23 and RAB8A do not

appear to bind the N-terminal domain in isolation. Nutlin is effective in competing many of the peptides from the N-terminal domain, however it should be noted that BOX-I is not competed as effectively from the N-terminal domain alone as it is from full-length MDM2 (Figure 4.10b, c).

4.8 Thermal denaturation assay - full-length MDM2

Thermal denaturation assays determine the melting point of a protein by measuring the amount of fluorescence of a probe, sypro orange, which is active when bound to hydrophobic regions of a protein. As the temperature is increased the protein unfolds revealing different hydrophobic sites, and the probe fluorescence is altered. The temperature at which the protein melts can be increased by stabilising ligands binding to a protein (Figure 4.11a)[204]. Full length MDM2 is somewhat resistant to thermal denaturation, with no clear melting temperature, but a broad melt-peak between 70-85°C (Figure 4.11b, c). This could be due to the high degree of disorder in the acidic domain, which might result in a large unstructured region of the protein resistant to thermal denaturation. MDM2 is also unusual in that it appears to bind sypro orange prior to denaturation which it is proposed is due to the dye binding into the hydrophobic pocket, resulting in high initial fluorescence[137]. Nutlin binding reduces this initial background presumably due to displacement of the dye bound in the hydrophobic pocket and this effect also contributes to the increase in visibility of the melt-peaks after addition of Nutlin. As previously observed for the N-terminal domain of MDM2[137], in the presence of Nutlin it is possible to see a melting point with full-length MDM2, which in this case is 83°C, with a secondary melt-peak visible at 56°C (Figure 4.11d, e). Binding the BOX-

I peptide results in a similar effect, with the main melt peak at 81°C. However in this case there is no secondary melt-peak (Figure 4.11f, g). This is in keeping with a model that Nutlin binds MDM2 with a higher affinity than BOX-I and therefore results in a more defined stabilization. The acidic domain binding peptide RB1 does not enhance the melting temperature of MDM2 and no clear melt-peak is visible (Figure 4.11h, i). As previously observed, Nutlin decreases the initial background reading of the assay (Figure 4.11b, d). RB1 actually increases this initial background, in contrast to the N-terminal binding ligands (Figure 4.11h), and this is also observed with the N-terminal domain of MDM2 which does not contain the RB1 binding site (Figure 4.13h). This may be due to the relatively high background observed with RB1 peptide alone, indicating that dye can bind the RB1 peptide itself. Interestingly, BOX-I slightly increases the initial background also, opposite to the effect observed with Nutlin (Figure 4.11f).

The IRF2 peptide does not have a similar effect to BOX-I and Nutlin on full-length MDM2. Two other newly identified peptides, one from RPS7, from a known MDM2 binding protein, and the CypB peptide were investigated in this assay. The RPS7 peptide does not cause a similar increase in melting temperature to Nutlin and BOX-I, however it does shift the broad minimum seen with ligand free protein to a higher temperature (Figure 4.12a, b). The CypB peptide has a substantial background fluorescence, which is likely caused by sypro binding to the peptide therefore at this concentration it was not possible to determine whether or not this peptide binds full-length MDM2 (Fig 4.12c, d). IRF2 and S7 peptides both increase the initial background relative to ligand free full length MDM2.

4.9 Thermal Denaturation Assay – N-Terminal MDM2 construct

Unlike full-length MDM2 the N-terminal domain of MDM2 in isolation does have a melt peak and this occurs at around 81°C. N-terminal MDM2 also has obvious melt peaks after the addition of Nutlin (Figure 4.13 a-d). Addition of Nutlin results in an increase in melting temperature for the N-terminal domain from 81°C to 85°C. This indicates that the N-terminal domain in isolation may be more stable than full-length MDM2 which has a melting temperature of 83°C after the addition of Nutlin (Figure 4.11c). Another possiblility is that the N-terminal domain of MDM2 binds Nutlin more effectively than full length MDM2. This is supported by the earlier observation that Nutlin competes BOX-I less effectively from the N-terminal domain in isolation (Figure 4.10). A secondary melt peak after the addition of Nutlin was also observed at 54°C. When BOX-I is added as a ligand the higher melting temperature is 81°C for full length MDM2 and 82°C for N-terminal MDM2, which fits with the model that BOX-I binds the same site as Nutlin with a lower affinity (Figure 4.13e, f). It is notable that MDM2 with BOX-I peptide has a higher melting temperature than with Nutlin at the earlier melt-point observed, from 54°C with Nutlin to 57°C with BOX-I. There is also a more distinct peak at 75°C which appears as a shoulder on the melting transition at the higher temperature when Nutlin is present. This may be because Nutlin stabilizes both higher melting transitions so the shoulder is better resolved with a less effective ligand, such as BOX-I. IRF2 peptide does not exhibit the earlier peak which is stabilized by BOX-I (Figure 4.14a, b), however the higher melting temperature is stabilized to 82°C in the N-terminal domain from 81°C in the protein without ligand. The S7 peptide and CypB

peptides do not stabilise the higher melting temperature, and actually have a negative effect on this melting temperature (Figure 4.14 c-f), however they do stabilise the earlier melting temperature. A low concentration of the CypB peptide was used to overcome the effect of the high background observed for this ligand with full length protein. With Nutlin the first melt-peak observed is 54°C, increasing to 57°C with the S7 peptide and 60°C with the CypB peptide. Nutlin and BOX-I both decrease the initial background for the N-terminal construct, unlike for full-length MDM2 where BOX-I slightly increases the initial fluorescence background. All the other peptide ligands, particularly RB1, increase the background however as before this may be due to dye binding the peptide ligands. Thermal denaturation melting temperatures and background levels are summarized in Table 4.1.

4.10 BOX-V-like sequences

MDM2 has multiple known peptide binding partners, including the second p53 binding site BOX-V. BOX-V does not have a well defined consensus sequence as there is for BOX-I, therefore the BOX-V peptide was used in a protein BLAST (NCBI) search against the proteins which are altered 2 hours after Nutlin treatment. 18 proteins were returned from this search, and peptides corresponding to the BOX-V like region tested for binding to MDM2 (Figure 4.15). The peptides which bound to MDM2 were derived from the proteins TRIM33, PCNA, RPL11 and elongin. RPL11 was not a hit at 2 hours in the PAcIFIC screen but was included as a known MDM2 binding protein containing this motif.

4.11 Discussion

The strategy used in this study to filter the large amount of proteomic mass spectrometry data was to search for motifs which are known to bind to MDM2 in the proteins which are upregulated at an acute time. The acute time was chosen because at this early stage the changes in protein level observed are more likely to be due to stabilization or destabilization on a proteomic level rather than further downstream effects. Nutlin directly inhibits protein-protein interactions at the MDM2 N-terminus[133], and allosterically regulates other MDM2 domains[91], therefore proteins detected by the mass spectrometry screen which are altered by Nutlin treatment can potentially bind either the N-terminal or other domains of MDM2. Highlighting the importance of MDM2 allostery is the observed increase in binding of BOX-I to GST purified MDM2 compared to SP column purified MDM2. The most likely reason for this is the presence or absence of another co-factor which inhibits BOX-I binding, candidates include RNA[80], zinc[80], ATP[61] or protein binders which may be retained by purification. The purification method does not affect the IRF peptides binding and the question this raises is whether these peptides bind the N-terminal domain of MDM2, a different domain, or indeed multiple domains. Addition or chelation of these cofactors in each MDM2 preparation may be a method to isolate how each of these ligands regulates MDM2.

The disordered acidic domain of MDM2 could adopt a more defined conformation in the presence of ligands, also known as disorder-to-order transition[205]. This may be a crucial part of the allosteric mechanism mediating MDM2 interactions. It could also be significant on both sides of the interaction, as linear motifs are frequently associated

with disordered regions of proteins[115] and highly disordered proteins such as p53 interact with MDM2 via linear motifs[95]. The allosteric mechanism of MDM2 coupled with speculation about the oligomeric status of MDM2 means many questions remain about MDM2 ability to bind peptide ligands, and how specific MDM2 consensus sequences are, so it was interesting to observe here the difference between IRF peptides and BOX-I binding and compare them to newly discovered MDM2 binding peptides.

IRF2-MDM2 binding has been shown to depend on residues found in the core hydrophobic motif which is similar to BOX-I[81]. The consensus motif used to search this data, [Hyd]-[Aro]-x-x-[Hyd], was deliberately chosen to have a very low level of complexity and likely high rate of occurrence in many proteins due to the high variability allowed by this motif. With a secondary peptide binding screen, the large amount of proteins containing this motif could then be narrowed down to those peptides which can bind MDM2 and further similarity with the BOX-I and IRF peptides it is constructed from could be found. Indeed, it seemed that a positively charged residue at the centre of this core was beneficial, as was an aspartate at position 14. Previous studies with the BOX-I peptide and PMI inhibitor have confirmed the importance of the core residues mimicked by Nutlin[131]. The threonine adjacent to the phenylalanine in position three and the proline directly C-terminal of the core motif can actually enhance BOX-I-MDM2 binding when converted to an alanine, highlighting the variability which may be permitted around core residues. Drawbacks with this approach include identification of so many peptides, however it could be argued that many consensus motifs have low complexity, and that residues around the core motif can influence binding such as in the

case of TPR binding HSP90[206]. With advances in peptide arrays testing thousands of peptides for binding to a protein is rapidly becoming more high-throughput[207]. There are numerous examples of proteins recognizing 'non-canonical' motifs which act in the same way as those fitting a consensus, for example the 14-3-3 proteins have an extremely large interactome based on linear motif binding[208].

The peptides obtained containing this BOX-I like motif exhibited a range of binding levels in comparison with BOX-I, this is interesting because transiently binding proteins may be vital in the MDM2 interaction whereas studies which normally focus on high affinity ligands may overlook transient interactions. Cell signaling pathways rely on transient binding to transmit information, and MDM2 is at the hub of a number of signaling pathways including ribosomal regulation[96, 99], p53 regulation[47], mRNA translation[59] and transcriptional regulation[106] where this type of interaction may be important. It is possible that part of the reason why the p53-MDM2 interaction is so widely characterized because it is an example of a very high affinity interaction, and these interactions are readily detected.

The competition assays with known MDM2 ligands further reveals the high degree of complexity of MDM2 peptide binding. Peptides such as RAB8A, SNF2L4 are competed by Nutlin similarly to BOX-I. Many of the other peptides however do not respond in the expected manner, including the IRF peptides previously identified as important for MDM2 binding. Further increasing the complexity of MDM2 peptide binding models, RB1 is competitor of many of these peptides but enhances the binding of some other

peptides. The extremely weak binder RPS23 is greatly enhanced in the presence of RB1, suggesting that the RB1 peptide opens a previously hidden binding site. This is possibly the hydrophobic pocket, or an as yet uncharacterized region in another domain of MDM2. Recent studies have shown the 'open' or 'closed' state of the hydrophobic pocket is extensively regulated by the MDM2 lid[65], and possibly the C-terminus of p53[38]. These studies suggest that the regulation of this domain is extremely dynamic.

Comparison of full length MDM2 to the N-terminal domain the thermal denaturation assay reveals that the melt-peaks are much clearer in the N-terminal domain construct. This is potentially because the melt-peaks observed for full-length MDM2 represent the N-terminal domain, as the acidic domain is disordered and may not exhibit a melt over this temperature range and the RING domain is very thermostable. The multiple melt-peaks observed hint at a multi-stage unfolding mechanism, with part of the protein becoming denatured followed, at a higher temperature, by a more stable core analogous to what has been previously observed by limited trypsin proteolysis of full-length MDM2[91]. Different ligands stabilization of different peaks suggests that these ligands bind different parts of the N-terminal domain than BOX-I, or bind by a different mechanism. The thermal denaturation assay on full-length MDM2 also intriguingly suggests a two way allosteric mechanism, with the RB1 peptide increasing sypro binding at the hydrophobic pocket. However the high background fluorescence of this peptide means further work is needed to determine if this effect is genuine. This agrees with computer modeling observations about the regulation of hydrophobic pocket binding being regulated by various MDM2 ligands and domains[136]. If acidic domain ligands can

change the confirmation of the N-terminal domain this could open or close the pocket, by regulating either the N-terminal domain itself or the lid[139]. The charged region on the IRF peptides and some of the new candidate peptides may be a factor in the binding of these peptides to MDM2. Since studies have shown the BOX-I binding interaction initially depends on docking via charge interactions outside the MDM2 pocket before intercalating into the same binding site that Nutlin occupies[108]. If these peptides are not very efficient at binding deep into the hydrophobic pocket Nutlin may not be able to compete these peptides effectively. Although the pattern of stabilization is not the same as for Nutlin, the newly identified MDM2 ligands S7 and CypB both have an effect on the N-terminal domain of MDM2, indicating that they can bind there. Further work to determine how these peptides bind MDM2 could include peptide arrays replacing each amino acid with every other amino acid, and more in depth kinetics assays such as fluorescence polarization, fluorescence resonance transfer methods or surface plasmon resonance. MS mapping or ion mobility MS to investigate MDM2 conformation would also clarify the MDM2 peptide binding mechanism. MDM2 can be described as a highly allosteric peptide binding protein, with extensive cross-talk between domains based on the results showing the effect of different ligands on different MDM2 binding peptides.

The next obvious step after identifying MDM2 binding peptides derived from proteins altered by Nutlin treatment is to investigate whether the peptide binding translates to full-length protein binding, and whether the effects of Nutlin on MDM2 are limited to the inhibition of MDM2 functions previously described. Although Nutlin reactivates p53[133], newly identified MDM2 proteins containing this motif, or validated for MDM2

binding in another way, may have a completely different response to Nutlin. The proteins identified in the MS screen, or containing a BOX-I like motif may behave like p53, E2F1 or an as yet unidentified class of MDM2 ligands and investigating these further will expand the known MDM2 interactome. Chapter 5 is an investigation of the effects of Nutlin on proteins *in vivo* characterization of full length candidate proteins binding MDM2 *in vitro*, to address these questions.

A

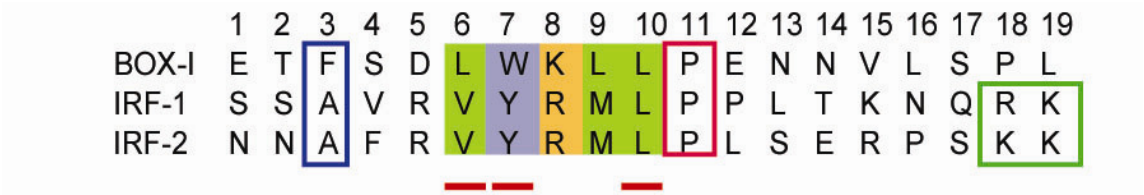

B

[LIVM]-[WYF]-[RK]-x-[LIVM] **[LIVM]-[WYF]-x-x-[LIVM]**

[Hyd]-[Aro]-[Pos]-x-[Hyd] **[Hyd]-[Aro]-x-x-[Hyd]**

Figure 4.1 – A) Alignment of BOX-I region of p53 with the IRF1 and IRF2 corresponding region. Residues essential for IRF binding MDM2 underlined in red, F residue important in BOX-I binding highlighted in blue, charged region only present in IRF peptides highlighted in green and proline highlighted in pink. B) Consensus motifs based on residues in position 6-10 constructed from this alignment, Hyd – Hydrophobic, Aro – Aromatic, Pos – Positively charged.

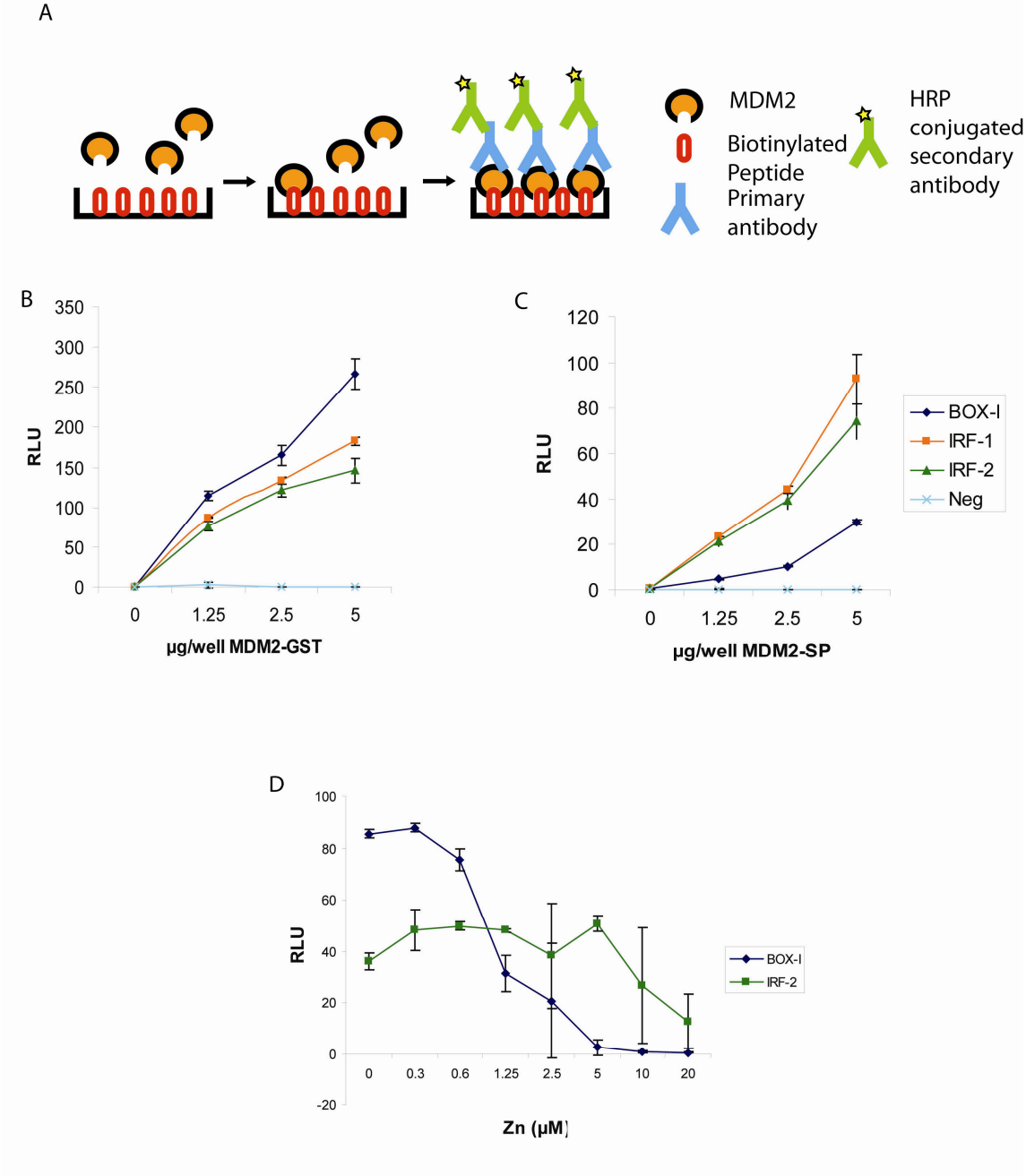

Figure 4.2 – A) Schematic of ELISA peptide binding assay. B) Binding of FL-MDM2 purified from cleavable GST tag to biotinylated BOX-I, IRF1 and IRF2 peptides (sequence as in Figure 4.1) and C) Binding of FL-MDM2 purified by SP column to peptides D) Zinc chloride competition ELISA of 2.5 µg/well MDM2 from BOX-I and IRF peptides immobilized as in B and C.

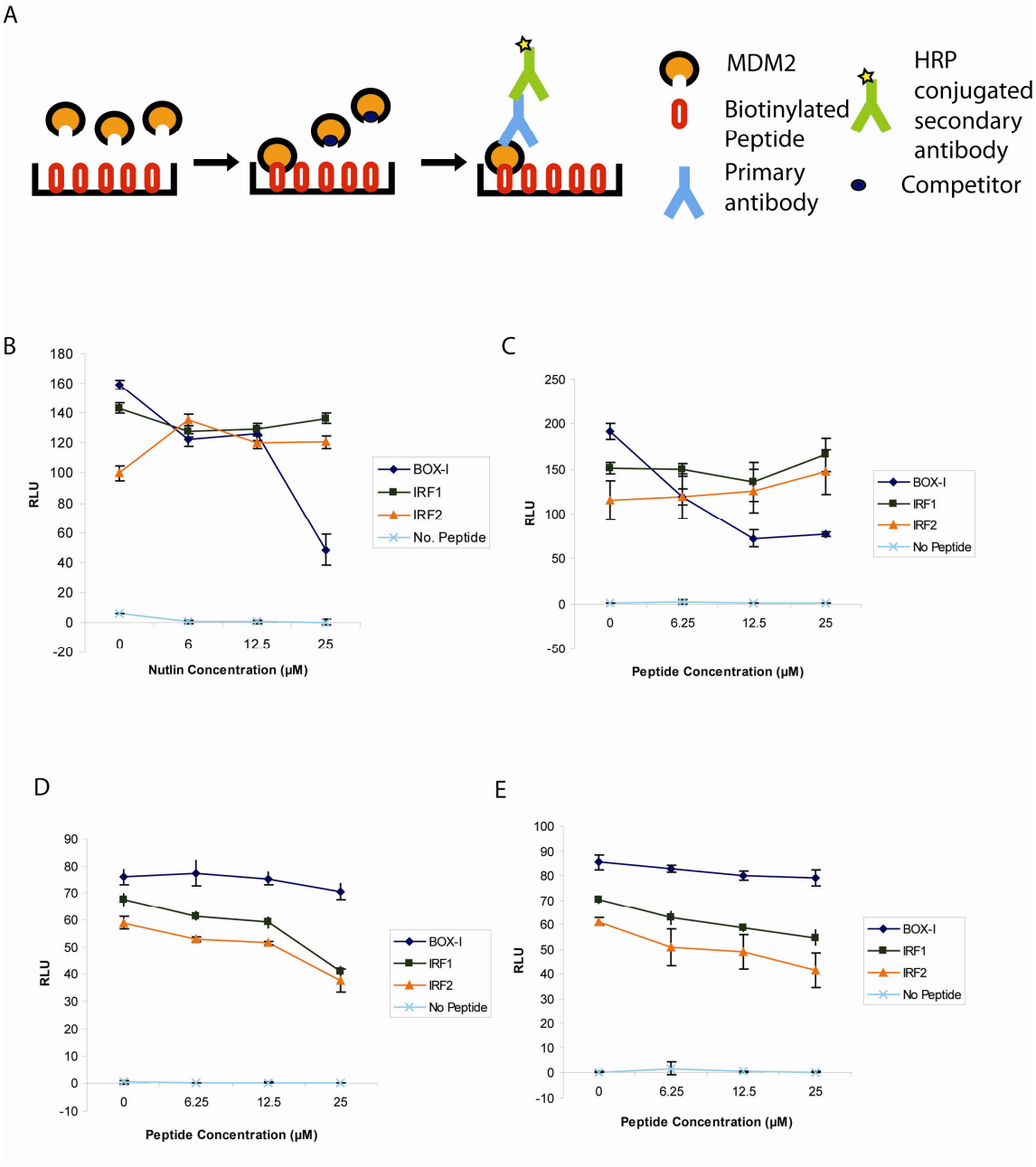

Figure 4.3 - A) Schematic of ELISA competition assay. B-E) Competition ELISA with Nutlin or untagged BOXI, IRF1 and IRF2 peptides (sequence as in Figure 4.1) from various MDM2 ligands. Legend indicates immobilized peptide. B) Nutlin competition, C) BOX-I competition, D) RB1 competition, E) BOX-V competition.

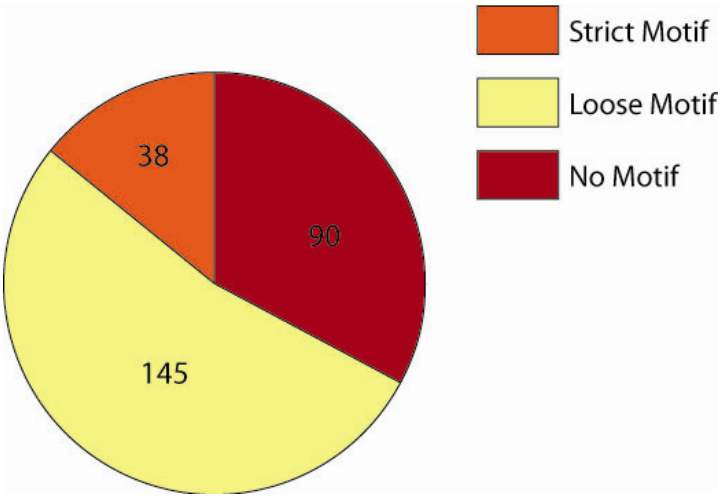

Figure 4.4 - Summary of number of motifs (Defined in Figure. 4.1) found in proteins with altered levels 2 hours after Nutlin treatment in PAcIFIC proteomics screen. (Full list in Appendix 4)

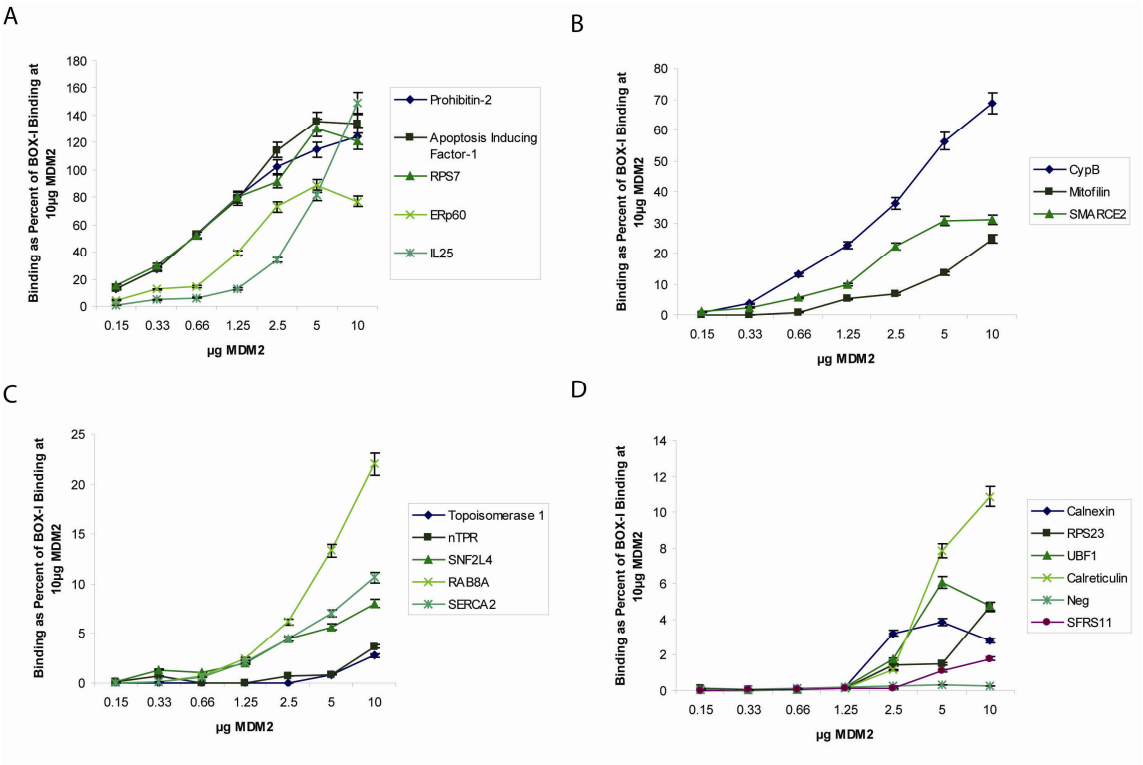

Figure 4.5 - Validation of peptides containing consensus motif binding by ELISA (Full sequences shown in alignment in Figure 4.7, method as in Figure 4.2). Results indicated as the amount of peptide binding as a fraction of BOX-I maximum binding with 10µg MDM2. Results are categorized as follows: A) Stronger than BOX-I, B) Intermediate, C) Weak, D) Very Weak.

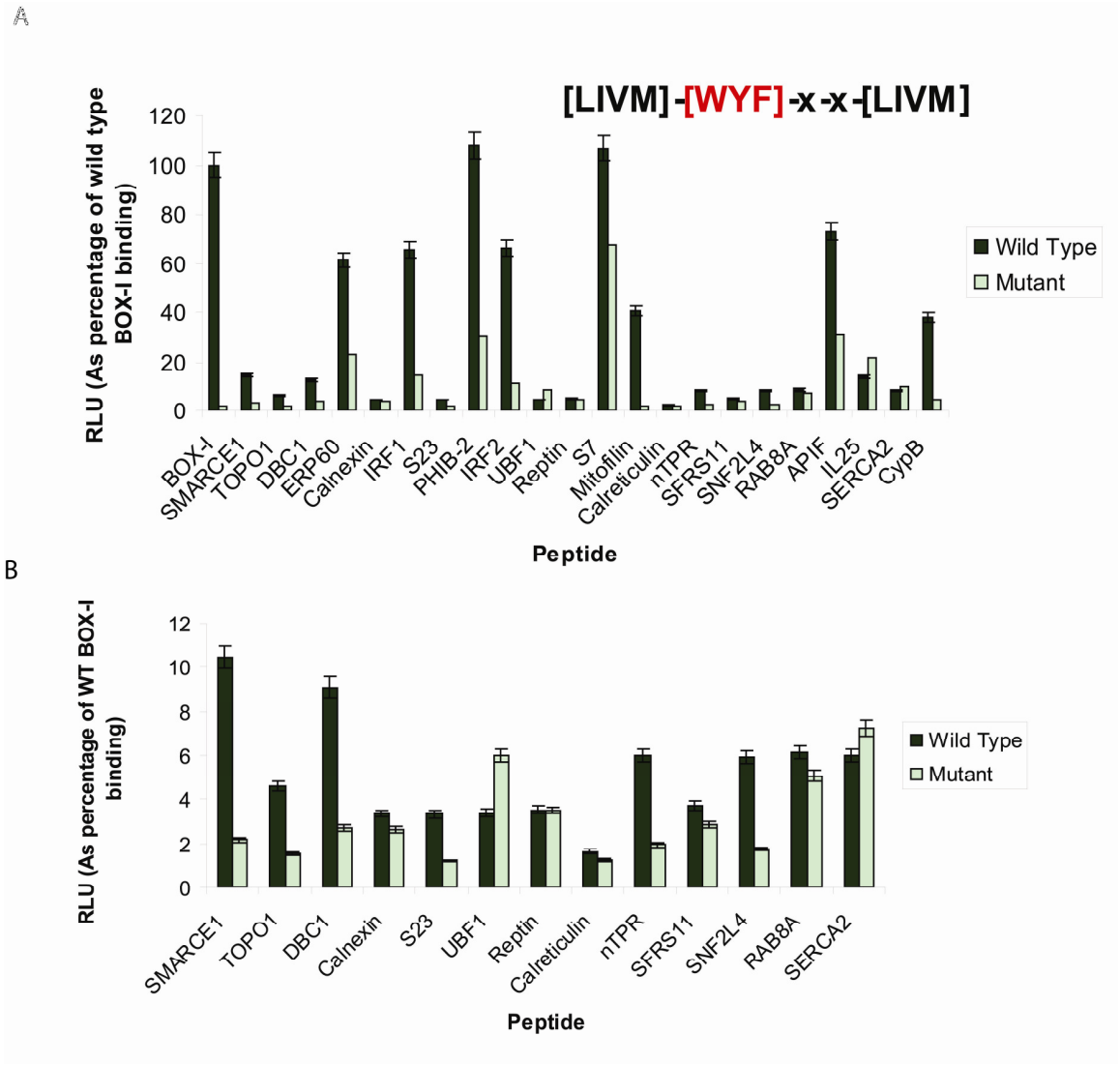

Figure 4.6 - A) ELISA binding of peptides to full length MDM2 (2.5 µg/well), sequences in Figure 4.7, compared to peptides with core W in the consensus motif defined in Figure 4.1 mutated to A. B) Weaker binding peptides (strong binders removed from graph for clarity).

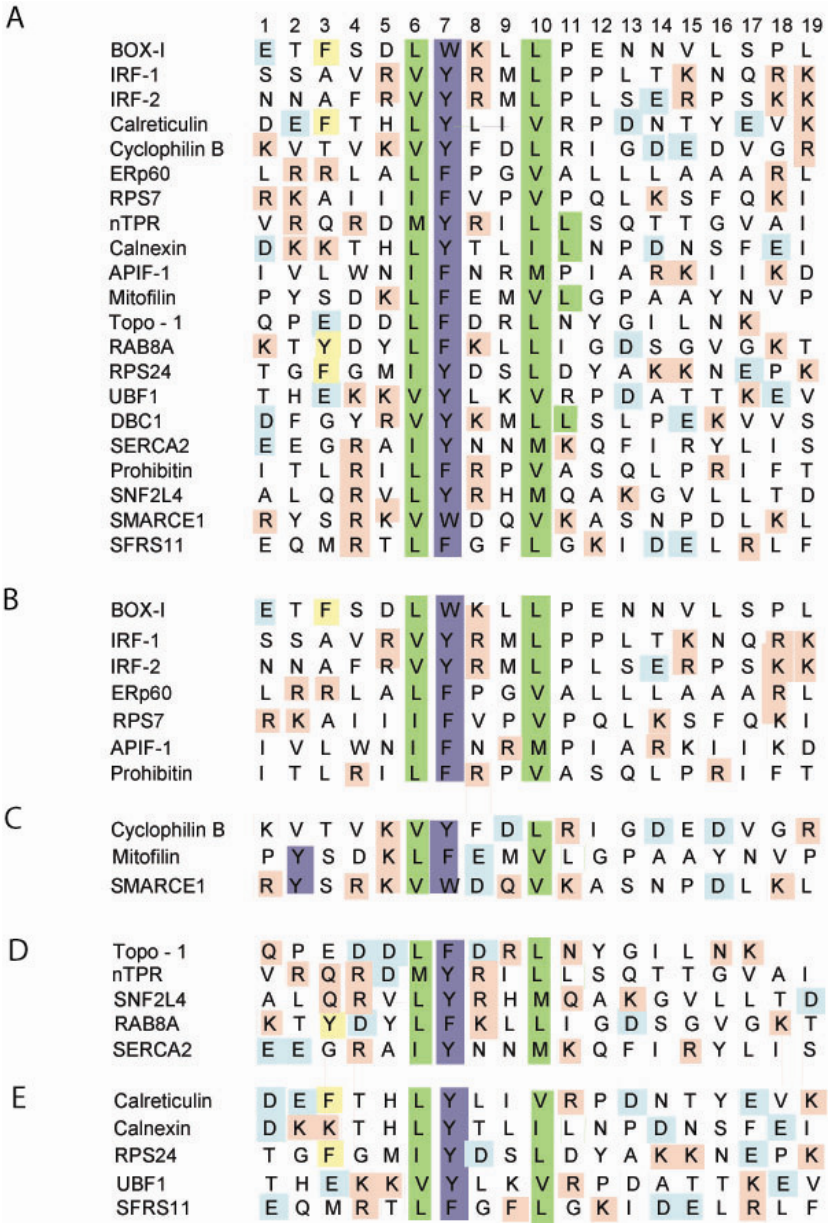

Figure 4.7 - Alignment of peptides which bind to full-length MDM2, A) All peptides B) Top binders, C) Intermediate binders, D) Weak binders, E) Very weak binders as defined in Figure 4.5. Green – core motif hydrophobic residues, Dark Blue – core motif aromatic residue, Light Blue – Negatively charged residues, Light Pink – Positively charged residues, Yellow – Aromatic residue at position 3 (Phenylalanine in BOX-I peptide).

A

	1	2	3	4	5	6	7	8	9	10	11	12	13	14	15	16	17	18	19		Total	%	% occ.
A	1		3		2						2	2	2	2	2	1	1	1		A	19	4.77	7.8
C																				C	0	0.00	1.9
D	3			3	3			2	1		1		1	**5**		2			2	D	23	5.78	5.3
E	3	2	2					1				1		1	3		1	3		E	17	4.27	6.3
F		1	3	1			**8**	1	1				1			1	1	1	1	F	20	5.03	3.9
G		1	2	1				1	1		1	1	3	1		2		2		G	16	4.02	7.2
H		1			2				1									1		H	5	1.26	2.3
I	2			1	2	4			1	2		3	1	2		1	2	1	3	I	25	6.28	5.3
K	2	2	1	1	4			3	1		2	1	1	2	3	1	2	4	4	K	34	8.54	5.9
L	1	1	2	1		**10**		1	4	**10**	**5**	2	4	2	1	3	3	1	3	L	54	13.57	9.1
M			1		1	1			4	3										M	10	2.51	2.3
N	1	1			1			2	1		1	1	1	2	2	3	1			N	17	4.27	4.3
P	1	1						1	2		**5**	2	3	1	2	1		2	1	P	22	5.53	5.2
Q	1	1	2						1		1	2	2				2			Q	12	3.02	4.2
R	2	2	1	**6**	3			**5**	2		2	1		1	2	1	1	2	1	R	32	8.04	5.1
S	1	1	2	1					1			3	2		2	1	2		2	S	18	4.52	6.8
T	2	3	1	2	1			2				1		2	2	2		1	1	T	20	5.03	5.9
V	1	2		2	1	**6**		2		**6**	1				2		4	2	2	V	31	7.79	6.6
W				1			2													W	3	0.75	1.4
Y		2	1	1	1		**11**					1				2	1			Y	20	5.03	3.2
	21	21	21	21	21	21	21	21	21	21	21	21	21	21	21	21	21	21	20		398	100	100

R-x-LV-YF-R-x-LV-LP-x-x-D

B

	1	2	3	4	5	6	7	8	9	10	11	12	13	14	15	16	17	18	19		Total	%	% occ.
A	2	3	6	7	5			2	4		7	6	5	3	5	4	8	5	6	A	78	6.44	7.8
C		2	1	2					1		2		2	1	1	2	1	5	1	C	21	1.73	1.9
D	7	3	6	6	7			7	7		4	4	4	**4**	2		2	3	1	D	67	5.53	5.3
E	5	7	6	5	8			6	1		6	11	7	5	8	6	7	6	8	E	102	8.42	6.3
F	4	1	3	1			**35**	4	2		2	2	2	2	3		1	4	1	F	67	5.53	3.9
G	4	3	3	4	4			6	3		7	4	2	6	6	2	5	3	5	G	67	5.53	7.2
H	1	2		3	1				1				1	1	2	1	1	1	1	H	16	1.32	2.3
I	1	2	2	2		13		2	1	11	2	4	4	2	1	2	5	1	8	I	63	5.20	5.3
K	9	3	3	10	7			5	11		3	6	7	6	5	4	3	5	4	K	91	7.51	5.9
L	5	6	8	3	6	**24**		4	7	**32**	**6**	3	3	5	5	4	3	4	5	L	133	10.98	9.1
M			2		1	7		1	2	7	2		2	3		1	2		1	M	31	2.56	2.3
N	2	6	5	1	3			2	6		4		4	1	3	3	2	2	5	N	49	4.05	4.3
P	4	2	3	3	4			1			1	3	1	6	6	7	3		2	P	46	3.80	5.2
Q		4		2	2			7	1		4	4	5	4	1	4	4	5	2	Q	49	4.05	4.2
R	5	5	3	**4**	6			**5**	6		1	6	3	4	3	1	5	2	2	R	61	5.04	5.1
S	5	4	6	2	3			4	4		4	5	4	3	7	7	5	3	1	S	67	5.53	6.8
T	3	8		3	2			3	5		3	2	4	4		6	1	6	5	T	55	4.54	5.9
V	4	2	6	4	3	**20**		2	1	14	3	3	3		5	8	5	5	4	V	92	7.60	6.6
W	1						11		1		1					1				W	15	1.24	1.4
Y		1	1	2	2		**18**	3			2	1	1	4	1	1		3	1	Y	41	3.39	3.2
	62	64	64	64	64	64	64	64	64	64	64	64	64	64	64	64	63	63	63		1211	100	

x-x-LV-YF-x-x-LV-x-x-x-x

Figure 4.8 – Tally chart of residue frequency in motifs which bind MDM2 compared to those which do not bind. A) Peptides binding MDM2 B) All other peptides from screen of MS dataset which did not bind MDM2. Residues which are overrepresented in the MDM2 binding peptides are highlighted in bold in both tables, and incorporated into the consensus defined in Figure 4.1 below the table.

A

No.	Sequence	Protein	No.	Sequence	Protein
1	ETFSDLWKLLPENNVLSPL	BOX-I	13	NNAFRVYRMLPLSERPSKK	IRF-2
2	RYSRKVWDQVKASNPDLKLW	SMARCE1-1	14	RKAIIIFVPVPQLKSFQKIQ	Ribosomal S7
3	NKQPEDDLFDRLNTGILNKH	Topoisomerase1-2	15	PYSDKLFEMVLGPAAYNVPL	Mitofilin
4	DFGYRVYKMLLSLPEKVVSP	DBC1	16	DEFTHLYTLIVRPDNTYEVK	Calreticulin
5	LRRLALFPGVALLLAAARL	eRP60	17	VRQRDMYRILLSQTTGVAIP	Nucleoprotein TPR
6	DKKTHLYTLILNPDNSFEIL	Calnexin-1	18	EQMRTLFGFLGKIDELRLFP	SRFS11
7	KVTVKVYFDLRIGDEDVGRV	CyclophilinB-2	19	ALQRVLYRHMQAKGVLLTDG	SNF2L4
8	SSAVRVYRMLPPLTKNQRK	IRF-1	20	KTYDYLFKLLLIGDSGVGKT	RAB8A
9	TGFGMIYDSLDYAKKNEPKH	Ribosomal S24	21	IVLWNIFNRMPIARKIIKDG	Apoptosis inducing factor 1-2
10	I TLRILFRPVASQLPRIFTS	Prohibitin-2	22	GVGASLWAALLLGAVALRPA	IL25
11	KEYQDAFLFNELKGETMDTS	Reptin	23		Negative
12	THEKKVYLKVRPDATTKEVK	UBF-1	24	EEGRAIYNNMKQFIRYLISS	SERCA2-2

B

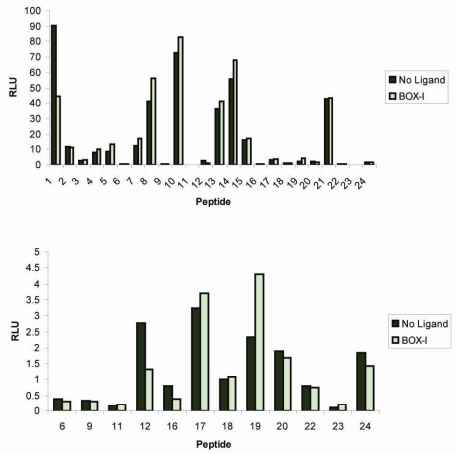

C

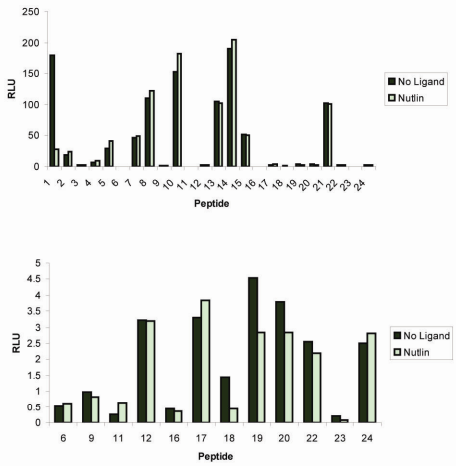

D

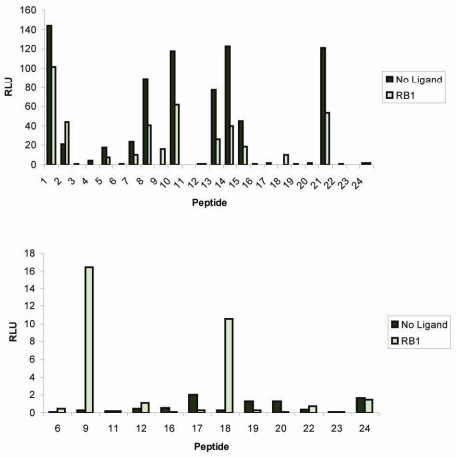

E

Peptide	1	2	3	4	5	6	7	8	9	10	11	12
Nutlin	-	-		+								
BOX-I	-			+	+		+			-		-
RB1	-	+		-	-		-	-	++			

Peptide	13	14	15	16	17	18	19	20	21	22	23	24
Nutlin					-	-	-	-		-		
BOX-I						-	+	-				-
RB1	-	-	-		-	+	-		-			

Figure 4.9 - ELISA plates for competition assays for unbound vs. incubated with ligand (20 µM) MDM2 (2.5 µg/well); B) Nutlin C) BOX-I D) RB1, lower binding peptides are shown without strong binders below initial graph. E) Summary of MDM2 ligand effects on peptides. Legend A) indicates which numbers represent peptides in axes.

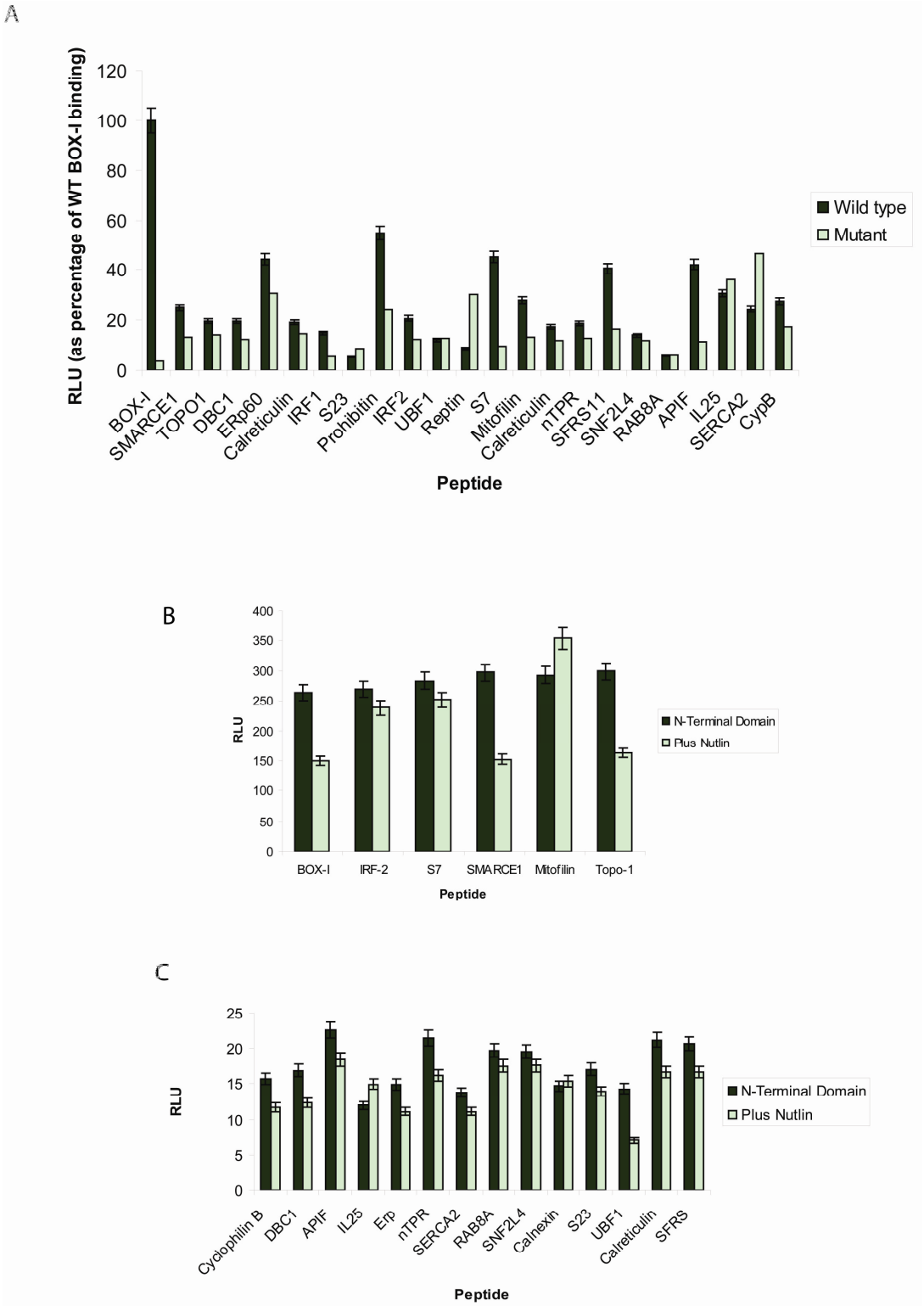

Figure 4.10 – ELISA of N-terminal MDM2 (residues 1-126) binding peptides identified as binding to full-length MDM2 (Sequences in figure 4.7). A) All peptides compared to core motif W to A mutant peptides, B) Strong binding peptides plus or minus Nutlin (40 μM) C) Weaker binding peptides plus or minus Nutlin (40 μM).

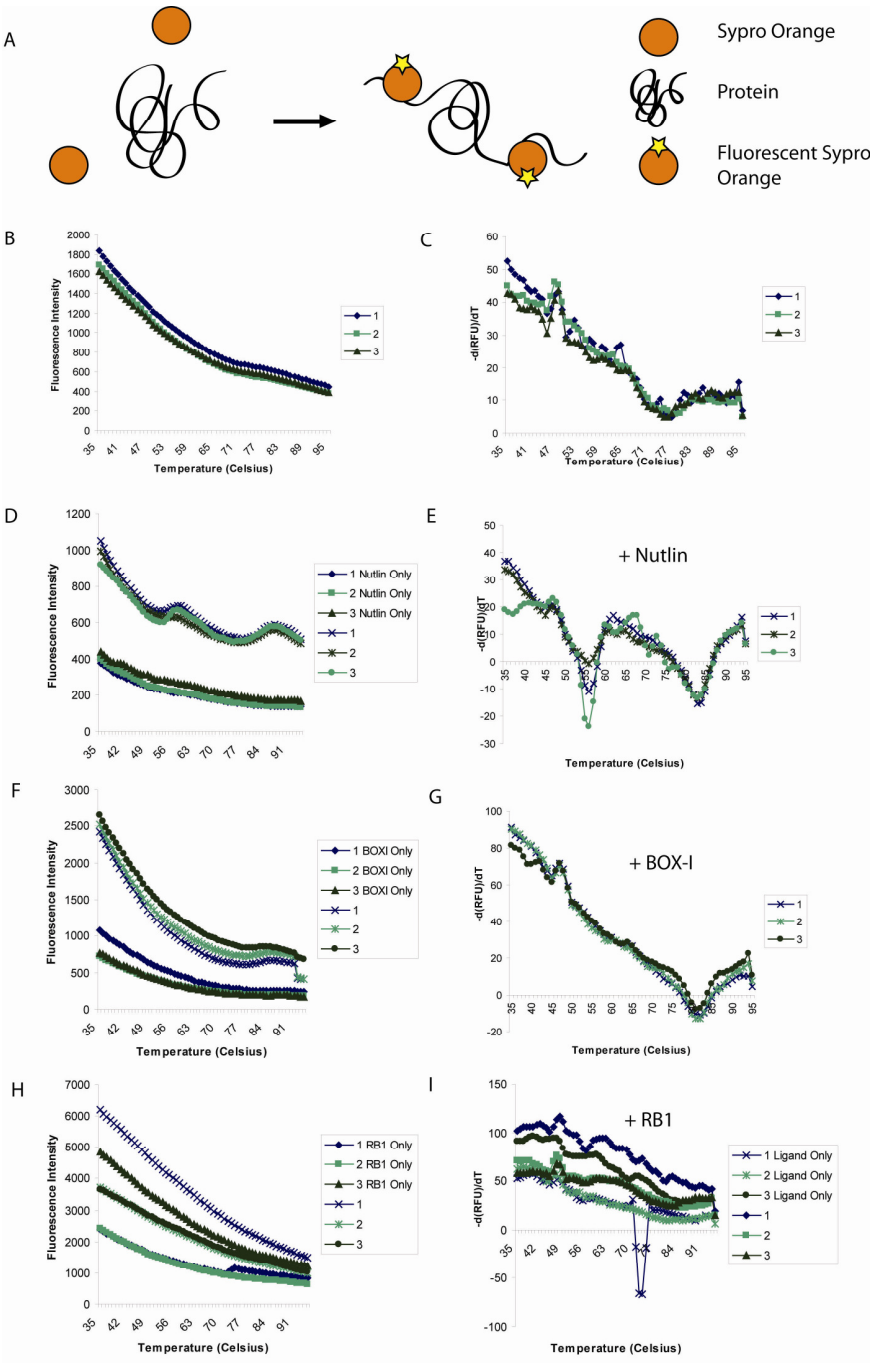

Figure 4.11 - A) Schematic of thermal denaturation assay. Left column of graphs are raw data, right column are corresponding data transformed as –d(RFU)/dT, where RFU is relative fluorescence units. 1,2 and 3 represent three replicates of identical samples. B,C) FL-MDM2 with no ligand D,E) FL-MDM2 with Nutlin F, G) FL-MDM2 with BOX-I peptide, H, I) FL-MDM2 with RB1 peptide. Ligand only measurements (background) are also shown in D,F, H and I. Ligand concentrations were all 20 µM and MDM2 concentration was 5 µM.

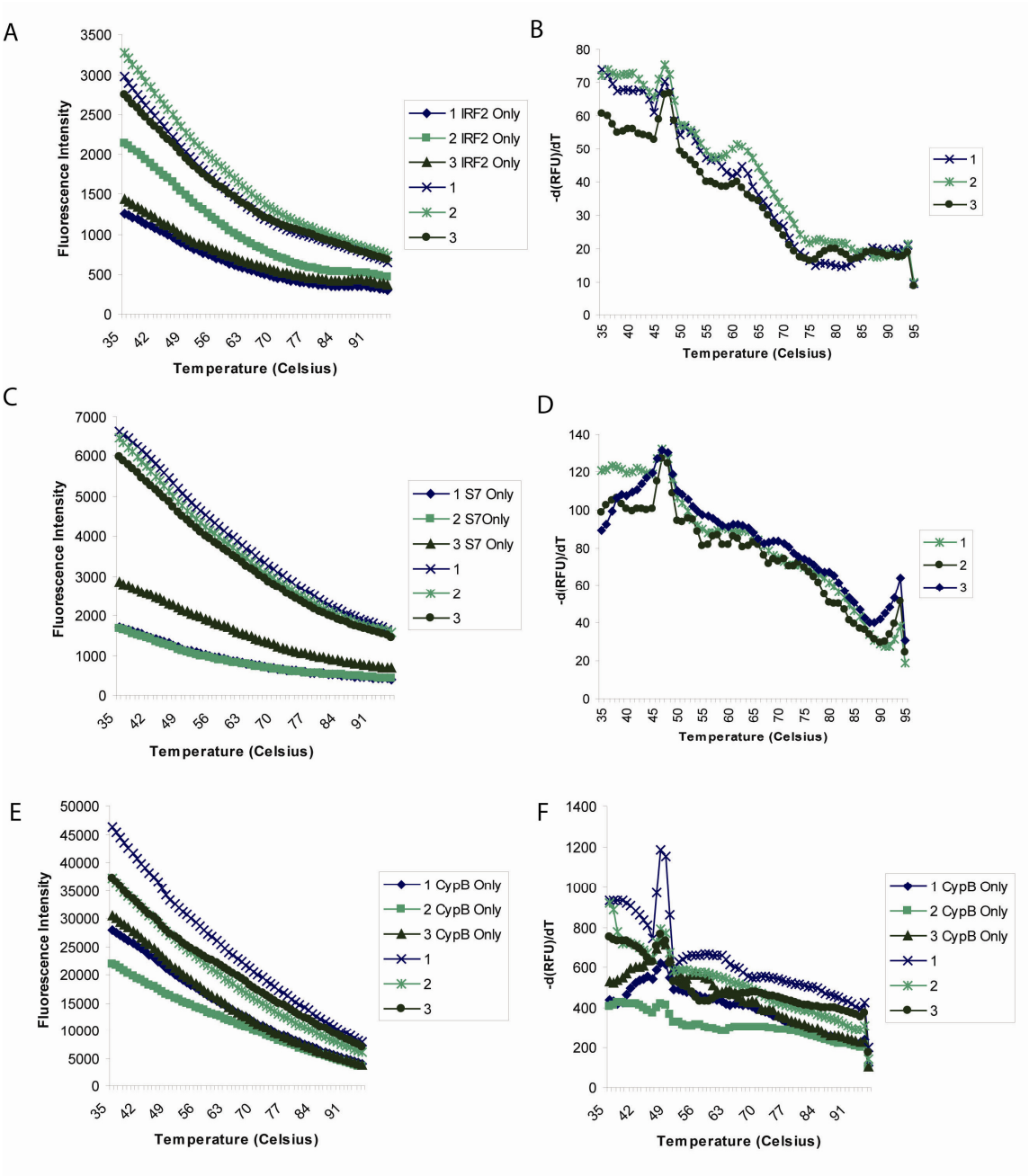

Figure 4.12 - Thermal denaturation assay for full-length MDM2 with conditions and presentation as in Figure 4.11. A), B) IRF2 peptide C), D) S7 peptide E), F) CypB peptide. 1, 2 and 3 represent replicates of identical samples, and ligand only controls are shown in A, C, E and F

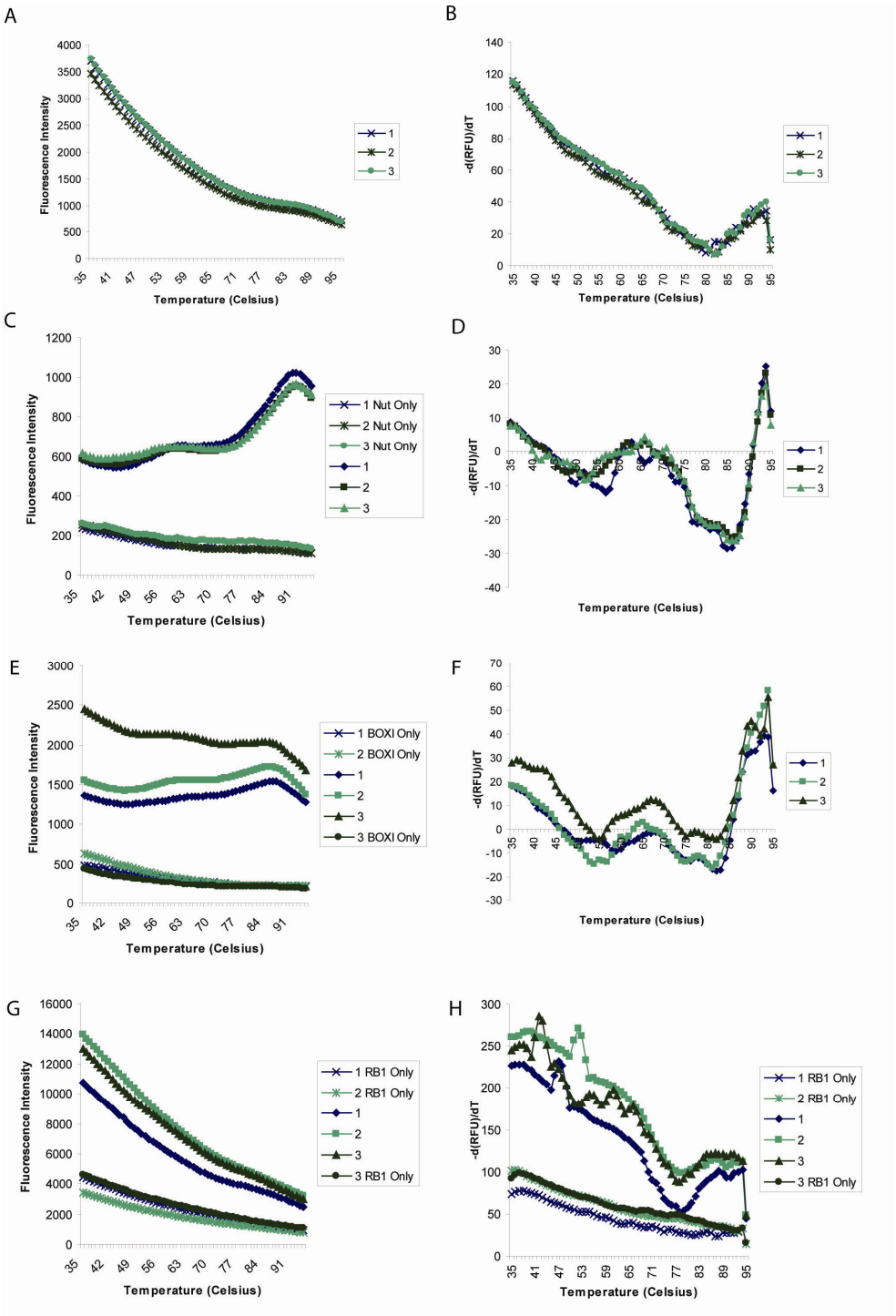

Figure 4.13 - Thermal denaturation assay of N-terminal construct MDM2 (aa 1-126) with A),B) No ligand, C), D), Nutlin, E), F) BOX-I, G), H) RB1. A, B and C represent three identical replicates, ligand only controls are shown in C, E, G and H. Presentation and concentrations as in figure 4.11.

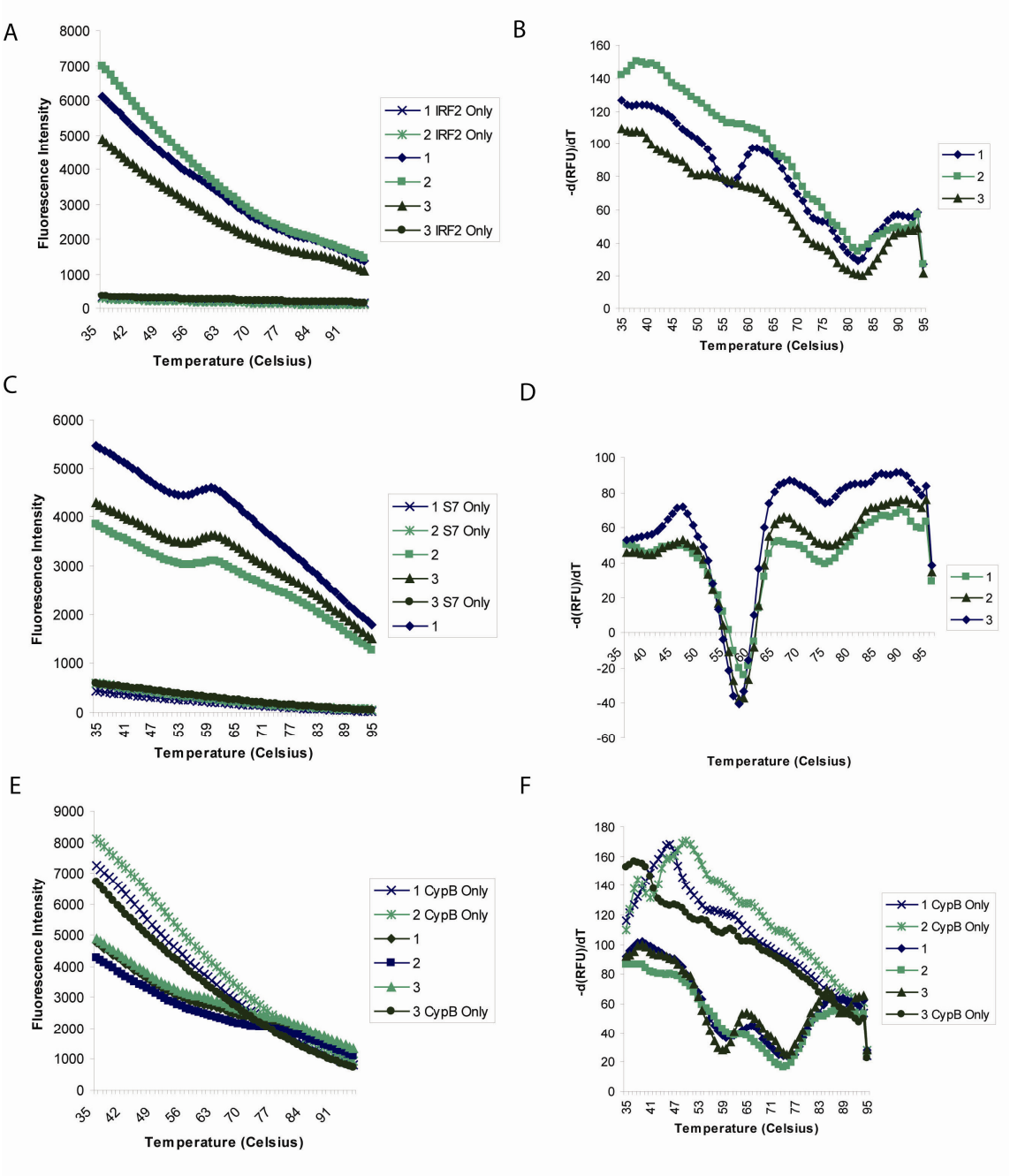

Figure 4.14 - Thermal denaturation assay of N-terminal construct MDM2 with A), B) IRF2 peptide, C), D) S7 peptide, E), F) CypB peptide. A, B and C represent identical replicates and ligand only controls are shown in A, C, E and F. Presentation and concentrations as in figure 4.11 (except CypB peptide at 5 µM).

		Melt Temp. (℃)	Initial Background (RFU)			Melt Temp. (℃)	Initial Background (RFU)
Full Length MDM2	**No Ligand**	-	1715 ± 106	**N-Terminal MDM2**	**No Ligand**	81 ± 1	3634 ± 152
	Nutlin	56 ± 0 83 ± 0	989 ± 66		**Nutlin**	54 ± 3 85 ± 1	594 ± 16
	BOX-I	81 ± 0.6	2530 ± 109		**BOX-I**	57 ± 2 75 ± 1 82 ± 1	1791 ± 581
	RB1	-	4523 ± 1443		**RB1**	-	12568 ± 1648
	IRF2	-	3000 ± 264		**IRF2**	82 ± 1	5996 ± 1069
	S7	90 ± 1	6366 ± 340		**S7**	57 ± 1 74 ± 1	4539 ± 832
	CypB	-	40220 ± 5194		**CypB**	60 ± 2 76 ± 1	4650 ± 330

Table 4.1 Summary of thermal denaturation assays figures 4.11-4.14. Melt temperature corresponds to peak minima in d(-RFU)/dT vs. Temperature graphs and initial background is RFU at 35°C.

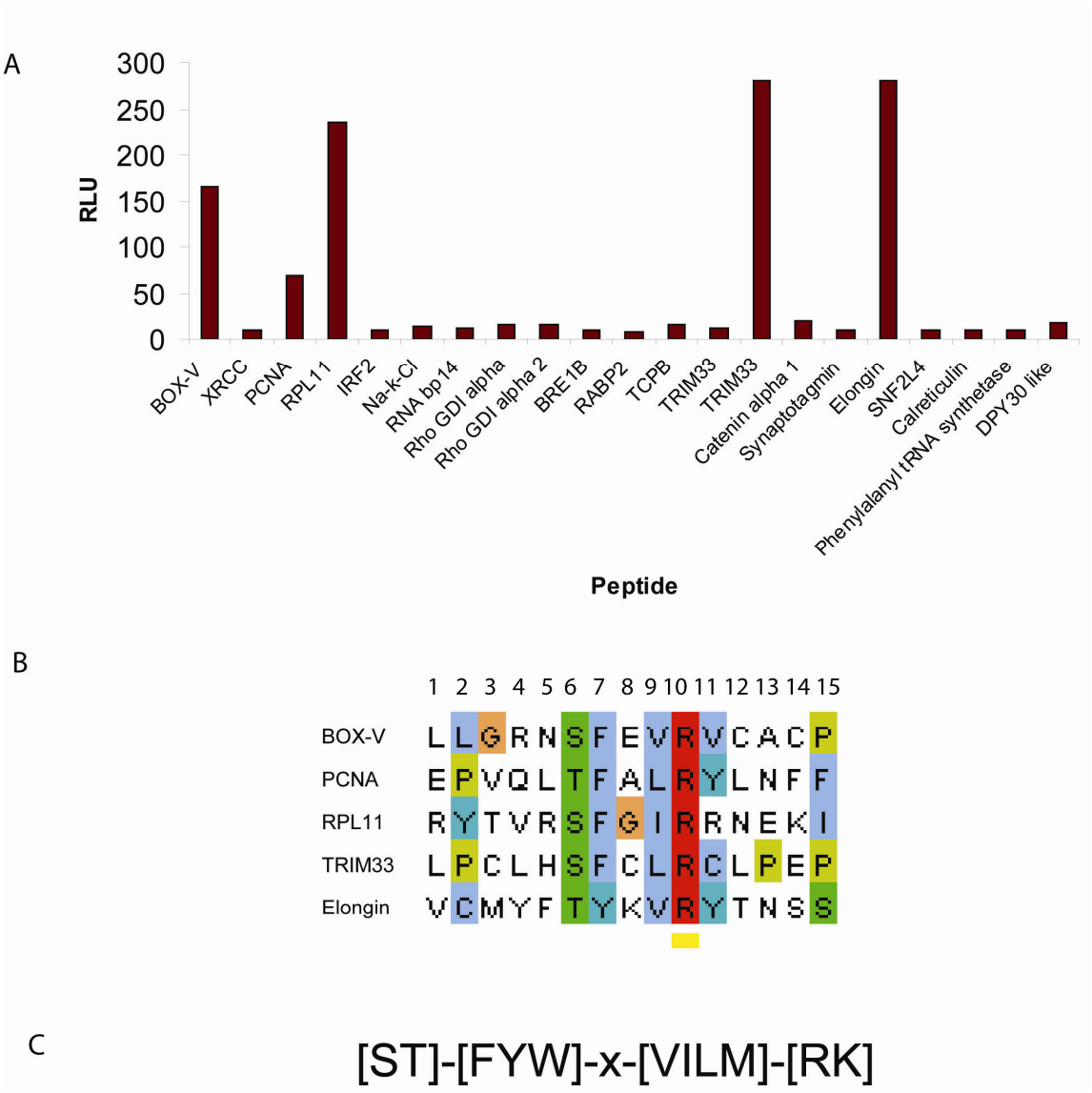

Figure 4.15 - Peptides with similarity to BOX-V binding by ELISA to full-length MDM2 B) Alignment of binding peptides containing BOX-V motif from early PAcIFIC hits which bind full length MDM2 C) Proposed BOX-V like motif based on peptides which bind MDM2

5 - Validation of full-length MDM2 binding proteins and the effects of Nutlin in cells

5.1 Introduction

In Chapters Three and Four proteins which responded to Nutlin treatment were identified by proteomic MS, and motifs with similarity to the BOX-I sequence from p53 derived from these proteins were shown to bind full-length or N-terminal domain MDM2. Further work is required to investigate the response of these proteins to Nutlin treatment, and establish whether these motifs have a role in full-length protein-protein interactions. Although some of these peptide motifs have been shown to bind MDM2 *in vitro*, this does not necessarily translate to mediating *in vivo* protein-protein interactions. The proteins with motifs which were investigated in Chapter Four by thermal denaturation, CypB and RPS7, were selected for further investigation by cell biology and biochemical assays.

CypB is a peptidyl-prolyl isomerase which has been implicated in cancer progression[209, 210], but it is unclear by which mechanisms this occurs. RPS7 is a previously validated MDM2 binding ribosomal protein, which has been shown to be a substrate for MDM2 ubiquitination and also plays a role in the regulation of the p53-MDM2-MDM4 axis[96]. The region of RPS7 which MDM2 binds has been mapped, and this includes the BOX-I like motif identified in Chapter Four. Of the proteins identified in the iTRAQ MS screen APE1, which has been shown to bind MDM2[97], and NPM, another previously validated MDM2 binding protein[103], were detected at multiple times after Nutlin treatment. These proteins were further investigated to determine the effect Nutlin treatment has on these

proteins in particular. Pyruvate kinase was also tested for binding to MDM2, as a cancer target which was detected in the iTRAQ screen. Although fully validating each of these proteins would require more work, preliminary experiments here identify that they are related to MDM2 and represent leads which can be further investigated to expand the MDM2 interactome.

5.2 Confirmation of Nutlin effects on cellular proteins by western blot

Nutlin treatment of cells results in an increase in p53 protein levels as early as one hour after treatment, and subsequent increases in MDM2 and p21 (Chapter 3, Section 3.2). IRF2 protein levels after Nutlin treatment were also increased as early as two hours, and this persisted over the time course (Fig 5.1). Although IRF2 was not detected in either mass spectrometry screen, it is a known MDM2 binding partner and substrate[81] and was used to design the BOX-I like motif used to screen the MS results (Chapter 4). Results obtained for the IRF2 response to Nutlin and relating to the IRF2 BOX-I like peptide therefore validate the results for new peptides derived from the MS results. Proteins which were detected in the PAcIFIC MS screen containing BOX-I like motifs were investigated for response to Nutlin treatment by western blot. The PAcIFIC hits RPS7, CypB and ERp60 were also detected in the iTRAQ screen, although none passed the 1.33 threshold set for iTRAQ quantification ratio. CypB however was approaching the 1.33 threshold by 12 hours after Nutlin treatment (Fig. 5.2). RPS7 was detected in both screens, although only detected as changed in level in the PAcIFIC screen at two and four hours after treatment. This was due to the absence of detection in the untreated cells, as RPS7 is a well-validated MDM2 binding protein however it warrants further

investigation (Fig. 5.2b). CypB levels were detected as increased at two hours after Nutlin treatment by western blot, with this increase maintained over the whole time course (Fig. 5.3). RPS7 was detected on a gel as higher molecular weight species as well as faintly detected at 20 kDa, and the level of these higher molecular weight species was slightly increased after Nutlin treatment (Fig. 5.3). Changes were not detectable by western blot for ERp60 which was detected at increased levels in the PAcIFIC screen. However this could be antibody dependent, an advantage of MS based protein detection methods is that they do not rely on the specificity and affinity of antibodies (Fig. 5.2d, 5.3). The protein APE1 was detected at multiple time points in the iTRAQ screen, although it was not detected by PAcIFIC. It has previously been shown that this protein increases in level after Nutlin treatment, binds p53 and is ubiquitinated[97]. The western blot for APE1 after Nutlin treatment indicated that this protein was increased in level to a greater extent than any other protein tested in this study except for p53 (Fig. 5.4b). Over-exposure of this blot also revealed an increase in ubiquitination of APE1 after Nutlin treatment. In the PAcIFIC screen DNA-PK appeared decreased, whereas in the iTRAQ screen it was shown to increase over the time course (Fig. 5.4c,d). As the western blot shows there is an increased level of DNA-PK after Nutlin treatment (Fig. 5.4e). The decrease detected in the PAcIFIC screen was possibly due to some relocalisation of DNA-PK

5.3 Immunoprecipitation of MDM2 binding motif containing proteins

CelluSpots™[173] peptide arrays printed with peptides representing all of the motifs discovered in Chapter 4, and W to A mutant controls of these peptides, were probed with

full-length or N-terminal MDM2. The peptide derived from ERp60, which has high alanine content, bound both forms of MDM2 in this assay format (Fig. 5.5). Other peptides which bound MDM2 in this format included peptides derived from BAT3 and ribosomal protein L24, although the array binding detected was low for all peptides other than ERp60. Surprisingly the positive control peptide, BOX-I, did not bind by this peptide array assay. As the most intense binding peptide co-immunoprecipitation of ERp60 with MDM2 from MCF7 cell lysate was attempted. Although there was a low intensity band in the elution lane at approximately the correct molecular weight (Fig. 5.6a) there was a high level of background, and it was not possible to co-immunoprecipate MDM2 with ERp60 in the solid phase. CypB was also tested for MDM2 binding using co-immunoprecipiation, and was not co-immunoprecipitated with MDM2 (Fig. 5.6b). There was however, a smear present in the load lane for cells treated with Nutlin, which which could represent modified forms of CypB (Fig. 5.6b).

5.4 CypB stabilization by drug treatment

To further investigate the effects of Nutlin treatment on CypB, samples were treated with drugs and analysed on gradient SDS-PAGE gels. Treatment of MCF7 cells with the proteasome inhibitor MG-132 stabilised levels of CypB, Nutlin treatment resulted in a similar level of stabilization in the absence of the proteasome inhibitor (Fig. 5.7). In all samples a higher molecular weight band was observed at around 30 kDa, which could represent a CypB dimer or a modified form of CypB and has potential to be identified by MALDI, for example. Interestingly, after Nutlin and MG-132 treatment other high molecular weight bands were observed on the CypB blot with a polyclonal antibody.

These bands were stabilized to a greater extent with MG-132 than any other drug, therefore it is possible they are intermediates in the CypB degradation pathway.

Cyclosporine is an immunosuppresant drug which binds members of the cyclophilin protein family. Nutlin induced increase in CypB was greater than for cyclosporine treatment alone, and also resulted in a greater stabilization of the higher molecular weight bands observed. MDM2 is stabilized by all drug treatments, particularly the combination of Nutlin and MG-132 or of cyclosporine and MG-132. These results indicate that CypB is also stabilized by Nutlin treatment, although they do not show whether or not this is due to a direct MDM2 effect or further downstream.

5.5 Full-length CypB binds MDM2 in vitro

Full length CypB protein contains three BOX-I like motifs (Fig. 5.8a), one of which has been shown to bind MDM2 (Chapter Four). Full-length CypB was purified to test for MDM2 binding *in vitro*. CypB coated on an ELISA plate bound both full-length MDM2 and N-terminal domain MDM2 to a greater extent than to free GST which was used as a control (Fig. 5.8b). In a similar pattern to that observed for MDM2 binding to the CypB motif peptide this interaction was not affected by the addition of BOX-I peptide or Nutlin, and was competed by BOX-V peptide and enhanced by RB1 peptides (Fig. 5.8c,d). Interestingly, all ligands competed with the CypB peptide for binding at the N-terminal domain (Fig. 5.8e), suggesting that this domain has intrinsic or less specific peptide binding activity. This also confirms that the enhancement of CypB binding observed with the full-length protein is most likely due to RB1 peptide binding a domain

other than the N-terminal domain. CypB with the core Y47 residue in the BOX-I like motif shown to bind MDM2 in Chapter Four mutated to alanine unexpectedly caused a slight enhancement of CypB binding to MDM2 (Fig. 5.9a). This is contrary to the MDM2 binding CypB peptide, which loses MDM2 binding activity with this mutation (Chapter Four). Nutlin actually enhanced binding of the mutant protein to MDM2 and had no effect on the wild type protein, which again was unexpected (Fig. 5.9b). Mutation of this residue in PyMOL revealed a slight increase in the exposure of the residues surrounding the core of the motif, which may explain this effect (Fig. 5.9d,e). To map the interface where CypB binds MDM2, overlapping MDM2 peptides were coated onto an ELISA plate and incubated with full-length CypB. Peptides from the N-terminal domain and RING domain bound to CypB, although no acidic domain peptides bound CypB outside experimental error (Fig. 5.10). Although these peptides bind CypB, this does not necessarily map the binding interface, as in the full-length protein these peptides may be occluded. However binding to overlapping peptides, such as with the RING peptides may indicate a binding site.

5.5 In vivo ubiquitination assays

In vivo ubiquitination assays detect ubiqutination by pull-down of transfected His-tagged ubiquitin, which may be conjugated to ubiquitination substrates. p53 transfected into H1299 cells, which do not have a detectable level of p53 transcription, exhibits a large increase in ubiquitination when cells are co-transfected with MDM2. p53 ubiquitination is not detected without MDM2 co-transfection (Fig 5.11a). IRF2 is ubiquitinated in the absence of MDM2 in H1299 cells, however there is a slight increase in the level of

polyubiquitination after the cotransfection of MDM2 indicating that MDM2 stimulates this process. CypB was not co-immunoprecipitated in this assay either with or without MDM2 transfection and Nutlin treatment (Fig. 5.11b), indicating MDM2 may not ubiquitinate CypB *in vivo*. APE1 has previously been shown to be ubiqitinated by MDM2[97] and here it was confirmed that there is an increased level of APE1 ubiquitination after Nutlin treatment, compared to untreated cells (Fig. 5.11c). This is visualized as a single band, unlike polyubiquitinated p53 and IRF2. Interestingly the APE1 band in the elution lane was at the same molecular weight as the load lane, suggesting this protein is usually ubiquitinated or is sticking to the nickel column.

5.4 In vitro ubiquitination assays of CypB

To further investigate if MDM2 can ubiquitinate CypB, *in vitro* ubiquitination assays were carried out. Full-length MDM2 purified by GST cleavage was shown to be active towards p53 due to the presence of ubiqutination bands as well as full length p53, increasing with a titration of MDM2 (Fig. 5.12a,b). When CypB was used as a substrate in the assay there were no ubiquitination bands visible, and the initial level of CypB appeared to decrease (Fig. 5.12a). Addition of CypB to the p53 ubiquitination reaction did not inhibit MDM2 ubiquitination of p53 (Fig. 5.12b).The decrease in CypB was observed with polyclonal, monoclonal and anti-His antibodies therefore it is unlikely that this is because of epitope masking. There are very low intensity higher molecular weight bands visible with a longer exposure using the anti-his antibody (Fig. 5.12c) which are potentially modified forms of CypB. In some exposures a higher molecular weight band was detected at about 30 kDa, which was also observed after MG-132

treatment of cells (Fig.5.7). This band also decreased over the MDM2 titration. This could potentially be due to a high rate of ubiquitination occurring too fast to be captured by the assay in this format. Using K48A mutant ubiquitin, which is unable to form poly-ubiquitin chains at this residue[211], decreased the level of substrate reduction for CypB (Fig. 5.12d) compared to with wild type ubiquitin.

5.6 Pyruvate kinase binds MDM2

Pyruvate kinase (PK) was detected in the iTRAQ screen, and although it was not classed as upregulated by the ProteinPilot quantitation algorithm it was manually assigned as a potential hit based on presence of multiple peptides suitable for quantitation. PK may therefore be a potential candidate for Nutlin regulation (Fig. 5.13a). PK was selected to test for MDM2 binding due to the pivotal role of pyruvate kinase in many cancers[212]. The protein bound MDM2 by ELISA, and PK-MDM2 binding was observed both for MDM2 in the solid phase and pyruvate kinase in the solid phase by ELISA (Fig. 5.13b,c). PK has multiple instances of a BOX-I like motif, although two of these motifs are buried structurally (Fig. 5.14a,b), the final two overlapping motifs are exposed at the PK surface (Fig. 5.14c). Together these data indicate that PK protein is an iTRAQ result which may warrant further investigation.

5.7 MDM2 regulates nucleophosmin oligomerisation

The nucleolar shuttle protein nucleophosmin (NPM) was detected at most time points in the iTRAQ MS screen as upregulated after Nutlin treatment. When testing whether this effect could also be detected by western blot SDS-PAGE resistant oligmers were visible

on a gradient gel (Fig. 5.15a). The amount of NPM oligomers, which run at the correct molecular weight to be pentamers as previously reported[213], decreases as the amount of monomers increase. This demonstrates Nutlin treatment results in the deoligomerisation of NPM. To validate this, MCF7 cells were treated with siRNA to MDM2, and both the soluble and insoluble fraction analysed by SDS-PAGE (Fig. 5.15b). As the level of MDM2 was reduced, there was an increase in NPM oligomerisation, contrary to the effect observed with Nutlin treatment. Adding purified MDM2 exogenously to cell lysates also decreased the amount of NPM oligomers, indicating this effect is due to increased levels of MDM2 rather than an off target or downstream effect caused by Nutlin (Fig. 5.15c). Transfection of MDM2 into H1299 cells resulted in a deoligomerisation effect, similar to adding exogenous MDM2 or Nutlin treatment (Fig. 5.15d). Together these data indicate that Nutlin activates the de-oligomerisation of NPM, and that this is a process which is mediated by MDM2.

5.8 Discussion

Validation of proteomic MS screens by biological methods is increasingly required, even if the data is confirmed using MS based proteomic methods. As the PAcIFIC screen discussed in Chapter Three represents pilot data it is imperative to support these results with cell biology and biochemical validation. The western blots carried out here for CypB and APE1 confirm the mass spectrometry results, and may clarify the ambiguity of the DNA-PK quantitation difference between label free and iTRAQ quantification. The peptide array format used here did not detect MDM2 binding of the BOX-I peptide, however it did detect MDM2 binding to a peptide derived from the

chaperone ERp60. The reason for this could be that the format of the array favours a conformation of BOX-I which does not bind MDM2. The negative result for the ERp60 co-immunoprecipitation and the lack of corroboration for these MS results by western blot demonstrates that not all leads acquired by the methods used in this study are possible to validate by biological methods. The method could be refined by using motif search engines such as SLiMFinder which categorise motifs based on conservation and structural features as well as sequence features[116]. It may also be useful to use other protein-protein interaction assays, such as fluorescence resonance energy transfer (FRET) or bioluminescence resonance energy transfer (BRET) which could identify proximity of proteins in cells.

Cyclophilin B (CypB) was more clearly linked to Nutlin inhibition of MDM2 than ERp60, due to the detection of a large increase in CypB after Nutlin treatment. In particular, the similarity of the Nutlin effect to MG-132 treatment on CypB levels shows Nutlin treatment is stabilizing this protein, potentially by inhibition of CypB ubiquitination. Another possiblility is that this is linked to the cyclophilins role in quality control of protein translation, if protein degradation is inhibited protein folding machinery may respond due to proteostatic mechanisms[18]. If this is the case then Nutlin and MDM2 are also implicated in the regulation of these pathways on a broader scale than the p53 pathway alone. Pin1 is a peptidyl prolyl isomerase which has been shown to demonstrate this kind of a response, in particular controlling the degree of p53 ubiquitination[214]. Although it was not possible to detect ubiquitinated CypB in the *in vivo* assay, the depletion of substrate in the *in vitro* assay was interesting due to the fact

that this usually represents ubiquitination. It has been proposed that the Pin1 protein has E4 activity and pre-assembles ubiquitin chains[214], it is possible that CypB could have a similar function. Although higher molecular weight species were not detected in the *in vitro* experiment, those stabilized in the MG-132 experiments are uncharacterized. If higher molecular weight species of CypB could be identified by further mass spectrometry, this could provide an answer to what is happening in these assays.

Purified CypB full-length protein binds both full-length MDM2 and the N-terminal domain in isolation. This was detected by ELISA, which does not mimic cellular conditions. Another factor that could influence this result is that CypB is a peptidyl-prolyl isomerase. If the MDM2 used in this assay has a PPI dependent folding step, it may actually be a CypB substrate. An interesting point about this interaction is that the full-length protein responds to competitors in a similar way to the CypB peptide, suggesting this peptide may indeed play a vital role in the CypB-MDM2 interaction. The lack of competition by Nutlin, and enhancement by the acid domain ligand RB1 is similar for peptide and protein, although thermal denaturation results (Chapter Four) suggest the CypB peptide is indeed binding the N-terminal domain. In particular, the RB1 stimulation of this binding interaction is interesting because this has not been observed for other MDM2 ligands, rather it is usually an inhibitory interaction[91], and may indicate a different mechanism of MDM2 allostery between the N-terminal and acidic domains. Nutlin enhances the binding of Y47A mutant CypB to full length MDM2. Mutating this residue in the crystal structure shows an increase in the depth of the pocket containing the potential MDM2 binding motif, this possibly allows MDM2 to

access residues in the region around the core. The CypB site around the motif has been shown to be a docking site for the ER chaperones calnexin and calreticulin, which was not affected by cyclosporine[215]. This indicates CypB can bind via a secondary binding site which is not the cyclosporine binding pocket, therefore the region with the BOX-I like motif may be another CypB site which can form protein-protein interfaces. It has been shown in computational studies that the surrounding residues of the BOX-I motif contribute to the interaction with MDM2[216], and if this CypB motif is binding the hydrophobic pocket it could be reliant on residues around the pocket which dock peptides[108]. The primary Nutlin binding site does not seem likely to be the CypB binding site as Nutlin cannot compete CypB. Although the protein was discovered due to the presence of a BOX-I motif a possibility is that this pattern of hydrophobic residues can interact in a different way with MDM2. Indeed in the previous chapter, thermal denaturation results show BOX-I has a slightly different profile than Nutlin which may indicate that peptides have subtle difference in binding than the drug. The initial structure of MDM2 with Nutlin has multiple drug molecules bound[133], raising the possibility of multiple binding pockets in the N-terminal domain. As Nutlin enhances the binding of CypB Y47A mutant to MDM2, maybe the CypB motif binding site is regulated by the state of the hydrophobic pocket, and the intercalation of Nutlin, or the core residues of the BOX-I like motifs activates another binding site in the N-terminal domain. The regulation of the pocket by the lid domain may further complicate this allostery. Although PK was only shown to bind MDM2 by ELISA and not investigated *in vitro*, the presence of BOX-I like motifs on the surface of the protein suggest this

might be a good lead to investigate further. This may also shed more light on the contradictions highlighted by the experiments carried out here with CypB.

Nucleophosmin (NPM) is a previously validated MDM2 binding protein[103], which serves as an internal validation for the iTRAQ MS screen. Although MDM2 has been shown to bind NPM, and participate in a complex with NPM and ARF the Nutlin effect on this pathway has not been demonstrated. In cancer NPM can be present as a fusion protein with ALK which is a constitutively active tyrosine kinase promoting the survival of cancerous cells[217]. NPM mediated oligomerisation has been shown to be important for this function[218]. Nutlin has a striking effect on the oligomerisation of NPM, which is similar to the effect of increasing the level of MDM2 in the cell either by transfection of exogenous addition of purified protein. This demonstrates that Nutlin stabilization of MDM2 is a factor causing the NPM de-oligomerisation, and as this has previously been shown to be mediated by NPM binding the MDM2 N-terminal domain[103]. These findings raise the possiblility that Nutlin allosterically activates not only the acidic domain, but also areas of the N-terminal domain other than the hydrophobic pocket to interact with binding partners (Fig 5.16). This is especially interesting regarding the therapeutic potential of Nutlin as NPM targeting drugs have been designed which target this oligomerisation interface[213].

Although the peptide motifs identified in the last two chapters bind by ELISA, the environment in the cell has very different conditions than those in *in vitro* assays. Some of these motifs may be unable to bind *in vivo*, represent transient binding partners or

docking signals and it is possible in full length proteins these motifs are occluded. MDM2 has chaperone activity for p53 and part of the function of a chaperone protein is based on binding unfolded, disordered regions. If the peptide binding ability of MDM2 is linked to chaperone activity, it does not necessarily follow that purified proteins containing these motifs will be able to bind MDM2. To validate further the protein-protein interactions identified here it would be necessary to develop more robust co-immunoprecipitation techniques, to complement the results obtained by ELISA. Further site directed mutagenesis of CypB motif and potential PK binding site would validate whether this motif is definitely linked to MDM2 binding or not. Whilst more work is required to fully identify the role MDM2 and Nutlin play in the regulation of each of the proteins discussed in this chapter, CypB and PK have been identified as new MDM2 binding proteins and the Nutlin mode of action regarding NPM has been further elucidated. These leads were generated from the original proteomic MS screen, and the range of questions raised by the initial attempts to validate these proteins highlight the complexity of the MDM2 interactome and mechanism and the benefits and pitfalls of MS based screens. It has been shown that proteomic MS can be a valuable tool to investigate an interactome, however this is only the beginning of understanding how complex the MDM2 protein-protein interaction networks is.

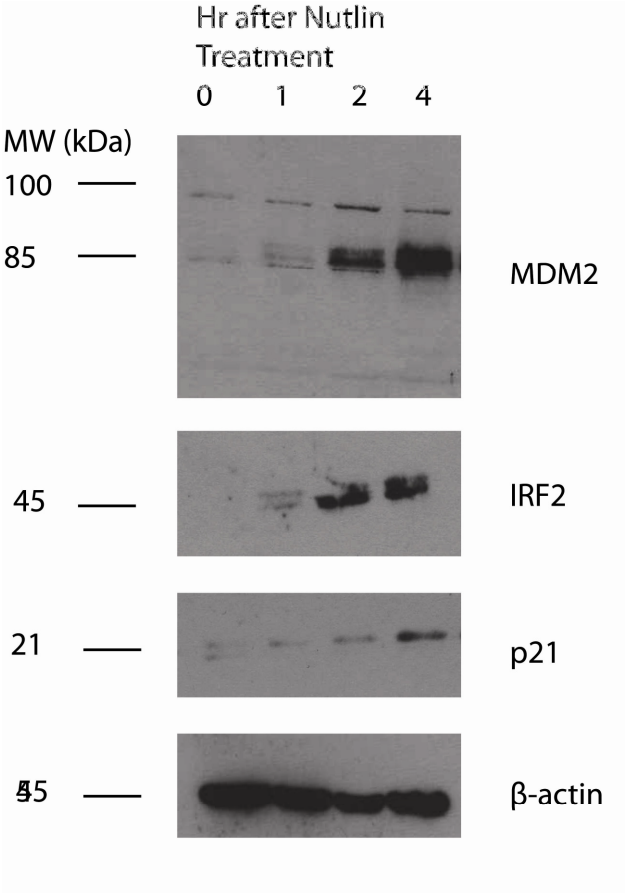

Figure 5.1 – Protein levels visualized by western blot for MDM2 and IRF2 levels in total lysate after 40 μM Nutlin treatment of MCF7 cells, B-actin is a loading control.

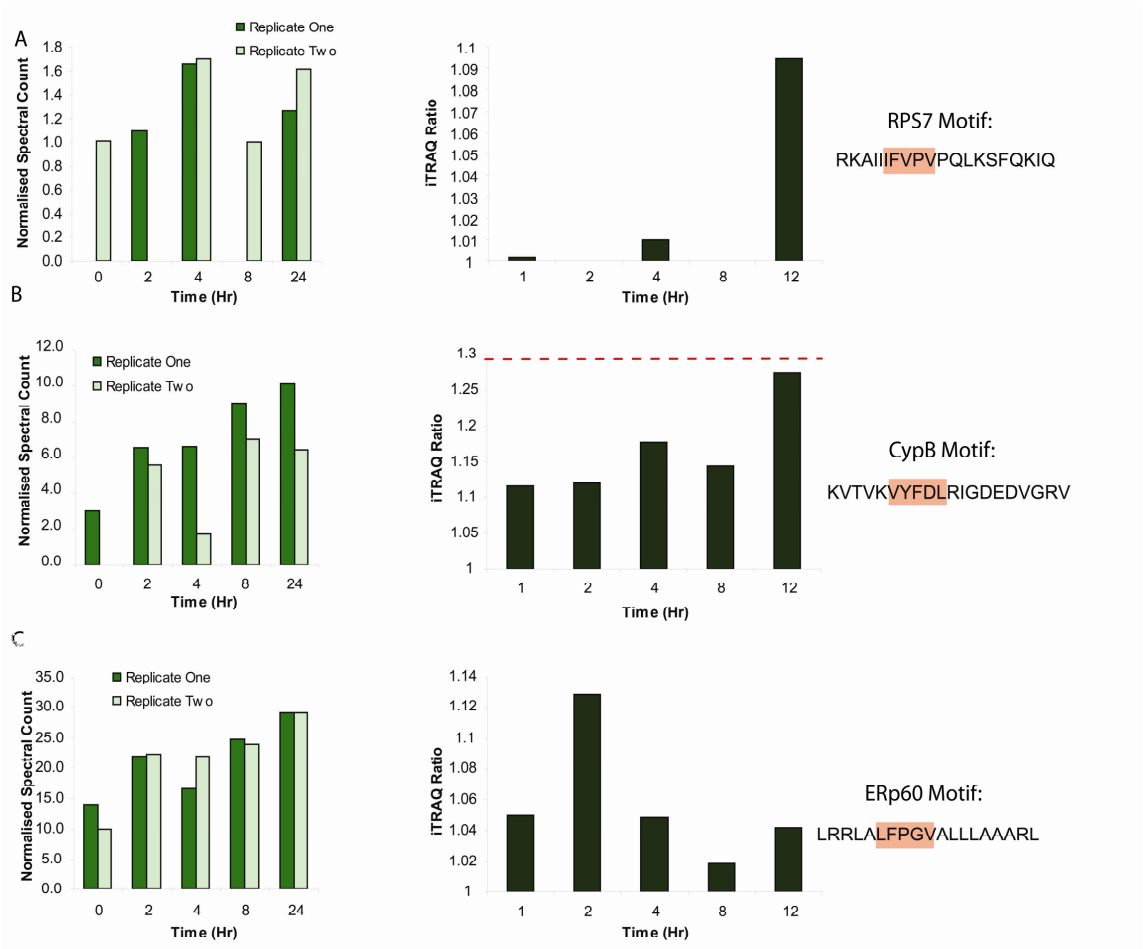

Figure 5.2 – MS screen quantitation results (left spectral count result from PAcIFIC, right iTRAQ) and BOX-I like motifs corresponding to the motif discussed in Chapter 4 which were found in the sequence of; A) RPS7, B) CypB, C) ERp60.

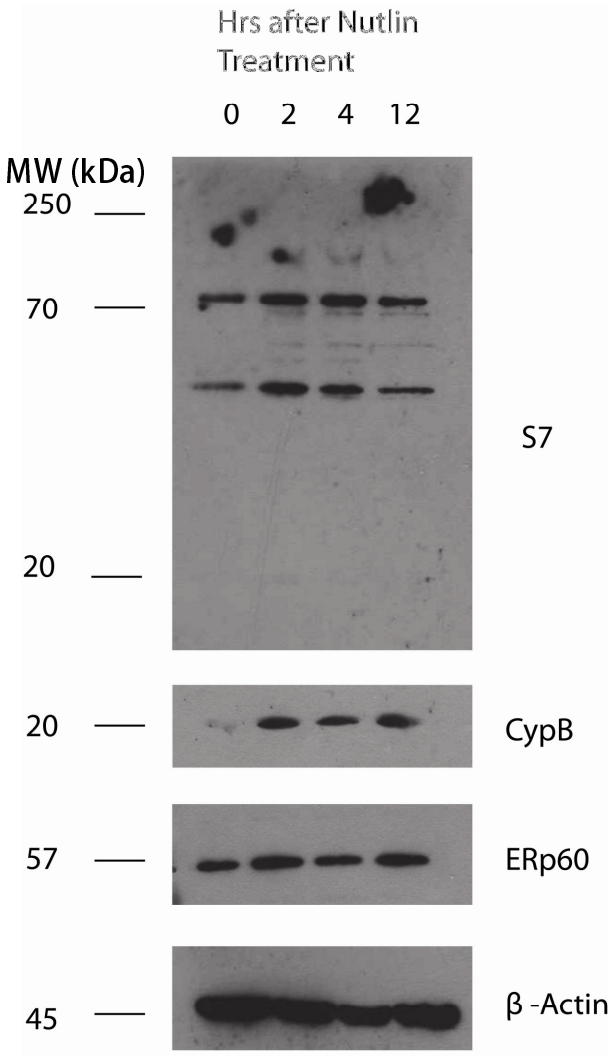

Figure 5.3 – Protein levels visualized by western blot for RPS7, ERp60 and CypB after 40 μM Nutlin treatment in MCF7 cells.

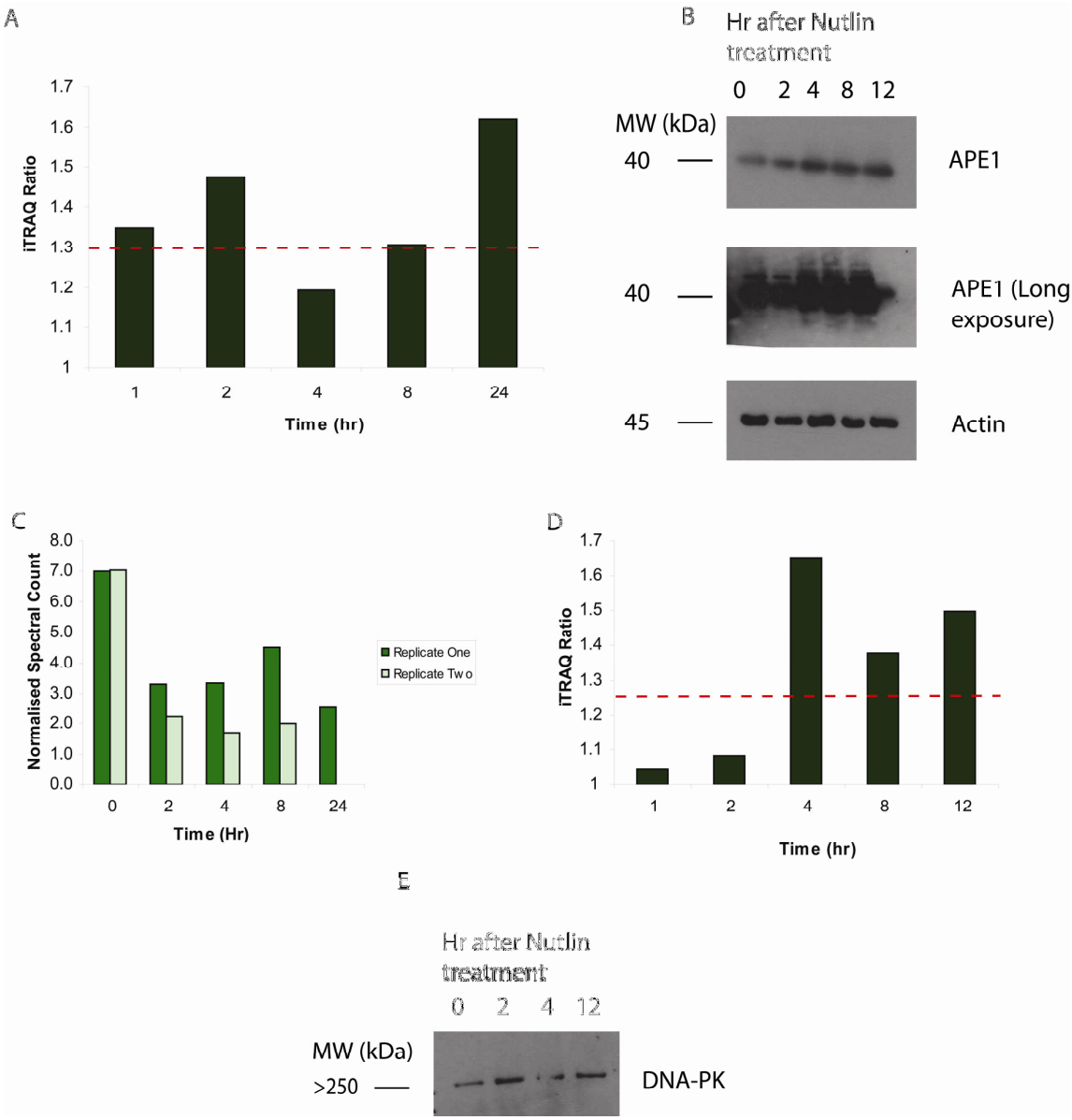

Figure 5.4 – APE1 levels after Nutlin treatment by A) iTRAQ MS and; B) detected by western blot C) DNA-PK PAcIFIC spectral counting quantitation results, D) iTRAQ quantiation results and E) DNA-PK levels visualized by western blot after Nutlin treatment in MCF7 cells. Western blot for β-actin loading control is shown in Fig. 5.3

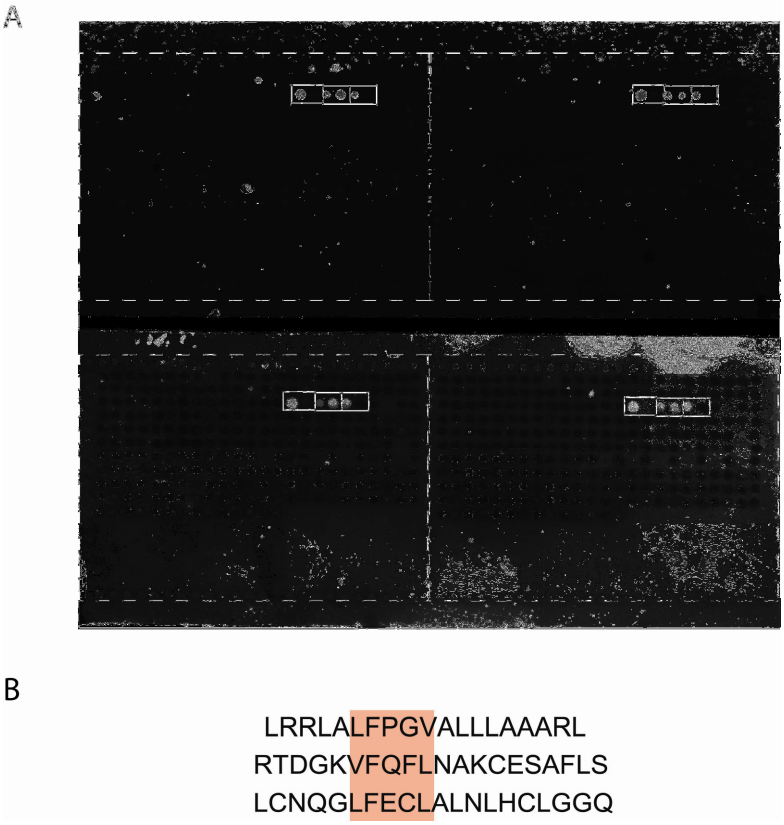

Figure 5.5 – A) CelluSpots (Intavis) peptide array probed with N-terminal domain MDM2 (aa 1-126) (top) or full length MDM2 (bottom) (conc.). Peptides with a positive signal are highlighted by white boxes. B) Sequence of peptides which bound by this assay

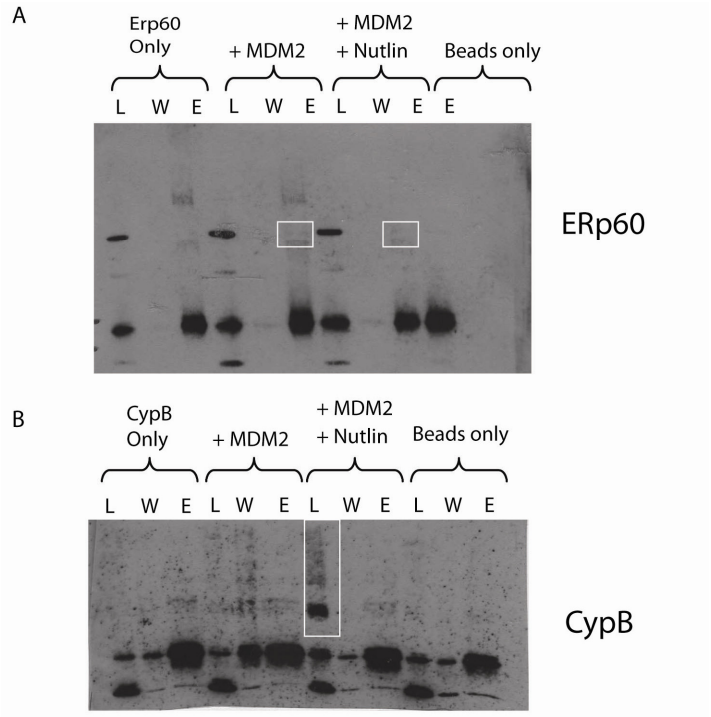

Figure 5.6 – Western blot for co-immunoprecipitation of A) ERp60, elution bands highlighted with white box, and B) CypB, smear highlighted with white box, with MDM2. Polyclonal anti-MDM2 (2A10) was bound to protein G coated beads and proteins which bound eluted with low pH. (L – Load (Cell lysate), W – Wash (Not bound to beads), E – Elution).

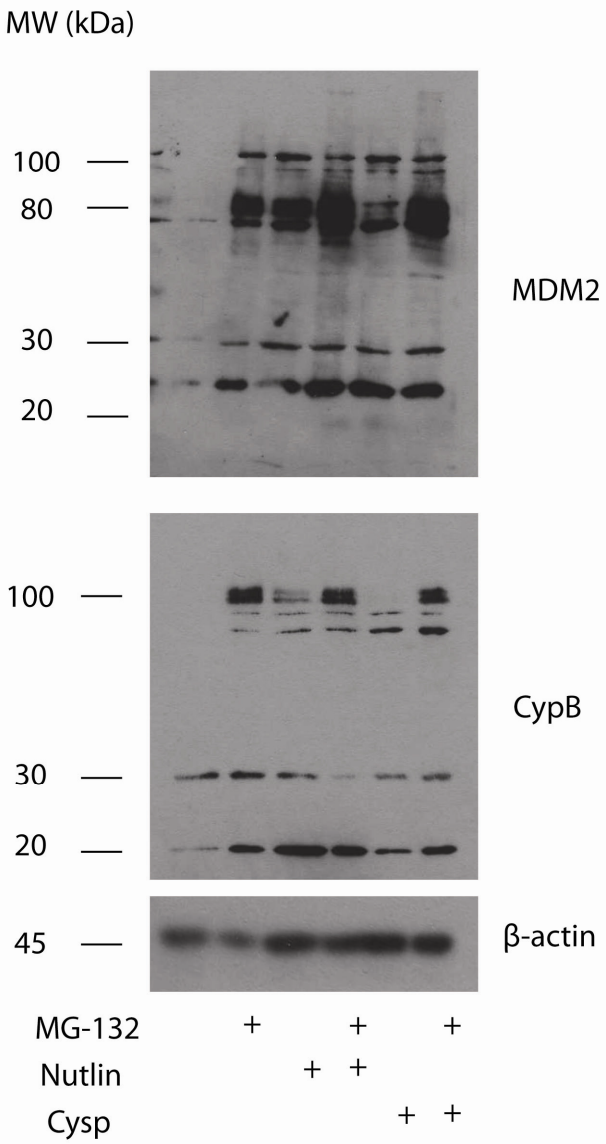

Figure 5.7 – Western blot to visualize protein levels of MDM2 and CypB after treatment with MG-132 (10 μM), Nutlin (40 μM) and cyclosporine (Cysp 10 μg/ml). β-actin blot included as loading control.

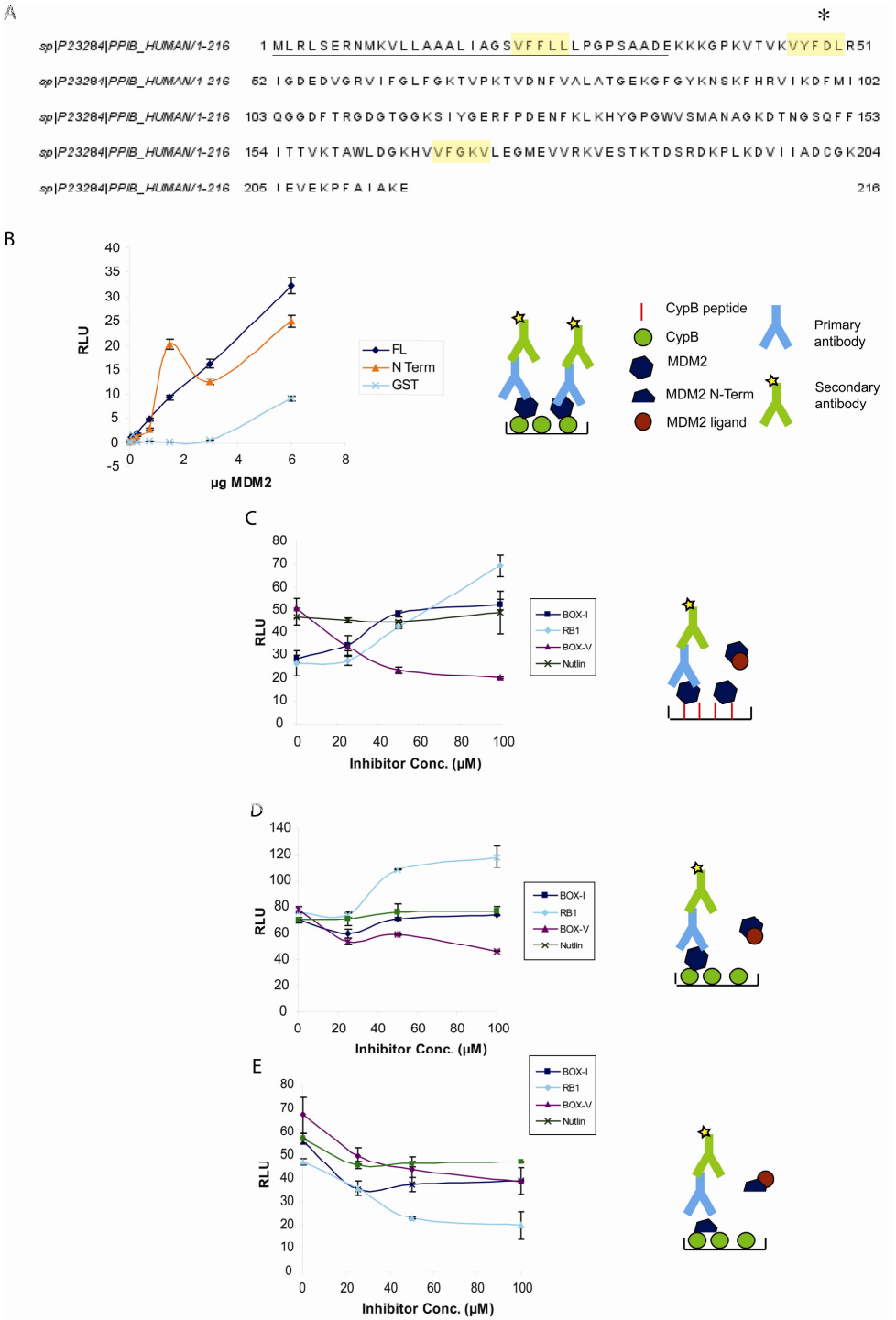

Figure 5.8 A) CypB primary amino acid sequence with BOX-I like motifs highlighted in yellow, and MDM2 binding peptide highlighted with asterisk. Cleaved leader sequence is underlined. B) Full-length CypB binding full-length and N-terminal domain MDM2 by ELISA illustrated in schematic. Competition assay with known MDM2 peptide ligands of; C) Full-length MDM2 from immobilized CypB peptide, D) Full-length MDM2 from CypB protein E) N-terminal domain MDM2 from CypB protein.

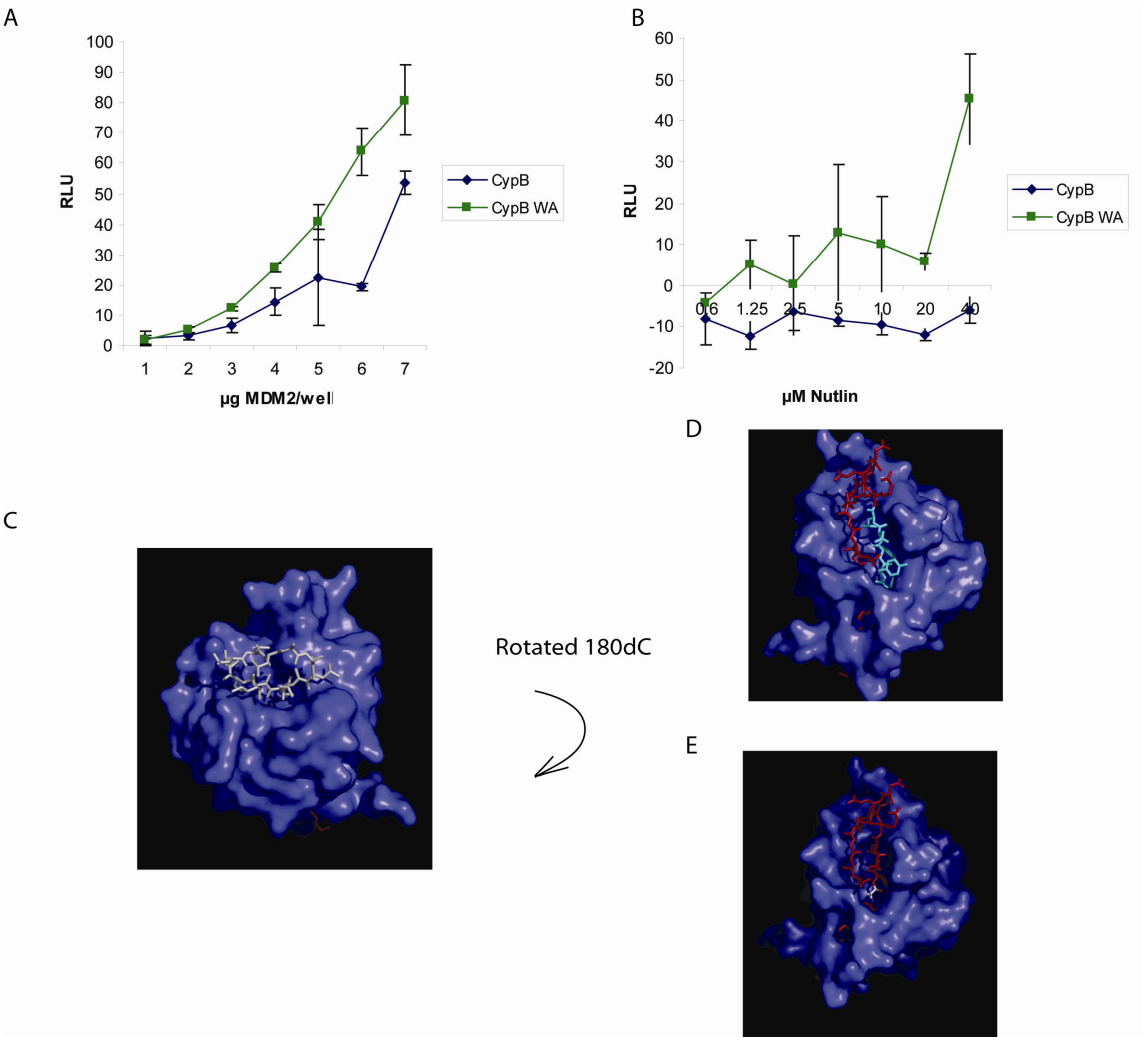

Figure 5.9 – Immobilized A) CypB wild type and B) CypB W to A mutant protein binding full-length MDM2 by ELISA. C) Structure of CypB bound to cyclosporine (gray) PDB:1CYN D) with BOX-I like MDM2 binding motif highlighted in red and E) with BOX-I like motif with W to A mutated in silico highlighted in red.

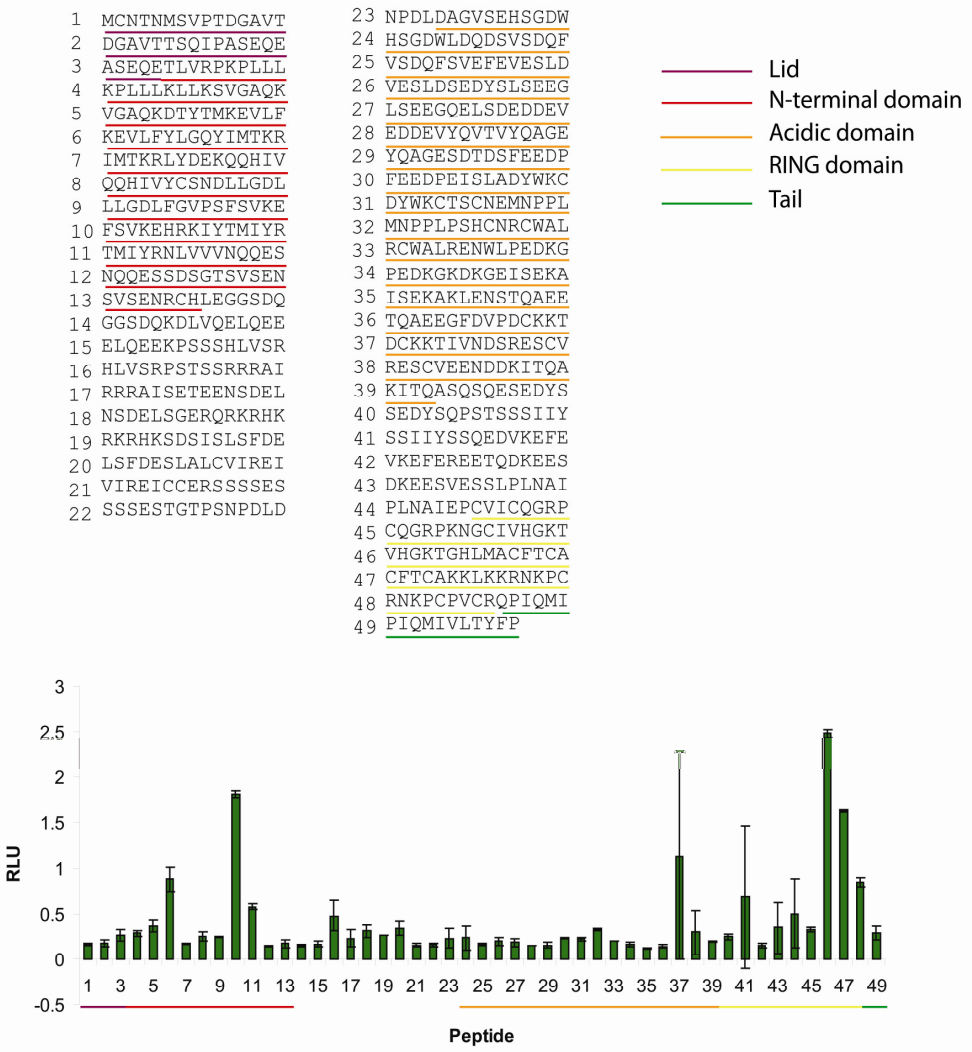

Figure 5.10 – A) Overlapping MDM2 peptides and domain they are found in. B) Full-length CypB (10 µg/well) binding to immobilized overlapping peptides from MDM2 by ELISA.

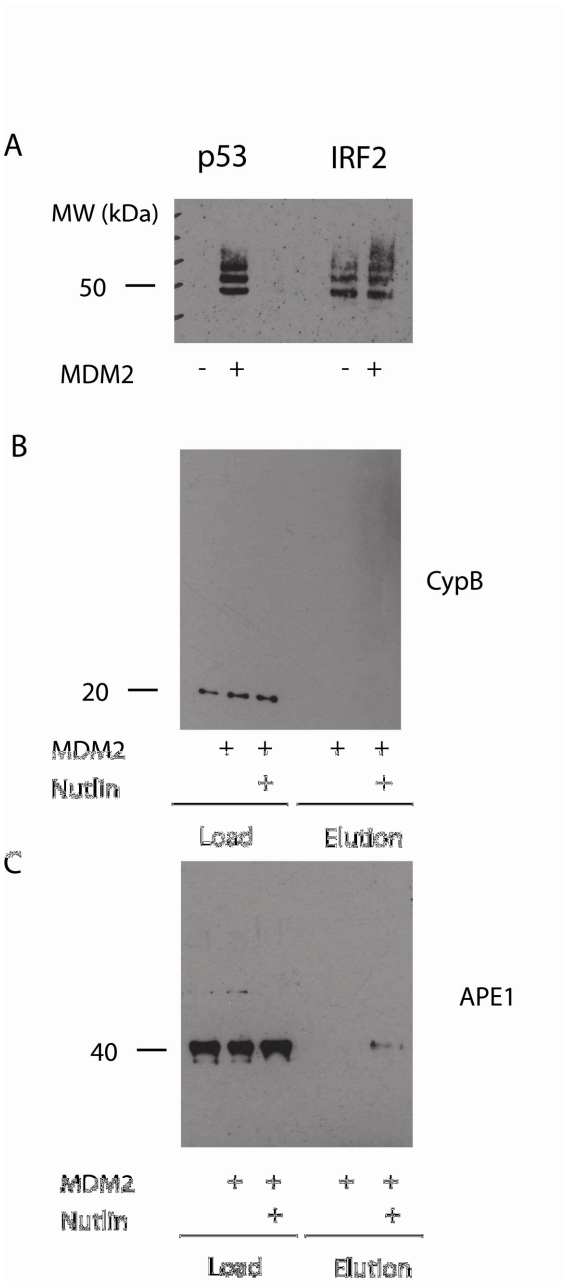

Figure 5.11 – A) In vivo ubiquitination assay (described in Chapter 2) for p53 and IRF2 with and without co-transfection of MDM2 in H1299 cells. In vivo ubiquitination of B) CypB C) APE1. Load lanes (1-3) are cell lysate, Elution lanes are fraction eluted from column after extensive washing.

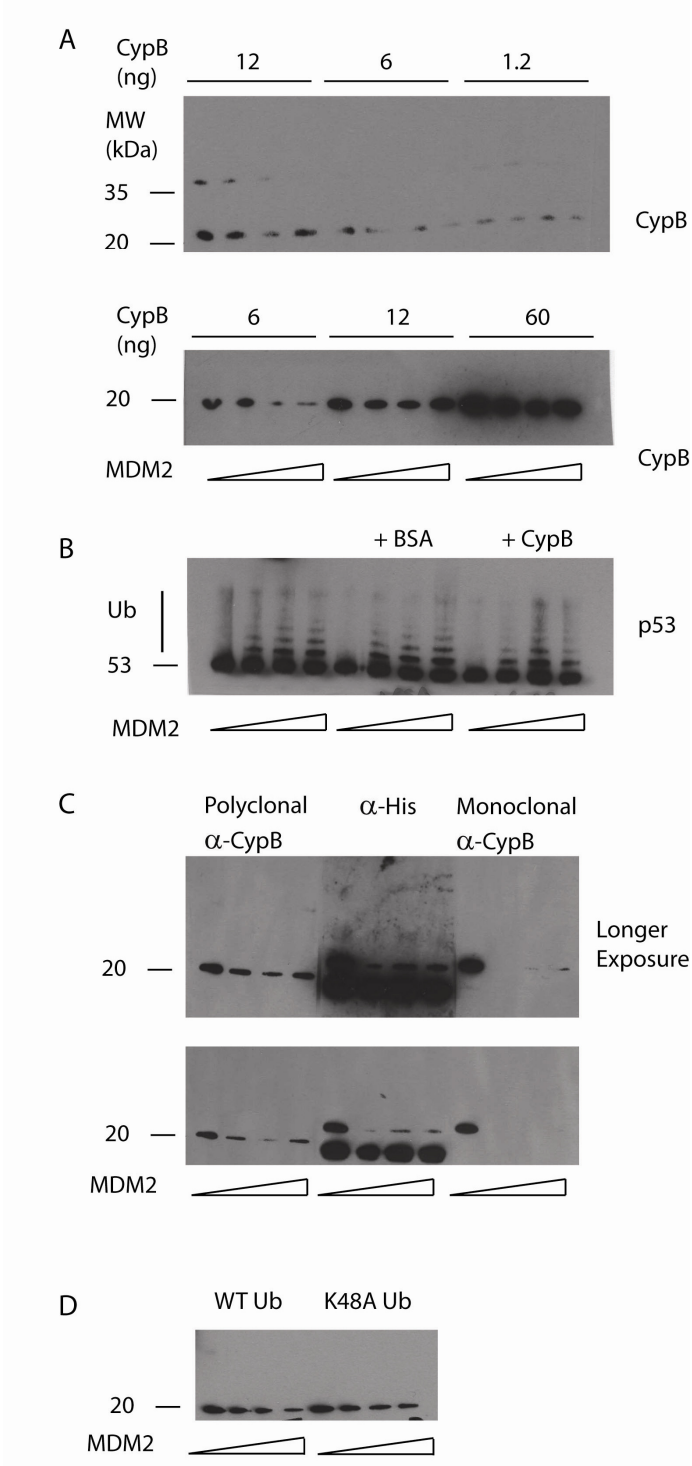

Figure 5.12 – In vitro ubiquitination assays with MDM2 (conc.) as the E3 ligase for A) CypB (detected with polyclonal anti-CypB), B) p53 with either BSA and CypB as potential competitors, Ub – ubiquitinated p53. C) CypB with a range of antibodies used for detection, D) CypB with mutant (K48A) ubiquitin.

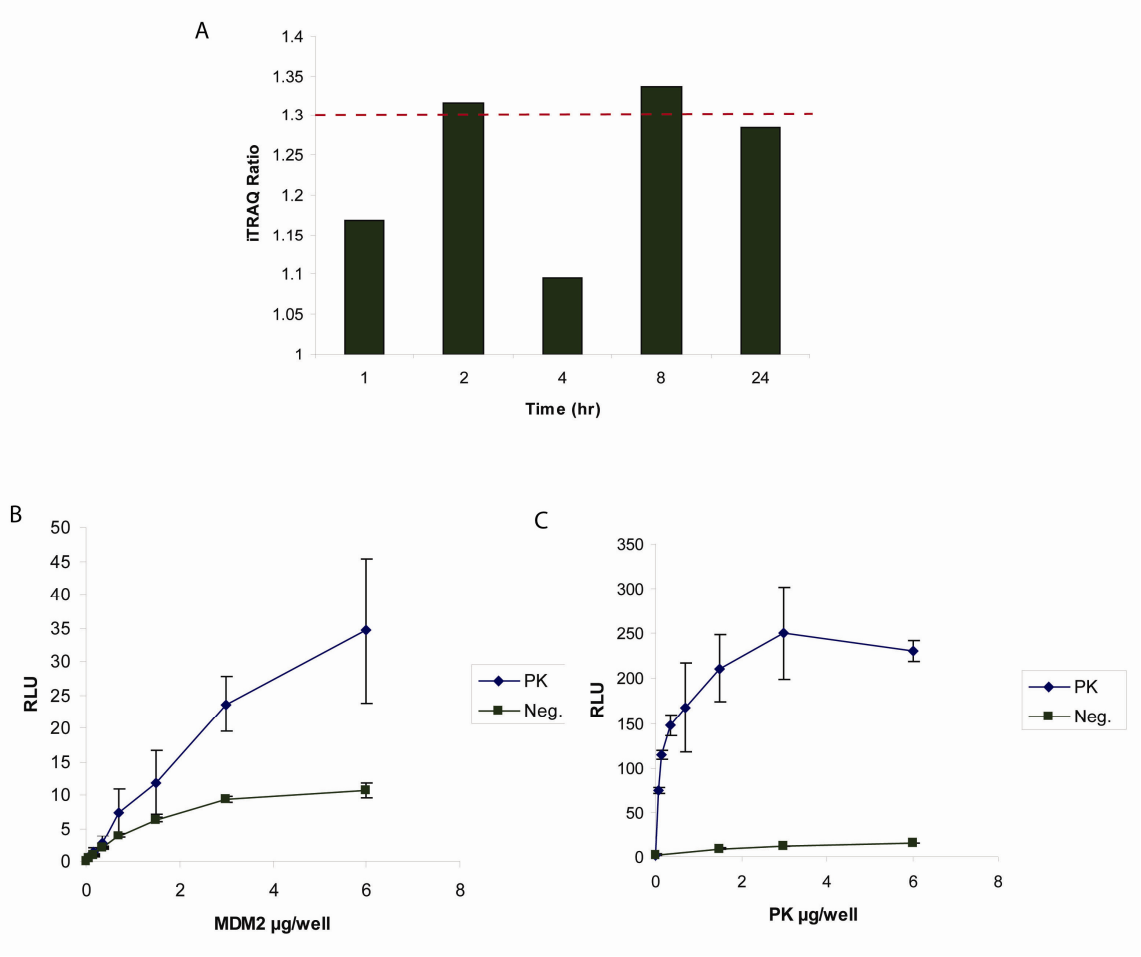

Figure 5.13 – A) iTRAQ MS result showing pyruvate kinase levels over Nutlin time course. B) Pyruvate kinase binding MDM2 by protein-protein ELISA with immobilized PK detected with anti-MDM2 antibody (2A10), C) with immobilized MDM2 detected with anti-PK antibody.

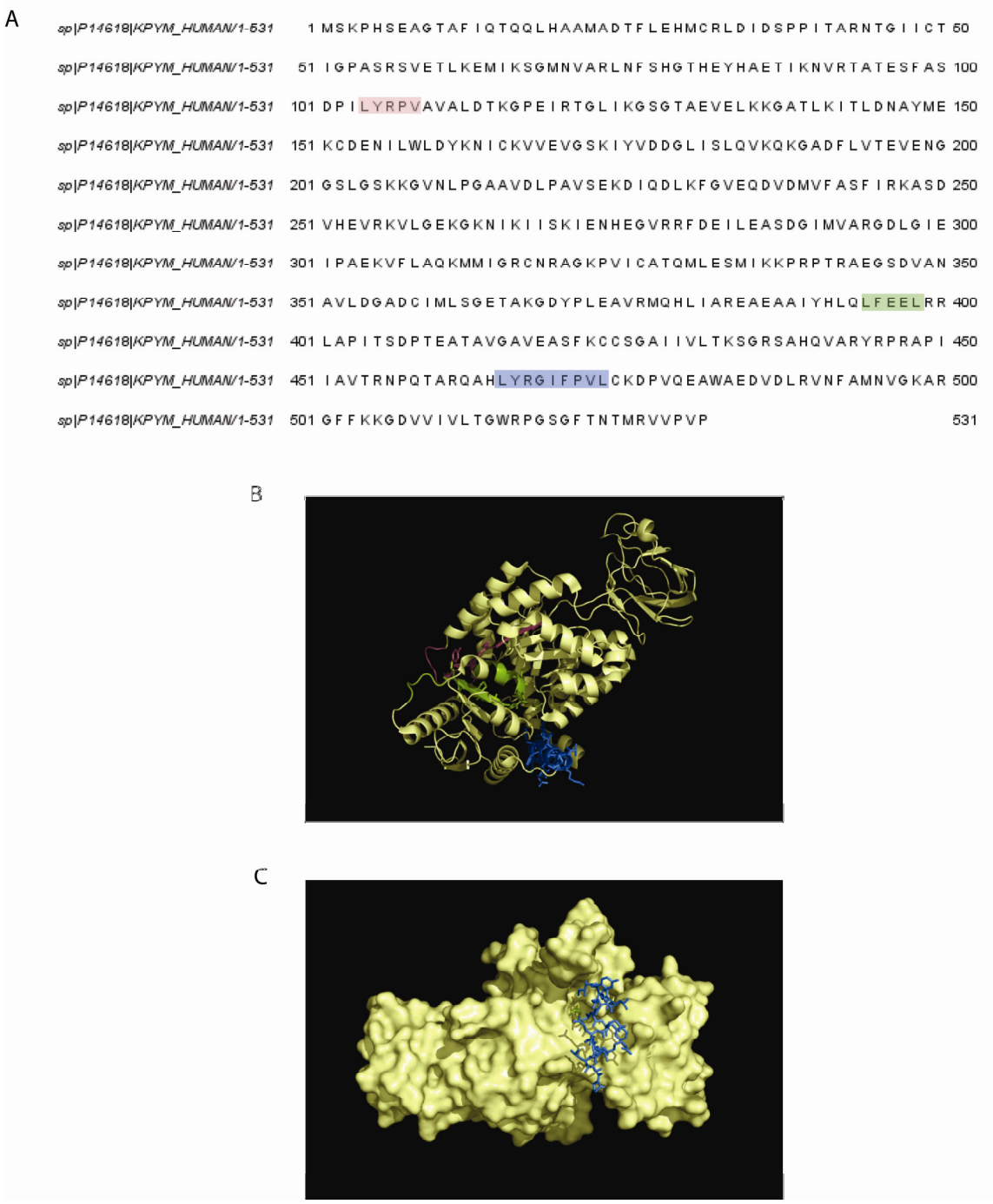

Figure 5.14 – A) PK primary amino acid sequence with BOX-I like motifs highlighted. B) PK structure with motifs highlighted in same colours as in A C) Position of BOX-I like motif on PK surface PDB: 1ZJH.

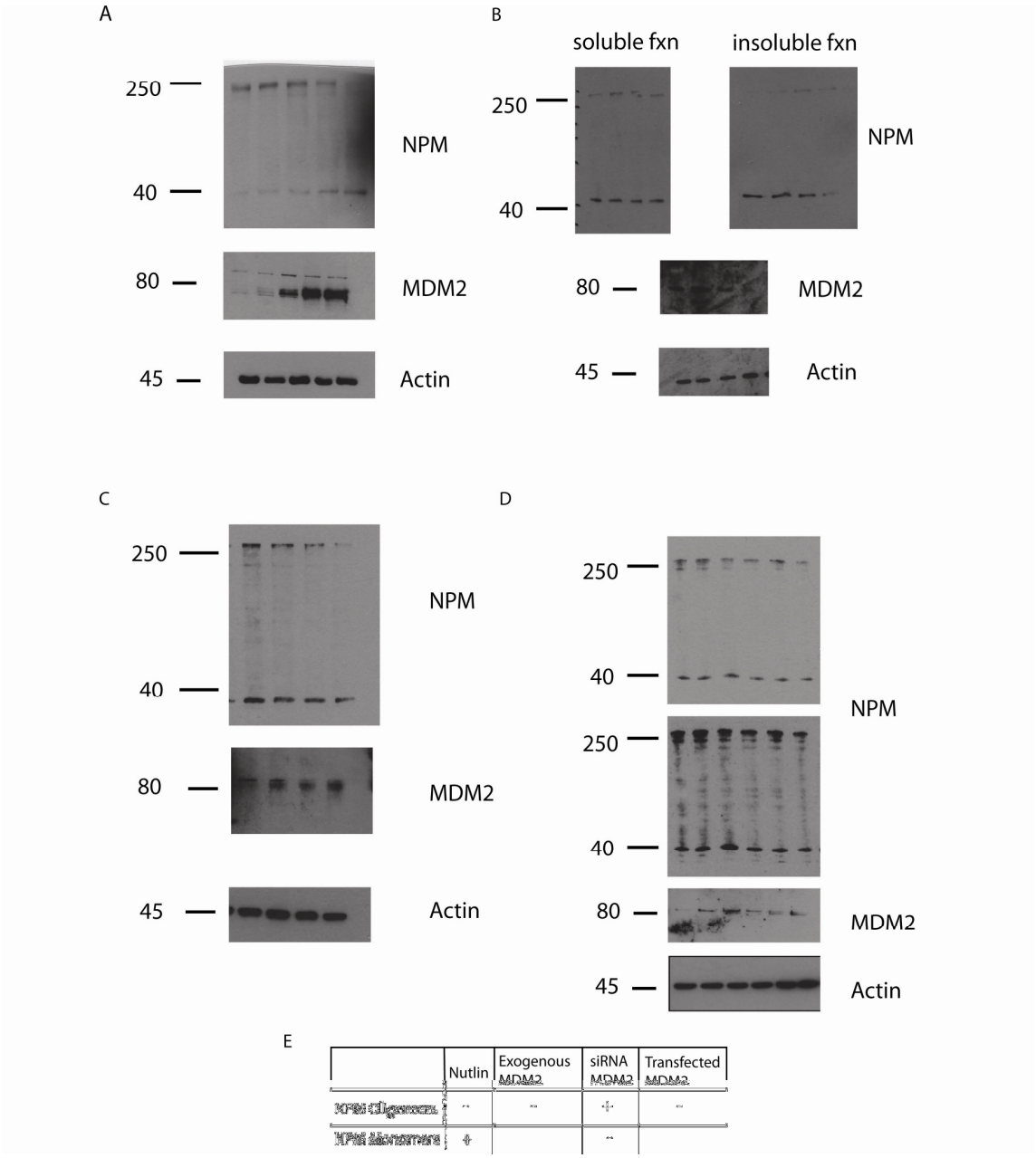

Figure 5.15 – Nucleophosmin response to Nutlin treatment. A) In MCF7 cells after Nutlin treatment B) after siRNA to MDM2, C) after addition of exogenous MDM2 to lysates, D) after transfection of MDM2 into H1299 cells E) Summary of NPM response to Nutlin and MDM2

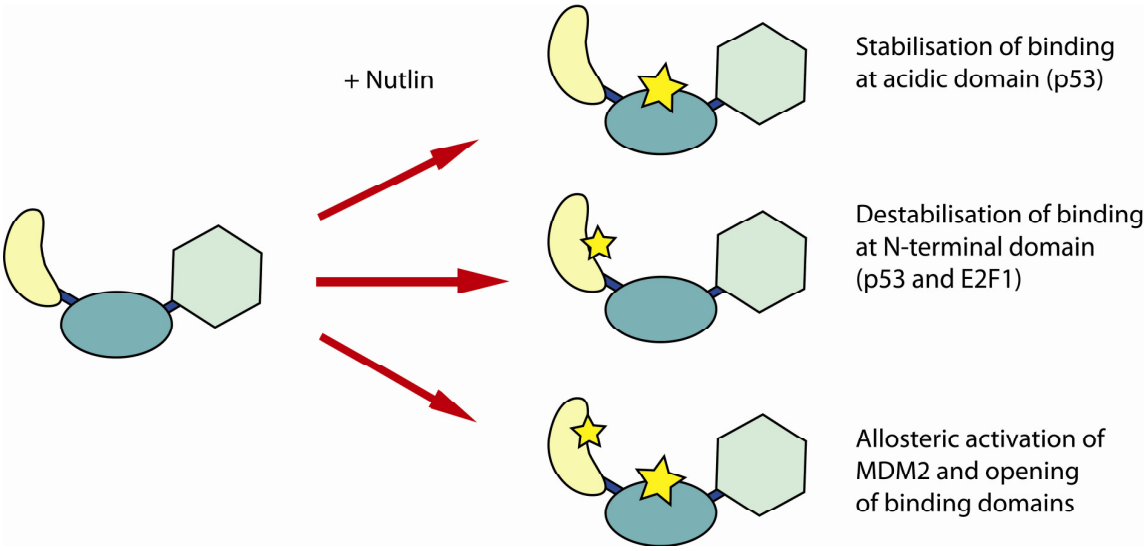

Figure 5.16 – Model of MDM2 activation response to Nutlin

6 - Linear motifs as tools for investigating protein-protein interactions

6.1 Introduction

There are different methods which can be used to find linear motifs; one is through known binding partners and sequence similarity, and another is by optimization of known peptide ligands to discover the critical residues. For example if a protein has a known high affinity peptide ligand this can be used as a starting point to search for similar peptides which also bind, as with the MDM2 binding peptides 12.1 and PMI which are similar to BOX-I[130]. In either case the peptide ligand can be used as the base to design a peptidomimetic protein-protein interaction inhibitor, an example of this is Nutlin which mimics the BOX-I region of p53 and blocks binding to MDM2[133]. The protein AGR2 is a protein disulphide isomerase[219] which has been shown to promote transformation in Barrett's oesophagus and downregulates p53[125]. Little is known about the AGR2 interactome and the exact function of AGR2 in transformation and cancer pathways is yet to be elucidated. A 12-mer AGR2 binding peptide, HLPTTIYYGPPG was obtained by phage peptide display and optimized to the core hexapeptide PTTIYY[124]. This peptide aptamer was then validated as a modulator of p53 localisation and AGR2 localisation, although it is not yet clear by which pathway this is occurring[128]. To validate the potential of this peptide as a drug template, it was conjugated to the optimized version of the cell penetrating peptide penetratin (RRMKWKK) and used to treat MCF7 cells.

6.2 A six-mer peptide which binds AGR2

The PTTIYY peptide binds to AGR2, shown by ELISA (Fig. 6.1) and previously by MS[220]. Previously identified peptides derived from proteins which are similar to PTTIYY were also tested by this method. These peptides exhibited an above background signal for AGR2 binding, although none were as effective in binding as the phage display derived peptide. The peptides derived from the protein SMG7 showed the largest amount of binding.

6.3 Penetratin-PTTIYY causes stabilization of p21 and contributes to UV mediated stabilization of p53

Variation in MCF7 cells used by different groups has previously been reported, and two types of MCF7 cell were identified each with different levels of AGR2, described here as high or low MCF7 cells (Fig. 6.2). It has previously been shown that transfected PTTIYY can alter the localization of AGR2 and p53, and affect the morphology of nuclei[128]. To investigate this further, Pen-PTTIYY was used to treat cells over a time course and overall levels of p53, p21 and AGR2 monitored by western blot. As a negative control the point mutated Pen-PTTIYA and the truncated peptide Pen-PTTI were used, as it has previously been shown the YY residues are important for AGR2 binding[124]. Pen-PTTIYY aptamer treatment resulted in stabilization of p21 relative to the truncated control, as did treatment with Pen-PTTIYA (Fig.6.2a). There was no change in p53 levels, however the increase in p21 suggests p53 may be transcriptionally activated by the aptamers. When the aptamers were added to the cells in combination with a dose of UV radiation, the p53 level was increased dramatically only in those cells treated with Pen-PTTIYY, along with the level of p21 (Fig. 6.2b). A375 cells which do not have

detectable levels of AGR2 were not affected by the aptamer. It has been observed that UV treatment can induce p21 degradation[221], and comparison of high AGR2 MCF7 cells to low AGR2 MCF7 cells after low UV treatment demonstrated that aptamer treatment rescues p21 from this degradation in the high AGR2 cells. In the low AGR2 cells both UV and aptamer treatment had little effect on any proteins, potentially there is a mild stabilization of p53 with UV treatment (Fig. 6.2c). Subcellular fractionation of MCF7 cells was carried out, and treatment of high AGR2 MCF7 cells with the Pen-PTTIYY aptamer resulted in relocalisation of AGR2 and p53 both to the nucleus as early as 4 hours after treatment with aptamer and UV or the proteasome inhibitor MG-132 (Fig. 6.3).

6.4 Transcriptional activation of p53 pathway in response to PTTIYY treatment

A super array (SABiosciences) representing genes in the p53 pathway was used to analyse transcriptional activation in response to aptamer treatment (Fig. 6.4). This assay measures the levels of various mRNAs which are associated with the p53 pathway. There were differences in transcription detected between aptamer treated cells and cells which were untreated, and also differences between Pen-PTTIYY treated cells and those treated with the truncated control peptide (Fig. 6.4a). Activated genes included BAX, which is consistent with the hypothesis that PTTIYY activates p53 transcriptionally. MDM4 is also induced relative to control and untreated cells, which is a link between AGR2 and the p53-MDM2-MDM4 axis. There was a slight increase in RB1, which is another tumour suppressor closely linked to MDM2 and p53. Interestingly, titration of

AGR2 into A375 cells resulted in a corresponding increase in the transcription of RB1 (Fig. 6.4b).

6.5 Discussion

The Pen-PTTIYY aptamer was discovered by phage peptide display, and it was shown here to bind AGR2 with high affinity. Sequences resembling this peptide which were discovered in proteins also bound AGR2 to a lesser extent, with peptides from SMG7 and MEKK3 binding slightly to AGR2. These peptides may be weaker binders due to a more transient interaction, such those which can occur in cells and are important for cell signaling cascades. These results demonstrate that phage peptide display can be a useful method for beginning to investigate proteins with few known binding partners, and as a way to identify protein-protein interaction interfaces. Phage peptides with high affinity such as this are useful as tools for molecular biology, to co-immunoprecipitate proteins and in some cases act in a similar way to antibodies, although they are much quicker and cheaper to produce.

The cellular effects of the AGR2 aptamer include relocalisation of AGR2 and p53. This may be one of the modes of negative regulation of the p53 pathway by AGR2, and targeting AGR2 may result in more nuclear p53 and therefore more active p53. p53 is a transcription factor controlling apoptosis related genes such as BAX, and this function takes place in nuclei. The activation of RB1 transcription by AGR2 transfection is also interesting, as this protein can bind MDM2 and act as a tumour suppressor, further linking AGR2 to p53 related cancer pathways. This is not observed in cells with low

AGR2, suggesting the aptamer is functioning in the high AGR2 cells because this is one of the dominant regulators of the p53 pathway when there are high levels of AGR2. Several drugs based on peptides are in development including a peptidomimetic which targets the Smac-XIAP interaction as a potential anti-tumour therapeutic[222]. Nutlin is similar to these drugs, because of the high similarity to BOX-I, however this was discovered by a high-throughput screen rather than rationally designed based on the peptide[133]. The results here show that this AGR2 derived peptide may be a viable template for further development as an AGR2 binding drug.

This demonstration of cellular effects of the aptamer targeting AGR2 highlights the importance of linear motif interactions in regulation of interactomes. Using the phage display derived peptide as a protein-protein interaction inhibitor of unknown protein-protein interactions is a slightly different approach than that of Nutlin to inhibit a known protein-protein interaction. The ability to target interfaces without knowing the binding partners of a protein makes peptide aptamers like this a useful approach to finding new binding partners for a protein, as well as investigating by which mechanisms and pathways they contribute to cancer cell survival.

One approach to investigating linear motifs is to alter the interactome of a protein with a drug and look for similarity in sequence between which the proteins that are affected, and this is the route described in the previous chapters. The PTTIYY-AGR2 example described in this chapter uses phage display as the basis for discovering a peptide which may block a protein-protein interface. This can be optimized as a drug and also used to

search databases for similar sequences in potential AGR2 binding proteins, and is another approach to the problem of discovering new protein-protein interactions via linear motif mechanisms. The advantage of the method described here, is that little prior knowledge about a protein mechanism is required to follow the phage display route. Phage peptide display, and the aptamers which are derived from the technique are a complementary method to the studies described in Chapters Three and Four. For the MDM2 interactome Nutlin was used in combination with information about linear motifs which bind MDM2 to identify potential new binding proteins, whereas for AGR2 there was little prior knowledge about which peptide sequences AGR2 is capable of binding. The phage peptide display provided both information about potential AGR2 binding sequences, and may be developed further as a peptidomimetic. This demonstrates that it is possible to find out about the interactome of a relatively new target using similar methods that are applied to well characterized targets. Both of these methods contribute to our understanding of the interactome of a protein, by providing protein leads for further validation and are tools for finding out which pathways and processes a protein is involved in.

A

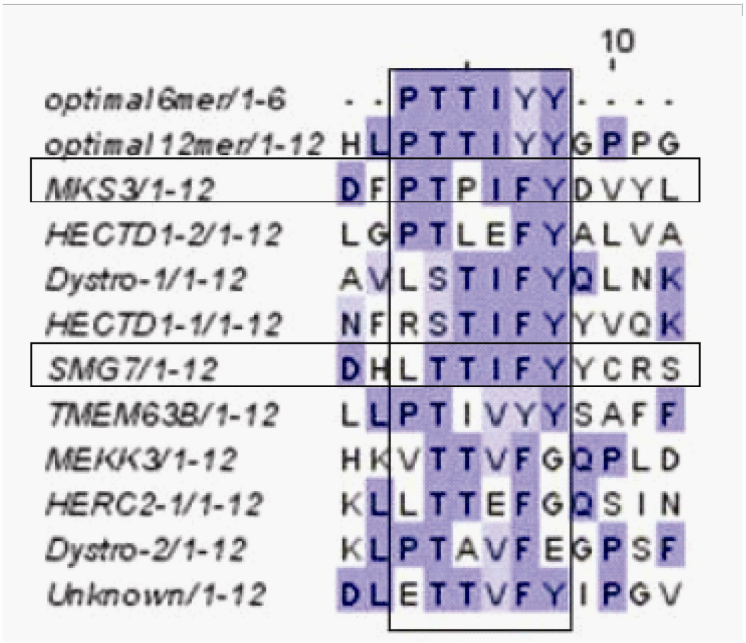

B

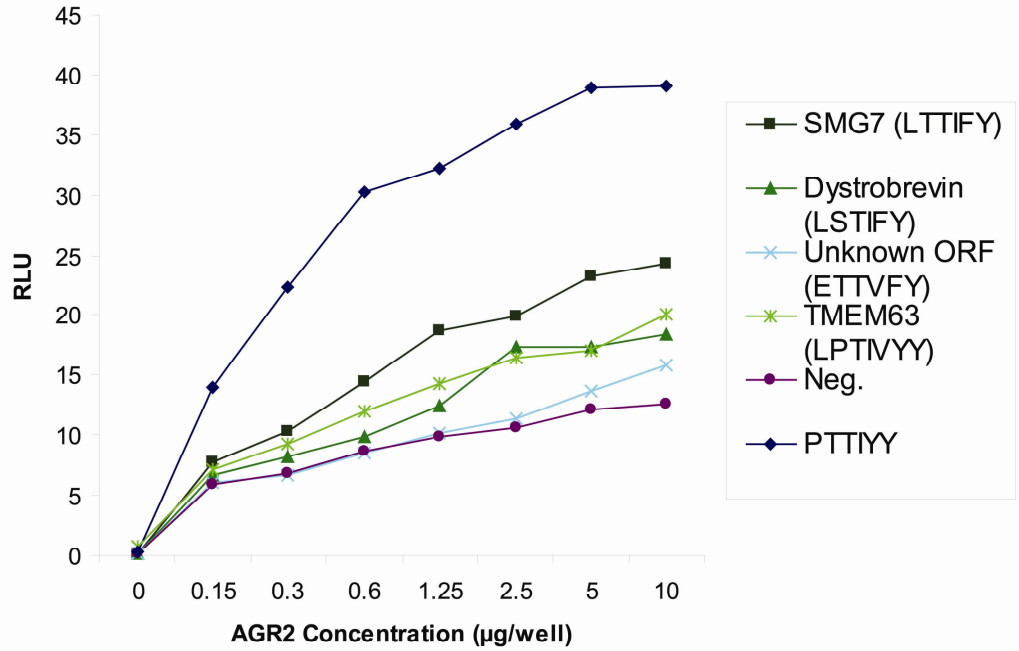

Figure 6.1 –A) Alignment of sequences with PTTIYY similarity from proteins in swisprot found by BLAST (NCBI). B) ELISA binding of AGR2 to immobilised PTTIYY and peptides with sequence similarity to PTTIYY detailed in A.

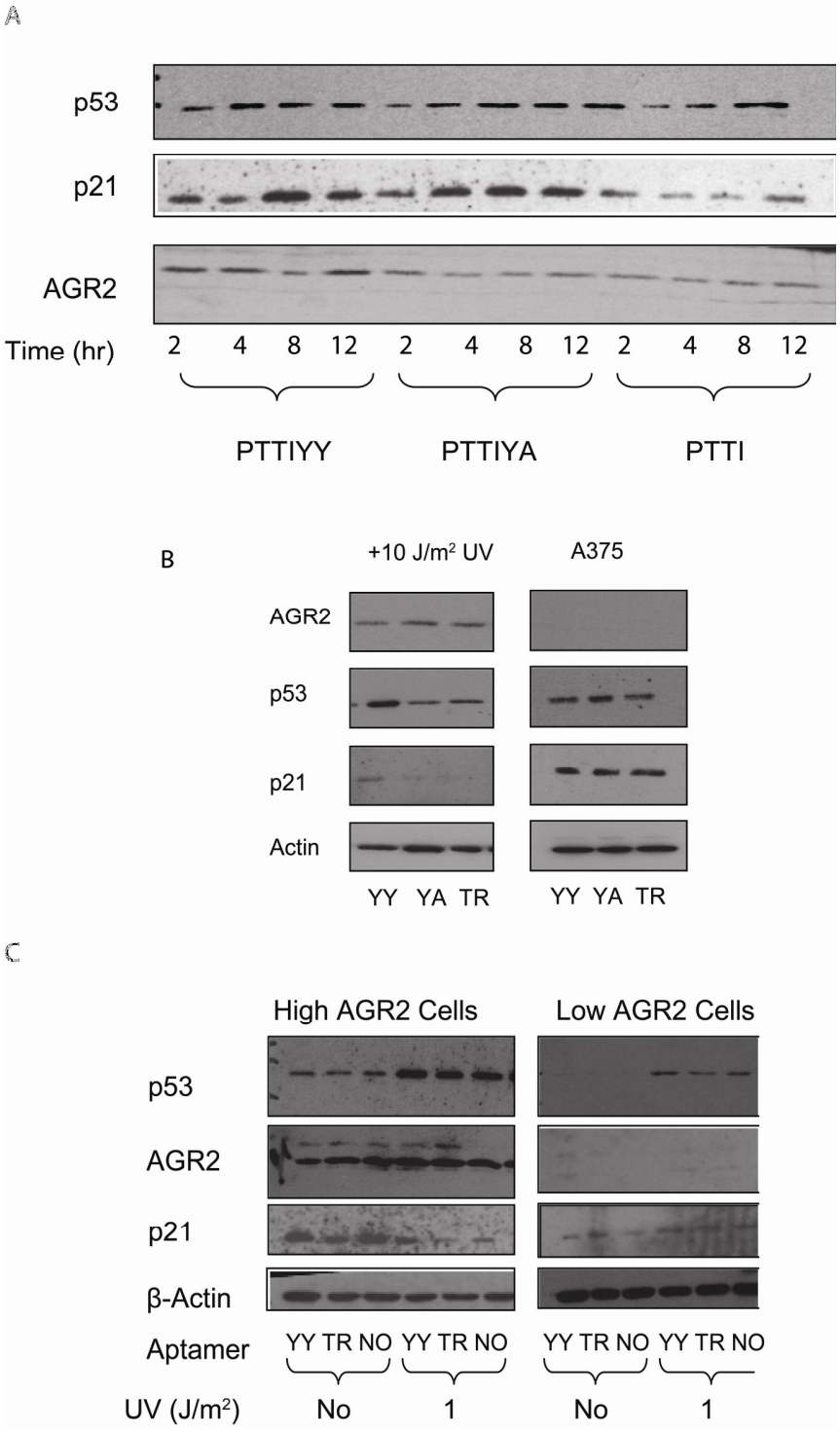

Figure 6.2 – A) Levels of p53, p21 and AGR2 after aptamer treatment over time course detected by western blot. B) Effect of aptamers in combination with UV on MCF7 cells and on control A375 cells. C) Aptamer effect with low dose (1J/m2) UV on high and low AGR2 expressing MCF7 cells. YY – Pen-PTTIYY, YA – Pen-PTTIYA, TR – Pen-PTTI, No – No treatment

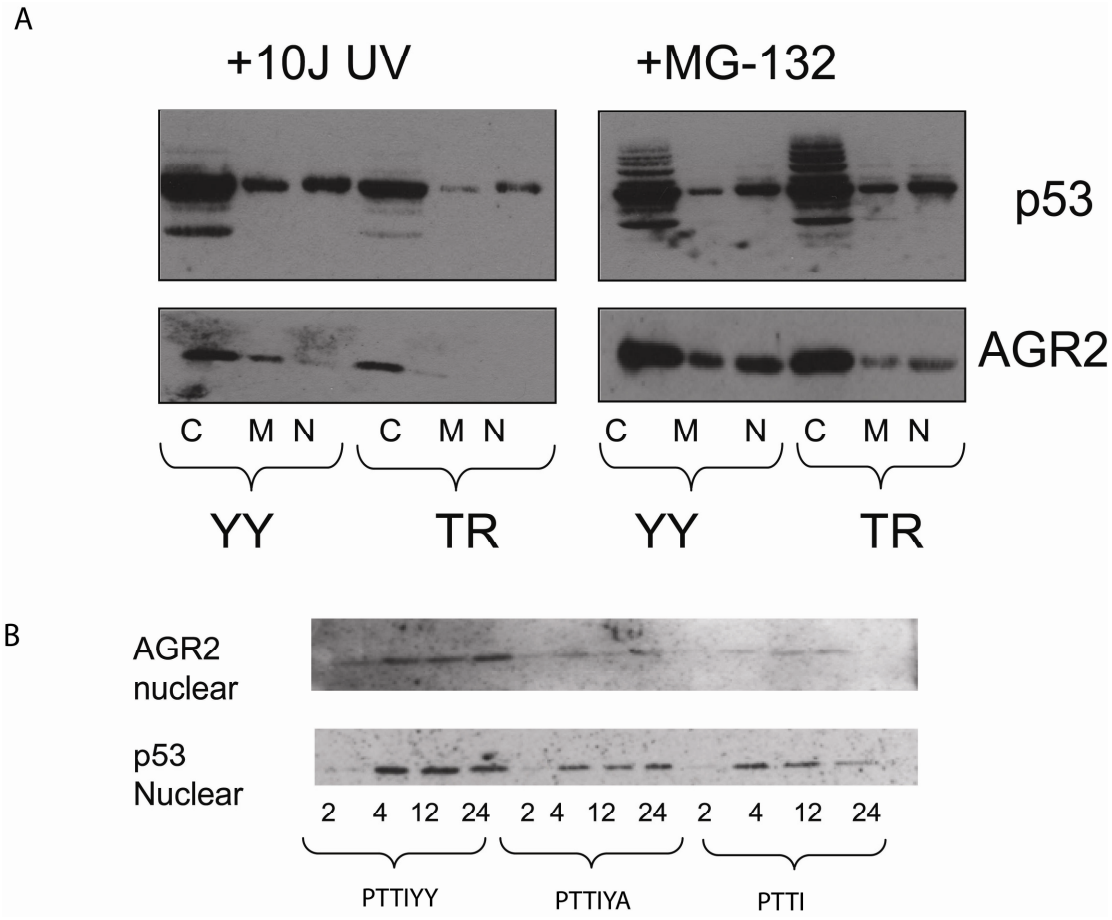

Figure 6.3 – A) Western blot showing subcellular localization of AGR2 and p53 after aptamer treatment and combination with UV or MG-132 treatment, and after subceullar fractionation. B) Change in p53 and AGR2 levels over time in the nuclear fraction. YY – Pen-PTTIYY, TR – Pen-PTTI, C – Cytoplasm, M – Membrane, N – Nucleus.

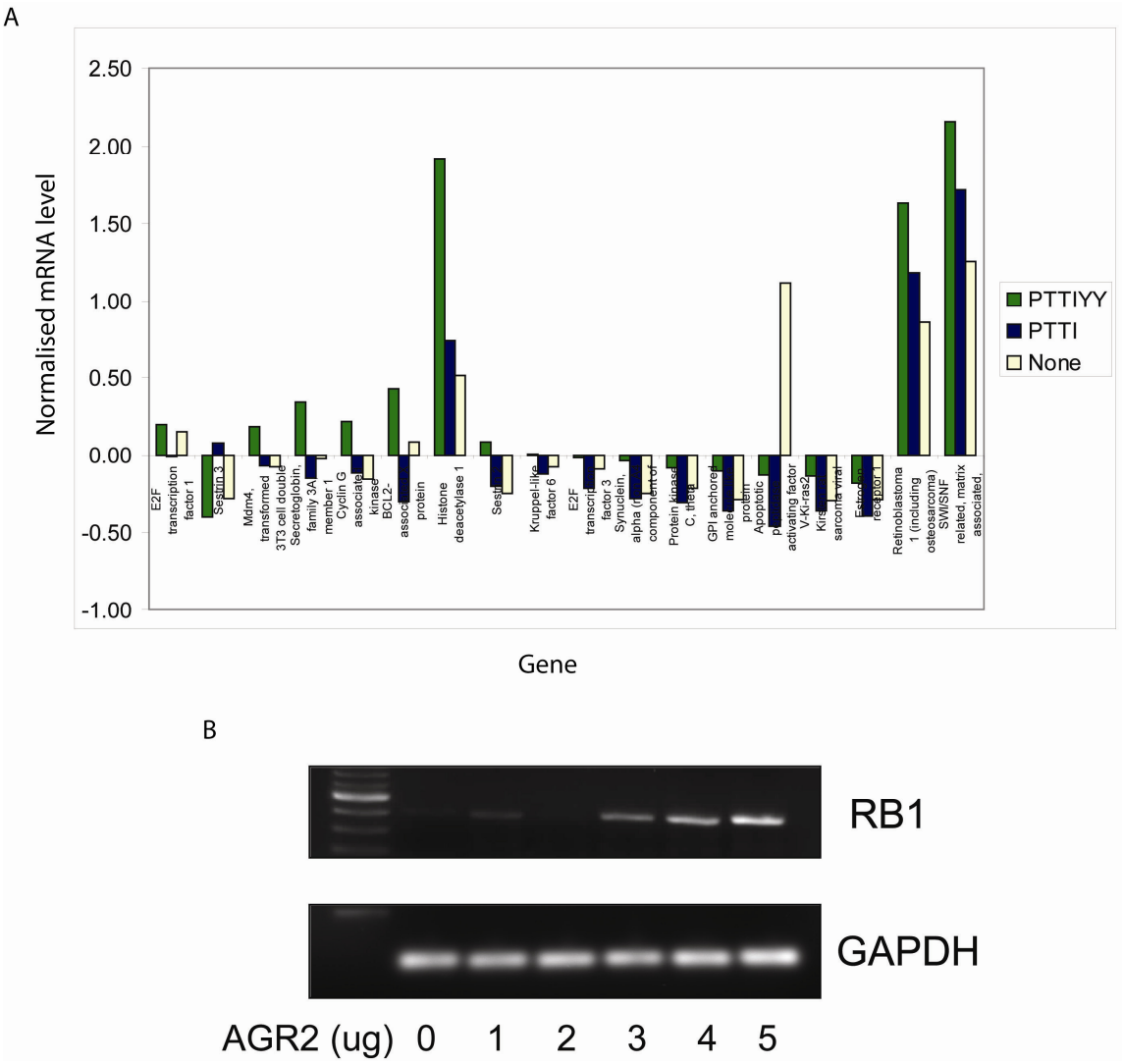

Figure 6.4 – A) Super array quantitation of transcription levels of a subset of genes after treatment with AGR2 targeting aptamers PTTIYY or PTTI (control). B) Increase in RB1 transcript levels after AGR2 transfection detected by RT-PCR. GAPDH is included as a loading control.

7 – Conclusions and Future Work

The aim of this work was to use proteomic mass spectrometry to investigate the MDM2 interactome, and investigate the utility of this method for discovering new protein-protein interactions. A difficulty with quantitative proteomic studies on global protein levels can occur when filtering the large amount of information which may be obtained to highlight interesting leads and phenomena. Therefore to complement the analysis of the proteomic results obtained here, the results were screened for the presence of an MDM2 binding motif. This represents a new approach to filtering proteomic data, by using linear motifs derived from proteins already known interact with MDM2 to highlight potential members of the MDM2 interactome. Over a time course of treatment with the drug Nutlin, many known MDM2 binding proteins which have altered levels detected by both the less stringent label-free quantitation method and the iTRAQ screen, validating the proteomic mass spectrometry approach. There were also important differences between the two separate proteomic methods, and it may be useful to carry out several proteomic screens based on the problem being investigated. It has been shown here that even relatively small scale proteomics experiments can yield interesting information for biologists, and communication between mass spectrometrists and biologists is vital to understand this data and the significance of it. Considering the bias towards known proteins as drug targets, particularly those for which structural information is available this type of experiment could highlight new targets. In the future it would be interesting to compare more proteomic mass spectrometry experiments

targeting to MDM2, and further investigate the similarities and differences in the proteins identified by different proteomics methods.

The method used in this project to investigate the proteomics data involved searching for sequences with similarity to known MDM2 binding proteins, p53 and IRF2. Although peptides from both of these proteins exhibit binding to MDM2, the consensus sequence differs slightly from the residues known to mimic BOX-I. The primary result of this approach was to identify new MDM2 binding peptides, which depend on a core aromatic residue. Interestingly, these peptides do not appear to behave exactly as the BOX-I peptide. This can be linked to computational and experimental observations about the conformational flexibility of the N-terminal domain of MDM2, and studies which show extensive allosteric communication between the domains of MDM2. It is suggested by this data that the MDM2 N-terminus may have multiple binding sites, regulated by the lid and acidic domain and the Nutlin/BOX-I pocket is only one aspect of the N-terminal domain binding capabilities. There is potential to continue this research by further defining the residues which are important for MDM2 binding at the N-terminal domain, and linking this to structural and computational studies to ascertain the effect these ligands have on MDM2 allosterically. The other interesting result regarding the function of the N-terminal domain obtained in this work was the regulation of nucleophosmin oligomerisation after Nutlin treatment. If MDM2 binds nucleophosmin and causes de-oligomerisation, Nutlin actually enhances this function. Therefore where previously Nutlin has been described as an MDM2 inhibitor, it is also an activator of MDM2.

Using consensus sequences to identify MDM2 binding peptides, and potentially binding proteins, is an approach which is linked to the AGR2 binding peptide aptamer examined in Chapter Six. The peptide is an optimized binder, as selection by phage display selects for high affinity peptides, however it can still be used to mine databases for similar sequences in potential AGR2 binding proteins and as a tool. These two approaches both use the model of linear motif interactions to find or inhibit protein-protein interactions and this is a promising approach both as a starting point for drug design and to investigate protein-protein interaction mechanisms.

CypB and pyruvate kinase were both identified *in vitro* as novel MDM2 binding proteins, and this represents the beginning of work to fully validate these proteins *in vivo* and *in vitro*. Further experiments, such as co-immunoprecipitations and FRET could be used to further validate these interactions. As CypB and pyruvate kinase are identifications from label-free and iTRAQ screens respectively, this is a promising result for the role of proteomic mass spectrometry in target identification for cancer biology. CypB is involved in protein folding, and pyruvate kinase in metabolism which links MDM2 to proteostatic pathways. In particular, the identification of many proteins which are as yet unlinked to the p53 pathway highlights the fact that MDM2 is not solely involved in p53 regulation, although non-ubiquitin ligase functions of MDM2 may often be overlooked. Ubiquitin ligases are integral to the control of protein degradation, and a role in quality control of cellular proteins may be linked with this function. These proteomic studies have revealed that there are wide ranging effects after Nutlin

treatment, and this could be useful in identifying off-target effects as well as new proteins which can be targeted in combination with current drugs to reactivate tumour suppressor pathways. It is possible that many proteins have a large interactome, and the regulation of these networks depends on the balance of regulatory proteins and metabolites. Stimuli such as stress and drugs for example, can therefore cause wide ranging changes in the cell, some of which will be compensated for by feedback loops and some of which effect cellular responses. Although it is a common approach to examine one protein-protein interaction at a time, the situation in the cell is much more complicated in practice and proteomics experiments are one way of addressing this complexity.

Most of the work to validate proteins from the mass spectrometry screens here was carried out on proteins which are affected at early time points after Nutlin treatment. It is striking that some of these proteins are affected throughout the time course, and others follow more transient patterns of stabilization and destabilization. This contrasts with genetic studies, which may be monitoring longer term changes. Changes in the proteome are the first cellular reaction to drugs and stimuli. The dynamic nature of the proteome can be investigated using experiments which monitor changes in global protein levels over time, and give a more complete picture of the events occurring in a cell. The experiments in this thesis work towards understanding the total interactome of MDM2 starting with a global approach then becoming more focused, and further work can build upon the new concepts described here.

References

1. WHO, W. H. O., Cancer Factsheet No. 297, Accessed 31st May 2011. (World Health Organisation, 2011).
2. Hanahan, D. & Weinberg, Robert A. Hallmarks of Cancer: The Next Generation. Cell 144, 646-674 (2011).
3. Allen, M. & Louise Jones, J. Jekyll and Hyde: the role of the microenvironment on the progression of cancer. The Journal of Pathology 223, 163-177 (2011).
4. Curiel, D. T., Douglas, J. T., Hemminki, A. & Hemminki, K. in Cancer Gene Therapy (ed. Nickoloff, J. A.) 9-18 (Humana Press, 2005).
5. Martens, J. H. A. & Stunnenberg, H. G. The molecular signature of oncofusion proteins in acute myeloid leukemia. FEBS Letters 584, 2662-2669 (2010).
6. Hanahan, D. & Weinberg, R. A. The Hallmarks of Cancer. Cell 100, 57-70 (2000).
7. Begg, A. C., Stewart, F. A. & Vens, C. Strategies to improve radiotherapy with targeted drugs. Nat Rev Cancer 11, 239-253 (2011).
8. Cairns, R. A., Harris, I. S. & Mak, T. W. Regulation of cancer cell metabolism. Nat Rev Cancer 11, 85-95 (2011).
9. Balch, W. E., Morimoto, R. I., Dillin, A. & Kelly, J. W. Adapting Proteostasis for Disease Intervention. Science 319, 916-919 (2008).
10. Traxler, P., Bold, G., Buchdunger, E., Caravatti, G., Furet, P., Manley, P., O'Reilly, T., Wood, J. & Zimmermann, J. Tyrosine kinase inhibitors: From rational design to clinical trials. Medicinal Research Reviews 21, 499-512 (2001).
11. Lopes, N. M., Adams, E. G., Pitts, T. W. & Bhuyan, B. K. Cell kill kinetics and cell cycle effects of taxol on human and hamster ovarian cell lines. Cancer Chemotherapy and Pharmacology 32, 235-242 (1993).
12. Dewit, L., Oussoren, Y. & Bartelink, H. The effects of cis-diamminedichloroplatinum (II) and radiation on the proliferation kinetics of mouse duodenal crypt cells and on a partially synchronized crypt cell population. International Journal of Radiation Oncology Biology Physics 12, 1977-1985 (1986).
13. Rajkumar, S. V., Richardson, P. G., Hideshima, T. & Anderson, K. C. Proteasome Inhibition As a Novel Therapeutic Target in Human Cancer. Journal of Clinical Oncology 23, 630-639 (2005).
14. Buchdunger, E., Zimmermann, J., Mett, H., Meyer, T., Moeller, M., Druker, B. J. & Lydon, N. B. Inhibition of the Abl Protein-Tyrosine Kinase in Vitro and in Vivo by a 2-Phenylaminopyrimidine Derivative. Cancer Research 56, 100-104 (1996).
15. Baselga, J., Norton, L., Albanell, J., Kim, Y.-M. & Mendelsohn, J. Recombinant Humanized Anti-HER2 Antibody (Herceptin™) Enhances the Antitumor

Activity of Paclitaxel and Doxorubicin against HER2/neu Overexpressing Human Breast Cancer Xenografts. Cancer Research 58, 2825-2831 (1998).
16. Porter, J. R., Fritz, C. C. & Depew, K. M. Discovery and development of Hsp90 inhibitors: a promising pathway for cancer therapy. Current Opinion in Chemical Biology 14, 412-420 (2010).
17. Whitesell, L., Mimnaugh, E. G., De Costa, B., Myers, C. E. & Neckers, L. M. Inhibition of heat shock protein HSP90-pp60v-src heteroprotein complex formation by benzoquinone ansamycins: essential role for stress proteins in oncogenic transformation. Proceedings of the National Academy of Sciences 91, 8324-8328 (1994).
18. Powers, E. T., Morimoto, R. I., Dillin, A., Kelly, J. W. & Balch, W. E. Biological and Chemical Approaches to Diseases of Proteostasis Deficiency. Annual Review of Biochemistry 78, 959-991 (2009).
19. Joerger, A. C. & Fersht, A. R. Structural Biology of the Tumor Suppressor p53. Annual Review of Biochemistry 77, 557-582 (2008).
20. Thomas, P. D., Campbell, M. J., Kejariwal, A., Mi, H., Karlak, B., Daverman, R., Diemer, K., Muruganujan, A. & Narechania, A. PANTHER: A Library of Protein Families and Subfamilies Indexed by Function. Genome Research 13, 2129-2141 (2003).
21. Mi, H., Dong, Q., Muruganujan, A., Gaudet, P., Lewis, S. & Thomas, P. D. PANTHER version 7: improved phylogenetic trees, orthologs and collaboration with the Gene Ontology Consortium. Nucleic Acids Research 38, 204-210 (2010).
22. Robles, A. I. & Harris, C. C. Clinical Outcomes and Correlates of TP53 Mutations and Cancer. Cold Spring Harbor Perspectives in Biology 2, a001016 (2010).
23. Coulombe, B., Jeronimo, C. l., Langelier, M.-F., Cojocaru, M. & Bergeron, D. Interaction Networks of the Molecular Machines That Decode, Replicate, and Maintain the Integrity of the Human Genome. Molecular & Cellular Proteomics 3, 851-856 (2004).
24. Causier, B. Studying the interactome with the yeast two-hybrid system and mass spectrometry. Mass Spectrometry Reviews 23, 350-367 (2004).
25. Ellis, R. J. Macromolecular crowding: obvious but underappreciated. Trends in Biochemical Sciences 26, 597-604 (2001).
26. Reich, N. C. & Levine, A. J. Specific interaction of the SV40 T antigen-cellular p53 protein complex with SV40 DNA. Virology 117, 286-290 (1982).
27. Jenkins, L. M. M., Yamaguchi, H., Hayashi, R., Cherry, S., Tropea, J. E., Miller, M., Wlodawer, A., Appella, E. & Mazur, S. J. Two Distinct Motifs within the p53 Transactivation Domain Bind to the Taz2 Domain of p300 and Are Differentially Affected by Phosphorylationâ€ Biochemistry 48, 1244-1255 (2009).
28. Natan, E., Baloglu, C., Pagel, K., Freund, S. M. V., Morgner, N., Robinson, C. V., Fersht, A. R. & Joerger, A. C. Interaction of the p53 DNA-Binding Domain with Its N-Terminal Extension Modulates the Stability of the p53 Tetramer. Journal of Molecular Biology 409, 358-368 (2011).

29. Ward, J. J., Sodhi, J. S., McGuffin, L. J., Buxton, B. F. & Jones, D. T. Prediction and Functional Analysis of Native Disorder in Proteins from the Three Kingdoms of Life. Journal of Molecular Biology 337, 635-645 (2004).
30. Delphin, C., Cahen, P., Lawrence, J. J. & Baudier, J. Characterization of baculovirus recombinant wild-type p53. European Journal of Biochemistry 223, 683-692 (1994).
31. Wang, P., Reed, M., Wang, Y., Mayr, G., Stenger, J. E., Anderson, M. E., Schwedes, J. F. & Tegtmeyer, P. p53 domains: structure, oligomerization, and transformation. Mol. Cell. Biol. 14, 5182-5191 (1994).
32. Wells, M., Tidow, H., Rutherford, T. J., Markwick, P., Jensen, M. R., Mylonas, E., Svergun, D. I., Blackledge, M. & Fersht, A. R. Structure of tumor suppressor p53 and its intrinsically disordered N-terminal transactivation domain. Proceedings of the National Academy of Sciences 105, 5762-5767 (2008).
33. Boeckler, F. M., Joerger, A. C., Jaggi, G., Rutherford, T. J., Veprintsev, D. B. & Fersht, A. R. Targeted rescue of a destabilized mutant of p53 by an in silico screened drug. Proceedings of the National Academy of Sciences 105, 10360-10365 (2008).
34. Khoo, K. H., Joerger, A. C., Freund, S. M. V. & Fersht, A. R. Stabilising the DNA-binding domain of p53 by rational design of its hydrophobic core. Protein Engineering, Design and Selection 22, 421-430 (2009).
35. Jeffrey, P., Gorina, S. & Pavletich, N. Crystal structure of the tetramerization domain of the p53 tumor suppressor at 1.7 angstroms. Science 267, 1498-1502 (1995).
36. Khoo, K. H., Mayer, S. & Fersht, A. R. Effects of Stability on the Biological Function of p53. Journal of Biological Chemistry 284, 30974-30980 (2009).
37. Nicholson, J. & Hupp, T. R. The molecular dynamics of MDM2. Cell Cycle 9, 1878-81 (2010).
38. Poyurovsky, M. V., Katz, C., Laptenko, O., Beckerman, R., Lokshin, M., Ahn, J., Byeon, I.-J. L., Gabizon, R., Mattia, M., Zupnick, A., Brown, L. M., Friedler, A. & Prives, C. The C terminus of p53 binds the N-terminal domain of MDM2. Nat Struct Mol Biol 17, 982-989 (2010).
39. Liu, W.-L., Midgley, C., Stephen, C., Saville, M. & Lane, D. P. Biological significance of a small highly conserved region in the N terminus of the p53 tumour suppressor protein. Journal of Molecular Biology 313, 711-731 (2001).
40. Uversky, V. N., Oldfield, C. J. & Dunker, A. K. Intrinsically Disordered Proteins in Human Diseases: Introducing the D2 Concept. Annual Review of Biophysics 37, 215-246 (2008).
41. Wright, P. E. & Dyson, H. J. Linking folding and binding. Current Opinion in Structural Biology 19, 31-38 (2009).
42. Chen, J., Wu, X., Lin, J. & Levine, A. J. mdm-2 inhibits the G1 arrest and apoptosis functions of the p53 tumor suppressor protein. Mol. Cell. Biol. 16, 2445-2452 (1996).
43. Maslon, M. M. & Hupp, T. R. Drug discovery and mutant p53. Trends in Cell Biology 20, 542-555 (2010).

44. Salminen, A. & Kaarniranta, K. Control of p53 and NF-[kappa]B signaling by WIP1 and MIF: Role in cellular senescence and organismal aging. Cellular Signalling 23, 747-752 (2010).
45. Maddocks, O. & Vousden, K. Metabolic regulation by p53. Journal of Molecular Medicine 89, 237-245 (2011).
46. Hernández-Acosta, N. C., Cabrera-Socorro, A., Morlans, M. P., Delgado, F. J. G., Suárez-Solá, M. L., Sottocornola, R., Lu, X., González-Gómez, M. & Meyer, G. Dynamic expression of the p53 family members p63 and p73 in the mouse and human telencephalon during development and in adulthood. Brain Research 1372, 29-40 (2010).
47. Honda, R., Tanaka, H. & Yasuda, H. Oncoprotein MDM2 is a ubiquitin ligase E3 for tumor suppressor p53. FEBS Letters 420, 25-27 (1997).
48. Inoue, T., Geyer, R. K., Yu, Z. K. & Maki, C. G. Downregulation of MDM2 stabilizes p53 by inhibiting p53 ubiquitination in response to specific alkylating agents. FEBS Letters 490, 196-201 (2001).
49. O'Keefe, K., Li, H. & Zhang, Y. Nucleocytoplasmic Shuttling of p53 Is Essential for MDM2-Mediated Cytoplasmic Degradation but Not Ubiquitination. Mol. Cell. Biol. 23, 6396-6405 (2003).
50. Foster, B. A., Coffey, H. A., Morin, M. J. & Rastinejad, F. Pharmacological Rescue of Mutant p53 Conformation and Function. Science 286, 2507-2510 (1999).
51. Basse, N., Kaar, J. L., Settanni, G., Joerger, A. C., Rutherford, T. J. & Fersht, A. R. Toward the Rational Design of p53-Stabilizing Drugs: Probing the Surface of the Oncogenic Y220C Mutant. Chemistry & biology 17, 46-56 (2010).
52. Lambert, J. M. R., Gorzov, P., Veprintsev, D. B., Söderqvist, M., Segerbäck, D., Bergman, J., Fersht, A. R., Hainaut, P., Wiman, K. G. & Bykov, V. J. N. PRIMA-1 Reactivates Mutant p53 by Covalent Binding to the Core Domain. Cancer Cell 15, 376-388 (2009).
53. Weissman, A. M. Themes and variations on ubiquitylation. Nat Rev Mol Cell Biol 2, 169-178 (2001).
54. Groettrup, M., Xirodimas, D. P. & Scheffner, M. in Conjugation and Deconjugation of Ubiquitin Family Modifiers (ed. Harris, J. R.) 116-135 (Springer New York).
55. Leng, R. P., Lin, Y., Ma, W., Wu, H., Lemmers, B., Chung, S., Parant, J. M., Lozano, G., Hakem, R. & Benchimol, S. Pirh2, a p53-Induced Ubiquitin-Protein Ligase, Promotes p53 Degradation. Cell 112, 779-791 (2003).
56. Esser, C., Scheffner, M. & Hohfeld, J. The Chaperone-associated Ubiquitin Ligase CHIP Is Able to Target p53 for Proteasomal Degradation. Journal of Biological Chemistry 280, 27443-27448 (2005).
57. Dornan, D., Wertz, I., Shimizu, H., Arnott, D., Frantz, G. D., Dowd, P., O' Rourke, K., Koeppen, H. & Dixit, V. M. The ubiquitin ligase COP1 is a critical negative regulator of p53. Nature 429, 86-92 (2004).
58. Woods, D. B. & Vousden, K. H. Regulation of p53 Function. Experimental Cell Research 264, 56-66 (2001).

59. Candeias, M. M., Malbert-Colas, L., Powell, D. J., Daskalogianni, C., Maslon, M. M., Naski, N., Bourougaa, K., Calvo, F. & Fahraeus, R. p53 mRNA controls p53 activity by managing Mdm2 functions. Nat Cell Biol 10, 1098-1105 (2008).
60. Fang, S., Jensen, J. P., Ludwig, R. L., Vousden, K. H. & Weissman, A. M. Mdm2 Is a RING Finger-dependent Ubiquitin Protein Ligase for Itself and p53. Journal of Biological Chemistry 275, 8945-8951 (2000).
61. Wawrzynow, B., Zylicz, A., Wallace, M., Hupp, T. & Zylicz, M. MDM2 Chaperones the p53 Tumor Suppressor. Journal of Biological Chemistry 282, 32603-32612 (2007).
62. Bartel, F., Harris, L. C., Wurl, P. & Taubert, H. MDM2 and Its Splice Variant Messenger RNAs: Expression in Tumors and Down-Regulation Using Antisense Oligonucleotides. Molecular Cancer Research 2, 29-35 (2004).
63. Shloush, J., Vlassov, J. E., Engson, I., Duan, S., Saridakis, V., Dhe-paganon, S., Raught, B., Sheng, Y. & Arrowsmith, C. H. Structural and Functional Comparison of the RING Domains of Two p53 E3 Ligases, Mdm2 and Pirh2. Journal of Biological Chemistry 286, 4796-4808 (2010).
64. Wawrzynow, B., Pettersson, S., Zylicz, A., Bramham, J., Worrall, E., Hupp, T. R. & Ball, K. L. A Function for the RING Finger Domain in the Allosteric Control of MDM2 Conformation and Activity. Journal of Biological Chemistry 284, 11517-11530 (2009).
65. Worrall, E., Wawrzynow, B., Worrall, L., Walkinshaw, M., Ball, K. & Hupp, T. Regulation of the E3 ubiquitin ligase activity of MDM2 by an N-terminal pseudo-substrate motif. Journal of Chemical Biology 2, 113-129 (2009).
66. Uldrijan, S., Pannekoek, W.-J. & Vousden, K. H. An essential function of the extreme C-terminus of MDM2 can be provided by MDMX. EMBO J 26, 102-112 (2007).
67. Kussie, P. H., Gorina, S., Marechal, V., Elenbaas, B., Moreau, J., Levine, A. J. & Pavletich, N. P. Structure of the MDM2 Oncoprotein Bound to the p53 Tumor Suppressor Transactivation Domain. Science 274, 948-953 (1996).
68. Uhrinova, S., Uhrin, D., Powers, H., Watt, K., Zheleva, D., Fischer, P., McInnes, C. & Barlow, P. N. Structure of Free MDM2 N-terminal Domain Reveals Conformational Adjustments that Accompany p53-binding. Journal of Molecular Biology 350, 587-598 (2005).
69. Muttray, A. F., O'Toole, T. F., Morrill, W., Van Beneden, R. J. & Baldwin, S. A. An invertebrate mdm homolog interacts with p53 and is differentially expressed together with p53 and ras in neoplastic Mytilus trossulus haemocytes. Comparative Biochemistry and Physiology Part B: Biochemistry and Molecular Biology 156, 298-308 (2010).
70. Lane, D. P., Fang Cheok, C., Brown, C., Madhumalar, A., Ghadessy, F. J. and Verma, C. MDM2 and p53 are highly conserved from placozoans to man. Cell Cycle 9 (2010).
71. Wang, M. & Pickart, C. M. Different HECT domain ubiquitin ligases employ distinct mechanisms of polyubiquitin chain synthesis. EMBO J 24, 4324-4333 (2005).

72. Clamp, M., Cuff, J., Searle, S. M. & Barton, G. J. The Jalview Java alignment editor. Bioinformatics 20, 426-427 (2004).
73. Linke, K., Mace, P. D., Smith, C. A., Vaux, D. L., Silke, J. & Day, C. L. Structure of the MDM2/MDMX RING domain heterodimer reveals dimerization is required for their ubiquitylation in trans. Cell Death Differ 15, 841-848 (2008).
74. Itahana, K., Mao, H., Jin, A., Itahana, Y., Clegg, H. V., Lindström, M. S., Bhat, Krishna P., Godfrey, V. L., Evan, G. I. & Zhang, Y. Targeted Inactivation of Mdm2 RING Finger E3 Ubiquitin Ligase Activity in the Mouse Reveals Mechanistic Insights into p53 Regulation. Cancer Cell 12, 355-366 (2007).
75. Sivakolundu, S. G., Nourse, A., Moshiach, S., Bothner, B., Ashley, C., Satumba, J., Lahti, J. & Kriwacki, R. W. Intrinsically Unstructured Domains of Arf and Hdm2 Form Bimolecular Oligomeric Structures In Vitro and In Vivo. Journal of Molecular Biology 384, 240-254 (2008).
76. Worrall, E. G. in Novel concepts in mdm2 protein regulation (University of Edinburgh, Edinburgh, 2009).
77. Yu, G. W., Rudiger, S., Veprintsev, D., Freund, S., Fernandez-Fernandez, M. R. & Fersht, A. R. The central region of HDM2 provides a second binding site for p53. Proceedings of the National Academy of Sciences of the United States of America 103, 1227-1232 (2006).
78. Azmi, A. S., Philip, P. A., Beck, F. W. J., Wang, Z., Banerjee, S., Wang, S., Yang, D., Sarkar, F. H. & Mohammad, R. M. MI-219-zinc combination: a new paradigm in MDM2 inhibitor-based therapy. Oncogene 30, 117-126 (2010).
79. Poyurovsky, M. V., Jacq, X., Ma, C., Karni-Schmidt, O., Parker, P. J., Chalfie, M., Manley, J. L. & Prives, C. Nucleotide Binding by the MDM2 RING Domain Facilitates Arf-Independent MDM2 Nucleolar Localization. Molecular Cell 12, 875-887 (2003).
80. Burch, L., Shimizu, H., Smith, A., Patterson, C. & Hupp, T. R. Expansion of Protein Interaction Maps by Phage Peptide Display Using MDM2 as a Prototypical Conformationally Flexible Target Protein. Journal of Molecular Biology 337, 129-145 (2004).
81. Pettersson, S., Kelleher, M., Pion, E., Wallace, M. & Ball, K. L. Role of Mdm2 acid domain interactions in recognition and ubiquitination of the transcription factor IRF-2. Biochem J 418, 575-585 (2009).
82. Mayo, L. D., Turchi, J. J. & Berberich, S. J. Mdm-2 Phosphorylation by DNA-dependent Protein Kinase Prevents Interaction with p53. Cancer Research 57, 5013-5016 (1997).
83. Cheng, Q. & Chen, J. Mechanism of p53 stabilization by ATM after DNA damage. Cell Cycle 9, 472-478 (2010).
84. Inuzuka, H., Tseng, A., Gao, D., Zhai, B., Zhang, Q., Shaik, S., Wan, L., Ang, X. L., Mock, C., Yin, H., Stommel, J. M., Gygi, S., Lahav, G., Asara, J., Xiao, Z.-X. J., Kaelin Jr, W. G., Harper, J. W. & Wei, W. Phosphorylation by Casein Kinase I Promotes the Turnover of the Mdm2 Oncoprotein via the SCF[beta]-TRCP Ubiquitin Ligase. Cancer Cell 18, 147-159 (2010).

85. Xirodimas, D. P., Saville, M. K., Bourdon, J.-C., Hay, R. T. & Lane, D. P. Mdm2-Mediated NEDD8 Conjugation of p53 Inhibits Its Transcriptional Activity. Cell 118, 83-97 (2004).
86. Sundqvist, A., Liu, G., Mirsaliotis, A. & Xirodimas, D. P. Regulation of nucleolar signalling to p53 through NEDDylation of L11. EMBO Rep 10, 1132-1139 (2009).
87. Jiang, M., Chiu, S. Y. & Hsu, W. SUMO-specific protease 2 in Mdm2-mediated regulation of p53. Cell Death Differ 18, 1005-15 (2011).
88. Deisenroth, C. & Zhang, Y. Ribosome biogenesis surveillance: probing the ribosomal protein-Mdm2-p53 pathway. Oncogene 29, 4253-4260 (2010).
89. Pang, L. Y., Scott, M., Hayward, R. L., Mohammed, H., Whitelaw, B. A., Smith, G. C. M. & Hupp, T. R. p21WAF1 is component of a positive feedback loop that maintains the p53 transcriptional program. Cell Cycle 10, 932-950 (2011).
90. Bourougaa, K., Naski, N., Boularan, C., Mlynarczyk, C., Candeias, M. M., Marullo, S. & Fåhraeus, R. Endoplasmic Reticulum Stress Induces G2 Cell-Cycle Arrest via mRNA Translation of the p53 Isoform p53/47. Molecular cell 38, 78-88 (2010).
91. Wallace, M., Worrall, E., Pettersson, S., Hupp, T. R. & Ball, K. L. Dual-Site Regulation of MDM2 E3-Ubiquitin Ligase Activity. Molecular Cell 23, 251-263 (2006).
92. Shimizu, H., Burch, L. R., Smith, A. J., Dornan, D., Wallace, M., Ball, K. L. & Hupp, T. R. The Conformationally Flexible S9-S10 Linker Region in the Core Domain of p53 Contains a Novel MDM2 Binding Site Whose Mutation Increases Ubiquitination of p53 in Vivo. J. Biol. Chem. 277, 28446-28458 (2002).
93. Meek, D. W. & Hupp, T. R. The regulation of MDM2 by multisite phosphorylation--Opportunities for molecular-based intervention to target tumours? Seminars in Cancer Biology 20, 19-28 (2010).
94. Fraser, J. A., Vojtesek, B. & Hupp, T. R. A Novel p53 Phosphorylation Site within the MDM2 Ubiquitination Signal. Journal of Biological Chemistry 285, 37762-37772 (2010).
95. Tompa, P. Structure and Function of Intrinsically Disordered Proteins (Chapman and Hall, 2009).
96. Zhu, Y., Poyurovsky, M. V., Li, Y., Biderman, L., Stahl, J., Jacq, X. & Prives, C. Ribosomal Protein S7 Is Both a Regulator and a Substrate of MDM2. Molecular Cell 35, 316-326 (2009).
97. Busso, C. S., Iwakuma, T. & Izumi, T. Ubiquitination of mammalian AP endonuclease (APE1) regulated by the p53-MDM2 signaling pathway. Oncogene 28, 1616-1625 (2009).
98. Bennett, E. J., Rush, J., Gygi, S. P. & Harper, J. W. Dynamics of Cullin-RING Ubiquitin Ligase Network Revealed by Systematic Quantitative Proteomics. Cell 143, 951-965 (2010).
99. Lohrum, M. A. E., Ludwig, R. L., Kubbutat, M. H. G., Hanlon, M. & Vousden, K. H. Regulation of HDM2 activity by the ribosomal protein L11. Cancer Cell 3, 577-587 (2003).

100. Chen, D., Zhang, Z., Li, M., Wang, W., Li, Y., Rayburn, E. R., Hill, D. L., Wang, H. & Zhang, R. Ribosomal protein S7 as a novel modulator of p53-MDM2 interaction: binding to MDM2, stabilization of p53 protein, and activation of p53 function. Oncogene 26, 5029-5037 (2007).
101. Macias, E., Jin, A., Deisenroth, C., Bhat, K., Mao, H., Lindström, M. S. & Zhang, Y. An ARF-Independent c-MYC-Activated Tumor Suppression Pathway Mediated by Ribosomal Protein-Mdm2 Interaction. Cancer Cell 18, 231-243 (2010).
102. Zhang, Y., Wang, J., Yuan, Y., Zhang, W., Guan, W., Wu, Z., Jin, C., Chen, H., Zhang, L., Yang, X. & He, F. Negative regulation of HDM2 to attenuate p53 degradation by ribosomal protein L26. Nucleic Acids Research 38, 6544-6554 (2010).
103. Kurki, S., Peltonen, K., Latonen, L., Kiviharju, T. M., Ojala, P. M., Meek, D. & Laiho, M. Nucleolar protein NPM interacts with HDM2 and protects tumor suppressor protein p53 from HDM2-mediated degradation. Cancer cell 5, 465-475 (2004).
104. Sun, X.-X., Wang, Y.-G., Xirodimas, D. P. & Dai, M.-S. Perturbation of 60 S Ribosomal Biogenesis Results in Ribosomal Protein L5- and L11-dependent p53 Activation. Journal of Biological Chemistry 285, 25812-25821 (2010).
105. Zhang, Z., Wang, H., Li, M., Rayburn, E. R., Agrawal, S. & Zhang, R. Stabilization of E2F1 protein by MDM2 through the E2F1 ubiquitination pathway. Oncogene 24, 7238-7247 (2005).
106. Stevens, C., Pettersson, S., Wawrzynow, B., Wallace, M., Ball, K., Zylicz, A. & Hupp, T. R. ATP stimulates MDM2-mediated inhibition of the DNA-binding function of E2F1. FEBS Journal 275, 4875-4886 (2008).
107. Huart, A.-S., MacLaine, N. J., Meek, D. W. & Hupp, T. R. CK1 alpha Plays a Central Role in Mediating MDM2 Control of p53 and E2F-1 Protein Stability. Journal of Biological Chemistry 284, 32384-32394 (2009).
108. Joseph, T. L., Madhumalar, A., Brown, C. J., Lane, D. P. & Verma, C. S. Differential binding of p53 and nutlin to MDM2 and MDMX: Computational studies. Cell Cycle 9, 1167-81 (2010).
109. Wade, M., Wang, Y. V. & Wahl, G. M. The p53 orchestra: Mdm2 and Mdmx set the tone. Trends in Cell Biology 20, 299-309 (2010).
110. Neduva, V., Linding, R., Su-Angrand, I., Stark, A., Masi, F. d., Gibson, T. J., Lewis, J., Serrano, L. & Russell, R. B. Systematic Discovery of New Recognition Peptides Mediating Protein Interaction Networks. PLoS Biol 3, e405 (2005).
111. Neduva, V. & Russell, R. B. Linear motifs: Evolutionary interaction switches. FEBS Letters 579, 3342-3345 (2005).
112. Fischer, E. Synthetical Chemistry in its Relation to Biology. Faraday Lecture (1907).
113. Fischer, E. Einfluss der Configuration auf die Wirkung der Enzyme. Ber. Dtsch. Chem. Ges. 27, 2985-2993 (1894).

114. Espinoza-Fonseca, L. M. Reconciling binding mechanisms of intrinsically disordered proteins. Biochemical and Biophysical Research Communications 382, 479-482 (2009).
115. Fuxreiter, M., Tompa, P. & Simon, I. n. Local structural disorder imparts plasticity on linear motifs. Bioinformatics 23, 950-956 (2007).
116. Edwards, R. J., Davey, N. E. & Shields, D. C. SLiMFinder: A Probabilistic Method for Identifying Over-Represented, Convergently Evolved, Short Linear Motifs in Proteins. PLoS ONE 2, e967 (2007).
117. Rosenbaum, J. C., Fredrickson, E. K., Oeser, M. L., Garrett-Engele, C. M., Locke, M. N., Richardson, L. A., Nelson, Z. W., Hetrick, E. D., Milac, T. I., Gottschling, D. E. & Gardner, R. G. Disorder Targets Misorder in Nuclear Quality Control Degradation: A Disordered Ubiquitin Ligase Directly Recognizes Its Misfolded Substrates. Molecular cell 41, 93-106 (2011).
118. Tompa, P. & Fuxreiter, M. Fuzzy complexes: polymorphism and structural disorder in protein-protein interactions. Trends in Biochemical Sciences 33, 2-8 (2008).
119. Burch, L. R., Scott, M., Pohler, E., Meek, D. & Hupp, T. Phage-peptide Display Identifies the Interferon-responsive, Death-activated Protein Kinase Family as a Novel Modifier of MDM2 and p21WAF1. Journal of Molecular Biology 337, 115-128 (2004).
120. Cwirla, S. E., Peters, E. A., Barrett, R. W. & Dower, W. J. Peptides on phage: a vast library of peptides for identifying ligands. Proceedings of the National Academy of Sciences of the United States of America 87, 6378-6382 (1990).
121. Katz, C., Levy-Beladev, L., Rotem-Bamberger, S., Rito, T., Rudiger, S. G. D. & Friedler, A. Studying protein-protein interactions using peptide arrays. Chemical Society Reviews 40, 2131-2145.
122. Vagner, J., Qu, H. & Hruby, V. J. Peptidomimetics, a synthetic tool of drug discovery. Current Opinion in Chemical Biology 12, 292-296 (2008).
123. Stephen, C. W., Helminen, P. & Lane, D. P. Characterisation of Epitopes on Human p53 using Phage-displayed Peptide Libraries: Insights into Antibody-Peptide Interactions. Journal of Molecular Biology 248, 58-78 (1995).
124. Murray, E., McKenna, E. O., Burch, L. R., Dillon, J., Langridge-Smith, P., Kolch, W., Pitt, A. & Hupp, T. R. Microarray-Formatted Clinical Biomarker Assay Development Using Peptide Aptamers to Anterior Gradient-2. Biochemistry 46, 13742-13751 (2007).
125. Pohler, E., Craig, A. L., Cotton, J., Lawrie, L., Dillon, J. F., Ross, P., Kernohan, N. & Hupp, T. R. The Barrett's Antigen Anterior Gradient-2 Silences the p53 Transcriptional Response to DNA Damage. Mol Cell Proteomics 3, 534-547 (2004).
126. Ramachandran, V., Arumugam, T., Wang, H. & Logsdon, C. D. Anterior Gradient 2 Is Expressed and Secreted during the Development of Pancreatic Cancer and Promotes Cancer Cell Survival. Cancer Res 68, 7811-7818 (2008).
127. Wang, Z., Hao, Y. & Lowe, A. W. The Adenocarcinoma-Associated Antigen, AGR2, Promotes Tumor Growth, Cell Migration, and Cellular Transformation. Cancer Res 68, 492-497 (2008).

128. Fourtouna, A., Murray, E., Nicholson, J., Maslon, M. M., Pang, L. Y., Dryden, D. T. F., Hupp, T. R. The Anterior Gradient-2 Pathway as a Model for Developing Peptide-Aptamer Anti-Cancer Drug Leads that Stimulate p53 Function. Current Chemical Biology 3, 124-137 (2009).
129. Phan, J., Li, Z., Kasprzak, A., Li, B., Sebti, S., Guida, W., Schonbrunn, E. & Chen, J. Structure-based design of high-affinity peptides inhibiting the interaction of p53 with MDM2 and MDMX. Journal of Biological Chemistry, - (2009).
130. Pazgier, M., Liu, M., Zou, G., Yuan, W., Li, C., Li, C., Li, J., Monbo, J., Zella, D., Tarasov, S. G. & Lu, W. Structural basis for high-affinity peptide inhibition of p53 interactions with MDM2 and MDMX. Proceedings of the National Academy of Sciences 106, 4665-4670 (2009).
131. Li, C., Pazgier, M., Li, C., Yuan, W., Liu, M., Wei, G., Lu, W.-Y. & Lu, W. Systematic Mutational Analysis of Peptide Inhibition of the p53-MDM2/MDMX Interactions. Journal of Molecular Biology 398, 200-213 (2010).
132. Stengel, F., Baldwin, A. J., Painter, A. J., Jaya, N., Basha, E., Kay, L. E., Vierling, E., Robinson, C. V. & Benesch, J. L. P. Quaternary dynamics and plasticity underlie small heat shock protein chaperone function. Proceedings of the National Academy of Sciences 107, 2007-2012 (2010).
133. Vassilev, L. T., Vu, B. T., Graves, B., Carvajal, D., Podlaski, F., Filipovic, Z., Kong, N., Kammlott, U., Lukacs, C., Klein, C., Fotouhi, N. & Liu, E. A. In Vivo Activation of the p53 Pathway by Small-Molecule Antagonists of MDM2. Science 303, 844-848 (2004).
134. Xu, H., Ye, H., Osman, N. E., Sadler, K., Won, E.-Y., Chi, S.-W. & Yoon, H. S. The MDM2-Binding Region in the Transactivation Domain of p53 Also Acts as a Bcl-XL-Binding Motif. Biochemistry 48, 12159-12168 (2009).
135. Brown, C. J., Cheok, C. F., Verma, C. S. & Lane, D. P. Reactivation of p53: from peptides to small molecules. Trends in Pharmacological Sciences 32, 53-62 (2010).
136. Dastidar, S., Lane, D. & Verma, C. Modulation of p53 binding to MDM2: computational studies reveal important roles of Tyr100. BMC Bioinformatics 10, S6 (2009).
137. Worrall, E. G., Worrall, L., Blackburn, E., Walkinshaw, M. & Hupp, T. R. The Effects of Phosphomimetic Lid Mutation on the Thermostability of the N-terminal Domain of MDM2. Journal of Molecular Biology 398, 414-428 (2010).
138. McCoy, M. A., Gesell, J. J., Senior, M. M. & Wyss, D. F. Flexible lid to the p53-binding domain of human Mdm2: Implications for p53 regulation. Proceedings of the National Academy of Sciences of the United States of America 100, 1645-1648 (2003).
139. Dastidar, S. G., Raghunathan, D., Nicholson, J., Hupp, T. R., Lane, D. P. & Verma, C. S. Chemical states of the N-terminal "lid" of MDM2 regulate p53 binding: Simulations reveal complexities of modulation. Cell Cycle 10, 82-9 (2011).

140. Brennan, R. C., Federico, S., Bradley, C., Zhang, J., Flores-Otero, J., Wilson, M., Stewart, C. F., Zhu, F., Guy, K. & Dyer, M. A. Targeting the p53 Pathway in Retinoblastoma with Subconjunctival Nutlin-3a. Cancer Research (2011).
141. Ooi, M. G., Hayden, P. J., Kotoula, V., McMillin, D. W., Charalambous, E., Daskalaki, E., Raje, N. S., Munshi, N. C., Chauhan, D., Hideshima, T., Buon, L., Clynes, M., O'Gorman, P., Richardson, P. G., Mitsiades, C. S., Anderson, K. C. & Mitsiades, N. Interactions of the Hdm2/p53 and Proteasome Pathways May Enhance the Antitumor Activity of Bortezomib. Clinical Cancer Research 15, 7153-7160 (2009).
142. Wasinger, V. C., Cordwell, S. J., Cerpa-Poljak, A., Yan, J. X., Gooley, A. A., Wilkins, M. R., Duncan, M. W., Harris, R., Williams, K. L. & Humphery-Smith, I. Progress with gene-product mapping of the Mollicutes: Mycoplasma genitalium. Electrophoresis 16, 1090-1094 (1995).
143. Cohen, A. A., Geva-Zatorsky, N., Eden, E., Frenkel-Morgenstern, M., Issaeva, I., Sigal, A., Milo, R., Cohen-Saidon, C., Liron, Y., Kam, Z., Cohen, L., Danon, T., Perzov, N. & Alon, U. Dynamic Proteomics of Individual Cancer Cells in Response to a Drug. Science 322, 1511-1516 (2008).
144. Voet, D. & Voet, J. G. Biochemistry (John Wiley & Sons, 2011).
145. Sayed, D. & Abdellatif, M. MicroRNAs in Development and Disease. Physiological Reviews 91, 827-887 (2011).
146. Sperling, J., Azubel, M. & Sperling, R. Structure and Function of the Pre-mRNA Splicing Machine. Structure 16, 1605-1615 (2008).
147. Johnson, R. S., Martin, S. A., Biemann, K., Stults, J. T. & Watson, J. T. Novel fragmentation process of peptides by collision-induced decomposition in a tandem mass spectrometer: differentiation of leucine and isoleucine. Analytical Chemistry 59, 2621-2625 (1987).
148. Ünlü, M., Morgan, M. E. & Minden, J. S. Difference gel electrophoresis. A single gel method for detecting changes in protein extracts. Electrophoresis 18, 2071-2077 (1997).
149. Wu, C. C. & MacCoss, M. J. Shotgun proteomics: Tools for the analysis of complex biological systems. Current Opinion in Molecular Therapeutics 4, 242 - 250 (2002).
150. Yates, J. R. r. & Chen, E. L. Cancer proteomics by quantitative shotgun proteomics. Molecular Oncology 1, 144-59 (2007).
151. Mann, M. & Wilm, M. Error-Tolerant Identification of Peptides in Sequence Databases by Peptide Sequence Tags. Analytical Chemistry 66, 4390-4399 (1994).
152. Perkins, D. N., Pappin, D. J. C., Creasy, D. M. & Cottrell, J. S. Probability-based protein identification by searching sequence databases using mass spectrometry data. ELECTROPHORESIS 20, 3551-3567 (1999).
153. Wu, L. & Han, D. K. Overcoming the dynamic range problem in mass spectrometry-based shotgun proteomics. Expert Review of Proteomics 3, 611-619 (2006).

154. Jmeian, Y. & El Rassi, Z. Liquid-phase-based separation systems for depletion, prefractionation and enrichment of proteins in biological fluids for in-depth proteomics analysis. ELECTROPHORESIS 30, 249-261 (2009).
155. Griffiths, W. J. in Proteomics in Functional Genomics (eds. Jolles, P. & Jornvall, H.) (Birkhauser, 2000).
156. Panchaud, A., Scherl, A., Shaffer, S. A., von Haller, P. D., Kulasekara, H. D., Miller, S. I. & Goodlett, D. R. Precursor Acquisition Independent From Ion Count: How to Dive Deeper into the Proteomics Ocean. Analytical Chemistry 81, 6481-6488 (2009).
157. Ross, P. L., Huang, Y. N., Marchese, J. N., Williamson, B., Parker, K., Hattan, S., Khainovski, N., Pillai, S., Dey, S., Daniels, S., Purkayastha, S., Juhasz, P., Martin, S., Bartlet-Jones, M., He, F., Jacobson, A. & Pappin, D. J. Multiplexed Protein Quantitation in Saccharomyces cerevisiae Using Amine-reactive Isobaric Tagging Reagents. Molecular & Cellular Proteomics 3, 1154-1169 (2004).
158. Thingholm, T. E., Palmisano, G., Kjeldsen, F. & Larsen, M. R. Undesirable Charge-Enhancement of Isobaric Tagged Phosphopeptides Leads to Reduced Identification Efficiency. Journal of Proteome Research 9, 4045-4052 (2010).
159. Ow, S. Y., Salim, M., Noirel, J., Evans, C., Rehman, I. & Wright, P. C. iTRAQ Underestimation in Simple and Complex Mixtures: "The Good, the Bad and the Ugly". Journal of Proteome Research 8, 5347-5355 (2009).
160. Everley, P. A., Krijgsveld, J., Zetter, B. R. & Gygi, S. P. Quantitative Cancer Proteomics: Stable Isotope Labeling with Amino Acids in Cell Culture (SILAC) as a Tool for Prostate Cancer Research. Molecular & Cellular Proteomics 3, 729-735 (2004).
161. Sury, M. D., Chen, J.-X. & Selbach, M. The SILAC Fly Allows for Accurate Protein Quantification in Vivo. Molecular & Cellular Proteomics 9, 2173-2183 (2010).
162. Walther, D. M. & Mann, M. Accurate Quantification of More Than 4000 Mouse Tissue Proteins Reveals Minimal Proteome Changes During Aging. Molecular & Cellular Proteomics 10 (2010).
163. Larance, M., Bailly, A. P., Pourkarimi, E., Hay, R. T., Buchanan, G., Coulthurst, S., Xirodimas, D. P., Gartner, A. & Lamond, A. I. Stable-isotope labeling with amino acids in nematodes. Nat Meth advance online publication (2011).
164. Yao, X., Freas, A., Ramirez, J., Demirev, P. A. & Fenselau, C. Proteolytic 18O Labeling for Comparative Proteomics: Model Studies with Two Serotypes of Adenovirus. Analytical Chemistry 73, 2836-2842 (2001).
165. Neilson, K. A., Ali, N. A., Muralidharan, S., Mirzaei, M., Mariani, M., Assadourian, G., Lee, A., van Sluyter, S. C. & Haynes, P. A. Less label, more free: Approaches in label-free quantitative mass spectrometry. PROTEOMICS 11, 535-553 (2011).
166. Old, W. M., Meyer-Arendt, K., Aveline-Wolf, L., Pierce, K. G., Mendoza, A., Sevinsky, J. R., Resing, K. A. & Ahn, N. G. Comparison of Label-free Methods for Quantifying Human Proteins by Shotgun Proteomics. Molecular & Cellular Proteomics 4, 1487-1502 (2005).

167. Carvahlo, P. C., Hewel, J., Barbosa, V. C. & Yates, J. R. r. Identifying differences in protein expression levels by spectral counting and feature selection. Genet. Mol. Res. 7, 342-356 (2008).
168. Kirkpatrick, D. S., Gerber, S. A. & Gygi, S. P. The absolute quantification strategy: a general procedure for the quantification of proteins and post-translational modifications. Methods 35, 265-273 (2005).
169. Swainston, N., Jameson, D. & Carroll, K. A QconCAT informatics pipeline for the analysis, visualization and sharing of absolute quantitative proteomics data. PROTEOMICS 11, 329-333 (2011).
170. Bhanot, G., Alexe, G., Venkataraghavan, B. & Levine, A. J. A robust meta-classification strategy for cancer detection from MS data. PROTEOMICS 6, 592-604 (2006).
171. Ohta, S., Bukowski-Wills, J.-C., Sanchez-Pulido, L., Alves, F. d. L., Wood, L., Chen, Z. A., Platani, M., Fischer, L., Hudson, D. F., Ponting, C. P., Fukagawa, T., Earnshaw, W. C. & Rappsilber, J. The Protein Composition of Mitotic Chromosomes Determined Using Multiclassifier Combinatorial Proteomics. Cell 142, 810-821 (2010).
172. Bradford, M. M. A rapid and sensitive method for the quantitation of microgram quantities of protein utilizing the principle of protein-dye binding. Analytical Biochemistry 72, 248-254 (1976).
173. Wu, C., Shawn, S.-C. L.,. in Peptide Microarrays Methods and Protocols 197-202 (Springer, 2009).
174. Chang, Y. C., Lee, Y. S., Tejima, T., Tanaka, K., Omura, S., Heintz, N. H., Mitsui, Y. & Magae, J. mdm2 and bax, downstream mediators of the p53 response, are degraded by the ubiquitin-proteasome pathway. Cell Growth Differ 9, 79-84 (1998).
175. Zhang, Z., Wang, H., Li, M., Agrawal, S., Chen, X. & Zhang, R. MDM2 Is a Negative Regulator of p21WAF1/CIP1, Independent of p53. Journal of Biological Chemistry 279, 16000-16006 (2004).
176. Hendrickson, E. L., Xia, Q., Wang, T., Leigh, J. A. & Hackett, M. Comparison of spectral counting and metabolic stable isotope labeling for use with quantitative microbial proteomics. Analyst 131, 1335-1341 (2006).
177. Peng, Y., Chen, L., Li, C., Lu, W. & Chen, J. Inhibition of MDM2 by hsp90 Contributes to Mutant p53 Stabilization. Journal of Biological Chemistry 276, 40583-40590 (2001).
178. Sievers, C., Billig, G., Gottschalk, K. & Rudel, T. Prohibitins Are Required for Cancer Cell Proliferation and Adhesion. PLoS ONE 5, e12735 (2010).
179. Banks, D., Wu, M., Higa, L. A., Gavrilova, N., Quan, J., Ye, T., Kobayashi, R., Sun, H. & Zhang, H. L2DTL/CDT2 and PCNA interact with p53 and regulate p53 polyubiquitination and protein stability through MDM2 and CUL4A/DDB1 complexes. Cell Cycle 5, 1719-29 (2006).
180. Zhang, Z. & Zhang, R. Proteasome activator PA28[gamma] regulates p53 by enhancing its MDM2-mediated degradation. EMBO J 27, 852-864 (2008).

181. Gobert, C. l., Bracco, L., Rossi, F., Olivier, M., Tazi, J., Lavelle, F. o., Larsen, A. K. & Riou, J.-F. o. Modulation of DNA Topoisomerase I Activity by p53. Biochemistry 35, 5778-5786 (1996).
182. Fernandez-Fernandez, M. R., Rutherford, T. J. & Fersht, A. R. Members of the S100 family bind p53 in two distinct ways. Protein Science 17, 1663-1670 (2008).
183. Roperch, J. P., Lethrone, F., Prieur, S., Piouffre, L., Israeli, D., Tuynder, M., Nemani, M., Pasturaud, P., Gendrom, M. C., Dausset, J., Oren, M., Amson, R. B. & Telerman, A. SIAH-1 promotes apoptosis and tumor suppression through a network involving the regulation of protein folding, unfolding, and trafficking: identification of common effectors with p53 and p21 (Waf1). Proceedings of the National Academy of Sciences 96, 8070-3 (1999).
184. Malanga, M., Pleschke, J. M., Kleczkowska, H. E. & Althaus, F. R. Poly(ADP-ribose) Binds to Specific Domains of p53 and Alters Its DNA Binding Functions. Journal of Biological Chemistry 273, 11839-11843 (1998).
185. Yoshida, Y., Izumi, H., Torigoe, T., Ishiguchi, H., Itoh, H., Kang, D. & Kohno, K. p53 Physically Interacts with Mitochondrial Transcription Factor A and Differentially Regulates Binding to Damaged DNA. Cancer Research 63, 3729-3734 (2003).
186. Wang, M., Gu, C., Qi, T., Tang, W., Wang, L., Wang, S. & Zeng, X. BAF53 Interacts with p53 and Functions in p53-mediated p21-gene Transcription. Journal of Biochemistry 142, 613-620 (2007).
187. Wang, Y., Cao, W., Yu, Z. & Liu, Z. Downregulation of a mitochondria associated protein SLP-2 inhibits tumor cell motility, proliferation and enhances cell sensitivity to chemotherapeutic reagents. Cancer Biol. Ther 8, 1651-8 (2009).
188. Constantinou, C. & Clemens, M. J. Regulation of translation factors eIF4GI and 4E-BP1 during recovery of protein synthesis from inhibition by p53. Cell Death Differ 14, 576-585 (2006).
189. Fang, F., Flegler, A. J., Du, P., Lin, S. & Clevenger, C. V. Expression of Cyclophilin B is Associated with Malignant Progression and Regulation of Genes Implicated in the Pathogenesis of Breast Cancer. The American Journal of Pathology 174, 297-308 (2009).
190. Dobbs, T. A., Tainer, J. A. & Lees-Miller, S. P. A structural model for regulation of NHEJ by DNA-PKcs autophosphorylation. DNA Repair 9, 1307-1314 (2010).
191. Szklarczyk, D., Franceschini, A., Kuhn, M., Simonovic, M., Roth, A., Minguez, P., Doerks, T., Stark, M., Muller, J., Bork, P., Jensen, L. J. & Mering, C. v. The STRING database in 2011: functional interaction networks of proteins, globally integrated and scored. Nucleic Acids Research 39, D561-D568 (2011).
192. Rutkevich, L. A. & Williams, D. B. Participation of lectin chaperones and thiol oxidoreductases in protein folding within the endoplasmic reticulum. Current Opinion in Cell Biology 23, 157-66 (2011).
193. Kozak, M. Initiation of translation in prokaryotes and eukaryotes. Gene 234, 187-208 (1999).

194. Kim, J. H., Hahm, B., Kim, Y. K., Choi, M. & Jang, S. K. Protein-protein interaction among hnRNPs shuttling between nucleus and cytoplasm. Journal of Molecular Biology 298, 395-405 (2000).
195. Rajagopalan, S., Andreeva, A., Teufel, D. P., Freund, S. M. & Fersht, A. R. Interaction between the Transactivation Domain of p53 and PC4 Exemplifies Acidic Activation Domains as Single-stranded DNA Mimics. Journal of Biological Chemistry 284, 21728-21737 (2009).
196. Jayaraman, L., Moorthy, N. C., Murthy, K. G. K., Manley, J. L., Bustin, M. & Prives, C. High mobility group protein-1 (HMG-1) is a unique activator of p53. Genes & Development 12, 462-472 (1998).
197. Shoshan-Barmatz, V., De Pinto, V., Zweckstetter, M., Raviv, Z., Keinan, N. & Arbel, N. VDAC, a multi-functional mitochondrial protein regulating cell life and death. Molecular Aspects of Medicine 31, 227-285 (2010).
198. Tsubota, A., Matsumoto, K., Mogushi, K., Nariai, K., Namiki, Y., Hoshina, S., Hano, H., Tanaka, H., Saito, H. & Tada, N. IQGAP1 and vimentin are key regulator genes in naturally occurring hepatotumorigenesis induced by oxidative stress. Carcinogenesis 31, 504 - 511 (2010).
199. Lain, S., Midgley, C., Sparks, A., Lane, E. B. & Lane, D. P. An Inhibitor of Nuclear Export Activates the p53 Response and Induces the Localization of HDM2 and p53 to U1A-Positive Nuclear Bodies Associated with the PODs. Experimental Cell Research 248, 457-472 (1999).
200. Burkard, T., Planyavsky, M., Kaupe, I., Breitwieser, F., Burckstummer, T., Bennett, K., Superti-Furga, G. & Colinge, J. Initial characterization of the human central proteome. BMC Systems Biology 5, 17 (2011).
201. Phu, L., Izrael-Tomasevic, A., Matsumoto, M. L., Bustos, D. J., Dynek, J. N., Fedorova, A. V., Bakalarski, C. E., Arnott, D., Deshayes, K., Dixit, V. M., Kelley, R. F., Vucic, D. & Kirkpatrick, D. S. Improved quantitative mass spectrometry methods for characterizing complex ubiquitin signals. Molecular & Cellular Proteomics 10 (2010).
202. De Castro, E., Sigrist, C. J. A., Gattiker, A., Bulliard, V., Langendijk-Genevaux, P. S., Gasteiger, E., Bairoch, A. & Hulo, N. ScanProsite: detection of PROSITE signature matches and ProRule-associated functional and structural residues in proteins. Nucleic Acids Research 34, 362-365 (2006).
203. Fraser, J. A. & Hupp, T. R. Chemical genetics approach to identify peptide ligands that selectively stimulate DAPK-1 kinase activity. Biochemistry 46, 2655-73 (2007).
204. Cummings, M. D., Farnum, M. A. & Nelen, M. I. Universal Screening Methods and Applications of ThermoFluor®. Journal of Biomolecular Screening 11, 854-863 (2006).
205. Dyson, H. J. & Wright, P. E. Coupling of folding and binding for unstructured proteins. Current Opinion in Structural Biology 12, 54-60 (2002).
206. Cheung-Flynn, J., Roberts, P. J., Riggs, D. L. & Smith, D. F. C-terminal Sequences outside the Tetratricopeptide Repeat Domain of FKBP51 and FKBP52 Cause Differential Binding to Hsp90. Journal of Biological Chemistry 278, 17388-17394 (2003).

207. Katz, C., Levy-Beladev, L., Rotem-Bamberger, S., Rito, T., Rudiger, S. G. D. & Friedler, A. Studying protein-protein interactions using peptide arrays. Chemical Society Reviews (2011).
208. Chan, P. M., Ng, Y. W. & Manser, E. A robust protocol to map binding sites of the 14-3-3 interactome: Cdc25C requires phosphorylation of both S216 and S263 to bind 14-3-3. Mol Cell Proteomics 10 (2011).
209. Theuerkorn, M., Fischer, G. & Schiene-Fischer, C. Prolyl cis/trans isomerase signalling pathways in cancer. Current Opinion in Pharmacology In Press, Corrected Proof (2011).
210. Lee, J. & Kim, S. S. An Overview of Cyclophilins in Human Cancers. The Journal of International Medical Research 38, 1561-1574 (2010).
211. Pickart, C. M. Targeting of substrates to the 26S proteasome. The FASEB Journal 11, 1055-1066 (1997).
212. Ferguson, E. C. & Rathmell, J. C. New roles for pyruvate kinase M2: working out the Warburg effect. Trends in Biochemical Sciences 33, 359-362 (2008).
213. Qi, W., Shakalya, K., Stejskal, A., Goldman, A., Beeck, S., Cooke, L. & Mahadevan, D. NSC348884, a nucleophosmin inhibitor disrupts oligomer formation and induces apoptosis in human cancer cells. Oncogene 27, 4210-4220 (2008).
214. Siepe, D. & Jentsch, S. Prolyl isomerase Pin1 acts as a switch to control the degree of substrate ubiquitylation. Nat Cell Biol 11, 967-972 (2009).
215. Kozlov, G., Bastos-Aristizabal, S., MÃ¤Ã¤ttÃ¤nen, P., Rosenauer, A., Zheng, F., Killikelly, A., Trempe, J.-F. o., Thomas, D. Y. & Gehring, K. Structural Basis of Cyclophilin B Binding by the Calnexin/Calreticulin P-domain. Journal of Biological Chemistry 285, 35551-35557 (2010).
216. Dastidar, S. G., Lane, D. P. & Verma, C. S. Multiple Peptide Conformations Give Rise to Similar Binding Affinities: Molecular Simulations of p53-MDM2. Journal of the American Chemical Society 130, 13514-13515 (2008).
217. Ergin, M., Denning, M. F., Izban, K. F., Amin, H. M., Martinez, R. L., Saeed, S. & Alkan, S. Inhibition of tyrosine kinase activity induces caspase-dependent apoptosis in anaplastic large cell lymphoma with NPM-ALK (p80) fusion protein. Experimental Hematology 29, 1082-1090 (2001).
218. Bischof, D., Pulford, K., Mason, D. Y. & Morris, S. W. Role of the nucleophosmin (NPM) portion of the non-Hodgkin's lymphoma- associated NPM-anaplastic lymphoma kinase fusion protein in oncogenesis. Mol. Cell. Biol. 17, 2312-2325 (1997).
219. Park, S.-W., Zhen, G., Verhaeghe, C., Nakagami, Y., Nguyenvu, L. T., Barczak, A. J., Killeen, N. & Erle, D. J. The protein disulfide isomerase AGR2 is essential for production of intestinal mucus. Proceedings of the National Academy of Sciences 106, 6950-6955 (2009).
220. Faull, P. A. in Exploring gas-phase protein conformations by ion mobility mass spectrometry
(University of Edinburgh, Edinburgh, 2009).
221. Fotedar, R., Bendjennat, M. & Fotedar, A. Role of p21Waf1 in the Cellular Response to UV. Cell Cycle 3, 132-135 (2004).

222. Sun, H., Nikolovska-Coleska, Z., Lu, J., Meagher, J. L., Yang, C. Y., Qiu, S., Tomita, Y., Ueda, Y., Jiang, S., Krajewski, K., Roller, P. P., Stuckey, J. A. & Wang, S. Design, Synthesis, and Characterization of a Potent, Nonpeptide, Cell-Permeable, Bivalent Smac Mimetic That Concurrently Targets Both the BIR2 and BIR3 Domains in XIAP. J. Am. Chem. Soc. 129, 15279-15294 (2007).

Appendix 1

All PAcIFIC Quantitation Results (TC – Time after Nutlin Treatment (Hr), Acc. Uniprot Accession Number)

Replicate One

Acc.	Gene	Normalized Spectral Count TC00	TC02	TC04	TC08	TC24
P61604	HSPE1	9.0	10.98554	11.61879	12.43262	11.37128
P63104	YWHAZ	1.0	3.295663	0	1.130238	1.263476
P62333	PSMC6 SUG2	2.0	1.098554	0	3.390716	0
P17980	PSMC3 TBP1	4.0	2.197109	0	3.390716	2.526952
O00231	PSMD11	2.0	1.098554	0	3.390716	1.263476
P55036	PSMD4 MCB1	1.0	1.098554	0	1.130238	1.263476
P52815	MRPL12 RPML12	10.0	9.886990	9.958967	10.17215	11.37128
Q99714	HSD17B10 ERAB	9.0	7.689881	3.319655	7.911671	11.37128
P46783	RPS10	1.0	4.394218	1.659827	0	0
P62263	RPS14 PRO2640	6.0	8.788436	4.979483	3.390716	3.790428
P08708	RPS17	9.0	7.7	8.299139	3.390716	2.526952
P39019	RPS19	11.0	13.18265	14.93845	12.43262	11.37128
P15880	RPS2 RPS4	6.0	5.492772	6.639311	0	3.790428
P60866	RPS20	6.0	7.689881	3.319655	3.390716	3.790428
P62266	RPS23	4.0	2.2	3.319655	1.130238	0
P62857	RPS28	1.0	2.2	0	0	0
P23396	RPS3 OK/SW-cl.26	5.0	7.689881	4.979483	3.390716	1.263476
P46782	RPS5	6.0	8.788436	6.639311	5.651194	10.10780
P62081	RPS7	0.0	1.098554	1.659827	0	1.263476
P08865	RPSA LAMBR	9.0	5.492772	8.299139	5.651194	5.053904
P08195	SLC3A2 MDU1	7.0	5.492772	6.639311	6.781433	6.317380
Q96IR7	HPDL GLOXD1	2.0	1.098554	1.659827	2.260477	3.790428
P10809	HSPD1 HSP60	74.0	90.08147	82.99139	87.02839	94.76070
P62906	RPL10A NEDD6	3.0	3.295663	0	0	1.263476
P62913	RPL11	8.0	10.98554	13.27862	9.041910	10.10780
P26373	RPL13 BBC1	1.0	2.197109	1.659827	0	0
P18621	RPL17	3.0	5.492772	3.319655	0	0
Q07020	RPL18	3.0	3.295663	3.319655	3.390716	1.263476
P46778	RPL21	5.0	7.689881	8.299139	4.520955	5.053904
P83731	RPL24	12.0	17.57687	16.59827	13.56286	16.42518
P61254	RPL26	3.0	4.394218	3.319655	2.260477	1.263476
P46776	RPL27A	2.0	5.5	3.319655	3.390716	0
P62888	RPL30	2.0	3.295663	0	1.130238	0

Acc.	Gene	Normalized Spectral Count TC00	TC02	TC04	TC08	TC24
P18124	RPL7	3.0	5.492772	0	0	1.263476
P62424	RPL7A SURF-3 SURF3	8.0	10.985545	13.278623	6.781431	5.053904
P62917	RPL8	1.0	1.1	1.659827	0	0
P11021	HSPA5 GRP78	19.0	45.04073	28.21707	44.07931	54.32947
Q8NFV4	ABHD11	0.0	1.098554	3.319655	3.390716	2.526952
P24752	ACAT1 ACAT MAT	4.0	4.394218	6.639311	4.520955	5.053904
Q99798	ACO2	1.0	6.591327	3.319655	3.390716	3.790428
P60709	ACTB	40.0	42.84362	59.75380	63.29337	68.22770
P54819	AK2 ADK2	3.0	3.295663	4.979483	1.130238	3.790428
Q9HDC9	APMAP C20orf3 UNQ1869/PRO430	2.0	1.098554	0	2.260477	1.263476
P12235	SLC25A4 ANT1	6.0	4.394218	1.659827	3.390716	1.263476
P05141	SLC25A5 ANT2	21.0	15.37976	24.89741	21.47453	17.68866
Q92667	AKAP1 AKAP149	4.0	4.394218	1.659827	3.390716	3.790428
P12814	ACTN1	7.0	14.28120	11.61879	5.651194	8.844332
O43707	ACTN4	27.0	18.67542	18.25810	18.08382	24.00604
P06733	ENO1 ENO1L1	9.0	7.689881	6.639311	10.17215	5.053904
P50995	ANXA11 ANX11	0.0	3.295663	0	0	0
P07355	ANXA2 ANX2	10.0	1.098554	0	0	11.37128
O95831	AIFM1 AIF PDCD8	3.0	1.098554	4.979483	1.130238	1.263476
P00505	GOT2	6.0	4.4	1.659827	5.651194	6.317380
P25705	ATP5A1 ATP5A	36.0	27.46386	14.93845	31.64668	29.05995
P06576	ATP5B ATPMB	43.0	31.85808	28.21707	27.12573	36.64080
P56385	ATP5I ATP5K	7.0	3.295663	0	2.260477	0
P48047	ATP5O ATPO	15.0	14.28120	6.639311	14.69310	8.844332
P53396	ACLY	1.0	0	0	2.260477	1.263476
O00148	DDX39	5.0	2.197109	0	2.260477	1.263476
P11586	MTHFD1 MTHFC	0.0	0	0	1.130238	1.263476
P27824	CANX	7.0	6.591327	0	2.260477	3.790428
Q14444	CAPRIN1 GPIAP1	5.0	2.2	0	2.260477	2.526952
P16152	CBR1 CBR CRN	0.0	1.1	0	2.260477	0
P35221	CTNNA1	14.0	9.886990	4.979483	13.56286	8.844332
Q13185	CBX3	11.0	13.2	14.93845	12.43262	8.844332
P45973	CBX5 HP1A	11.0	5.5	8.299139	3.390716	5.053904
Q00610	CLTC CLH17	1.0	2.197109	1.659827	3.390716	2.526952
P23528	CFL1 CFL	15.0	15.37976	24.89741	20.34429	15.16171
Q9NX63	CHCHD3	7.0	4.394218	0	1.130238	0
O75534	CSDE1 D1S155E	4.0	1.098554	4.979483	1.130238	0
Q14011	CIRBP A18HNRNP	1.0	1.098554	1.659827	0	0

Acc.	Gene	Normalized Spectral Count TC00	TC02	TC04	TC08	TC24
Q92879	CELF1 BRUNOL2 CUGBP CUGBP1 NAB50	5.0	3.2956636	4.9794838	5.6511942	5.0539043
P31930	UQCRC1	11.0	7.7	4.979483	6.781433	6.317380
P22695	UQCRC2	6.0	4.394218	3.319655	4.520955	3.790428
P07919	UQCRH	6.0	5.492772	6.639311	4.520955	6.317380
P14927	UQCRB UQBP	5.0	1.098554	3.319655	2.260477	1.263476
P10606	COX5B	5.0	5.492772	3.319655	3.390716	6.317380
P14854	COX6B1 COX6B	9.0	9.9	14.93845	7.911671	10.10780
P15954	COX7C	3.0	1.098554	1.659827	1.130238	0
Q07065	CKAP4	5.0	2.197109	0	1.130238	1.263476
P28838	LAP3 LAPEP PEPS	0.0	0	0	2.260477	0
O43175	PHGDH PGDH3	5.0	2.197109	1.659827	5.651194	0
P54886	ALDH18A1 GSAS P5CS PYCS	7.0	2.1971091	0	1.1302388	0
P60981	DSTN ACTDP DSN	4.0	1.098554	1.659827	4.520955	1.263476
P09622	DLD GCSL LAD	4.0	3.295663	0	3.390716	2.526952
Q92878	RAD50	1.0	1.098554	0	1.130238	1.263476
P33991	MCM4 CDC21	1.0	1.098554	3.319655	3.390716	1.263476
P11387	TOP1	5.0	3.3	0	2.260477	2.526952
P78527	PRKDC HYRC	7.0	3.295663	3.319655	4.520955	2.526952
P04843	RPN1	13.0	7.689881	6.639311	7.911671	8.844332
O75150	RNF40 BRE1B	2.0	0	1.659827	1.130238	1.263476
Q9UPN9	TRIM33 KIAA1113	9.0	6.591327	4.979483	9.041910	6.317380
P13804	ETFA	3.0	3.295663	3.319655	2.260477	5.053904
P38117	ETFB FP585	2.0	2.197109	1.659827	3.390716	5.053904
P68104	EEF1A1 EEF1A	5.0	6.591327	8.299139	4.520955	2.526952
P29692	EEF1D EF1D	4.0	6.591327	6.639311	7.911671	5.053904
P26641	EEF1G EF1G	7.0	6.591327	3.319655	5.651194	2.526952
P13639	EEF2 EF2	18.0	8.788436	11.61879	11.30238	11.37128
P49411	TUFM	11.0	19.8	13.27862	13.56286	15.16171
P30040	ERP29 C12orf8	2.0	4.394218	1.659827	11.30238	6.317380
P14625	HSP90B1 GRP94	4.0	14.3	16.59827	18.08382	24.00604
P30084	ECHS1	4.0	4.394218	8.299139	7.911671	10.10780
P58107	EPPK1 EPIPL	13.0	4.394218	4.979483	1.130238	0
P16422	EPCAM GA733-2	3.0	1.098554	0	1.130238	2.526952
P60842	EIF4A1 DDX2A	0.0	2.197109	1.659827	3.390716	0
Q04637	EIF4G1 EIF4F	3.0	1.098554	0	2.260477	2.526952
Q9GZV4	EIF5A2	1.0	1.098554	0	0	0
Q9BSJ8	ESYT1 FAM62A	11.0	6.591327	6.639311	11.30238	7.580856

Acc.	Gene	Normalized Spectral Count TC00	TC02	TC04	TC08	TC24
Q96AE4	FUBP1	18.0	18.67542	16.59827	16.95358	25.26952
Q92945	KHSRP FUBP2	19.0	19.77398	24.89741	22.60477	22.74256
P49327	FASN FAS	10.0	8.788436	8.299139	13.56286	10.10780
P21333	FLNA FLN FLN1	26.0	30.75952	51.45466	38.42812	32.85037
O75369	FLNB FLN1L FLN3	3.0	4.394218	1.659827	2.260477	3.790428
Q5SZK8	FREM2	0.0	0	0	2.260477	0
P04075	ALDOA ALDA	14.0	15.37976	14.93845	16.95358	13.89823
P11413	G6PD	0.0	0.0	1.659827	2.260477	0
P14314	PRKCSH G19P1	6.0	15.37976	9.958967	16.95358	17.68866
P04406	GAPDH GAPD	11.0	10.98554	9.958967	15.82334	15.16171
P43304	GPD2	7.0	7.689881	1.659827	7.911671	5.053904
Q08379	GOLGA2	4.0	0	0	0	0
Q8TBA6	GOLGA5 RETII	2.0	0	0	0	0
P01111	NRAS HRAS1	2.0	0	0	0	0
P62826	RAN ARA24	9.0	7.689881	14.93845	6.781433	10.10780
P62879	GNB2	4.0	0	1.659827	3.390716	6.317380
P08107	HSPA1A HSPA1;	15.0	15.37976	14.93845	13.56286	16.42518
P11142	HSPA8 HSC70	6.0	10.98554	13.27862	14.69310	10.10780
Q92598	HSPH1 HSP105	4.0	3.295663	3.319655	6.781433	2.526952
Q12931	TRAP1 HSP75	3.0	9.886990	4.979483	10.17215	10.10780
P04792	HSPB1 HSP27	8.0	8.788436	8.299139	6.781433	5.053904
P07900	HSP90AA1	15.0	13.2	8.299139	22.60477	20.21561
P08238	HSP90AB1	22.0	27.46386	26.55724	35.03740	31.58690
P30519	HMOX2 HO2	6.0	5.492772	0	1.130238	6.317380
P51858	HDGF HMG1L2	0.0	1.098554	1.659827	1.130238	0
Q99729	HNRNPAB ABBP1	7.0	5.492772	6.639311	3.390716	5.053904
P09651	HNRNPA1	21.0	19.77398	28.21707	20.34429	20.21561
P51991	HNRNPA3	2.0	2.197109	0	0	0
Q14103	HNRNPD AUF1	7.0	6.591327	1.659827	5.651194	6.317380
P31943	HNRNPH1 HNRPH	12.0	8.8	9.958967	11.30238	7.580856
P61978	HNRNPK HNRPK	24.0	24.1682	33.19655	25.99549	29.05995
P14866	HNRNPL HNRPL	6.0	1.098554	1.659827	1.130238	1.263476
P52272	HNRNPM HNRPM	23.0	26.36530	13.27862	38.42812	42.95818
O60506	SYNCRIP HNRPQ	2.0	3.295663	4.979483	2.260477	2.526952
Q00839	HNRNPU HNRPU	10.0	7.689881	1.659827	3.390716	5.053904
P22626	HNRNPA2B1	8.0	8.788436	6.639311	4.520955	1.263476
P07910	HNRNPC HNRPC	1.0	1.1	3.319655	0	0
P19367	HK1	3.0	4.394218	0	0	1.263476
P16401	HIST1H1B H1F5	2.0	4.4	4.979483	3.390716	7.580856
Q92522	H1FX	7.0	5.492772	6.639311	4.520955	3.790428

Acc.	Gene	Normalized Spectral Count TC00	TC02	TC04	TC08	TC24
Q12906	ILF3 DRBF MPHOSPH4 NF90	4.0	2.1971091	4.9794838	2.2604777	0
P50213	IDH3A	8.0	6.6	9.958967	7.911671	10.10780
P48735	IDH2	6.0	4.394218	0	4.520955	5.053904
Q04695	KRT17	2.0	0	1.659827	0	0
P05783	KRT18 CYK18	52.0	53.82917	92.95036	56.51194	58.11989
P08727	KRT19	57.0	62.6	91.29053	62.16313	63.17380
P35527	KRT9	4.0	0.0	0	0	0
P04264	KRT1 KRTA	16.0	6.591327	8.299139	4.520955	3.790428
Q8N1N4	KRT78 K5B KB40	6.0	9.886990	13.27862	7.911671	10.10780
P05787	KRT8 CYK8	174.0	138.4178	257.2733	166.1451	154.1440
Q86UP2	KTN1 CG1	8.0	4.394218	3.319655	3.390716	3.790428
P42166	TMPO LAP2	2.0	2.197109	3.319655	2.260477	1.263476
P20700	LMNB1 LMN2	4.0	2.197109	3.319655	0	0
P42704	LRPPRC LRP130	2.0	0.0	0	0	0
Q96AG4	LRRC59 PRO1855	17.0	16.47831	13.27862	13.56286	11.37128
P05455	SSB	3.0	4.394218	3.319655	4.520955	3.790428
P14174	MIF GLIF MMIF	15.0	12.0841	14.93845	13.56286	17.68866
P40926	MDH2	46.0	65.91327	63.07346	72.33528	87.17984
P43243	MATR3 KIAA0723	3.0	2.2	3.319655	0	1.263476
P11310	ACADM	2.0	1.098554	1.659827	1.130238	2.526952
O00264	PGRMC1 HPR6.6	6.0	4.394218	4.979483	5.651194	2.526952
P55145	MANF ARMET	0.0	1.098554	0	3.390716	1.263476
Q9HCC	MCCC2 MCCB	3.0	2.197109	1.659827	2.260477	2.526952
Q9Y5L4	TIMM13 TIM13B	0.0	3.295663	1.659827	1.130238	2.526952
O60220	TIMM8A DDP	2.0	6.591327	3.319655	4.520955	7.580856
O94826	TOMM70A	5.0	2.197109	1.659827	2.260477	1.263476
Q16891	IMMT HMP PIG4	8.0	5.492772	3.319655	1.130238	2.526952
O75439	PMPCB MPPB	0.0	2.197109	0	0	0
P60660	MYL6	2.0	7.689881	3.319655	6.781433	6.317380
P35579	MYH9	1.0	3.3	1.659827	6.781433	5.053904
O14745	SLC9A3R1 NHERF	4.0	6.591327	8.299139	6.781433	5.053904
P28331	NDUFS1	2.0	0	0	0	1.263476
Q09666	AHNAK PM227	25.0	12.1	11.61879	10.17215	11.37128
Q14697	GANAB G2AN	3.0	14.3	13.27862	13.56286	13.89823
P55769	NHP2L1	2.0	1.098554	1.659827	2.260477	2.526952
Q15233	NONO NRB54	20.0	19.8	3.319655	22.60477	22.74256
Q02818	NUCB1 NUC	2.0	3.295663	0	4.520955	1.263476
P17480	UBTF UBF UBF1	2.0	0	0	0	0
P19338	NCL	7.0	6.591327	9.958967	5.651194	6.317380

Acc.	Gene	Normalized Spectral Count TC00	TC02	TC04	TC08	TC24
P12270	TPR	6.0	0	0	1.130238	1.263476
P15531	NME1 NDPKA NM23	7.0	7.689881 7	6.639311 7	7.911671 9	6.317380 4
Q99733	NAP1L4 NAP2	3.0	3.295663	0	4.520955	1.263476
Q8WXF	PSPC1 PSP1	2.0	0	0	0	0
P62937	PPIA CYPA	31.0	36.3	33.19655	40.68859	39.16775
P23284	PPIB CYPB	3.0	6.591327	6.639311	9.041910	10.10780
P30405	PPIF CYP3	6.0	7.689881	9.958967	7.911671	7.580856
Q06830	PRDX1 PAGA	10.0	10.98554	9.958967	12.43262	10.10780
Q13162	PRDX4	3.0	9.9	8.299139	11.30238	10.10780
P30044	PRDX5 ACR1	4.0	5.492772	0	2.260477	1.263476
P30041	PRDX6 AOP2	3.0	2.197109	0	0	0
P51659	HSD17B4	1.0	4.394218	3.319655	3.390716	5.053904
P00558	PGK1 PGKA	6.0	3.3	3.319655	3.390716	3.790428
P18669	PGAM1 PGAMA	3.0	0	0	0	0
Q15149	PLEC PLEC1	20.0	6.591327	6.639311	4.520955	10.10780
P09874	PARP1 ADPRT	4.0	1.098554	0	1.130238	1.263476
Q15366	PCBP2	5.0	5.5	0	0	5.053904
P11940	PABPC1 PAB1	5.0	5.492772	3.319655	1.130238	2.526952
Q86U42	PABPN1 PAB2	4.0	3.295663	0	1.130238	1.263476
P26599	PTBP1 PTB	11.0	8.788436	6.639311	7.911671	11.37128
P02545	LMNA LMN1	9.0	15.37976	28.21707	9.041910	5.053904
O94906	PRPF6 C20orf14	3.0	2.197109	1.659827	2.260477	1.263476
Q92841	DDX17	9.0	6.591327	1.659827	6.781433	2.526952
P17844	DDX5 G17P1	27.0	23.06964	4.979483	15.82334	11.37128
P07737	PFN1	6.0	4.4	9.958967	5.651194	5.053904
P35232	PHB	20.0	20.87253	18.25810	13.56286	15.16171
Q99623	PHB2 BAP REA	11.0	5.492772	1.659827	1.130238	5.053904
P12004	PCNA	3.0	6.591327	6.639311	7.911671	5.053904
Q9UQ80	PA2G4 EBP1	1.0	4.394218	0	1.130238	0
P61289	PSME3	1.0	1.098554	0	2.260477	1.263476
P28066	PSMA5	1.0	0	0	0	1.263476
P60900	PSMA6 PROS27	7.0	3.295663	8.299139	6.781433	6.317380
O14818	PSMA7 HSPC	2.0	1.098554	1.659827	1.130238	0
P07237	P4HB ERBA2L PDI	13.0	39.54796	43.15552	40.68859	50.53904
P30101	PDIA3 ERP57	14.0	21.97109	16.59827	24.86525	29.05995
P13667	PDIA4 ERP70	2.0	18.67542	14.93845	15.82334	16.42518
Q15084	PDIA6 ERP5 P5	5.0	17.57687	23.23759	15.82334	18.95214
Q8N163	KIAA1967 DBC1	2.0	0	1.659827	0	0
P31949	S100A11 MLN70	3.0	1.1	0	1.130238	0

Acc.	Gene	Normalized Spectral Count TC00	TC02	TC04	TC08	TC24
B2RPK0	HMGB1P1 HMG1L1 HMGB1L1	6.0	8.7884363	9.9589676	0	6.3173804
P98179	RBM3 RNPL	7.0	2.197109	3.319655	5.651194	10.10780
Q9Y383	LUC7L2 CGI-59	2.0	4.394218	0	4.520955	2.526952
P32322	PYCR1	3.0	3.295663	4.979483	3.390716	3.790428
P11498	PC	3.0	4.394218	4.979483	3.390716	3.790428
P11177	PDHB PHE1B	4.0	1.098554	0	2.260477	3.790428
P14618	PKM2 OIP3 PK2	19.0	18.67542	11.61879	20.34429	20.21561
P43487	RANBP1	2.0	0	1.659827	0	0
Q13283	G3BP1 G3BP	3.0	2.197109	1.659827	3.390716	1.263476
P62491	RAB11A RAB11	6.0	6.6	4.979483	5.651194	7.580856
P51149	RAB7A RAB7	3.0	3.295663	1.659827	3.390716	5.053904
P62834	RAP1A KREV1	6.0	3.3	0	0	0
A6NIZ1		5.0	2.197109	3.319655	5.651194	2.526952
P52565	ARHGDIA GDIA1	2.0	0	0	0	0
P62745	RHOB ARH6 ARHB	3.0	2.2	1.659827	2.260477	2.526952
Q9P2E9	RRBP1 KIAA1398	5.0	4.394218	3.319655	5.651194	5.053904
Q96PK6	RBM14 SIP	10.0	4.394218	6.639311	4.520955	1.263476
P35637	FUS TLS	6.0	6.6	4.979483	6.781433	7.580856
Q9Y230	RUVBL2 INO80J	7.0	5.492772	9.958967	5.651194	5.053904
P16615	ATP2A2 ATP2B	7.0	4.394218	3.319655	5.651194	3.790428
P34897	SHMT2	12.0	15.37976	13.27862	18.08382	25.26952
Q9UQ35	SRRM2 KIAA0324	14.0	15.37976	11.61879	4.520955	6.317380
Q07955	SRSF1 ASF SF2	8.0	6.591327	8.299139	3.390716	1.263476
Q05519	SRSF11 SFRS11	4.0	2.197109	3.319655	1.130238	2.526952
Q13247	SRSF6 SFRS6	4.0	2.197109	3.319655	0	0
P50454	SERPINH1 CBP1	3.0	14.28120	13.27862	12.43262	17.68866
Q9H9B4	SFXN1	23.0	19.77398	16.59827	16.95358	21.47909
Q9Y5M8	SRPRB PSEC0230	1.0	1.098554	0	0	0
Q04837	SSBP1 SSBP	9.0	9.886990	13.27862	13.56286	12.63476
P62318	SNRPD3	7.0	4.4	3.319655	2.260477	2.526952
P05023	ATP1A1	13.0	6.591327	6.639311	5.651194	5.053904
P55011	SLC12A2 NKCC1	3.0	1.098554	0	1.130238	0
Q12874	SF3A3 SAP61	1.0	0	0	1.130238	1.263476
Q13435	SF3B2 SAP145	1.0	1.098554	0	1.130238	0
Q8WU6	U2AF1L4 U2AF1-	0.0	0	0	2.260477	0
P23246	SFPQ PSF	30.0	26.36530	28.21707	24.86525	32.85037
Q9GZT3	SLIRP C14orf156	9.0	7.689881	4.979483	4.520955	5.053904
Q7KZF4	SND1 TDRD11	5.0	10.98554	8.299139	6.781433	11.37128
Q9UJZ1	STOML2 SLP2	2.0	0	0	0	0

Acc.	Gene	Normalized Spectral Count TC00	TC02	TC04	TC08	TC24
P31040	SDHA SDH2 SDHF	7.0	6.591327	4.979483	7.911671	6.317380
P55809	OXCT1 OXCT SCOT	0.0	0	0	3.390716 5	3.790428 2
Q969G3	SMARCE1 BAF57	1.0	0	0	1.130238	0
P78371	CCT2 99D8.1	10.0	5.492772	6.639311	4.520955	5.053904
P48643	CCT5 CCTE	2.0	0	0	1.130238	0
P49368	CCT3 CCTG TRIC5	6.0	3.295663	4.979483	7.911671	1.263476
P50990	CCT8 C21orf112	6.0	2.197109	4.979483	2.260477	2.526952
P40227	CCT6A CCT6	5.0	2.197109	0	2.260477	1.263476
Q8NBS9	TXNDC5 TLP46	0.0	5.492772	0	6.781433	8.844332
P30048	PRDX3 AOP1	9.0	3.295663	4.979483	4.520955	6.317380
Q86V81	THOC4 ALY BEF	8.0	9.886990	11.61879	10.17215	10.10780
Q5JTV8	TOR1AIP1	3.0	1.098554	1.659827	2.260477	1.263476
P37837	TALDO1 TAL	0.0	1.098554	0	3.390716	1.263476
Q00059	TFAM TCF6	2.0	4.394218	1.659827	1.130238	0
Q13263	TRIM28 KAP1	12.0	9.886990	9.958967	12.43262	7.580856
P02786	TFRC	5.0	4.394218	1.659827	3.390716	2.526952
P37802	TAGLN2 KIAA0120	4.0	3.3	0	6.781433	5.053904
P55072	VCP	13.0	17.57687	13.27862	21.47453	15.16171
P29401	TKT	2.0	3.295663	4.979483	6.781433	3.790428
Q9BSH4	TACO1 CCDC44	2.0	5.492772	1.659827	3.390716	5.053904
P13693	TPT1	2.0	1.098554	3.319655	3.390716	0
P40939	HADHA HADH	7.0	5.492772	3.319655	3.390716	10.10780
P60174	TPI1 TPI	11.0	6.591327	14.93845	7.911671	6.317380
Q13641	TPBG 5T4	6.0	1.098554	0	0	0
P06753	TPM3	1.0	4.394218	3.319655	2.260477	2.526952
P67936	TPM4	0.0	1.098554	0	3.390716	0
Q9BQE3	TUBA1C TUBA6	4.0	0	0	0	0
P07437	TUBB TUBB5	17.0	15.4	16.59827	16.95358	15.16171
P68371	TUBB2C	6.0	16.47831	11.61879	18.08382	0
P04350	TUBB4 TUBB5	17.0	7.689881	0	9.041910	25.26952
O75347	TBCA	2.0	0	1.659827	1.130238	0
O43399	TPD52L2	1.0	1.098554	1.659827	2.260477	1.263476
O43290	SART1	4.0	1.098554	3.319655	0	1.263476
P62979	RPS27A UBA80	4.0	4.394218	1.659827	3.390716	6.317380
Q969H8	C19orf10 IL25	0.0	3.295663	0	5.651194	3.790428
O95292	VAPB	7.0	1.098554	0	0	0
Q00341	HDLBP HBP VGL	3.0	2.197109	0	0	0
P21796	VDAC1 VDAC	11.0	9.886990	16.59827	11.30238	7.580856
P45880	VDAC2	2.0	5.492772	3.319655	1.130238	3.790428

Acc.	Gene	Normalized Spectral Count TC00	TC02	TC04	TC08	TC24
Q9Y6X8	ZHX2 AFR1 KIAA0854 RAF	0.0	1.0985545	0	1.1302388	1.2634761

Replicate Two

Acc.	Gene	Normalized Spectral Count TC00	TC02	TC04	TC08	TC24
P61604	HSPE1	7.045928	8.954506	10.19414	11	11.28307
P27348	YWHAQ	4.026245	0	0	3	3.223733
Q16698	DECR1 DECR	1.006561	2.238627	1.699023	2	6.447466
P62333	PSMC6 SUG2	3.019684	1.119313	1.699023	3	1.611867
P17980	PSMC3 TBP1	11.07217	10.07382	5.097068	4	3.223733
O00231	PSMD11	5.032806	2.238627	5.097068	4	9.671199
Q9Y3D9	MRPS23 CGI-138	3.019684	1.119313	1.699023	2	1.611867
P52815	MRPL12 RPML12	10.06561	7.835193	10.19414	9	8.059333
Q8N983	MRPL43	1.006561	0	0	2	1.611867
Q8N5N7	MRPL50	1.006561	0	0	0	3.223733
Q99714	HSD17B10 ERAB	11.07217	13.43176	20.38827	13	11.28307
P46783	RPS10	4.026245	6.71588	5.097068	2	4.8356
P25398	RPS12	3.019684	3.35794	0	1	0
P62263	RPS14 PRO2640	2.013122	5.596567	5.097068	2	4.8356
P08708	RPS17	3.019684	3.35794	6.796091	4	6.447466
P39019	RPS19	12.07873	11.19313	11.89316	11	11.28307
P15880	RPS2 RPS4	6.039367	6.71588	8.495114	4	3.223733
P60866	RPS20	1.006561	4.477253	3.398046	2	4.8356
P62847	RPS24	2.013122	0	1.699023	1	0
P62857	RPS28	0	2.238627	1.699023	1	1.611867
P23396	RPS3 OK/SW-cl.26	5.032806	8.954506	8.495114	6	6.447466
P46782	RPS5	9.059051	15.67039	15.29121	12	12.89493
P62753	RPS6 OK/SW-cl.2	1.006561	2.238627	0	0	0
P62081	RPS7	1.006561	0	1.699023	1	1.611867
P08865	RPSA LAMBR LAMR1	0	3.35794	5.097068	3	6.447466
P08195	SLC3A2 MDU1	9.059051	6.71588	11.89316	8	8.059333
Q96IR7	HPDL GLOXD1	5.032806	5.596567	6.796091	7	8.059333
P10809	HSPD1 HSP60	71.46584	88.42575	95.14528	85	61.25093
P05387	RPLP2 D11S2243E	1.006561	4.477253	1.699023	2	1.611867

P62913	RPL11	5.032806	10.07382	11.89316	7	6.447466
P18621	RPL17	0	0	0	1	3.223733
Q07020	RPL18	2.013122	3.35794	0	1	0
P84098	RPL19	3.019684	4.477253	1.699023	3	3.223733
P46778	RPL21	1.006561	4.477253	3.398046	2	4.8356
P83731	RPL24	8.052489	16.7897	10.19414	9	8.059333
P61254	RPL26	1.006561	1.119313	0	1	1.611867
P46776	RPL27A	1.006561	1.119313	1.699023	1	1.611867
Q02878	RPL6 TXREB1	0	2.238627	5.097068	1	1.611867
P62424	RPL7A SURF-3 SURF3	7.045928	11.19313	8.495114	6	8.059333
P11021	HSPA5 GRP78	24.15747	40.29528	32.28143	36	22.56613
P24752	ACAT1 ACAT MAT	3.019684	3.35794	8.495114	5	4.8356
Q99798	ACO2	5.032806	8.954506	1.699023	3	4.8356
P60709	ACTB	27.17715	32.46009	49.27166	38	41.90853
P63261	ACTG1 ACTB ACTG	4.026245	0	0	0	0
P54819	AK2 ADK2	4.026245	5.596567	8.495114	6	8.059333
Q9HDC9	APMAP C20orf3	1.006561	0	0	2	1.611867
P12235	SLC25A4 ANT1	6.039367	3.35794	3.398046	4	3.223733
P05141	SLC25A5 ANT2	16.10498	7.835193	28.88339	22	19.3424
P12236	SLC25A6 ANT3	6.039367	8.954506	6.796091	10	9.671199
O43707	ACTN4	29.19027	24.62489	30.58241	19	16.11867
P06733	ENO1 ENO1L1 MBPB1	12.07873	5.596567	11.89316	14	11.28307
P07355	ANXA2 ANX2 ANX2L4	15.09842	11.19313	16.99023	9	16.11867
P08133	ANXA6 ANX6	4.026245	3.35794	0	0	1.611867
Q07812	BAX BCL2L4	1.006561	0	0	0	3.223733
O95831	AIFM1 AIF PDCD8	12.07873	5.596567	8.495114	5	8.059333
P00505	GOT2	9.059051	3.35794	3.398046	5	3.223733
P25705	ATP5A1 ATP5A	28.18371	24.62489	20.38827	22	19.3424
P06576	ATP5B ATPMB ATPSB	38.24932	34.69871	33.98046	34	33.8492
O75947	ATP5H My032	2.013122	1.119313	0	2	0
P56385	ATP5I ATP5K	4.026245	0	1.699023	4	6.447466
P48047	ATP5O ATPO	14.09186	14.55107	6.796091	13	9.671199
P53396	ACLY	3.019684	0	1.699023	1	1.611867
O00571	DDX3X DBX DDX3	0	4.477253	3.398046	0	3.223733
O15523	DDX3Y DBY	2.013122	0	0	1	0
P13995	MTHFD2 NMDMC	0	1.119313	0	3	0
Q6NUK1	SLC25A24 APC1	3.019684	2.238627	0	2	1.611867
P27824	CANX	9.059051	2.238627	3.398046	2	3.223733
P27797	CALR CRTC	1.006561	7.835193	5.097068	7	6.447466
P35221	CTNNA1	16.10498	7.835193	8.495114	15	8.059333
P35222	CTNNB1 CTNNB	1.006561	0	0	1	0
O60716	CTNND1 KIAA0384	2.013122	0	0	0	0
P07339	CTSD CPSD	0	10.07382	1.699023	7	4.8356

Acc.	Gene	Normalized Spectral Count TC00	TC02	TC04	TC08	TC24
Q13185	CBX3	14.09186	16.7897	11.89316	17	16.11867
P45973	CBX5 HP1A	9.059051	6.71588	8.495114	6	6.447466
O75390	CS	2.013122	2.238627	1.699023	1	1.611867
Q00610	CLTC CLH17 CLTCL2	4.026245	5.596567	1.699023	4	4.8356
P09497	CLTB	1.006561	0	0	1	0
P23528	CFL1 CFL	12.07873	16.7897	20.38827	15	8.059333
Q9NX63	CHCHD3	6.039367	2.238627	1.699023	2	3.223733
O75534	CSDE1 D1S155E	2.013122	1.119313	1.699023	2	0
Q9BR76	CORO1B	1.006561	2.238627	1.699023	0	1.611867
P12532	CKMT1A CKMT;	2.013122	5.596567	1.699023	7	6.447466
Q92879	CELF1 BRUNOL2	6.039367	5.596567	5.097068	3	6.447466
P31930	UQCRC1	6.039367	7.835193	3.398046	6	6.447466
P22695	UQCRC2	6.039367	0	6.796091	2	6.447466
P07919	UQCRH	7.045928	3.35794	6.796091	6	12.89493
P20674	COX5A	3.019684	0	0	0	0
P10606	COX5B	6.039367	7.835193	3.398046	5	1.611867
P14854	COX6B1 COX6B	8.052489	10.07382	6.796091	8	6.447466
P15954	COX7C	3.019684	2.238627	5.097068	4	3.223733
Q07065	CKAP4	6.039367	3.35794	0	2	0
O43175	PHGDH PGDH3	1.006561	1.119313	3.398046	4	1.611867
Q13011	ECH1	0	0	0	0	3.223733
P30038	ALDH4A1 ALDH4	1.006561	2.238627	0	2	3.223733
P54886	ALDH18A1 GSAS	3.019684	2.238627	0	0	3.223733
P15924	DSP	1.006561	1.119313	1.699023	1	1.611867
P60981	DSTN ACTDP DSN	7.045928	3.35794	3.398046	5	1.611867
Q9NR28	DIABLO SMAC	0	1.119313	1.699023	4	3.223733
P09622	DLD GCSL LAD PHE3	4.026245	4.477253	6.796091	8	3.223733
Q92878	RAD50	2.013122	2.238627	0	1	4.8356
P49736	MCM2 BM28 CCNL1	1.006561	1.119313	3.398046	5	1.611867
P25205	MCM3	2.013122	0	3.398046	2	1.611867
P33991	MCM4 CDC21	0	0	1.699023	2	3.223733
P11387	TOP1	6.039367	2.238627	0	2	3.223733
P78527	PRKDC HYRC HYRC1	7.045928	2.238627	1.699023	2	0
P04843	RPN1	8.052489	7.835193	8.495114	8	8.059333
Q9UPN9	TRIM33 KIAA1113	8.052489	3.35794	1.699023	4	4.8356
P13804	ETFA	4.026245	4.477253	3.398046	3	6.447466
P38117	ETFB FP585	1.006561	5.596567	0	3	1.611867
P68104	EEF1A1 EEF1A EF1A	2.013122	4.477253	1.699023	4	3.223733
P29692	EEF1D EF1D	7.045928	7.835193	5.097068	7	4.8356
P26641	EEF1G EF1G	4.026245	3.35794	6.796091	5	3.223733

Acc.	Gene	Normalized Spectral Count TC00	TC02	TC04	TC08	TC24
P30040	ERP29 C12orf8 ERP28	5.032806	7.835193	11.89316	8	9.671199
P14625	HSP90B1 GRP94 TRA1	3.019684	17.90901	8.495114	19	19.3424
P30084	ECHS1	6.039367	15.67039	10.19414	16	12.89493
P58107	EPPK1 EPIPL	10.06561	5.596567	1.699023	2	1.611867
P16422	EPCAM GA733-2	2.013122	3.35794	3.398046	4	4.8356
P60842	EIF4A1 DDX2A EIF4A	1.006561	5.596567	5.097068	3	0
Q99613	EIF3C EIF3S8; EIF3CL	0	0	1.699023	1	0
Q04637	EIF4G1 EIF4F EIF4G	2.013122	0	0	2	0
Q9BSJ8	ESYT1 FAM62A	8.052489	5.596567	5.097068	9	9.671199
P47756	CAPZB	2.013122	0	0	1	1.611867
Q96AE4	FUBP1	12.07873	22.38627	16.99023	14	16.11867
Q92945	KHSRP FUBP2	19.12466	13.43176	18.68925	20	12.89493
Q96I24	FUBP3 FBP3	2.013122	1.119313	0	1	1.611867
P49327	FASN FAS	18.1181	12.31245	6.796091	11	9.671199
P22830	FECH	2.013122	0	0	0	0
P21333	FLNA FLN FLN1	18.1181	15.67039	33.98046	29	16.11867
O75369	FLNB FLN1L FLN3	4.026245	4.477253	1.699023	7	6.447466
P04075	ALDOA ALDA	14.09186	13.43176	8.495114	21	9.671199
P07954	FH	5.032806	3.35794	5.097068	5	4.8356
P11413	G6PD	0	0	0	3	1.611867
P06744	GPI	2.013122	2.238627	3.398046	2	3.223733
P14314	PRKCSH G19P1	7.045928	15.67039	15.29121	15	11.28307
P04406	GAPDH GAPD	14.09186	10.07382	3.398046	13	9.671199
P43304	GPD2	6.039367	1.119313	0	4	4.8356
Q08379	GOLGA2	6.039367	4.477253	5.097068	1	4.8356
P01111	NRAS HRAS1	4.026245	0	0	4	6.447466
P62826	RAN ARA24 OK/SW-	6.039367	10.07382	15.29121	11	9.671199
P62879	GNB2	1.006561	1.119313	3.398046	3	4.8356
Q14344	GNA13	3.019684	0	0	0	0
P08107	HSPA1A HSPA1;	21.13778	20.14764	11.89316	23	19.3424
P11142	HSPA8 HSC70 HSP73	49.3215	39.17597	18.68925	21	51.57973
Q92598	HSPH1 HSP105	2.013122	2.238627	1.699023	3	3.223733
Q12931	TRAP1 HSP75	8.052489	7.835193	3.398046	7	4.8356
P04792	HSPB1 HSP27 HSP28	11.07217	10.07382	8.495114	8	9.671199
P07900	HSP90AA1 HSP90A	15.09842	16.7897	10.19414	20	17.73053
P08238	HSP90AB1 HSP90B	20.13122	27.98283	18.68925	32	27.40173
P30519	HMOX2 HO2	4.026245	1.119313	0	2	3.223733
Q99729	HNRNPAB ABBP1	6.039367	5.596567	6.796091	3	3.223733
P09651	HNRNPA1 HNRPA1	22.14435	20.14764	22.0873	17	20.95426

Acc.	Gene	Normalized Spectral Count TC00	TC02	TC04	TC08	TC24
P52597	HNRNPF HNRPF	7.045928	6.71588	6.796091	4	6.447466
P31943	HNRNPH1 HNRPH	10.06561	10.07382	11.89316	9	11.28307
P55795	HNRNPH2 FTP3	0	2.238627	0	1	0
P61978	HNRNPK HNRPK	19.12466	25.74421	30.58241	22	12.89493
P14866	HNRNPL HNRPL	5.032806	4.477253	5.097068	4	4.8356
P52272	HNRNPM HNRPM	24.15747	30.22146	10.19414	37	40.29666
O60506	SYNCRIP HNRPQ	9.059051	5.596567	3.398046	8	9.671199
O43390	HNRNPR HNRPR	2.013122	1.119313	0	0	1.611867
Q00839	HNRNPU HNRPU	9.059051	8.954506	5.097068	3	4.8356
P22626	HNRNPA2B1	8.052489	6.71588	3.398046	3	3.223733
P07910	HNRNPC HNRPC	3.019684	3.35794	8.495114	2	1.611867
P19367	HK1	3.019684	2.238627	0	3	4.8356
P16403	HIST1H1C H1F2	5.032806	4.477253	5.097068	5	9.671199
Q92522	H1FX	3.019684	3.35794	1.699023	3	3.223733
Q09028	RBBP4 RBAP48	4.026245	5.596567	5.097068	5	4.8356
Q16836	HADH HAD HADHSC	3.019684	3.35794	1.699023	4	6.447466
Q9Y4L1	HYOU1 GRP170	0	4.477253	3.398046	4	1.611867
Q14974	KPNB1 NTF97	7.045928	11.19313	8.495114	5	4.8356
Q8TEX9	IPO4 IMP4B RANBP4	0	3.35794	0	0	0
Q12906	ILF3 DRBF	3.019684	0	1.699023	1	0
P50213	IDH3A	7.045928	8.954506	6.796091	9	8.059333
P48735	IDH2	6.039367	6.71588	0	5	11.28307
P14923	JUP CTNNG DP3	2.013122	0	0	0	0
P05783	KRT18 CYK18 PIG46	38.24932	39.17597	81.55309	49	38.6848
P08727	KRT19	61.40023	52.60773	79.85407	50	30.62546
P04264	KRT1 KRTA	20.13122	7.835193	15.29121	13	14.5068
P13647	KRT5	1.006561	0	0	1	0
Q8N1N4	KRT78 K5B KB40	5.032806	5.596567	11.89316	6	6.447466
P05787	KRT8 CYK8	124.8136	125.3631	208.9798	142	87.04079
Q86UP2	KTN1 CG1 KIAA0004	6.039367	1.119313	3.398046	7	3.223733
P42166	TMPO LAP2	0	2.238627	0	2	1.611867
P42167	TMPO LAP2	7.045928	5.596567	5.097068	3	4.8356
P20700	LMNB1 LMN2 LMNB	2.013122	2.238627	1.699023	0	0
P46379	BAG6 BAT3 G3	0	1.119313	0	0	1.611867
P42704	LRPPRC LRP130	4.026245	2.238627	0	1	1.611867
Q96AG4	LRRC59 PRO1855	17.11154	10.07382	10.19414	11	9.671199
P05455	SSB	4.026245	4.477253	6.796091	5	3.223733
P40926	MDH2	45.29525	66.03948	62.86384	60	64.47466
P43243	MATR3 KIAA0723	5.032806	1.119313	0	2	0
P11310	ACADM	1.006561	2.238627	3.398046	1	3.223733

Acc.	Gene	Normalized Spectral Count TC00	TC02	TC04	TC08	TC24
Q9HCC0	MCCC2 MCCB	2.013122	3.35794	1.699023	2	1.611867
Q9Y5L4	TIMM13 TIM13B TIMM13A TIMM13B	0	3.35794	3.398046	3	4.8356
O60220	TIMM8A DDP DDP1	0	8.954506	6.796091	8	11.28307
Q15388	TOMM20 KIAA0016	2.013122	0	0	0	0
O94826	TOMM70A KIAA0719	4.026245	4.477253	5.097068	5	3.223733
Q16891	IMMT HMP PIG4	7.045928	2.238627	5.097068	2	3.223733
P60660	MYL6	7.045928	11.19313	6.796091	9	3.223733
P35579	MYH9	2.013122	2.238627	1.699023	2	1.611867
O14745	SLC9A3R1 NHERF	5.032806	5.596567	6.796091	7	4.8356
Q16718	NDUFA5	5.032806	2.238627	3.398046	3	4.8356
O00217	NDUFS8	4.026245	4.477253	3.398046	2	1.611867
P28331	NDUFS1	2.013122	0	0	0	0
O15394	NCAM2 NCAM21	4.026245	2.238627	3.398046	2	4.8356
Q09666	AHNAK PM227	11.07217	12.31245	3.398046	11	9.671199
Q14697	GANAB G2AN	3.019684	11.19313	11.89316	10	16.11867
Q15233	NONO NRB54	19.12466	15.67039	3.398046	17	17.73053
Q02818	NUCB1 NUC	4.026245	3.35794	3.398046	4	4.8356
Q9NR30	DDX21	0	0	0	3	3.223733
P19338	NCL	7.045928	8.954506	11.89316	8	4.8356
P06748	NPM1 NPM	25.16403	24.62489	32.28143	24	27.40173
O75607	NPM3	4.026245	2.238627	8.495114	7	6.447466
Q5SRE5	NUP188 KIAA0169	1.006561	0	0	1	0
P12270	TPR	8.052489	7.835193	10.19414	5	4.8356
P15531	NME1 NDPKA NM23	3.019684	7.835193	5.097068	13	6.447466
Q99733	NAP1L4 NAP2	1.006561	1.119313	0	2	3.223733
P50897	PPT1 PPT	0	0	0	1	1.611867
Q8WXF1	PSPC1 PSP1	2.013122	2.238627	1.699023	1	4.8356
P62937	PPIA CYPA	23.15091	31.34077	28.88339	20	37.07293
P23284	PPIB CYPB	0	5.596567	1.699023	7	6.447466
P30405	PPIF CYP3	5.032806	8.954506	6.796091	9	8.059333
Q02790	FKBP4 FKBP52	1.006561	2.238627	0	2	3.223733
Q9Y3E5	PTRH2 BIT1 PTH2	1.006561	1.119313	0	0	1.611867
Q06830	PRDX1 PAGA PAGB	7.045928	13.43176	11.89316	10	16.11867
Q13162	PRDX4	2.013122	7.835193	10.19414	10	12.89493
P30041	PRDX6 AOP2	3.019684	1.119313	1.699023	1	1.611867
P51659	HSD17B4 EDH17B4	3.019684	4.477253	1.699023	6	6.447466
Q9Y285	FARSA FARS FARSL	0	3.35794	1.699023	1	1.611867
P00558	PGK1 PGKA MIG10	12.07873	5.596567	13.59218	10	9.671199
Q15149	PLEC PLEC1	16.10498	8.954506	10.19414	8	6.447466

Acc.	Gene	Normalized Spectral Count TC00	TC02	TC04	TC08	TC24
Q15366	PCBP2	4.026245	4.477253	3.398046	4	4.8356
P11940	PABPC1 PAB1 PABP1 PABPC2	3.019684	4.477253	1.699023	3	4.8356
Q86U42	PABPN1 PAB2 PABP2	2.013122	2.238627	0	1	1.611867
P26599	PTBP1 PTB	9.059051	8.954506	11.89316	11	8.059333
P02545	LMNA LMN1	8.052489	10.07382	8.495114	5	8.059333
Q92841	DDX17	8.052489	0	0	0	0
P17844	DDX5 G17P1 HELR	22.14435	13.43176	15.29121	14	12.89493
P07737	PFN1	7.045928	7.835193	10.19414	7	12.89493
P35232	PHB	20.13122	13.43176	15.29121	14	6.447466
Q99623	PHB2 BAP REA	8.052489	8.954506	3.398046	8	9.671199
P12004	PCNA	1.006561	2.238627	3.398046	3	3.223733
Q9UQ80	PA2G4 EBP1	0	1.119313	0	3	1.611867
P61289	PSME3	0	0	0	4	3.223733
P25787	PSMA2 HC3 PSC3	3.019684	1.119313	0	3	1.611867
P60900	PSMA6 PROS27	5.032806	5.596567	5.097068	6	11.28307
O14818	PSMA7 HSPC	3.019684	0	0	2	1.611867
P07237	P4HB ERBA2L PDI	9.059051	34.69871	42.47557	35	33.8492
P30101	PDIA3 ERP57 ERP60	10.06561	22.38627	22.0873	24	29.0136
P13667	PDIA4 ERP70 ERP72	4.026245	15.67039	11.89316	21	16.11867
Q15084	PDIA6 ERP5 P5	7.045928	23.50558	22.0873	22	20.95426
Q9C005	DPY30	2.013122	5.596567	1.699023	5	4.8356
Q86UE4	MTDH AEG1 LYRIC	1.006561	0	0	3	1.611867
Q9BPW8	NIPSNAP1	2.013122	2.238627	0	3	1.611867
P31949	S100A11 MLN70	4.026245	2.238627	5.097068	2	4.8356
Q96FQ6	S100A16 S100F	4.026245	3.35794	5.097068	3	1.611867
Q16740	CLPP	0	1.119313	0	3	1.611867
B2RPK0	HMGB1P1 HMG1L1	4.026245	4.477253	8.495114	9	12.89493
P0C6E5		2.013122	0	1.699023	2	3.223733
P98179	RBM3 RNPL	10.06561	10.07382	6.796091	11	8.059333
Q9Y383	LUC7L2 CGI-59 CGI-74	2.013122	4.477253	0	3	3.223733
P32322	PYCR1	2.013122	4.477253	3.398046	3	11.28307
Q96C36	PYCR2	3.019684	0	0	2	1.611867
P11498	PC	4.026245	3.35794	1.699023	2	3.223733
P11177	PDHB PHE1B	1.006561	2.238627	3.398046	3	3.223733
P14618	PKM2 OIP3 PK2 PK3	13.0853	14.55107	13.59218	16	17.73053
Q6IAA8	PDRO C11orf59	2.013122	1.119313	0	2	1.611867
Q13283	G3BP1 G3BP	3.019684	2.238627	1.699023	5	1.611867
P62491	RAB11A RAB11	3.019684	4.477253	3.398046	2	4.8356

Acc.	Gene	Normalized Spectral Count TC00	TC02	TC04	TC08	TC24
P62834	RAP1A KREV1	6.039367	0	0	3	0
A6NIZ1		5.032806	6.71588	5.097068	5	3.223733
P18754	RCC1 CHC1	3.019684	2.238627	3.398046	1	6.447466
P62745	RHOB ARH6 ARHB	4.026245	1.119313	1.699023	1	1.611867
Q9P2E9	RRBP1 KIAA1398	4.026245	3.35794	1.699023	4	6.447466
Q8N7H5	PAF1 PD2	0	0	0	1	1.611867
Q96PK6	RBM14 SIP	6.039367	2.238627	10.19414	4	3.223733
Q14498	RBM39 HCC1 RNPC2	8.052489	2.238627	3.398046	2	4.8356
P35637	FUS TLS	6.039367	7.835193	6.796091	6	4.8356
Q9Y230	RUVBL2 INO80J TIP48	7.045928	2.238627	3.398046	4	4.8356
P31153	MAT2A AMS2 MATA2	0	0	0	1	3.223733
P16615	ATP2A2 ATP2B	9.059051	4.477253	0	5	0
P34897	SHMT2	13.0853	22.38627	16.99023	19	16.11867
Q9UQ35	SRRM2 KIAA0324	8.052489	11.19313	6.796091	5	6.447466
Q07955	SRSF1 ASF SF2	3.019684	2.238627	3.398046	2	3.223733
Q05519	SRSF11 SFRS11	3.019684	0	0	1	1.611867
P50454	SERPINH1 CBP1	4.026245	11.19313	13.59218	15	16.11867
Q9H9B4	SFXN1	24.15747	17.90901	16.99023	14	9.671199
Q9BWM7	SFXN3	5.032806	5.596567	5.097068	4	4.8356
P37108	SRP14	3.019684	1.119313	1.699023	1	1.611867
Q04837	SSBP1 SSBP	11.07217	12.31245	11.89316	9	16.11867
P62318	SNRPD3	7.045928	4.477253	3.398046	2	8.059333
P05023	ATP1A1	7.045928	2.238627	5.097068	3	8.059333
P55011	SLC12A2 NKCC1	1.006561	0	0	1	0
Q13813	SPTAN1 SPTA2	2.013122	1.119313	0	0	0
Q13838	BAT1 UAP56	4.026245	0	0	0	0
O75533	SF3B1 SAP155	5.032806	1.119313	0	1	0
Q15393	SF3B3 KIAA0017	0	1.119313	0	0	3.223733
Q8WU68	U2AF1L4 U2AF1-RS3	3.019684	1.119313	0	0	0
P23246	SFPQ PSF	24.15747	17.90901	18.68925	21	24.178
P37268	FDFT1	3.019684	0	0	0	1.611867
Q9GZT3	SLIRP C14orf156 DC23	5.032806	3.35794	5.097068	4	4.8356
Q7KZF4	SND1 TDRD11	9.059051	13.43176	10.19414	5	9.671199
Q9UJZ1	STOML2 SLP2	7.045928	3.35794	1.699023	3	0
P38646	HSPA9 GRP75	40.26245	45.89185	44.17459	40	37.07293
P31948	STIP1	5.032806	6.71588	5.097068	4	6.447466
P31040	SDHA SDH2 SDHF	5.032806	5.596567	5.097068	6	8.059333
Q96I99	SUCLG2	0	3.35794	1.699023	3	1.611867
P55809	OXCT1 OXCT SCOT	2.013122	4.477253	1.699023	2	3.223733
Q8TAQ2	SMARCC2 BAF170	3.019684	0	1.699023	1	1.611867

Acc.	Gene	Normalized Spectral Count TC00	TC02	TC04	TC08	TC24
P50991	CCT4 CCTD SRB	1.006561	1.119313	0	1	0
P48643	CCT5 CCTE KIAA0098	2.013122	1.119313	0	4	0
Q99832	CCT7 CCTH NIP7-1	1.006561	0	0	2	0
P49368	CCT3 CCTG TRIC5	8.052489	4.477253	3.398046	10	3.223733
P50990	CCT8 C21orf112 CCTQ	5.032806	1.119313	1.699023	2	1.611867
Q8NBS9	TXNDC5 TLP46	0	4.477253	5.097068	3	8.059333
P30048	PRDX3 AOP1	7.045928	12.31245	6.796091	9	6.447466
Q86V81	THOC4 ALY BEF	15.09842	8.954506	11.89316	11	9.671199
Q5JTV8	TOR1AIP1	2.013122	2.238627	1.699023	3	1.611867
P51532	SMARCA4 BAF190A	1.006561	0	3.398046	1	0
Q15369	TCEB1	1.006561	0	0	1	0
Q13263	TRIM28 KAP1 RNF96	11.07217	7.835193	10.19414	8	12.89493
P02786	TFRC	8.052489	2.238627	3.398046	3	4.8356
P37802	TAGLN2 KIAA0120	4.026245	4.477253	1.699023	6	8.059333
P55072	VCP	20.13122	24.62489	16.99023	22	12.89493
P29401	TKT	1.006561	5.596567	5.097068	4	4.8356
Q9BSH4	TACO1 CCDC44	1.006561	2.238627	1.699023	4	4.8356
Q9BVK6	TMED9 GP25L2	4.026245	2.238627	0	3	6.447466
P40939	HADHA HADH	16.10498	8.954506	6.796091	16	17.73053
P60174	TPI1 TPI	5.032806	10.07382	18.68925	9	17.73053
Q13641	TPBG 5T4	3.019684	7.835193	5.097068	6	1.611867
P09493	TPM1 C15orf13 TMSA	0	1.119313	1.699023	2	1.611867
P06753	TPM3	5.032806	2.238627	3.398046	6	6.447466
Q9BQE3	TUBA1C TUBA6	8.052489	7.835193	11.89316	8	4.8356
Q13748	TUBA3C TUBA2;	1.006561	1.119313	0	0	0
P68366	TUBA4A TUBA1	0	3.35794	0	0	0
P07437	TUBB TUBB5 OK/SW-	32.20996	13.43176	13.59218	18	11.28307
P68371	TUBB2C	17.11154	15.67039	13.59218	15	11.28307
O43290	SART1	3.019684	0	0	0	1.611867
P62979	RPS27A UBA80	3.019684	6.71588	3.398046	4	4.8356
P22314	UBA1 A1S9T UBE1	1.006561	0	0	1	1.611867
Q9Y3I0	C22orf28 HSPC117	2.013122	2.238627	1.699023	1	3.223733
Q969H8	C19orf10 IL25	0	3.35794	5.097068	5	6.447466
O75396	SEC22B SEC22L1	7.045928	1.119313	1.699023	2	3.223733
Q00341	HDLBP HBP VGL	0	1.119313	0	2	1.611867
P21796	VDAC1 VDAC	15.09842	8.954506	15.29121	8	6.447466
P45880	VDAC2	8.052489	2.238627	1.699023	1	0
P13010	XRCC5 G22P2	1.006561	3.35794	1.699023	4	8.059333
P12956	XRCC6 G22P1	4.026245	3.35794	0	3	3.223733

Appendix Two

Proteins altered two-fold after Nutlin treatment detected in PAcIFIC Screen in two replicates (FC – Fold Change)

At 2 hours after Nutlin treatment

Uniprot Accession	Gene	Replicate One		Replicate Two		FC 1	FC 2
		0HR	2HR	0HR	2Hr		
Q9UJZ1	STOML2	2	0	7.045928	3.35794	Down	0.476579
P53396	ACLY	1	0	3.019684	0	Down	Down
P28331	NDUFS1	2	0	2.013122	0	Down	Down
P60981	DSTN	4	1.098555	7.045928	3.35794	0.274639	0.476579
O43290	SART1	4	1.098555	3.019684	0	0.274639	Down
Q04637	EIF4G1	3	1.098555	2.013122	0	0.366185	Down
P55011	SLC12A2	3	1.098555	1.006561	0	0.366185	Down
P50990	CCT8	6	2.197109	5.032806	1.119313	0.366185	0.222403
O95831	AIFM1	3	1.098555	12.07873	5.596567	0.366185	0.46334
P04264	KRT1	16	6.591327	20.13122	7.835193	0.411958	0.389206
Q96PK6	RBM14	10	4.394218	6.039367	2.238627	0.439422	0.370672
P78527	PRKDC	7	3.295664	7.045928	2.238627	0.470809	0.317719
P56385	ATP5I	7	3.295664	4.026245	0	0.470809	Down
Q9Y383	LUC7L2	2	4.394218	2.013122	4.477253	2.197109	2.224034
Q02878	RPL6	1	2.197109	0	2.238627	2.197109	Up
P62857	RPS28	1	2.197109	0	2.238627	2.197109	Up
P23284	PPIB	3	6.591327	0	5.596567	2.197109	Up
P13010	XRCC5	2	4.394218	1.006561	3.35794	2.197109	3.336052
P12004	PCNA	3	6.591327	1.006561	2.238627	2.197109	2.224034
P14314	PRKCSH	6	15.37976	7.045928	15.67039	2.563294	2.224034
Q9BSH4	TACO1	2	5.492773	1.006561	2.238627	2.746386	2.224034
P07237	P4HB	13	39.54796	9.059051	34.69871	3.042151	3.830281
O60220	TIMM8A	2	6.591327	0	8.954506	3.295664	Up
Q13162	PRDX4	3	9.886991	2.013122	7.835193	3.295664	3.89206
Q15084	PDIA6	5	17.57687	7.045928	23.50558	3.515375	3.336052
P14625	HSP90B1 GRP94 TRA1	4	14.28121	3.019684	17.90901	3.570302	5.930758
Q9UQ80	PA2G4	1	4.394218	0	1.119313	4.394218	Up
Q14697	GANAB	3	14.28121	3.019684	11.19313	4.760403	3.706724
P50454	SERPINH1	3	14.28121	4.026245	11.19313	4.760403	2.780043

Uniprot Accession	Gene	Replicate One		Replicate Two		FC 1	FC 2
		0HR	2HR	0HR	2Hr		
Q9Y6X8	ZHX2	0	1.098555	0	1.119313	Up	Up
Q9Y5L4	TIMM13	0	3.295664	0	3.35794	Up	Up
Q9Y4L1	HYOU1	0	2.197109	0	4.477253	Up	Up
P60842	EIF4A1	0	2.197109	1.006561	5.596567	Up	5.560086
P55145	MANF	0	1.098555	0	2.238627	Up	Up

At 4 hours after Nutlin treatment

Uniprot Accession	Gene	Replicate One		Replicate Two		FC 1	FC 2
		0HR	4HR	0HR	4HR		
Q9Y383	LUC7L2	2	0	2.013122	0	Down	Down
Q9UJZ1	STOML2	2	0	7.045928	1.699023	Down	0.241135
Q9NX63	CHCHD3	7	0	6.039367	1.699023	Down	0.281325
Q9HDC9	APMAP	2	0	1.006561	0	Down	Down
Q99733	NAP1L4	3	0	1.006561	0	Down	Down
Q92878	RAD50	1	0	2.013122	0	Down	Down
Q86U42	PABPN1	4	0	2.013122	0	Down	Down
Q07065	CKAP4	5	0	6.039367	0	Down	Down
Q04637	EIF4G1	3	0	2.013122	0	Down	Down
Q02818	NUCB1	2	0	4.026245	3.398046	Down	0.843974
P62834	RAP1A	6	0	6.039367	0	Down	Down
P56385	ATP5I	7	0	4.026245	1.699023	Down	0.421987
P55011	SLC12A2	3	0	1.006561	0	Down	Down
P54886	ALDH18A1	7	0	3.019684	0	Down	Down
P53396	ACLY	1	0	3.019684	1.699023	Down	0.562649
P51991	HNRNPA3	2	0	1.006561	0	Down	Down
P48735	IDH2	6	0	6.039367	0	Down	Down
P48643	CCT5	2	0	2.013122	0	Down	Down
P47756	CAPZB	2	0	2.013122	0	Down	Down
P42704	LRPPRC	2	0	4.026245	0	Down	Down
P37802	TAGLN2	4	0	4.026245	1.699023	Down	0.421987
P30519	HMOX2	6	0	4.026245	0	Down	Down
P28331	NDUFS1	2	0	2.013122	0	Down	Down
P27824	CANX	7	0	9.059051	3.398046	Down	0.3751
P19367	HK1	3	0	3.019684	0	Down	Down
P17980	PSMC3	4	0	11.07217	5.097068	Down	0.460349
P11387	TOP1	5	0	6.039367	0	Down	Down
P09874	PARP1	4	0	6.039367	1.699023	Down	0.281325
P01111	NRAS	2	0	4.026245	0	Down	Down
Q99623	PHB2	11	1.659828	8.052489	3.398046	0.150893	0.421987
Q15233	NONO	20	3.319656	19.12466	3.398046	0.165983	0.177679
Q92841	DDX17	9	1.659828	8.052489	0	0.184425	Down
P43304	GPD2	7	1.659828	6.039367	0	0.237118	Down
P00505	GOT2	6	1.659828	9.059051	3.398046	0.276638	0.3751
P02786	TFRC	5	1.659828	8.052489	3.398046	0.331966	0.421987
P58107	EPPK1	13	4.979484	10.06561	1.699023	0.383037	0.168795
P60981	DSTN	4	1.659828	7.045928	3.398046	0.414957	0.482271
P48047	ATP5O	15	6.639312	14.09186	6.796091	0.442621	0.482271
Q09666	AHNAK	25	11.6188	11.07217	3.398046	0.464752	0.3069
P78527	PRKDC	7	3.319656	7.045928	1.699023	0.474237	0.241135

Uniprot Accession	Gene	Replicate One		Replicate Two		FC 1	FC 2
		0HR	4HR	0HR	4HR		
P16615	ATP2A2	7	3.319656	9.059051	0	0.474237	Down
Q8N1N4	KRT78	6	13.27862	5.032806	11.89316	2.213104	2.363127
P23284	PPIB	3	6.639312	0	1.699023	2.213104	Up
P12004	PCNA	3	6.639312	1.006561	3.398046	2.213104	3.375896
P29401	TKT	2	4.979484	1.006561	5.097068	2.489742	5.063844
Q13162	PRDX4	3	8.29914	2.013122	10.19414	2.76638	5.063844
P33991	MCM4	1	3.319656	0	1.699023	3.319656	Up
P07910	HNRNPC	1	3.319656	3.019684	8.495114	3.319656	2.813246
P07237	P4HB	13	43.15553	9.059051	42.47557	3.319656	4.688744
P14625	HSP90B1	4	16.59828	3.019684	8.495114	4.14957	2.813246
Q14697	GANAB	3	13.27862	3.019684	11.89316	4.426208	3.938545
P50454	SERPINH1	3	13.27862	4.026245	13.59218	4.426208	3.375896
Q15084	PDIA6	5	23.23759	7.045928	22.0873	4.647518	3.13476
P13667	PDIA4	2	14.93845	4.026245	11.89316	7.469226	2.953909
Q9Y5L4	TIMM13	0	1.659828	0	3.398046	Up	Up
P60842	EIF4A1	0	1.659828	1.006561	5.097068	Up	5.063844

At 8 hours after Nutlin treatment

Uniprot Accession	Gene	Replicate One		Replicate Two		FC 1	FC 2
		0HR	8HR	0HR	8HR		
Q9UJZ1	STOML2	2	0	7.045928	3	Down	0.425778
Q9BR76	CORO1B	1	0	1.006561	0	Down	N/A
Q8WXF1	PSPC1	2	0	2.013122	1	Down	0.496741
Q08379	GOLGA2	4	0	6.039367	1	Down	0.16558
P62834	RAP1A	6	0	6.039367	3	Down	0.496741
P46783	RPS10	1	0	4.026245	2	Down	0.496741
P43243	MATR3	3	0	5.032806	2	Down	0.397393
P42704	LRPPRC	2	0	4.026245	1	Down	0.24837
P30041	PRDX6	3	0	3.019684	1	Down	0.331161
P28331	NDUFS1	2	0	2.013122	0	Down	Down
P20700	LMNB1	4	0	2.013122	0	Down	Down
O43290	SART1	4	0	3.019684	0	Down	Down
P58107	EPPK1	13	1.130239	10.06561	2	0.086941	0.198696
Q16891	IMMT	8	1.130239	7.045928	2	0.14128	0.283852
Q9NX63	CHCHD3	7	1.130239	6.039367	2	0.161463	0.331161
P54886	ALDH18A1	7	1.130239	3.019684	0	0.161463	Down
P30519	HMOX2	6	1.130239	4.026245	2	0.188373	0.496741
Q15149	PLEC	20	4.520955	16.10498	8	0.226048	0.496741
Q07065	CKAP4	5	1.130239	6.039367	2	0.226048	0.331161
Q86U42	PABPN1	4	1.130239	2.013122	1	0.28256	0.496741
Q05519	SRSF11	4	1.130239	3.019684	1	0.28256	0.331161
P62318	SNRPD3	7	2.260478	7.045928	2	0.322925	0.283852
P27824	CANX	7	2.260478	9.059051	2	0.322925	0.220774
Q00839	HNRNPU	10	3.390717	9.059051	3	0.339072	0.331161
P50990	CCT8	6	2.260478	5.032806	2	0.376746	0.397393
P31949	S100A11	3	1.130239	4.026245	2	0.376746	0.496741
O95831	AIFM1	3	1.130239	12.07873	5	0.376746	0.413951
P05023	ATP1A1	13	5.651194	7.045928	3	0.434707	0.425778
P11387	TOP1	5	2.260478	6.039367	2	0.452096	0.331161
Q99729	HNRNPAB	7	3.390717	6.039367	3	0.484388	0.496741
P61289	PSME3	1	2.260478	0	4	2.260478	Up
P13010	XRCC5	2	4.520955	1.006561	4	2.260478	3.973926
O60220	TIMM8A	2	4.520955	0	8	2.260478	Up
P12004	PCNA	3	7.911672	1.006561	3	2.637224	2.980445
P14314	PRKCSH	6	16.95358	7.045928	15	2.825597	2.128889

Uniprot Accession	Gene	Replicate One		Replicate Two		FC 1	FC 2
		0HR	8HR	0HR	8HR		
P29401	TKT	2	6.781433	1.006561	4	3.390717	3.973926
Q13162	PRDX4	3	11.30239	2.013122	10	3.767463	4.967408
P50454	SERPINH1	3	12.43263	4.026245	15	4.144209	3.725556
Q14697	GANAB	3	13.56287	3.019684	10	4.520955	3.311605
P14625	HSP90B1	4	18.08382	3.019684	19	4.520955	6.29205
P12532	CKMT1A	1	5.651194	2.013122	7	5.651194	3.477186
P13667	PDIA4	2	15.82334	4.026245	21	7.911672	5.215778
Q9Y5L4	TIMM13	0	1.130239	0	3	Up	Up
Q9Y4L1	HYOU1	0	1.130239	0	4	Up	Up
Q969H8	IL25	0	5.651194	0	5	Up	Up
Q8NBS9	TXNDC5	0	6.781433	0	3	Up	Up
P60842	EIF4A1	0	3.390717	1.006561	3	Up	2.980445
P55145	MANF	0	3.390717	0	1	Up	Up
P11413	G6PD	0	2.260478	0	3	Up	Up

At 24 hours after Nutlin treatment

Uniprot Accession	Gene	Replicate One		Replicate Two		FC 1	FC 2
		0HR	24HR	0HR	24HR		
Q9UJZ1	STOML2	2	0	7.045928	0	Down	Down
Q12906	ILF3	4	0	3.019684	0	Down	Down
P62834	RAP1A	6	0	6.039367	0	Down	Down
P58107	EPPK1	13	0	10.06561	1.611867	Down	0.160136
P55011	SLC12A2	3	0	1.006561	0	Down	Down
P51991	HNRNPA 3 HNRPA3	2	0	1.006561	0	Down	Down
P48643	CCT5	2	0	2.013122	0	Down	N/A
P42704	LRPPRC	2	0	4.026245	1.611867	Down	0.40034
P30041	PRDX6	3	0	3.019684	1.611867	Down	0.533787
P20700	LMNB1	4	0	2.013122	0	Down	Down
O75534	CSDE1	4	0	2.013122	0	Down	Down
P22626	HNRNPA 2B1	8	1.263476	8.052489	3.223733	0.157935	0.40034
P49368	CCT3	6	1.263476	8.052489	3.223733	0.210579	0.40034
Q07065	CKAP4	5	1.263476	6.039367	0	0.252695	Down
Q92841	DDX17	9	2.526952	8.052489	0	0.280772	Down
Q16891	IMMT	8	2.526952	7.045928	3.223733	0.315869	0.457531
P60981	DSTN	4	1.263476	7.045928	1.611867	0.315869	0.228766
P78527	PRKDC	7	2.526952	7.045928	0	0.360993	Down
Q07020	RPL18	3	1.263476	2.013122	0	0.421159	Down
P50990	CCT8	6	2.526952	5.032806	1.611867	0.421159	0.320272
P43243	MATR3	3	1.263476	5.032806	0	0.421159	Down
O00264	PGRMC1	6	2.526952	8.052489	3.223733	0.421159	0.40034
P30101	PDIA3	14	29.05995	10.06561	29.0136	2.075711	2.882447
Q9BSH4	TACO1	2	5.053904	1.006561	4.8356	2.526952	4.804079
Q16740	CLPP	1	2.526952	0	1.611867	2.526952	Up
P30084	ECHS1	4	10.10781	6.039367	12.89493	2.526952	2.135146
P23284	PPIB	3	10.10781	0	6.447466	3.36927	N/A
Q15084	PDIA6	5	18.95214	7.045928	20.95426	3.790428	2.973954
O60220	TIMM8A	2	7.580856	0	11.28307	3.790428	Up
P07237	P4HB	13	50.53904	9.059051	33.8492	3.887619	3.736506
Q14697	GANAB	3	13.89824	3.019684	16.11867	4.632746	5.337866

Uniprot Accession	Gene	Replicate One		Replicate Two		FC 1	FC 2
		0HR	24HR	0HR	24HR		
P14625	HSP90B1	4	24.00605	3.019684	19.3424	6.001511	6.405439
P12532	CKMT1A	1	6.31738	2.013122	6.447466	6.31738	3.202719
P13667	PDIA4	2	16.42519	4.026245	16.11867	8.212594	4.003399
Q9Y6X8	ZHX2	0	1.263476	0	3.223733	Up	Up
Q9Y5L4	TIMM13	0	2.526952	0	4.8356	Up	Up
Q969H8	IL25	0	3.790428	0	6.447466	Up	Up
Q8NBS9	TXNDC5	0	8.844332	0	8.059333	Up	Up
P55145	MANF	0	1.263476	0	1.611867	Up	Up

Detected as changed in a single replicate only
After two hours Nutlin treatment

Detected in Replicate One Accession	Protein	Gene	2HR 0Hr	2Hr	FC
Q969G3	SWI/SNF-related matrix-associated actin-dependent regulator of chromatin subfamily E member 1	SMARCE1	1	0	N/A
Q8TBA6	Golgin subfamily A member 5	GOLGA5	2	0	N/A
Q8N163	Protein KIAA1967 (Deleted in breast cancer gene 1 protein)	DBC1	2	0	N/A
Q12874	Splicing factor 3A subunit 3 (SF3a60)	SF3A3	1	0	N/A
Q04695	Keratin, type I cytoskeletal 17	KRT17	2	0	N/A
P52565	Rho GDP-dissociation inhibitor 1	ARHGDIA	2	0	N/A
P43487	Ran-specific GTPase-activating protein	RANBP1	2	0	N/A
P35527	Keratin, type I cytoskeletal 9	KRT9	4	0	N/A
P28066	Proteasome subunit alpha type-5	PSMA5	1	0	N/A
P18669	Phosphoglycerate mutase 1	PGAM1	3	0	N/A
P17480	Nucleolar transcription factor 1 (UBF-1)	UBF1	2	0	N/A
O75347	Tubulin-specific chaperone A (CFA)	TBCA	2	0	N/A
O75150	E3 ubiquitin-protein ligase BRE1B	RNF40	2	0	N/A
O95292	Vesicle-associated membrane protein-associated protein B/C	VAPB	7	1.098555	0.156936
P14927	Cytochrome b-c1 complex subunit 7 (Complex III subunit 7)	UQCRB	5	1.098555	0.219711
Q14444	Caprin-1 (Cell cycle-associated protein 1)	CAPRIN1	5	2.197109	0.439422
P40227	T-complex protein 1 subunit zeta (TCP-1-zeta)	CCT6A	5	2.197109	0.439422
O00148	ATP-dependent RNA helicase DDX39	DDX39	5	2.197109	0.439422
P04350	Tubulin beta-4 chain	TUBB4	17	7.689882	0.452346
P12814	Alpha-actinin-1	ACTN1	7	14.28121	2.040173
Q00059	Transcription factor A, mitochondrial (mtTFA)	TFAM	2	4.394218	2.197109
P26373	60S ribosomal protein L13 (Breast basic conserved protein 1)	RPL13	1	2.197109	2.197109
P16401	Histone H1.5	HIST1H1B	2	4.394218	2.197109

Detected in Replicate One Accession	Protein	Gene	2HR 0Hr	2Hr	FC
P67936	Tropomyosin alpha-4 chain	TPM4	0	1.098555	N/A
P52907	F-actin-capping protein subunit alpha-1	CAPZA1	0	3.295664	N/A
P51858	Hepatoma-derived growth factor (HDGF)	HDGF	0	1.098555	N/A
P50995	Annexin A11	ANXA11	0	3.295664	N/A
P37837	Transaldolase	TALDO1	0	1.098555	N/A
P16152	Carbonyl reductase [NADPH]	CBR1	0	1.098555	N/A
O75439	Mitochondrial-processing peptidase subunit beta	PMPCB	0	2.197109	N/A

Detected in Replicate Two Accession	Protein	Gene	2HR 0Hr	2Hr	FC
Q99832	T-complex protein 1 subunit eta (TCP-1-eta)	CCT7	1.006561	0	N/A
Q96C36	Pyrroline-5-carboxylate reductase 2	PYCR2	3.019684	0	N/A
Q8TAQ2	SWI/SNF complex subunit SMARCC2	SMARCC2	3.019684	0	N/A
Q8N983	39S ribosomal protein L43, mitochondrial	MRPL43	1.006561	0	N/A
Q8N5N7	39S ribosomal protein L50, mitochondrial	MRPL50	1.006561	0	N/A
Q86UE4	Protein LYRIC (3D3/LYRIC)	MTDH	1.006561	0	N/A
Q5SRE5	Nucleoporin NUP188 homolog	NUP188	1.006561	0	N/A
Q15388	Mitochondrial import receptor subunit TOM20 homolog	TOMM20	2.013122	0	N/A
Q15369	Transcription elongation factor B polypeptide 1 (Elongin 15 kDa subunit)	TCEB1	1.006561	0	N/A
Q14344	Guanine nucleotide-binding protein subunit alpha-13	GNA13	3.019684	0	N/A
Q13838	Spliceosome RNA helicase BAT1	BAT1	4.026245	0	N/A
Q07812	Apoptosis regulator BAX	BAX	1.006561	0	N/A
P63261	Actin, cytoplasmic 2	ACTG1	4.026245	0	N/A
P62847	40S ribosomal protein S24	RPS24	2.013122	0	N/A
P61006	Ras-related protein Rab-8A (Oncogene c-mel)	RAB8A	2.013122	0	N/A
P51532	Transcription activator BRG1	SMARCA4	1.006561	0	N/A

Detected in Replicate Two Accession	Protein	Gene	2HR 0Hr	2Hr	FC
P29373	Cellular retinoic acid-binding protein 2	CRABP2	2.013122	0	N/A
P27348	14-3-3 protein theta	YWHAQ	4.026245	0	N/A
P25205	DNA replication licensing factor MCM3	MCM3	2.013122	0	N/A
P22830	Ferrochelatase, mitochondrial	FECH	2.013122	0	N/A
P22314	Ubiquitin-like modifier-activating enzyme 1 (Protein A1S9)	UBE1	1.006561	0	N/A
P20674	Cytochrome c oxidase subunit 5A, mitochondrial	COX5A	3.019684	0	N/A
P14923	Junction plakoglobin	JUP	2.013122	0	N/A
P13647	Keratin, type II cytoskeletal 5	KRT5	1.006561	0	N/A
P0C6E5	Putative high mobility group protein B3-like protein		2.013122	0	N/A
P09497	Clathrin light chain B	CLTB	1.006561	0	N/A
O60716	Catenin delta-1	CTNND1	2.013122	0	N/A
O15523	ATP-dependent RNA helicase DDX3Y	DDX3Y	2.013122	0	N/A
O75396	Vesicle-trafficking protein SEC22b	SEC22B	7.045928	1.119313	0.15886
O75533	Splicing factor 3B subunit 1	SF3B1	5.032806	1.119313	0.222403
Q14498	RNA-binding protein 39 (Hepatocellular carcinoma protein 1)	RBM39	8.052489	2.238627	0.278004
Q9Y3D9	28S ribosomal protein S23, mitochondrial	MRPS23	3.019684	1.119313	0.370672
Q13148	TAR DNA-binding protein 43 (TDP-43)	TARDBP	3.019684	1.119313	0.370672
P37108	Signal recognition particle 14 kDa protein (SRP14)	SRP14	3.019684	1.119313	0.370672
P25787	Proteasome subunit alpha type-2 (EC 3.4.25.1)	PSMA2	3.019684	1.119313	0.370672
Q16718	NADH dehydrogenase [ubiquinone] 1 alpha subcomplex subunit 5	NDUFA5	5.032806	2.238627	0.444807
Q16698	2,4-dienoyl-CoA reductase, mitochondrial	DECR1	1.006561	2.238627	2.224034
Q02790	Peptidyl-prolyl cis-trans isomerase FKBP4	FKBP4	1.006561	2.238627	2.224034
P62753	40S ribosomal protein S6 (Phosphoprotein NP33)	RPS6	1.006561	2.238627	2.224034
P30038	Delta-1-pyrroline-5-carboxylate dehydrogenase, mitochondrial	ALDH4A1	1.006561	2.238627	2.224034
Q9C005	Protein dpy-30 homolog (Dpy-30-like protein)	DPY30	2.013122	5.596567	2.780043

Detected in Replicate Two Accession	Protein	Gene	2HR 0Hr	2Hr	FC
Q9Y285	Phenylalanyl-tRNA synthetase alpha chain	FARSA	0	3.35794	N/A
Q9NR28	Diablo homolog, mitochondrial (Smac)	DIABLO	0	1.119313	N/A
Q96I99	Succinyl-CoA ligase [GDP-forming] subunit beta, mitochondrial	SUCLG2	0	3.35794	N/A
Q8TEX9	Importin-4 (Imp4)	IPO4	0	3.35794	N/A
Q15393	Splicing factor 3B subunit 3	SF3B3	0	1.119313	N/A
P68366	Tubulin alpha-4A chain	TUBA4A	0	3.35794	N/A
P55795	Heterogeneous nuclear ribonucleoprotein H2 (hnRNP H2)	HNRNPH2	0	2.238627	N/A
P46379	Large proline-rich protein BAG6 (BCL2-associated athanogene 6)	BAG6	0	1.119313	N/A
P13995	Bifunctional methylenetetrahydrofolate dehydrogenase/cyclohydrolase, mitochondrial	MTHFD2	0	1.119313	N/A
P09493	Tropomyosin alpha-1 chain	TPM1	0	1.119313	N/A
P07339	Cathepsin D	CTSD	0	10.07382	N/A
O00571	ATP-dependent RNA helicase DDX3X	DDX3X	0	4.477253	N/A

After four hours Nutlin treatment

Detected in Rep. One Accession	Protein	Gene	0Hr	4Hr	FC
Q9Y5M8	Signal recognition particle receptor subunit beta	SRPRB	1	0	N/A
Q9GZV4	Eukaryotic translation initiation factor 5A-2 (eIF-5A-2)	EIF5A2	1	0	N/A
Q969G3	SWI/SNF-related matrix-associated actin-dependent regulator of chromatin subfamily E member 1	SMARCE1	1	0	N/A
Q8TBA6	Golgin subfamily A member 5	GOLGA5	2	0	N/A
Q14444	Caprin-1 (Cell cycle-associated protein 1)	CAPRIN1	5	0	N/A
Q13435	Splicing factor 3B subunit 2	SF3B2	1	0	N/A
Q12874	Splicing factor 3A subunit 3	SF3A3	1	0	N/A
P63104	14-3-3 protein zeta/delta	YWHAZ	1	0	N/A
P62906	60S ribosomal protein L10a	RPL10A	3	0	N/A
P62888	60S ribosomal protein L30	RPL30	2	0	N/A
P55036	26S proteasome non-ATPase regulatory subunit 4	PSMD4	1	0	N/A
P52565	Rho GDP-dissociation inhibitor 1 (Rho GDI 1)	ARHGDIA	2	0	N/A
P40227	T-complex protein 1 subunit zeta (TCP-1-zeta)	CCT6A	5	0	N/A
P35527	Keratin, type I cytoskeletal 9	KRT9	4	0	N/A
P30044	Peroxiredoxin-5, mitochondrial	PRDX5	4	0	N/A
P28066	Proteasome subunit alpha type-5	PSMA5	1	0	N/A
P18669	Phosphoglycerate mutase 1	PGAM1	3	0	N/A
P18124	60S ribosomal protein L7	RPL7	3	0	N/A
P17480	Nucleolar transcription factor 1 (UBF-1)	UBF1	2	0	N/A
P04350	Tubulin beta-4 chain	TUBB4	17	0	N/A
O95292	Vesicle-associated membrane protein-associated protein B/C	VAPB	7	0	N/A
O00148	ATP-dependent RNA helicase DDX39	DDX39	5	0	N/A
Q92667	A-kinase anchor protein 1, mitochondrial	AKAP1	4	1.659828	0.414957
P16401	Histone H1.5	HIST1H1B	2	4.979484	2.489742

Detected in Rep. One Accession	Protein	Gene	0Hr	4Hr	FC
Q8NFV4	Abhydrolase domain-containing protein 11	ABHD11	0	3.319656	N/A
P52907	F-actin-capping protein subunit alpha-1	CAPZA1	0	1.659828	N/A
P51858	Hepatoma-derived growth factor (HDGF)	HDGF	0	1.659828	N/A
Q9Y3E5	Peptidyl-tRNA hydrolase 2, mitochondrial	PTRH2	1.006561	0	N/A
Q9BVK6	Transmembrane emp24 domain-containing protein 9	TMED9	4.026245	0	N/A
Q9BPW8	Protein NipSnap homolog 1	NIPSNAP1	2.013122	0	N/A
Q99832	T-complex protein 1 subunit eta (TCP-1-eta)	CCT7	1.006561	0	N/A
Q96I24	Far upstream element-binding protein 3 (FUSE-binding protein 3)	FUBP3	2.013122	0	N/A
Q96C36	Pyrroline-5-carboxylate reductase 2	PYCR2	3.019684	0	N/A
Q8N983	39S ribosomal protein L43, mitochondrial	MRPL43	1.006561	0	N/A
Q8N5N7	39S ribosomal protein L50, mitochondrial	MRPL50	1.006561	0	N/A
Q86UE4	Protein LYRIC (3D3/LYRIC)	MTDH	1.006561	0	N/A
Q6NUK1	Calcium-binding mitochondrial carrier protein SCaMC-1	SLC25A24	3.019684	0	N/A
Q6IAA8	Ragulator complex protein PDRO	PDRO	2.013122	0	N/A
Q5SRE5	Nucleoporin NUP188 homolog	NUP188	1.006561	0	N/A
Q15388	Mitochondrial import receptor subunit TOM20 homolog	TOMM20	2.013122	0	N/A
Q15369	Transcription elongation factor B polypeptide 1	TCEB1	1.006561	0	N/A
Q14344	Guanine nucleotide-binding protein subunit alpha-13	GNA13	3.019684	0	N/A
Q13838	Spliceosome RNA helicase BAT1	BAT1	4.026245	0	N/A
Q13813	Spectrin alpha chain, brain	SPTAN1	2.013122	0	N/A
Q13748	Tubulin alpha-3C/D chain	TUBA3C	1.006561	0	N/A
Q07812	Apoptosis regulator BAX	BAX	1.006561	0	N/A
Q02790	Peptidyl-prolyl cis-trans isomerase FKBP4	FKBP4	1.006561	0	N/A
P83916	Chromobox protein homolog 1	CBX1	2.013122	0	N/A
P63261	Actin, cytoplasmic 2	ACTG1	4.026245	0	N/A
P62753	40S ribosomal protein S6 (Phosphoprotein NP33)	RPS6	1.006561	0	N/A

Detected in Rep. One					
Accession	Protein	Gene	0Hr	4Hr	FC
P61006	Ras-related protein Rab-8A (Oncogene c-mel)	RAB8A	2.013122	0	N/A
P50991	T-complex protein 1 subunit delta (TCP-1-delta)	CCT4	1.006561	0	N/A
P37268	Squalene synthase (SQS)	FDFT1	3.019684	0	N/A
P35222	Catenin beta-1	CTNNB1	1.006561	0	N/A
P30038	Delta-1-pyrroline-5-carboxylate dehydrogenase, mitochondrial	ALDH4A1	1.006561	0	N/A
P29373	Cellular retinoic acid-binding protein 2	CRABP2	2.013122	0	N/A
P27348	14-3-3 protein theta	YWHAQ	4.026245	0	N/A
P25787	Proteasome subunit alpha type-2	PSMA2	3.019684	0	N/A
P25398	40S ribosomal protein S12	RPS12	3.019684	0	N/A
P22830	Ferrochelatase, mitochondrial	FECH	2.013122	0	N/A
P22314	Ubiquitin-like modifier-activating enzyme 1 (Ubiquitin-activating enzyme E1)	UBA1	1.006561	0	N/A
P20674	Cytochrome c oxidase subunit 5A, mitochondrial	COX5A	3.019684	0	N/A
P14923	Junction plakoglobin	JUP	2.013122	0	N/A
P13647	Keratin, type II cytoskeletal 5	KRT5	1.006561	0	N/A
P09497	Clathrin light chain B	CLTB	1.006561	0	N/A
P08133	Annexin A6	ANXA6	4.026245	0	N/A
O75947	ATP synthase subunit d, mitochondrial	ATP5H	2.013122	0	N/A
O75533	Splicing factor 3B subunit 1	SF3B1	5.032806	0	N/A
O60716	Catenin delta-1	CTNND1	2.013122	0	N/A
O43390	Heterogeneous nuclear ribonucleoprotein R (hnRNP R)	HNRNPR	2.013122	0	N/A
O15523	ATP-dependent RNA helicase DDX3Y	DDX3Y	2.013122	0	N/A
O75396	Vesicle-trafficking protein SEC22b	SEC22B	7.045928	1.699023	0.241135
Q14498	RNA-binding protein 39 (Hepatocellular carcinoma protein 1)	RBM39	8.052489	3.398046	0.421987
P51532	Transcription activator BRG1	SMARCA4	1.006561	3.398046	3.375896
P49736	DNA replication licensing factor MCM2	MCM2	1.006561	3.398046	3.375896
P27797	Calreticulin (CRP55) (Calregulin)	CALR	1.006561	5.097068	5.063844
Q9Y285	Phenylalanyl-tRNA synthetase alpha chain	FARSA	0	1.699023	N/A
Q9NR28	Diablo homolog, mitochondrial	DIABLO	0	1.699023	N/A

Detected in Rep. One Accession	Protein	Gene	0Hr	4Hr	FC
Q99613	Eukaryotic translation initiation factor 3 subunit C (eIF3c)	EIF3C	0	1.699023	N/A
P09493	Tropomyosin alpha-1 chain	TPM1	0	1.699023	N/A
P07339	Cathepsin D	CTSD	0	1.699023	N/A
O00571	ATP-dependent RNA helicase DDX3X	DDX3X	0	3.398046	N/A

After eight hours Nutlin treatment

Detected in Rep. One Accession	Protein	Gene	0Hr	8Hr	FC
Q9Y5M8	Signal recognition particle receptor subunit beta	SRPRB	1	0	N/A
Q9GZV4	Eukaryotic translation initiation factor 5A-2 (eIF-5A-2)	EIF5A2	1	0	N/A
Q8TBA6	Golgin subfamily A member 5	GOLGA5	2	0	N/A
Q8N163	Protein KIAA1967 (Deleted in breast cancer gene 1 protein)	DBC1	2	0	N/A
Q14011	Cold-inducible RNA-binding protein (A18 hnRNP)	CIRBP	1	0	N/A
Q13247	Serine/arginine-rich splicing factor 6	SRSF6	4	0	N/A
Q04695	Keratin, type I cytoskeletal 17	KRT17	2	0	N/A
P62917	60S ribosomal protein L8	RPL8	1	0	N/A
P62906	60S ribosomal protein L10a	RPL10A	3	0	N/A
P52565	Rho GDP-dissociation inhibitor 1 (Rho GDI 1)	ARHGDIA	2	0	N/A
P43487	Ran-specific GTPase-activating protein	RANBP1	2	0	N/A
P35527	Keratin, type I cytoskeletal 9	KRT9	4	0	N/A
P28066	Proteasome subunit alpha type-5	PSMA5	1	0	N/A
P26373	60S ribosomal protein L13 (Breast basic conserved protein 1)	RPL13	1	0	N/A
P18669	Phosphoglycerate mutase 1	PGAM1	3	0	N/A
P18124	60S ribosomal protein L7	RPL7	3	0	N/A
P17480	Nucleolar transcription factor 1 (UBF-1)	UBF1	2	0	N/A
O95292	Vesicle-associated membrane protein-associated protein B/C	VAPB	7	0	N/A
P62266	40S ribosomal protein S23	RPS23	4	1.130239	0.28256
Q14444	Caprin-1 (Cell cycle-associated protein 1)	CAPRIN1	5	2.260478	0.452096
P40227	T-complex protein 1 subunit zeta (TCP-1-zeta)	CCT6A	5	2.260478	0.452096
P14927	Cytochrome b-c1 complex subunit 7	UQCRB	5	2.260478	0.452096
O00148	ATP-dependent RNA helicase DDX39	DDX39	5	2.260478	0.452096
O43399	Tumor protein D54 (hD54)	TPD52L2	1	2.260478	2.260478
Q8NFV4	Abhydrolase domain-containing protein 11	ABHD11	0	3.390717	N/A
Q5SZK8	FRAS1-related extracellular matrix protein 2 (ECM3 homolog)	FREM2	0	2.260478	N/A
Q01105	Protein SET	SET	0	1.13023	N/A

Detected in Rep. One Accession	Protein	Gene	0Hr	8Hr	FC
P67936	Tropomyosin alpha-4 chain	TPM4	0	3.390717	N/A
P51858	Hepatoma-derived growth factor (HDGF)	HDGF	0	1.130239	N/A
P37837	Transaldolase	TALDO1	0	3.390717	N/A
P28838	Cytosol aminopeptidase	LAP3	0	2.260478	N/A
P16152	Carbonyl reductase [NADPH] 1	CBR1	0	2.260478	N/A
P11586	C-1-tetrahydrofolate synthase, cytoplasmic	MTHFD1	0	1.130239	N/A

Detected in Rep.Two Accession	Protein	Gene	0Hr	8Hr	FC
Q9Y3E5	Peptidyl-tRNA hydrolase 2, mitochondrial	PTRH2	1.006561	0	N/A
Q8N5N7	39S ribosomal protein L50, mitochondrial	MRPL50	1.006561	0	N/A
Q15388	Mitochondrial import receptor subunit TOM20 homolog	TOMM20	2.013122	0	N/A
Q14344	Guanine nucleotide-binding protein subunit alpha-13	GNA13	3.019684	0	N/A
Q13838	Spliceosome RNA helicase BAT1	BAT1	4.026245	0	N/A
Q13813	Spectrin alpha chain, brain	SPTAN1	2.013122	0	N/A
Q13748	Tubulin alpha-3C/D chain	TUBA3C	1.006561	0	N/A
Q07812	Apoptosis regulator BAX	BAX	1.006561	0	N/A
P63261	Actin, cytoplasmic 2	ACTG1	4.026245	0	N/A
P62753	40S ribosomal protein S6 (Phosphoprotein NP33)	RPS6	1.006561	0	N/A
P37268	Squalene synthase (SQS)	FDFT1	3.019684	0	N/A
P22830	Ferrochelatase, mitochondrial	FECH	2.013122	0	N/A
P20674	Cytochrome c oxidase subunit 5A, mitochondrial	COX5A	3.019684	0	N/A
P14923	Junction plakoglobin	JUP	2.013122	0	N/A
P08133	Annexin A6	ANXA6	4.026245	0	N/A
O60716	Catenin delta-1	CTNND	2.013	0	N/A

Detected in Rep.Two Accession	Protein	Gene	0Hr	8Hr	FC
Q14498	RNA-binding protein 39 (Hepatocellular carcinoma protein 1)	RBM39	8.052489	2	0.24837
O75396	Vesicle-trafficking protein SEC22b	SEC22B	7.045928	2	0.283852
Q8TAQ2	SWI/SNF complex subunit SMARCC2	SMARCC2	3.019684	1	0.331161
Q13148	TAR DNA-binding protein 43	TARDBP	3.019684	1	0.331161
P37108	Signal recognition particle 14 kDa protein (SRP14)	SRP14	3.019684	1	0.331161
P25398	40S ribosomal protein S12	RPS12	3.019684	1	0.331161
P18754	Regulator of chromosome condensation	RCC1	3.019684	1	0.331161
P42167	Lamina-associated polypeptide 2, isoforms beta/gamma	TMPO	7.045928	3	0.425778
Q9Y3I0	UPF0027 protein C22orf28	HSPC117	2.013122	1	0.496741
Q96I24	Far upstream element-binding protein 3 (FUSE-binding protein 3)	FUBP3	2.013122	1	0.496741
P83916	Chromobox protein homolog 1	CBX1	2.013122	1	0.496741
P62847	40S ribosomal protein S24	RPS24	2.013122	1	0.496741
P61006	Ras-related protein Rab-8A (Oncogene c-mel)	RAB8A	2.013122	1	0.496741
P29373	Cellular retinoic acid-binding protein 2	CRABP2	2.013122	1	0.496741
O75390	Citrate synthase, mitochondrial	CS	2.013122	1	0.496741
O15523	ATP-dependent RNA helicase DDX3Y	DDX3Y	2.013122	1	0.496741
O15394	Neural cell adhesion molecule 2	NCAM2	4.026245	2	0.496741
O00217	NADH dehydrogenase [ubiquinone] iron-sulfur protein 8, mitochondrial	NDUFS8	4.026245	2	0.496741
Q9C005	Protein dpy-30 homolog	DPY30	2.013122	5	2.483704
Q86UE4	Protein LYRIC (3D3/LYRIC)	MTDH	1.006561	3	2.980445
P49736	DNA replication licensing factor MCM2	MCM2	1.006561	5	4.967408
P27797	Calreticulin (CRP55) (Calregulin)	CALR	1.006561	7	6.954371
Q9Y285	Phenylalanyl-tRNA synthetase alpha chain	FARSA	0	1	N/A

Detected in Rep.Two Accession	Protein	Gene	0Hr	8Hr	FC
Q99613	Eukaryotic translation initiation factor 3 subunit C (eIF3c)	EIF3C	0	1	N/A
Q96I99	Succinyl-CoA ligase [GDP-forming] subunit beta, mitochondrial	SUCLG2	0	3	N/A
Q8N7H5	RNA polymerase II-associated factor 1 homolog (hPAF1)	PAF1	0	1	N/A
P55795	Heterogeneous nuclear ribonucleoprotein H2 (hnRNP H2)	HNRNPH2	0	1	N/A
P50897	Palmitoyl-protein thioesterase 1 (PPT-1)	PPT1	0	1	N/A
P31153	S-adenosylmethionine synthase isoform type-2	MAT2A	0	1	N/A
P13995	Bifunctional methylenetetrahydrofolate dehydrogenase/cyclohydrolase, mitochondrial	MTHFD2	0	3	N/A
P09493	Tropomyosin alpha-1 chain	TPM1	0	2	N/A
P07339	Cathepsin D	CTSD	0	7	N/A

After 24 hours Nutlin treatment

Detected in Rep. One Accession	Protein	Gene	0Hr	24Hr	FC
Q9Y5M8	Signal recognition particle receptor subunit beta	SRPRB	1	0	N/A
Q9GZV4	Eukaryotic translation initiation factor 5A-2 (eIF-5A-2)	EIF5A2	1	0	N/A
Q969G3	SWI/SNF-related matrix-associated actin-dependent regulator of chromatin subfamily E member 1	SMARCE1	1	0	N/A
Q8TBA6	Golgin subfamily A member 5	GOLGA5	2	0	N/A
Q8N163	Protein KIAA1967 (Deleted in breast cancer gene 1 protein)	DBC1	2	0	N/A
Q14011	Cold-inducible RNA-binding protein (A18 hnRNP)	CIRBP	1	0	N/A
Q13435	Splicing factor 3B subunit 2	SF3B2	1	0	N/A
Q13247	Serine/arginine-rich splicing factor 6	SRSF6	4	0	N/A
Q04695	Keratin, type I cytoskeletal 17	KRT17	2	0	N/A
Q00059	Transcription factor A, mitochondrial	TFAM	2	0	N/A
P62917	60S ribosomal protein L8	RPL8	1	0	N/A
P62910	60S ribosomal protein L32	RPL32	4	0	N/A
P62888	60S ribosomal protein L30	RPL30	2	0	N/A
P62266	40S ribosomal protein S23	RPS23	4	0	N/A
P52565	Rho GDP-dissociation inhibitor 1 (Rho GDI 1)	ARHGDIA	2	0	N/A
P43487	Ran-specific GTPase-activating protein	RANBP1	2	0	N/A
P35527	Keratin, type I cytoskeletal 9	KRT9	4	0	N/A
P26373	60S ribosomal protein L13 (Breast basic conserved protein 1)	RPL13	1	0	N/A
P18669	Phosphoglycerate mutase 1	PGAM1	3	0	N/A
P17480	Nucleolar transcription factor 1 (UBF-1)	UBF1	2	0	N/A
P13693	Translationally-controlled tumor protein (TCTP)	TPT1	2	0	N/A
O95292	Vesicle-associated membrane protein-associated protein B/C	VAPB	7	0	N/A
O75347	Tubulin-specific chaperone A (TCP1-chaperonin cofactor A)	TBCA	2	0	N/A
P40227	T-complex protein 1 subunit zeta (TCP-1-zeta)	CCT6A	5	1.263476	0.252695
P14927	Cytochrome b-c1 complex subunit 7 (Complex III subunit 7)	UQCRB	5	1.263476	0.252695

Detected in Rep. One Accession	Protein	Gene	0Hr	24Hr	FC
P62906	60S ribosomal protein L10a (CSA-19)	RPL10A	3	1.263476	0.421159
P18124	60S ribosomal protein L7	RPL7	3	1.263476	0.421159
O94906	Pre-mRNA-processing factor 6 (PRP6 homolog)	PRPF6	3	1.263476	0.421159
P16401	Histone H1.5	HIST1H1B	2	7.580856	3.790428
Q8NFV4	Abhydrolase domain-containing protein 11	ABHD11	0	2.526952	N/A
Q01105	Protein SET	SET	0	1.263476	N/A
P52907	F-actin-capping protein subunit alpha-1	CAPZA1	0	1.263476	N/A
P37837	Transaldolase	TALDO1	0	1.263476	N/A
P11586	C-1-tetrahydrofolate synthase, cytoplasmic	MTHFD1	0	1.263476	N/A

Detected in Rep.Two Accession	Protein	Gene	0Hr	24Hr	FC
Q99832	T-complex protein 1 subunit eta (TCP-1-eta)	CCT7	1.006561	0	N/A
Q5SRE5	Nucleoporin NUP188 homolog	NUP188	1.006561	0	N/A
Q15388	Mitochondrial import receptor subunit TOM20 homolog	TOMM20	2.013122	0	N/A
Q15369	Transcription elongation factor B polypeptide 1	TCEB1	1.006561	0	N/A
Q14344	Guanine nucleotide-binding protein subunit alpha-13	GNA13	3.019684	0	N/A
Q13838	Spliceosome RNA helicase BAT1	BAT1	4.026245	0	N/A
Q13813	Spectrin alpha chain, brain	SPTAN1	2.013122	0	N/A
Q13748	Tubulin alpha-3C/D chain	TUBA3C	1.006561	0	N/A
P83916	Chromobox protein homolog 1	CBX1	2.013122	0	N/A
P63261	Actin, cytoplasmic 2	ACTG1	4.026245	0	N/A
P62847	40S ribosomal protein S24	RPS24	2.013122	0	N/A
P62753	40S ribosomal protein S6 (Phosphoprotein NP33)	RPS6	1.006561	0	N/A
P51532	Transcription activator BRG1	SMARCA4	1.006561	0	N/A
P50991	T-complex protein 1 subunit delta (TCP-1-delta)	CCT4	1.006561	0	N/A
P35222	Catenin beta-1	CTNNB1	1.006561	0	N/A
Detected in Rep.Two					

Accession	Protein	Gene	0Hr	24Hr	FC
P20674	Cytochrome c oxidase subunit 5A, mitochondrial	COX5A	3.019684	0	N/A
P14923	Junction plakoglobin	JUP	2.013122	0	N/A
P13647	Keratin, type II cytoskeletal 5	KRT5	1.006561	0	N/A
P09497	Clathrin light chain B	CLTB	1.006561	0	N/A
O75947	ATP synthase subunit d, mitochondrial	ATP5H	2.013122	0	N/A
O75533	Splicing factor 3B subunit 1	SF3B1	5.032806	0	N/A
O60716	Catenin delta-1	CTNND1	2.013122	0	N/A
O15523	ATP-dependent RNA helicase DDX3Y	DDX3Y	2.013122	0	N/A
Q96FQ6	Protein S100-A16	S100A16	4.026245	1.611867	0.40034
P08133	Annexin A6	ANXA6	4.026245	1.611867	0.40034
O00217	NADH dehydrogenase [ubiquinone] iron-sulfur protein 8, mitochondrial	NDUFS8	4.026245	1.611867	0.40034
O75396	Vesicle-trafficking protein SEC22b	SEC22B	7.045928	3.223733	0.457531
Q16836	Hydroxyacyl-coenzyme A dehydrogenase, mitochondrial (HCDH)	HADH	3.019684	6.447466	2.135146
P18754	Regulator of chromosome condensation	RCC1	3.019684	6.447466	2.135146
Q9C005	Protein dpy-30 homolog	DPY30	2.013122	4.8356	2.40204
Q8N5N7	39S ribosomal protein L50, mitochondrial	MRPL50	1.006561	3.223733	3.202719
Q07812	Apoptosis regulator BAX	BAX	1.006561	3.223733	3.202719
Q02790	Peptidyl-prolyl cis-trans isomerase FKBP4 (PPIase FKBP4)	FKBP4	1.006561	3.223733	3.202719
P30038	Delta-1-pyrroline-5-carboxylate dehydrogenase, mitochondrial	ALDH4A1	1.006561	3.223733	3.202719
Q16698	2,4-dienoyl-CoA reductase, mitochondrial	DECR1	1.006561	6.447466	6.405439
P27797	Calreticulin (CRP55) (Calregulin)	CALR	1.006561	6.447466	6.405439
Q9Y285	Phenylalanyl-tRNA synthetase alpha chain	FARSA	0	1.611867	N/A
Q9NR30	Nucleolar RNA helicase 2	DDX21	0	3.223733	N/A
Q9NR28	Diablo homolog, mitochondrial (Smac)	DIABLO	0	3.223733	N/A
Q96I99	Succinyl-CoA ligase [GDP-forming] subunit beta, mitochondrial	SUCLG2	0	1.611867	N/A

Detected in Rep.Two Accession	Protein	Gene	0Hr	24Hr	FC
Q13011	Delta(3,5)-Delta(2,4)-dienoyl-CoA isomerase, mitochondrial	ECH1	0	3.223733	N/A
P50897	Palmitoyl-protein thioesterase 1	PPT1	0	1.611867	N/A
P46379	Large proline-rich protein BAG6	BAG6	0	1.611867	N/A
P31153	S-adenosylmethionine synthase isoform type-2	MAT2A	0	3.223733	N/A
P09493	Tropomyosin alpha-1 chain	TPM1	0	1.611867	N/A
P07339	Cathepsin D	CTSD	0	4.8356	N/A
O00571	ATP-dependent RNA helicase DDX3X	DDX3X	0	3.223733	N/A

Appendix 3

	Sequence	Protein
1	ETFSDLWKLLPENNVLSPL	BOX-I
2	SSAVRVYRMLPPLTKNQRK	IRF-1
3	NNAFRVYRMLPLSERPSKK	IRF-2
4	NNVLPVFDNLMQQKLVDQNI	CathepsinD
5	DEFTHLYTLIVRPDNTYEVK	Calreticulin
6	RPLVVVYYSVDFSFDYRAAT	Erp72-1
7	KQLEPVYNSLAKKYKGQKGL	Erp72-2
8	FLDEYIFLAVGRVGSTSENI	DDX3X
9	KNRIAIYELLFKEGVMVAKK	Ribosomal S10
10	LIAGSVFFLLLPGPSAADEK	CyclophilinB-1
11	KVTVKVYFDLRIGDEDVGRV	CyclophilinB-2
12	DGKHVVFGKVLEGMEVVRKV	CyclophilinB-3
13	GTPGRVFDMLNRRYLSPKYI	eIF4A-1
14	DQIYDIFQKLNSNTQVVLLS	eIF4A-2
15	DTLCDLYETLTITQAVIFIN	eIF4A-3
16	GLAFSLYQAMAKDQAVENIL	Serpin H1
18	KYKKKMWGWLWTEAGAQSEL	PDIA6
20	VERSRIFSKLCLNIRLAVKE	CCD44-1
21	EERNVFKFICDASSLHQVR	CCD44-2
22	VNLDKLWTLVSEQTRVNAAK	Ribosomal L27
23	AREKKLYANMFERLAEEENK	Rotamase-1
24	KLYANMFERLAEEENKAKAE	Rotatmase-2
25	AFLRSMWGVLSALGRSGAEL	TFAM
26	LRRLALFPGVALLLAAARL	eRP60
27	RTDGKVFQFLNAKCESAFLS	Ribosomal L24
28	LCNQGLFECLALNLHCLGGQ	BAT3
29	EEEDEVWQVIIGARAEMTSK	Smac
30	PDDAEVYRLIEVTGLARSEI	AFP Regulator Two
31	ERAYDIYSRLLRERIVCVMG	CLPP-1
32	TAGLAIYDTMQYILNPICTW	CLPP-2
33	KCGDLVFAKMKGYPHWPARI	HDGF
34	RKAIIIFVPVPQLKSFQKIQ	Ribosomal S7
35	ETFSGVYKKLTGKDVNFEFP	Ribosomal S7-2

	Sequence	Protein
37	VRQRDMYRILLSQTTGVAIP	Nucleoprotein TPR
39	VNSVLLFTILNPIYSITTDV	hnRNPL
40	SVLKPLWKGIRQHRGKGLAA	SAP155
41	EKNRKLFDLLDVLEFNQVVI	BAT1
42	NVNEIFYDLVRQINRKTPVE	Rap1A
43	VADGMVFGALLPCEECSGQL	PARP1
44	PQGTVIFEDISIEHFEGTVT	NrasUpstream-1
45	GDSKKLFFHVKEVQDGIELQ	NrasUpstream-2
46	DRNVEMFMTIEKSLVQNNCL	SMARCC22
47	DEVCRIFYDMKVRKCSTPEE	Destrin
48	GLEEAVYRNIQACKELAQTT	TCP Theta
49	LKEKPLWFDVYDAFPPLREP	Ribosomal S23
50	LTNPELFQRVGIIPPKGCLL	Proteasome S23
51	DKKTHLYTLILNPDNSFEIL	Calnexin-1
53	KSRTTLFRKIGDFRSLEKIS	Apoptosis inducing factor 1
54	IVLWNIFNRMPIARKIIKDG	Apoptosis inducing factor 1-2
55	EQMRTLFGFLGKIDELRLFP	SRFS11
56	PYSDKLFEMVLGPAAYNVPL	Mitofilin
57	RKAHQLWLSVEALKYSMKTS	Mitofilin-2
58	HASIHLWDLLEGKEKPVCGT	Caprin1
59	LTNPELFQRVGIIPPKGCLL	Proteasome S10B
60	RSLLDLFLDMEAATGQEVEL	Proteasome regulatory S9
61	THLAKLYDNLLEQNLIRVIE	Proteasome regulatory S9-2
62	PVEKRVFKNLQLFMENKQPE	Topoisomerase1
63	NKQPEDDLFDRLNTGILNKH	Topoisomerase1-2
64	KTKKTMFGKMYFPDVEAHGP	Desmoyokin
65	FLDEYIFLAVGRVGSTSENI	DDX3Y
66	DHSHLLYSTIPRMQEPGQIV	Catenin d 1-1
67	PEVVRIYISLLKESKTPAIL	Catenin d 1-2
68	KKLGEMWKNLNDSEKQPYIT	HMG3M
69	TRSKDIFDQLAKSLAPSIHG	MCM3-1
70	SRFDLLFIMLDQMDPEQDRE	MCM3-2
71	KTYDYLFKLLLIGDSGVGKT	RAB8A
72	TGFGMIYDSLDYAKKNEPKH	Ribosomal S24

	Sequence	Protein
74	RLLARMWNDLSEKKKAKYKA	UBF-1-2
75	DFGYRVYKMLLSLPEKVVSP	DBC1
78	NEAKGVYEKVGEATETALTC	SERCA2-1
79	EEGRAIYNNMKQFIRYLISS	SERCA2-2
80	IPVQLLWVNLVTDGLPATAL	SERCA2-3
81	ADMADVYKLLVQLKVVEDGI	Catenin a1-1
84	SFFEEVFTELQEKYGEIEEM	Splicing factor U2AF
85	I TLRILFRPVASQLPRIFTS	Prohibitin-2
86	ALQRVLYRHMQAKGVLLTDG	SNF2L4
87	EGPDAMYVKLISSDGHEFIV	Elongin15
88	WSDRSIFSGIGSTAEPVSQS	LYRIC
89	DSPREVFFRVAADMFSDGNF	BAX
90	FNMPNLYQKLESDPRTRTLL	STIP1
91	RYSRKVWDQVKASNPDLKLW	SMARCE1-1
92	KIIGGMWRDLTDEEKQEYLN	SMARCE1-2
93	FGVALLFGGVDEKGPQLFHM	PSA5
94	VAKECADLWPRIASNAGSIA	Ribosomal L23

Appendix 4

Proteins up or downregulated after two hours Nutlin treatment containing BOX-I like motifs.

Accession	Core Motif Residues	Gene
P13667	VYysV	PDIA4
P13667	VYnsL	PDIA4
P12532	VYarL	KCRU
P12532	VFadL	KCRU
P12532	LFdpV	KCRU
P60842	VFdmL	IF4A1
P60842	IFqkL	IF4A1
P60842	LYetL	IF4A1
Q14697	LYnpM	GANAB
Q14697	LYgsV	GANAB
Q14697	LFgkM	GANAB
Q14697	VFllL	GANAB
Q14697	IWldI	GANAB
Q14697	VWndM	GANAB
Q14697	LYvhM	GANAB
Q14697	VWydI	GANAB
Q14697	LYlpV	GANAB
Q14697	LFvaL	GANAB
P50454	LYqaM	SERPH
P07237	LFifI	PDIA1
P07237	IWdkL	PDIA1
Q15084	MWgwL	PDIA6
P13010	IFtdL	XRCC5
P13010	VFkkI	XRCC5
P13010	VYvqL	XRCC5
P13010	MFssL	XRCC5
P13010	LFqcL	XRCC5
P13010	IWnmL	XRCC5
P13010	LFpII	XRCC5
Q9BSH4	IFskL	TACO1
Q9BSH4	VFkfI	TACO1
Q9BSH4	VYdnI	TACO1
P14314	VWaaI	GLU2B
P23284	VFflL	PPIB

Accession	Core Motif Residues	Gene
Q15149	LWevM	PLEC1
Q15149	IYqaL	PLEC1
Q15149	LFqaM	PLEC1
Q15149	VYqaM	PLEC1
Q15149	LFqaM	PLEC1
P54886	LYeaM	P5CS
P54886	LFdqI	P5CS
O75534	IFedI	CSDE1
O75534	LFfhV	CSDE1
P09874	VFgaL	PARP1
P14866	LFtiL	HNRPL
P14866	LYgnV	HNRPL
O95292	LFfiV	VAPB
P07355	VYkeM	ANXA2
P07355	LYdsM	ANXA2
P07355	LYyyI	ANXA2
O75439	VFdyL	MPPB
P16152	VYlaL	CBR1
P50995	LYhdI	ANX11
P51858	VFakM	HDGF
P52907	VFndV	CAZA1
P12270	MYriL	TPR
P12270	VFgtV	TPR
P17480	VYlkV	UBF1
P17480	MWndL	UBF1
P18669	LWtvL	PGAM1
P18669	MWlpV	PGAM1
P28066	LFggV	PSA5
P31948	LYqkL	STIP1
P42704	IWdtL	LPPRC
P42704	VFsaL	LPPRC
P42704	LWseI	LPPRC
P42704	LYnlI	LPPRC
P42704	IYrgI	LPPRC

Accession	Core Motif Residues	Gene		Accession	Core Motif Residues	Gene
P23284	VFgkV	PPIB		P42704	VWnkI	LPPRC
Q13641	VFlgI	TPBG		P42704	LFrkV	LPPRC
Q13641	IFllV	TPBG		P42704	IYkpV	LPPRC
P11310	VFedV	ACADM		P42704	LYehL	LPPRC
P30519	LYfpM	HMOX2		P62879	IWdaM	GBB2
P30519	LFenV	HMOX2		Q12874	IFdqL	SF3A3
P30519	IFneL	HMOX2		Q12874	LFgkI	SF3A3
O00231	LFldM	PSD11		Q12874	IYeyV	SF3A3
O00231	LYdnL	PSD11		Q12874	LWakL	SF3A3
P62333	LFqrV	PRS10		Q8N163	VFtgI	K1967
O95831	LFrkI	AIFM1		Q8N163	VFfqL	K1967
O95831	IFnrM	AIFM1		Q8N163	VWtiM	K1967
P05023	LYlgV	AT1A1		Q8N163	LFleM	K1967
P05023	VFlgV	AT1A1		Q8N163	VYkmL	K1967
P05023	IFdnL	AT1A1		Q8N163	LFgnL	K1967
P05023	VYdeV	AT1A1		Q8TBA6	LFdfL	GOGA5
P78527	VYelL	PRKDC		Q8TBA6	MYgkV	GOGA5
P78527	IFnfV	PRKDC		Q8TBA6	VFviI	GOGA5
P78527	LFevL	PRKDC		Q8TBA6	IYmaL	GOGA5
P78527	MYveL	PRKDC		Q8TBA6	LWvmI	GOGA5
P78527	VYtpV	PRKDC		Q969G3	VWdqV	SMCE1
P78527	VFlaL	PRKDC		Q969G3	MWrdL	SMCE1
P78527	LFrhL	PRKDC		Q9BQE3	VFvdL	TBA1C
P78527	IFldV	PRKDC		P27797	LYtlI	CALR
P78527	LYepL	PRKDC		P29401	VYclL	TKT
P78527	LFkrL	PRKDC		P29401	VWeaM	TKT
P78527	VFeaL	PRKDC		P29401	IYsqI	TKT
P78527	VYkgI	PRKDC		P29401	MFrsV	TKT
P78527	MYsrL	PRKDC		P15531	VWegL	NDKA
P78527	VFneL	PRKDC		P30038	VYrgL	AL4A1
P78527	IFenL	PRKDC		P30038	VYriL	AL4A1
P78527	VFflL	PRKDC		P30038	LWkqV	AL4A1
P78527	LYfqL	PRKDC		P30038	LWpqI	AL4A1
P78527	IYkmM	PRKDC		P30038	IFgpV	AL4A1
P78527	MYniL	PRKDC		P30101	LFpgV	PDIA3
P78527	LFssL	PRKDC		P32322	LFlaV	P5CR1
P78527	LFsgI	PRKDC		P55809	MYanL	SCOT1

Accession	Core Motif Residues	Gene		Accession	Core Motif Residues	Gene
P78527	LYrsI	PRKDC		P55809	LWegL	SCOT1
P78527	IWddI	PRKDC		Q02790	LYanM	FKBP4
P78527	VYpfI	PRKDC		Q02790	MFerL	FKBP4
P78527	MYerM	PRKDC		Q16698	VFftL	DECR
P78527	MYaaL	PRKDC		P83731	VFqfL	RL24
P78527	LFqvM	PRKDC		O75396	LFrkL	SC22B
P78527	MYsiM	PRKDC		O75396	VFfiM	SC22B
P60981	IFydM	DEST		P40939	VYkkV	ECHA
P50990	VYrnI	TCPQ		P40939	VFkgL	ECHA
Q9UJZ1	LYlrI	STML2		P40939	IFsnL	ECHA
Q9UJZ1	VYgaL	STML2		P40939	VFedL	ECHA
P56385	LFlgV	ATP5I		P16615	VYekV	AT2A2
P55011	IWgvM	S12A2		P16615	IYnnM	AT2A2
P55011	LFirL	S12A2		P16615	LWvnL	AT2A2
P55011	VYvgI	S12A2		P05141	LYdeI	ADT2
P55011	IFqaL	S12A2		P35221	VYklL	CTNA1
P55011	MWisL	S12A2		P35221	IYkqL	CTNA1
P55011	LYiyV	S12A2		P35221	VYdgI	CTNA1
P55011	MYinL	S12A2		P07919	LFdfL	QCR6
Q04637	IFasM	IF4G1		P07919	LFnnL	QCR6
Q04637	LFrrV	IF4G1		P06733	IYeaL	ENOA
Q04637	MFqqL	IF4G1		P06733	LYrhI	ENOA
Q04637	LFifV	IF4G1		P06733	VYhnL	ENOA
Q04637	LYeiL	IF4G1		Q16718	LYtkI	NDUA5
Q04637	VWlyL	IF4G1		Q16718	LWepL	NDUA5
Q04637	LFreI	IF4G1		P07437	LFkrI	TBB5
Q04637	VFdwI	IF4G1		Q9UPN9	VFcpV	TRI33
P53396	LYkfI	ACLY		Q9UPN9	IFtlI	TRI33
P53396	IWtmV	ACLY		P11387	VFknL	TOP1
P53396	VFknM	ACLY		P11387	LFdrL	TOP1
P53396	VYegV	ACLY		P25787	VYsgM	PSA2
P53396	VYedL	ACLY		P37108	VYitL	SRP14
P53396	IYagM	ACLY		Q8WU68	VFteL	U2AF4
Q9Y4L1	MFydM	HYOU1		Q9Y3D9	LWfdV	RT23
Q9Y4L1	LFerV	HYOU1		Q16891	LFemV	IMMT
Q9Y4L1	VYpiL	HYOU1		Q16891	LWlsV	IMMT
Q9Y4L1	LFsrM	HYOU1		Q9Y230	LFneL	RUVB2
Q9Y4L1	VFetL	HYOU1		P02786	VFfII	TFR1
Q9Y4L1	LFfrV	HYOU1		P02786	LYtpV	TFR1
Q9Y4L1	IFteV	HYOU1		P02786	LFgnM	TFR1
Q9Y6X8	VYrII	ZHX2		P02786	IFgvI	TFR1
Q969H8	LWaaL	CS010		P02786	MFsdM	TFR1
Q99798	VYghL	ACON		P02786	LYtlI	TFR1
Q99798	VYnfL	ACON		P27824	LYtlI	CALX

Accession	Core Motif Residues	Gene		Accession	Core Motif Residues	Gene
P46783	IYelL	RS10		P27824	VFlvI	CALX
P51659	LYkpL	DHB4		O75533	LFnqI	SF3B1
P51659	VFeeI	DHB4		O75533	LWkgI	SF3B1
P35579	LFcvV	MYH9		O75533	LYeyL	SF3B1
P35579	IFyyL	MYH9		O75533	LFeyI	SF3B1
P35579	MFrwL	MYH9		O75533	VWpnV	SF3B1
P35579	LWkdV	MYH9		O75533	VYwkI	SF3B1
P35579	MFrtV	MYH9		O75533	IYnsI	SF3B1
P35579	LFtkV	MYH9		P43304	LYdIV	GPDM
P45880	IYqkV	VDAC2		P43304	LYirL	GPDM
P46776	LWtlV	RL27A		P43304	LYyeM	GPDM
P68371	LFkrI	TBB2C		Q86UP2	LFfwL	KTN1
P11021	VFevV	GRP78		Q86UP2	LYdeV	KTN1
P30040	VYlgM	ERP29		Q86UP2	LWneL	KTN1
P30040	VYdaL	ERP29		Q86UP2	LFpkV	KTN1
Q00059	MWgvL	TFAM		O00571	IFlaV	DDX3X
P12814	IWtiI	ACTN1		P07339	VFdnL	CATD
Q00839	LFphV	HNRPU		P08865	MWwmL	RSSA
P13693	IYrdL	TCTP		P13995	VWeiI	MTDC
P13693	MFsdI	TCTP		P42166	VYvqL	LAP2A
Q96IR7	LWqsV	HPDL		P46379	LFecL	BAT3
Q99623	MYqrL	PHB2		P68366	VFvdL	TBA4A
P13639	LFyeL	EF2		Q15393	VFgvI	SF3B3
P13639	VFdaI	EF2		Q15393	MFekI	SF3B3
P13639	VFsgL	EF2		Q15393	VYhvV	SF3B3
P13639	LYasV	EF2		Q15393	MFacL	SF3B3
P13639	IYgvL	EF2		Q15393	MFffL	SF3B3
Q09666	MFgkM	AHNK		Q15393	LFcqI	SF3B3
P04350	LFkrI	TBB4		Q15393	VYfeM	SF3B3
A6NIZ1	IFydL	RP1BL		Q15393	LYlnI	SF3B3
O00148	LFdlL	DDX39		Q15393	VFnqV	SF3B3
Q07065	IFteV	CKAP4		Q15393	VYttL	SF3B3
Q07065	IYteV	CKAP4		Q16740	MWpgI	CLPP
Q07065	LYgdV	CKAP4		Q16740	IYsrL	CLPP
Q07065	LFvkV	CKAP4		Q16740	IYdtM	CLPP
Q14444	LWdlL	CAPR1		Q8TEX9	LFysL	IPO4
Q5JTV8	LWsrI	TOIP1		Q8TEX9	LFpiV	IPO4
P58107	VYaaM	EPIPL		Q8TEX9	LFaaL	IPO4
P58107	LFqaI	EPIPL		Q8TEX9	VFeeV	IPO4
P58107	LFqaM	EPIPL		Q8TEX9	VFklL	IPO4
P58107	LWelL	EPIPL		Q8TEX9	LFplL	IPO4
P58107	LYerL	EPIPL		Q8TEX9	LFsfL	IPO4
P58107	VFakL	EPIPL		Q96I99	IFegI	SUCB2
P58107	LFqaM	EPIPL		Q96I99	LFlkI	SUCB2
P58107	LYqaM	EPIPL		Q96I99	IFggI	SUCB2
P58107	LYgrL	EPIPL		Q9NR28	VWqvI	DBLOH

Accession	Core Motif Residues	Gene		Accession	Core Motif Residues	Gene
P58107	VFqaM	EPIPL		Q9Y285	VFrsI	SYFA
P58107	LWdlL	EPIPL		Q9Y285	VFrvV	SYFA
P58107	LWqaM	EPIPL		Q9Y285	IFleM	SYFA
P58107	LWdlL	EPIPL		O15523	IFlaV	DDX3Y
P58107	LFqaM	EPIPL		O60716	LYstI	CTND1
P58107	LFqaM	EPIPL		O60716	IYisL	CTND1
P58107	IYalI	EPIPL		P0C6E5	MWknL	HMG3M
P58107	LWalL	EPIPL		P14923	LFyaI	PLAK
P58107	IYqaM	EPIPL		P14923	LFvqL	PLAK
P58107	MWkgV	EPIPL		P14923	LYssV	PLAK
P58107	LFqaM	EPIPL		P20674	IYpyV	COX5A
P58107	VWelL	EPIPL		P22314	LFgqL	UBA1
P58107	VWdvL	EPIPL		P22314	LYkvV	UBA1
P58107	VWdvL	EPIPL		P25205	IFdqL	MCM3
P58107	IYqaM	EPIPL		P25205	LFimL	MCM3
P58107	MWkgV	EPIPL		P35222	LFyaI	CTNB1
P58107	LFqaM	EPIPL		P35222	LFvqL	CTNB1
P58107	VWelL	EPIPL		P35222	LYspI	CTNB1
P58107	VWdvL	EPIPL		P37268	IFylV	FDFT
P58107	VWdvL	EPIPL		P37268	IYqyM	FDFT
P58107	IYqaM	EPIPL		P37268	IYhrI	FDFT
P58107	MWkgV	EPIPL		P51532	LWalL	SMCA4
P58107	LFqaM	EPIPL		P51532	LYrhM	SMCA4
P58107	VWelL	EPIPL		P51532	MFqhI	SMCA4
P58107	VWdvL	EPIPL		P51532	LFcqM	SMCA4
P58107	VWdvL	EPIPL		P51532	LFmrM	SMCA4
P58107	IYqaM	EPIPL		P51532	VFiqL	SMCA4
P58107	MWkgV	EPIPL		P51532	VFtsV	SMCA4
P58107	LFqaM	EPIPL		P61006	LFklL	RAB8A
P58107	VWelL	EPIPL		P62834	IFydL	RAP1A
P58107	VWdvL	EPIPL		P62847	IYdsL	RS24
P58107	VWdvL	EPIPL		P63261	VFpsI	ACTG
P58107	IYqaM	EPIPL		P63261	MYvaI	ACTG
P58107	MWkgV	EPIPL		P63261	MYpgI	ACTG
P58107	LFqaM	EPIPL		Q05519	LFgfL	SFR11
P58107	VWelL	EPIPL		Q07812	VFfrV	BAX
P58107	VWdvL	EPIPL		Q07812	IWkkM	BAX
P58107	VWdvL	EPIPL		Q13838	LFdlL	UAP56
P58107	IYqaM	EPIPL		Q14344	IYsnV	GNA13
P58107	MWkgV	EPIPL		Q14344	IFetI	GNA13
P58107	LFqaM	EPIPL		Q14344	VFsnV	GNA13
P58107	LFlsL	EPIPL		Q14344	VFrdV	GNA13
Q15149	IYevL	PLEC1		Q15369	MYvkL	ELOC
Q15149	LYedL	PLEC1		Q15388	VFqmL	TOM20
Q15149	IWtiI	PLEC1		Q5SRE5	LWtiL	NU188
Q15149	LFnaI	PLEC1		Q5SRE5	VFqyL	NU188

Accession	Core Motif Residues	Gene		Accession	Core Motif Residues	Gene
Q15149	LYdaM	PLEC1		Q5SRE5	VYglL	NU188
Q15149	IYqsL	PLEC1		Q5SRE5	MFphL	NU188
Q15149	LFndV	PLEC1		Q5SRE5	VYsfL	NU188
Q15149	MYrrV	PLEC1		Q5SRE5	IYmlL	NU188
Q15149	LWhqL	PLEC1		Q5SRE5	VWtdL	NU188
Q15149	VYaaL	PLEC1		Q5SRE5	VYacL	NU188
Q15149	LFqaM	PLEC1		Q5SRE5	LFlnL	NU188
Q15149	IWeiI	PLEC1		Q5SRE5	MWscL	NU188
Q15149	LYqqL	PLEC1		Q5SRE5	LFgtL	NU188
Q15149	IYnaL	PLEC1		Q5SRE5	IYyvV	NU188
Q15149	LFqaL	PLEC1		Q5SRE5	LFldV	NU188
Q15149	LYseL	PLEC1		Q86UE4	IFsgI	LYRIC
Q15149	VWelI	PLEC1		Q8TAQ2	MFmtI	SMRC2
Q15149	IYeaM	PLEC1		Q96C36	LFlaV	P5CR2
Q15149	LFqaM	PLEC1		Q99832	LYdkL	TCPH